Effect of Hyaluronan on Pancreatic cancer cell hallmark responses; Focus on cell migration.

A thesis submitted to the University of Manchester for the degree of
Doctor of Philosophy
in the Faculty of Biology, Medicine and Health

2023

EDUARDO A PENA ALARCON

School of Medical Sciences / Division of Cancer Sciences

Table of Contents

TOTAL WORD COUNT: 37718

List of Figures

List of Tables

List of Abbreviations

4-MU	4-methylumbeliferone
BMI	Body mass index
ANOVA	Analysis of variance
ATTC	American Type Culture Collection
BSA	Bovine Serum Albumin
°C	Degrees celsius
CAFs	Cancer associated fibroblasts
CD44	Cluster of differentiation 44
CEMIP	Cell Migration Inducing Hyaluronidase 1
CM	Conditioned media
CTGF	Connective tissue growth factor
DMEM	Dulbecco's modified Eagle's media
DPBS	Dulbecco's phosphate-buffered saline
DSS	Dextran sulphate
ECM	Extracellular matrix
EMT	Epithelial mesenchymal transition
FAP	Fibroblast activation protein
FBS	Foetal bovine serum
FGF-2	Fibroblast growth factor 2
GAGs	Glycosaminoglycans
GFAP	Glial acidic fibrillary protein
GM-CSF	Granulocyte-macrophage colony-stimulating factor
G-MDSC	Granulocytic MDSCs
GPI-anchored	Glycosylphosphatidylinositol-anchored
H4C4	CD44s blocking antibody
HA	Hyaluronan
HABP	HA binding protein
HAdase	Hyaluronidase from bovine testes type I-S
HARE	Hyaluronan receptor for endocytosis
HAS	Hyaluronan synthase
HAS1	Hyaluronan synthase 1
HAS2	Hyaluronan synthase 2
HAS3	Hyaluronan synthase 3
HEPES	4-(2-hydroxyethyl)-1-piperazineethanesulfonic acid
HGF	Hepatocyte growth factor
H-HA	High molecular weight hyaluronan
hPSCs	Human PSCs

HYALs	Hyaluronidases
iCAF	Inflammatory CAFs
IL-10	Interleukin-10
KIAA1199	Cell Migration Inducing Hyaluronidase 1
L-HA	Low molecular weight hyaluronan
LIF	Leukaemia inhibitory factor
LYVE-1	Lymphatic vessel endothelial receptor-1
MCT1	Monocarboxylate transporter 1
MCT4	Monocarboxylate transporter 4
MDSCs	Such myeloid derived suppressor cells
M-HA	Medium molecular weight hyaluronan
Min	Minute
ml	Mililitre
mM	Milimolar
M-MDSC	Monocytic MDSCs
MMPs	Matrix metalloproteinases family
myCAF	Myofibroblast CAFs
NaCL	Sodium chloride
nM	Nanometer
nm	Nano molar
NU-S	NU-Serum
OXPHOS	Oxidative phosphorylation
PanIN	Pancreatic intraepithelial neoplasia
PBS	Phosphate buffer saline
PDAC	Pancreatic ductal adenocarcinoma
PDGF	Platelet derived growth factor
PDGFRα	Platelet derived growth factor receptor alpha
PDGFRβ	Platelet derived growth factor receptor beta
PEGPH20	PEGylated recombinant hyaluronidase PH-20
PFA	Paraformaldehyde
PMA	12-O-tetradecanoyl-phorbol-13-acet
PSCs	Pancreatic stellate cells
PVDF	Polyvinylidene difluoride
RHAMM	Receptor for HA-mediated motility
rcf	Relative centrifugal force
rpm	Rotations per minute
SHH	Sonic hedgehog
SRB	Sulforhodamine B protein
STAB2	Stabilin-2

TAMs	Tumour associated macrophages
TBS	Tris-buffer saline solution
TBST	Tris-buffer saline with 0.1% Tween 20
TCA	Trichloroacetic acid
TGF-β1	Transforming growth factor beta-1
TIMP-2	Tissue inhibitor of metalloproteinase 2
TME	Tumour microenvironment
TMEM2	Transmembrane protein 2
Tregs	Regulatory T cells
TSP-2	Tromosbospondin-2
μl	Micro litre
μM	Micro molar
UDP	Uridine diphosphate
UDP-GlcUA	UDP-glucuronic acid
UDP-GlncNAc	UDP-N-acetylglucosamine
UGT	UDP-glucuronosyltransferase
UL-HA	Ultra-Low molecular weight hyaluronan
WST-8	Water-soluble tetrazolium dye-8 / Cell count Kit-8
α-SMA	α-smooth muscle actin

Abstract

The microenvironment of pancreatic ductal adenocarcinoma (PDAC) is characterized by an extensive desmoplastic reaction, an alteration of the tumour stroma where activated pancreatic stellate cells (PSC) produce large deposits of extracellular matrix where hyaluronan (HA) stands out. The large deposits of HA have been shown to increase interstitial pressure and collapse blood vessels creating an impenetrable barrier for chemotherapy drugs. Clinical trials attempting to disrupt large deposits of HA have failed to improve chemotherapy outcomes. There are a limited number of studies that have investigated the functional role of HA in PDAC, therefore this study attempted to understand the role of exogenous and endogenous HA in two cancer hallmarks, proliferation, and migration. We used conditioned media rich in HA derived from PSCs and commercial HA to analyse the exogenous effects on PDAC proliferation and migration. This study also characterised the endogenous production of HA, the proteins involved in HA turnover and how endogenous HA affects PDAC cell proliferation and migration. Proliferation was assessed by the cell counting kit and sulforhodamine assays and migration was analysed by gap closure assays. HA production was assessed with an HA-ELISA-like assay and HA in PDAC cells was assessed by an immunofluorescence-like assay. The proteins involved in HA turnover were analysed by immunoblotting, cell membrane enrichment kits, immunofluorescence and siRNA knock downs. We found that PSC-conditioned media did not affect PDAC cell proliferation. Despite PSC-conditioned media increasing migration, we found that this effect was independent of HA. Exogenous HA did not affect PDAC cell proliferation. However exogenous HA had a differential effect on migration. BXPC3 cells expressing variants of HA receptors CD44 and RHAMM, increased migration with exogenous high molecular weight HA. This was abolished by blocking hyaluronidases (HYALs), HA degrading enzymes, with dextran sulphate. PDAC cells differentially produced HA. Disrupting endogenous HA by removing pericellular HA or inhibiting HA synthesis differentially decreased the migration of BXPC3 cells but did on affect PDAC cell proliferation. The combination of these two treatments had an additive effect in decreasing migration. Knocking down hyaluronan synthase 2 (HAS2) had a similar effect and greatly reduced migration in BXPC3 cells. This study provides evidence of differentially expressed HA turnover systems that can affect migration and proliferation in PDAC. Further studies investigating the role of HA in PDAC could provide insight into why the recent therapeutic attempts to target HA in the stroma have failed.

Declaration

No portion of the work referred to in the thesis has been submitted in support of an application for another degree or qualification of this or any other university or other institute of learning.

Copyright Statement

i.   The author of this thesis (including any appendices and/or schedules to this thesis) owns certain copyright or related rights in it (the "Copyright") and they have given the University of Manchester certain rights to use such Copyright, including for administrative purposes.

ii.   Copies of this thesis, either in full or in extracts and whether in hard or electronic copy, may be made only in accordance with the Copyright, Designs and Patents Act 1988 (as amended) and regulations issued under it or, where appropriate, in accordance with licensing agreements which the University has from time to time. This page must form part of any such copies made.

iii.   The ownership of certain Copyright, patents, designs, trademarks and other intellectual property (the "Intellectual Property") and any reproductions of copyright works in the thesis, for example graphs and tables ("Reproductions"), which may be described in this thesis, may not be owned by the author and may be owned by third parties. Such Intellectual Property and Reproductions cannot and must not be made available for use without the prior written permission of the owner(s) of the relevant Intellectual Property and/or Reproductions.

iv.   Further information on the conditions under which disclosure, publication and commercialisation of this thesis, the Copyright and any Intellectual Property and/or Reproductions described in it may take place is available in the University IP Policy (see http://documents.manchester.ac.uk/DocuInfo.aspx?DocID=24420), in any relevant Thesis restriction declarations deposited in the University Library, The University Library's regulations (see http://www.library.manchester.ac.uk/about/regulations/) and in the University's policy on Presentation of Theses.

Acknowledgements

First, I would like to express my most sincere thanks and utmost respect to my supervisor Dr Jason Bruce, for his guidance, knowledge, and continued support. Thanks also to Dr Ayse Latif from the University of Manchester for facilitating the BXPC3 cells for our studies.

My special thanks to the members of the Bruce Lab, particularly to Daniel Richardson, Pishya Sritangos, Rosa Sanchez-Alvares and Sarah Sugden for their warm welcome and support during my first years of the PhD.

I would also like to acknowledge all my friends from the Michael Smith Building, especially Gabby, Pablo and Blanca. Thanks for all your support, company, and friendship. I wish you all the best in your future careers.

Thanks to my sponsor, the Agencia Nacional de Investigación y Desarrollo (ANID) from the Chilean government for the grant to fund my PhD studies. Becas Chile 2018 Folio: 72190660.

Finally, I would like to thank my friends and family for all their love and support over the past years and during my whole life.

I would like to give special thanks to my partner Fernanda for her unconditional support over the years, without which I would not have been able to achieve this feat. I dedicate this thesis to her.

Chapter 1   Introduction

1.1 Pancreatic Cancer

Pancreatic cancer has some of the worst survival statistics and very limited treatment options. This is due to a combination of different factors such as a general lack of symptoms and late detection. This means that by the time of diagnosis the disease has advanced to a late stage and is often found metastasising. In addition, pancreatic cancer usually presents with a dense tumour microenvironment, making it almost impenetrable to most cytotoxic chemotherapy drugs. Understanding the underlying molecular pathology, potential vulnerabilities and the nature of the tumour microenvironment are critical if we are to identify novel drug targets and develop new drugs to treat this devastating disease.

1.1.1 Epidemiology of pancreatic cancer

According to data from the analysis of the Global Burden of Disease study 2017, the global recorded deaths from pancreatic cancer increased 2.3 times from 196000 in 1990 to 441000 in 2017 (Collaborators, 2019). In the year 2020, there had been an increase of 55% in the incidence of pancreatic cancer, a 63% increase in prevalence and a 53% increase in mortality in the last 25 years (Lippi and Mattiuzzi, 2020). Despite that, the incidence of pancreatic cancer is estimated to be only 14th among all cancers (1.8%). However, it is the 6th cause of death of all cancers worldwide (4.8%) (Lippi and Mattiuzzi, 2020). Furthermore, projections for the year 2030 have set pancreatic cancer to become the 2nd leading cause of cancer deaths (Rahib et al., 2014). Survival rates are overwhelmingly low, although progress has been made. The overall 5-year survival rate increased from less than 5% in 1990 up to 9% in 2019 in the USA and Europe, which remains very low (Klein, 2021). There are three main recognized risk factors associated with pancreatic cancer: smoking, diabetes mellitus and high body mass index (BMI) (Collaborators, 2019). In recent years other risk factors have been under study, such as high alcohol consumption, pancreatitis and the microbiota (Klein, 2021). Individuals with a family history of pancreatic cancer have a higher risk of developing the disease, accounting for approximately 10% of all pancreatic cancers (Hruban et al., 2010). As most diagnosis of pancreatic cancer occurs in older patients, with a median age of 71 years, age has also been associated with a higher risk of developing the disease (Midha, Chawla and Garg, 2016).

1.1.2 Treatments for pancreatic cancer

The poor survival rates reported for pancreatic cancer patients are mainly related to late detection because patients are asymptomatic and are usually diagnosed at advanced stages (Vincent et al., 2011). Surgical resection is the only potential cure for treatment however more than 80% of patients do not qualify due do the advance of the diseases, therefore surgical resections are performed in only 10% of patients. Tumours are typically resected by pancreatic-duodenectomy (Whipple´s procedure) and patients receiving surgery have a 10-25% 5 year overall survival (Mizrahi et al., 2020).

The standard adjuvant treatment for pancreatic cancer was gemcitabine (Neoptolemos et al., 2010), but several recent changes have improved these original treatments. In the ESPAC-3 clinical trial, Gemcitabine plus capecitabine has shown better patient outcomes than gemcitabine alone (Neoptolemos et al., 2017). The PRODIGE24/CCTG clinical trial compared patient outcomes between treatments with gemcitabine and mFOLFIRINOX (oxaliplatin, irinotecan, and leucovorin). mFOLFIRINOX was associated with improved overall survival compared to gemcitabine (54-4 months vs 35 months)(Conroy et al., 2018). Despite the advances in cancer treatment more than 70% of patients relapse within 2 years (McGuigan et al., 2018). One of the main reasons limiting the effects of chemotherapy treatment is due in part to the high desmoplastic reaction characterizing the stromal compartment of pancreatic cancer which has been found to increase the interstitial pressure collapsing blood vessels, limiting the access of chemotherapy drugs to the tumour(Provenzano et al., 2012). Hyaluronan has been found to be the main factor responsible for the increased interstitial pressure due to its ability to attract water (Toole, 2004).

1.1.3 PDAC cancer hallmarks

The biology of a tumour is a complex network of interactions between cells and the environment, with a series of acquired traits that enable the success of aberrant growth and metastasis of cancer cells. The general framework for understanding the features that allow the success of cancer cells was laid in the seminal papers by Douglas Hanahan and Robert Weinberg (Hanahan and Weinberg, 2000). They proposed a set of six basic functional capabilities acquired by cancer cells during their development. Self-sufficiency in growth signals, insensitivity to anti-growth signals, tissue invasion and metastasis, limitless replicative potential, sustained angiogenesis, and evading apoptosis. These where later complimented by four additional attributes, two emerging hallmarks: avoiding immune destruction and deregulating cellular energetics. And two enabling characteristics: Tumour promoting inflammation and genome instability (Hanahan and Weinberg, 2011). In PDAC some of the attributes are more prominent than others in leading tumorigenesis, cancer progression and metastasis, with the tumour microenvironment having an essential role.

1.1.4 Pathology of pancreatic cancer

The pancreas is an organ with two main functions, endocrine and exocrine. Histologically the tissue is divided into two main compartments. The parenchyma is the functional compartment composed of both endocrine and exocrine tissue. The second compartment is the stroma which is the extracellular compartment that harbours the interstitial support tissue, the extracellular matrix, several types of mesenchymal and immune cells, blood vessels, and nerves (Whatcott et al., 2015). The endocrine tissue is formed by hormone producing cells (insulin, glucagon) while the exocrine cells secrete digestive enzymes (amylase, lipase, trypsinogen) (Roder et al., 2016). Malignant pancreatic tumours can originate from either exocrine or endocrine pancreatic cells. However, only 5% of cancers originate from endocrine cells compared to more than 90% of cancer originating from exocrine cells, with the most common exocrine cancer classified as pancreatic ductal adenocarcinoma (PDAC) (Grant, Hua and Singh, 2016).

PDAC arises from the exocrine tissue formed by acinar cells (enzyme producing cells) and epithelial cells found in the lining of pancreatic ducts. The classic hypothesis was that PDACs originated from ductal cells (Hruban et al., 2000; Hruban, Wilentz and Kern, 2000), however, newer evidence suggests a more complex origin (Perez-Mancera et al., 2012). Acinar cells have been reported to undergo a process called acinar-ductal-metaplasia (ADM), and this process could be a precursor to neoplasia (Kopp et al., 2012; Rooman and Real, 2012; Strobel et al., 2007). Independently of the cell origin, PDAC tumours arise from lesions found in the ducts of the pancreatic tissue. These lesions are called pancreatic intraepithelial neoplasia (PanIN) and are thought to originate in more than 90% of PDACs (Wood et al., 2022), while less than 10% of tumours originate from intraductal papillary mucinous neoplasms (IPMNs) (Basturk et al., 2015; Felsenstein et al., 2018). PanINs are classified into three stages, low grade (PanIN-1), intermediate grade (PanIN-2) and high grade (PanIN-3) (Guo, Xie and Zheng, 2016). This classification is based on the ductal morphology in histological samples where cells gradually increase in atypia (abnormal non-cancerous changes) towards higher grade lesions (Iacobuzio-Donahue, 2012). A revised classification has been proposed for describing PanINs that involves only two categories, low grade PanIN and high grade PanIN. This is thought to provide greater consensus among reporting these types of precursor lesions and updated to match the current knowledge (Basturk et al., 2015).

1.1.5 Oncogenes and tumour suppressor, mutations and aberrant signalling

The proposed mechanism for PDAC progression begins with the appearance of low grade PanINs, which progressively accumulate somatic mutations overtime evolving into higher grade PanINs, that will eventually develop into cancer (Iacobuzio-Donahue, 2012). PDAC cells are characterized for presenting several somatic mutations, with the most common activating mutations found in the *KRAS2* oncogene. Mutations in *KRAS2* are present in more than 90% of pancreatic tumours and are critical for tumourigenesis (Hidalgo, 2010). In addition to *KRAS2* activation, tumours may also present inactivation of tumour suppressor genes *CDKN2A/INK4*, TP53 and *DPC4/SMAD4* (Hidalgo, 2010; Mizrahi et al., 2020). Mutations in KRAS arise in early stages in low grade PanINs while mutations in tumour suppressor genes start to appear in high grade PanINs and PDAC (**Figure 1**) (Iacobuzio-Donahue, 2012).

The mutations in *KRAS2* generate aberrant activation of proliferation, migration, and survival pathways (Furukawa, 2022; Jonckheere, Vasseur and Van Seuningen, 2017; Schubbert, Shannon and Bollag, 2007). KRAS is a member of the small GTPase super family, that functions as a binary switch between an inactive GDP (guanosine diphosphate)-bound state to a GTP (guanosine diphosphate)- bound activated state (Colicelli, 2004). When KRAS is activated, it can bind to several
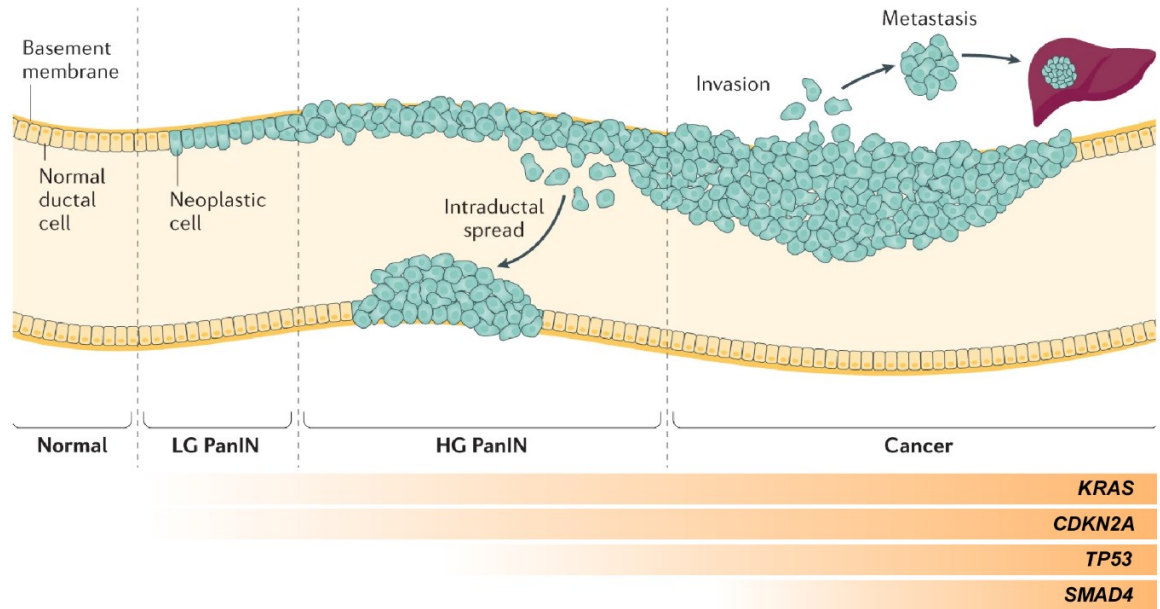
Figure 1. Model the progression of pancreatic ductal adenocarcinoma. PDAC begins in the ducts of the pancreas where non-invasive lesions can be found in the epithelial lining of the ducts. These lesions begin with mutations in KRAS which unleashes uncontrolled proliferation. Low grade PanINs evolve into high grade PanINs. High grade PanIN continues to grow and present atypical phenotypes accompanied by mutations in other genes, mainly CKN2A, TP53 and SMAD4. Eventually, an invasive phenotype in the intraepithelial lesions breaks through the basement membrane and invades the surrounding stroma evolving into pancreatic cancer. Modified from (Hayashi, Hong and Iacobuzio-Donahue, 2021).

effector proteins activating downstream signalling pathways regulating cell cycle, cell differentiation cell motility cell survival, among others (Vigil et al., 2010). The three most frequent KRAS mutations found in PDAC are G12D (41%) followed by G12V (34%) and G12R (16%). These mutations generate a constant GTP-bound KRAS overstimulating downstream signalling pathways that lead to cancer growth (Waters and Der, 2018).

Mutations in the tumour suppressor *CDKN2A/INK4* result in a loss of G1/S checkpoint control leading to increases in cell proliferation (Bardeesy et al., 2006; Kim and Sharpless, 2006). Mutations in the tumour suppressor *TP53* lead to a loss of apoptosis regulation, aberrant activation of the cell cycle, induce several metabolic changes and even support metastasis (Morton et al., 2010; Petitjean et al., 2007; Weissmueller et al., 2014). Mutations in the tumour suppressor *DPC4/SMAD4* produce the loss of the intracellular TGF-β signalling pathway, these results in increased migration, autocrine activation, and immune evasion (Chen et al., 2014; Hayashi, Hong and Iacobuzio-Donahue, 2021; Hurwitz et al., 2023). Although these are the main four mutations characteristic of most PDACs there are several more such as mutations in the TGF-β pathway (*TGFBR1*, *TGFBR2* and *ACVR1B*) and germline mutations in *BRCA2, FANCC, FANCG and STK11/LKB1* that contribute to maintenance, progression and metastasis (Iacobuzio-Donahue, 2012).

1.1.6 Pancreatic cancer microenvironment

The tumour microenvironment (TME) is an important component of pancreatic cancer. Not only does it provide a physical structure providing a scaffold that supports cancer cells, but it is also formed by a great number of biochemicals cues and different cell types that are indispensable for maintaining tumour growth, progression and metastasis (Hosein, Brekken and Maitra, 2020). An important part of PDAC development is its interaction with the microenvironment. This interaction is mutually beneficial where cancer cells are able to modify their microenvironment and in turn the microenvironment supports several cancer hallmarks (Herting, Karpovsky and Lesinski, 2021).

1.1.7 Extracellular matrix

The extracellular matrix (ECM) is a three-dimensional network of numerous macromolecules that provide structural support for tissues to function and it is highly dynamic with the ability to be remodelled upon the requirements of the tissue (Theocharis et al., 2016). It is an intertwined network of collagens, laminin fibronectin, proteoglycans, glycoproteins, hyaluronan and many other molecules that interact and bind to each other as well as interacting with different types of cells (Hynes and Naba, 2012). The ECM can be classified into two categories, the basement membrane, a thin layer of ECM that directly supports epithelial and endothelial tissues, and the interstitial matrix which is a broader matrix where several stromal cells coexist (Piersma, Hayward and Weaver, 2020). In healthy tissues, the basement membrane is formed mainly by a network of collagen IV and laminin (Mouw, Ou and Weaver, 2014). Interstitial ECM is formed by large quantities of collagen and fibronectin fibrils that grant the ECM mechanical strength, and by proteoglycans that like hyaluronan (HA) maintain hydration due to its highly hydrophilic structure (Toole, 2004).

Cancer cells can bind to the ECM through several receptors present on the cell's surface such as integrins, syndecans, discoidin and hyaluronan receptors (Leitinger and Hohenester, 2007; Misra et al., 2015; Xian, Gopal and Couchman, 2010). These interactions with the ECM can control cellular processes like cell proliferation, adhesion, differentiation, survival, motility, angiogenesis and many others (Karamanos et al., 2021).

During PDAC tumorigenesis, ECM remodelling begins early on in low grade PanIN where stromal cells can be activated increasing the secretion and deposition of extracellular matrix components, in a process known as fibrosis (Detlefsen et al., 2005). These activated stromal cells are responsible for the increase of several ECM components like collagen (I, III, V) periostin, fibronectin, and HA are all found to be present from early stages of PanIN and throughout the progression of PDAC (Berchtold et al., 2015; Dawson et al., 2013; Provenzano et al., 2012; Tian et al., 2019; Yan et al., 2021).

In PDAC the ECM undergoes several transformations that change its structure, one example is collagen fibres have been found to be highly aligned compared to non-neoplastic tissue, and this collagen alignment correlates with a worse prognosis (Drifka et al., 2016; Drifka et al., 2015). Increases in ECM stiffness due to large deposits of collagens have been reported to alter PDAC cell behaviour and even contribute to chemoresistance (Rice et al., 2017). The changes in collagen deposits are only part of a greater process in the PDAC stroma, characterized by extensive fibrosis generated by activated stromal cells, where cancer associated fibroblasts (CAFs) and pancreatic stellate cells (PSCs) are the main culprits (Apte et al., 2004; Hosein, Brekken and Maitra, 2020). The extensive fibrosis found in PDAC is called desmoplastic reaction and it generally composes more than 90% of the tumour volume (Orth et al., 2019). The desmoplastic reaction will be more profoundly discussed at a later point.

1.1.8 Desmoplastic reaction

One of the defining characteristics of PDACs is the excessive deposits of ECM surrounding the tumours (Erkan et al., 2008; Yen et al., 2002). Over 90% of the proteins found in PDAC ECM are derived from CAFs with less than 10% coming from PDAC cells (Tian et al., 2019). The desmoplastic ECM is formed by large deposits of collagen I, collagen III, collagen IV and HA accompanied by extensive staining of α-smooth muscle actin (α-SMA) a marker for CAFs and PSCs (**Figure 2**) (Whatcott et al., 2015). Within the ECM collagen I and HA quantity are correlated to survival, the median difference in survival of patients with high and low HA was 15 months, while the median difference in survival between high and low collagen I was 8.2 months (**Figure 2**) (Whatcott et al., 2015). Interestingly metastatic lesions from the lung, liver and peritoneal cavities also present a desmoplastic stroma (**Figure 2**) (Whatcott et al., 2015). Collagen I is known to promote the malignant phenotype of PDAC cells in vitro and induce chemoresistance by increasing cell proliferation and reducing apoptosis in response to 5-fluorouracil (Armstrong et al., 2004; Koenig et al., 2006; Rice et al., 2017; Shields et al., 2011) Collagen I can also be a source of proline for PDAC cells promoting cell survival (Olivares et al., 2017). Collagen IV can also promote PDAC by enhancing proliferation,

migration and inhibiting apoptosis (Ohlund et al., 2013) HA has been shown to promote growth by acting as fuel for PDAC cells (Kim et al., 2021) and by partially decreasing cell adhesion (Kultti et al., 2014). Several other ECM proteins can be found increased in the desmoplastic stroma which includes laminin, tenascin, and fibronectin that are also involved in promoting the malignant phenotype (Apte et al., 1999; Haber et al., 1999; Leppanen et al., 2019; Opitz et al., 2021; Paron et al., 2011).

The desmoplastic reaction found in PDAC is induced through the secretion of several factors from PDAC cells, transforming growth factor beta-1 (TGF-β1), fibroblast growth factor 2(FGF-2), sonic hedgehog (SHH) and platelet derived growth factor (PDGF) are the main factors responsible for CAF-induce ECM production and proliferation (Bachem et al., 2005; Bailey et al., 2008; Lohr et al., 2001). In a mouse model, the inhibition of SHH was studied to try an improve drug delivery (gemcitabine) into the blood vessel collapse tissue of PDAC surrounding PDACs (Olive et al., 2009). Inhibition of SHH effectively depleted the desmoplastic stroma and improved vascular perfusion for gemcitabine delivery and delayed disease progression. This strategy was later applied to humans in a clinical trial with unsuccessful results (NCT01130142). The inhibition of SHH had the opposite effect decreasing patient survival when it was combined with gemcitabine treatment (Sahai et al., 2020). This was further studied in mouse models discovering that the desmoplastic reaction acts both as a tumour promoter as well as a tumour constraint, suggesting that this dual function is due to the different stromal populations in the tumour (Hosein, Brekken and Maitra, 2020).

The excess deposit of ECM poses one of the biggest difficulties to overcome in PDAC as it acts as a barrier that limits the accessibility of chemotherapeutic drugs for PDAC treatment (Neesse et al., 2015). In the desmoplastic stroma of a mouse model blood vessels were found to be collapsed and tumour perfusion was limited due to the high interstitial pressure exerted mainly by the ability of HA to hold water (DuFort et al., 2016; Jacobetz et al., 2013; Provenzano et al., 2012). The high interstitial pressure could be reversed using a PEGylated recombinant hyaluronidase PH-20 (PEGPH20) (Thompson et al., 2010). This allowed blood vessels to reopen and increased perfusion allowing chemotherapeutic agents, like gemcitabine, to reach the tumours in mouse models effectively reducing tumour size (DuFort et al., 2016; Jacobetz et al., 2013; Provenzano et al., 2012). However, a phase III clinical trial applying this concept returned unsuccessful results when PEGPH20 was used as it did not improve the overall survival of treated patients (Van Cutsem et al., 2020). The heterogeneity of stromal cells participating in the desmoplastic reaction might be the reason why these therapeutic strategies have failed, therefore further studies are needed to understand why these strategies failed.
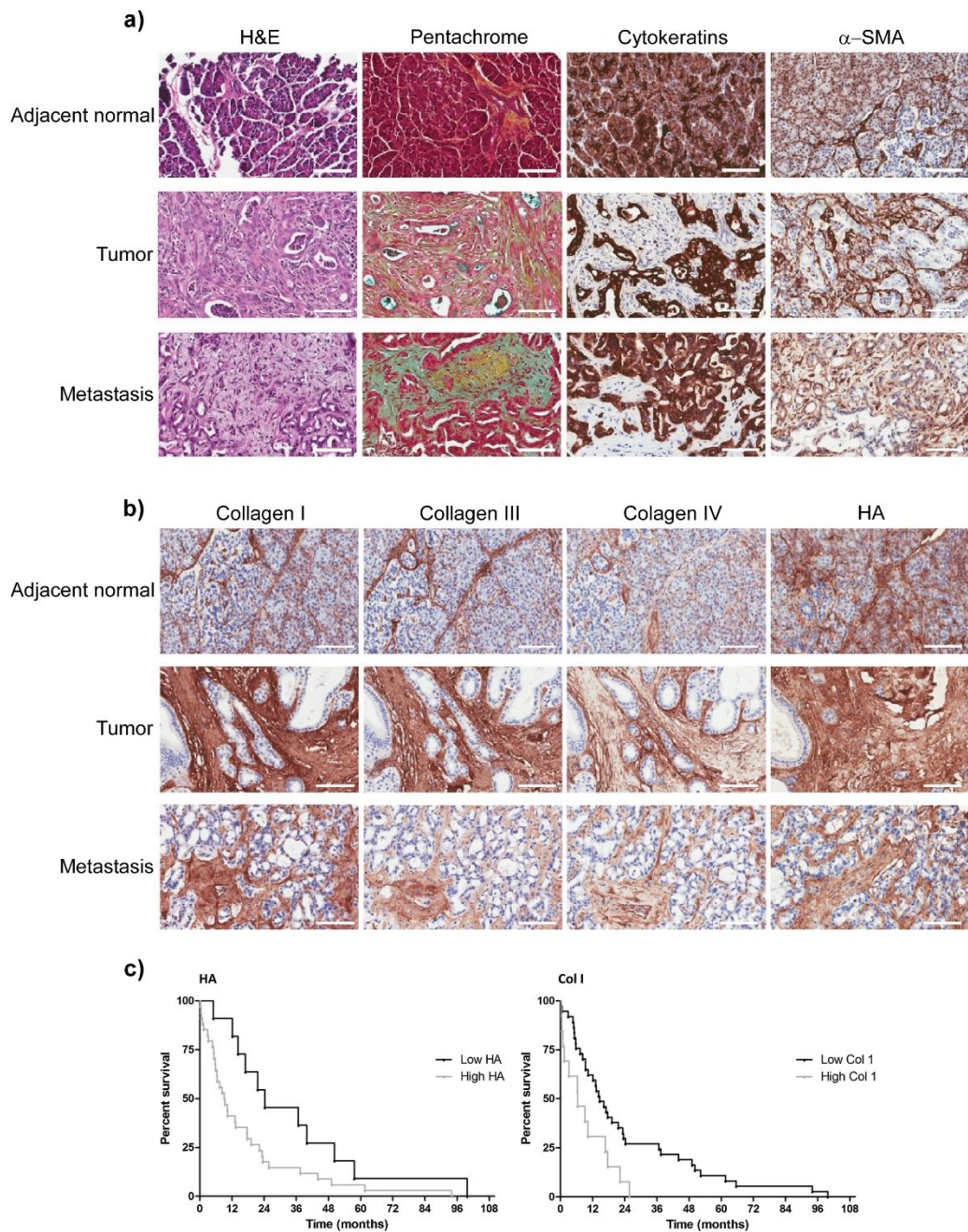
Figure 2. The stroma of PDAC tumours is characterized by an extensive desmoplastic reaction. a) Tissue from primary and metastatic PDAC displays abundant collagen and glycosaminoglycans (yellow and light blue) staining in the stroma, accompanied by extensive staining for the CAF marker α-SMA. **b)** Abundant collagen I, II and IV together with HA is present in PDAC tissue of primary tumours and metastasis. **c)** Kaplan-Meier survival curves for high and low quantities of HA and collagen I. The media difference between low HA and high HA was 15 months, while for high collagen I and low collagen I was 8.2 months. Figure modified from Whatcott et al. 2015 (Whatcott et al., 2015).

1.1.9 PDAC cells can recruit and activate different cell types in the stroma.

PDACs are known to be immunologically cold tumours, with low infiltration of cytotoxic T cells and a high presence of immunosuppressing cells (Blando et al., 2019; Pineda et al., 2021; Zhao et al., 2009). PDAC can modulate the TME into an immunosuppressive environment by inducing the recruitment of immunosuppressing cells, such myeloid derived suppressor cells (MDSCs), regulatory T cells (T_{regs}) and tissue associated macrophages which in turn reduce the recruitment of proinflammatory cells (Khaled, Ammori and Elkord, 2014) (Ullman et al., 2022).

Myeloid derived suppressor cells: Tumour derived factors such as cytokines and chemokines (VEGF, CSF, IL-6), IL-10) that are systemically released can interrupt the normal progression of myeloid cell differentiation (Messmer et al., 2015). One of the main pathways that cause the interruption of myeloid differentiation is thought to be the activation of the transducer and activator of transcription 3 (STAT3) (Gabrilovich, 2004). Pathological interruption of differentiation results in immature myeloid cells named MDSCs. There are two main types of MDSCs, granulocytic MDSCs (G-MDSC) and monocytic MDSCs (M-MDSC) (Gabrilovich, Ostrand-Rosenberg and Bronte, 2012). Circulating MDSCs were found to be increased in PDAC patients compared to healthy patients (Khaled, Ammori and Elkord, 2014; Trovato et al., 2019), and tissue infiltrating G-MDSC and MDSCs have been reported in several studies (Khaled, Ammori and Elkord, 2014; Sivakumar et al., 2021; Trovato et al., 2019). PDAC cells secrete granulocyte-macrophage colony-stimulating factor (GM-CSF) that recruits MDSCs from the bone marrow to the tumour stroma, where they have immunosuppression activity by limiting the activity of anti-tumour T cells (Bayne et al., 2012). PDACs can also secret the chemokine CCL2 that can recruit CCR2^{+} macrophages from the bone marrow that infiltrate the tumour and are characterized by an immunosuppressive phenotype (Sanford et al., 2013). Once in the tumour stroma MDSCs have immunosuppressing effects by four main mechanisms: metabolite depletion (e.g L-arginine), production of reactive oxygen and nitrogen species, direct contact inhibition, and secretion of soluble factors (e.g. TGF-β) (Trovato et al., 2020).

Tumour associated macrophages: Macrophages are late stage differentiated myeloid cells that form part of the innate immune defence (Lankadasari et al., 2019). Tumour associated macrophages (TAMs) found in PDAC tissue can either be recruited from circulation (monocytes) or arise from embryonic precursors residing within the tissue that have self-renewal capabilities (Zhu et al., 2017). They can be categorized into two separate groups, classic activation M1 and alternative activation M2 macrophages, which are differentiated by local environmental signalling (Lankadasari et al., 2019). The M1 macrophages are characterized by an anti-tumoral phenotype while the M2 macrophages are characterized by a pro-tumoral phenotype (Murray et al., 2014; Yang, Liu and Liao, 2020). The M2 macrophages, mainly derived from circulating monocytes, exert their pro-tumoral activity by generating an immunosuppressing environment mediated by the secretion of anti-inflammatory cytokines such as TGF-β and interleukin-10 (IL-10) abrogating T cell anti-tumoral activity while recruiting immunosuppressing T_{regs} (Habtezion, Edderkaoui and Pandol, 2016; Ostuni

et al., 2015). While tissue resident TAMs are reported to be associated with a more pro-fibrotic phenotype (Zhu et al., 2017).

Cancer associated fibroblasts: Fibroblasts are one of the most abundant cell types in the stroma (Maia and Wiemann, 2021). They are distributed along the stromal tissue of all organs in a quiescent state, resting until an alteration occurs in the tissue that can activate them (Kalluri, 2016). The origin of fibroblasts has not been fully established but they are thought to arise from mesenchymal cells of the embryonic tissue called mesenchyme with either mesoderm or neural crest origin (Sahai et al., 2020). Because of the unclear origins of fibroblasts, it is difficult to differentiate them, but fibroblasts can be identified by a combination of markers and morphological characteristics. Fibroblasts tend to have a spindle like shape and can express markers like vimentin, desmin, platelet derived growth factor receptor (PDGFRα and PDGFRβ), fibroblast specific protein 1, and fibroblast activation protein (FAP) and α-smooth muscle actin (Maia and Wiemann, 2021). CAFs can also originate from other stromal resident cells like endothelial cells, smooth muscle cells and myoepithelial cells (Shiga et al., 2015).

In the context of cancer, fibroblasts can become activated and are categorized as cancer associated fibroblasts or CAFs (Gieniec et al., 2019). PDAC cells can secrete TGF-β, PDGF, sonic hedgehog and fibroblast growth factor-2, all of which induce CAF activation, proliferation, and matrix deposition (Apte et al., 2004; Bachem et al., 2005; Bailey et al., 2008). Even though CAFs are a heterogeneous group of cells in the tissue, in PDAC it is thought that the majority of CAFs derive from quiescent resident pancreatic stellate cells that can be identified by increased expression of α-SMA and FAP (Apte et al., 1998; Apte et al., 1999; Arina et al., 2016; Bachem et al., 2005). It is important to note that these markers are also expressed by several different cell types (Santi, Kugeratski and Zanivan, 2018).

Recently CAFs have been categorized according to their functional phenotype into myofibroblast CAFs (myCAF) and inflammatory CAFs (iCAF) in an organoid in vitro model (Ohlund et al., 2017). In this study, myCAFs were characterized by expressing high levels of α-SMA and low levels of IL-6 (α-SMA^{high}IL-6^{low}), whereas the iCAF phenotype was characterized by low expression of α-SMA and high levels of IL-6 (α-SMA^{low}IL-6^{high}). These two phenotypes have distinct functions, the α-SMA^{high}IL-6^{low} had ECM synthesis functions while the α-SMA^{low}IL-6^{high} secreted cytokines, like IL-6, are known to promote tumorigenesis on PDAC cells via activation of STAT3 (Huang et al., 2019). This heterogeneity of CAFs becomes important, as seen in a PDAC mouse model where α-SMA positive cells can be selectively targeted and eliminated (Ozdemir et al., 2015). Eliminating α-SMA positive cells from the tumour stroma of these mice generated more invasive and undifferentiated PDAC cells and diminished animal survival. This demonstrates the highly heterogenous nature of CAFs in the tumour tissue and the interconnections with PDAC cells are extremely complicated and require continued study.

Pancreatic stellate cells: Pancreatic stellate cells are "star" shaped mesenchymal cells residing around the acinar, pancreatic ducts and blood vessels of the pancreas and comprise 4-7% of parenchymal cells (Apte et al., 1998; Bachem et al., 1998). PSCs share similarities to hepatic stellate cells that reside in the liver as they both are quiescent vitamin A storing cells, which led to the identification of PSCs by autofluorescence of cytoplasmic lipid droplets of vitamin A (Watari, Hotta and Mabuchi, 1982). PSCs express intermediate filament proteins like desmin and glial acidic fibrillary protein (GFAP) that can be used as markers for identification to differentiate them from fibroblast, as well as α-SMA which is differentially expressed when PSCs are activated and acquire an ECM producing phenotype (Apte et al., 2004; Bachem et al., 2005; Haber et al., 1999; Ohlund et al., 2017). Even though α-SMA is not a specific marker for activation of PSCs it is important to note that α-SMA considered a marker for ECM synthesising phenotype in PSCs (Ohlund et al., 2017).

PSCs can become activated in pathological instances like chronic pancreatitis and cancer (Mews et al., 2002). As previously mentioned, PDAC cells can secrete several factors that can activate PSCs such as TGF- β, PDGF, SHH, FGF-2 and IL-1 (Bachem et al., 1998; Biffi et al., 2019; Hwang et al., 2012). The stronger promoters of ECM deposition by activated PSCs are TGF-β FGF-2 and SHH, which induce the deposition of several ECM components like collagen, fibronectin and hyaluronan (Apte et al., 2004; Bachem et al., 2005; Junliang et al., 2019). ECM degrading enzymes from the matrix metalloproteinases family (MMPs) like MMP-2 and MMP-9 can be secreted by PSCs, as well as MMP inhibitors like tissue inhibitor of metalloproteinase 2 (TIMP-2), which suggests that PSCs actively participate in matrix remodelling and turnover (Phillips et al., 2003; Schneiderhan et al., 2007).

In addition to ECM deposition, activated PSCs can secrete several factors that act in a paracrine or autocrine manner. Activated PSCs secrete hepatocyte growth factor (HGF), Tromosbospondin-2 (TSP-2) and PDGF that can promote the growth of PDAC cells (Farrow, Berger and Rowley, 2009; Pothula et al., 2016; Vonlaufen et al., 2008). Furthermore, PSCs can induce chemoresistance against gemcitabine in PDAC cells via Nocth-HES1 signalling (Cao et al., 2015) and by c-MET phosphorylation on PDAC cells through paracrine secretion of HGF by PSCs (Firuzi et al., 2019). Another cytokine found to be secreted by activated PSCs was the leukaemia inhibitory factor (LIF) (Shi et al., 2019). LIF was present throughout the development of PDAC in a mouse model, actively promoting PDAC progression through STAT3 activation and inducing chemoresistance to gemcitabine (Shi et al., 2019). PSCs can secrete connective tissue growth factor (CTGF) (Eguchi et al., 2013) and PDGF in an autocrine manner increasing their activation and proliferation in a self-stimulating loop (Habisch et al., 2010). The constant crosstalk of PDAC cells and PSCs are replicated in several *in vivo* mice models, when both cell types were co-injected in a xenograft model, PSCs replicated the desmoplastic reaction reported in human tissue. PSCs also promoted tumour growth when injected together, compared to mice that were only injected with PDAC cells alone (Bachem et al., 2005; Hwang et al., 2008; Vonlaufen et al., 2008; Xu et al., 2010). In one mouse model where PDAC metastasis was studied, PSCs were able to migrate along with

metastasizing PDAC cells to metastatic sites, highlighting the closed interconnected fate of PDAC and PSCs (Xu et al., 2010).

It is important to remember that activated PSCs can also acquire an iCAF phenotype that is mainly induced by PDAC cell secreted IL-1 (Biffi et al., 2019). This inflammatory phenotype of PSCs is characterized by low α-SMA expression and high IL-6 secretion (Ohlund et al., 2017). This becomes important since high levels of IL-6 have been found in patients with PDAC and are correlated to tumour size and liver metastasis (Talar-Wojnarowska et al., 2009). Secretion of IL-6 by PSCs has been reported to directly promote invasion and progression of PDAC cells through a STAT3 dependent pathway (Nagathihalli et al., 2016; Ohlund et al., 2017). Other cytokines IL-11, LIF and chemokines CXCL1 and CXLC2 are also expressed by the activated inflammatory PSCs and promote PDAC progression (Al-Ismaeel et al., 2019; Ohlund et al., 2017; Shi et al., 2019; Steele et al., 2016).

PSCs can also promote PDAC progression indirectly by affecting other cells in the tumour tissue. PSCs express galectin-1 that induces T cell apoptosis (Tang et al., 2015) inducing an immune escape environment. PSCs can also sequester cytotoxic T cells in the stroma limiting access to the tumour by secreting the chemotactic cytokine CXCL12 (Ene-Obong et al., 2013). The immunosuppressive environment observed in PDAC can also be promoted by PSCs by inducing TAMs into an M2 suppressive phenotype by secreting GM-CSF and reactive oxygen species (Zhang et al., 2017).

Metabolic coupling between PDAC cells and PSCs has been reported to occur through two different pathways. In a co-culture system, PDAC cells induced a change in metabolism from oxidative phosphorylation (OXPHOS) to glycolysis in activated PSCs. This produced increased secretion of lactate by PSCs through monocarboxylate transporter 4 (MCT4) and uptake of lactate by PDAC cells through monocarboxylate transporter 1 (MCT1) supporting the tumour progression (Shao et al., 2020). PDAC cells can induce autophagy in activated PSCs which leads to cell catabolism and the release of alanine from PSCs. This alanine can be captured by PDAC cells and shuttled into oxidative phosphorylation promoting growth, more importantly in nutrient deprived environments (Sousa et al., 2016).

As shown above, the closely regulated crosstalk between PSCs and PDAC cells is essential for tumour progression and metastasis (**Figure 3**). This remains under active study as there are still many unanswered questions. One of the most prominent ECM macromolecules synthesized by PSCs is HA. Most studies in PDAC have been centred around removing HA from the tumour tissue to recover collapsed blood vessels and overcome chemoresistance. However, research on how HA interacts with PDAC cells is limited and given the recent failure of one of the most promising clinical trials focused on removing HA from the stroma, the need for understanding how HA and PDAC interact is even more necessary.
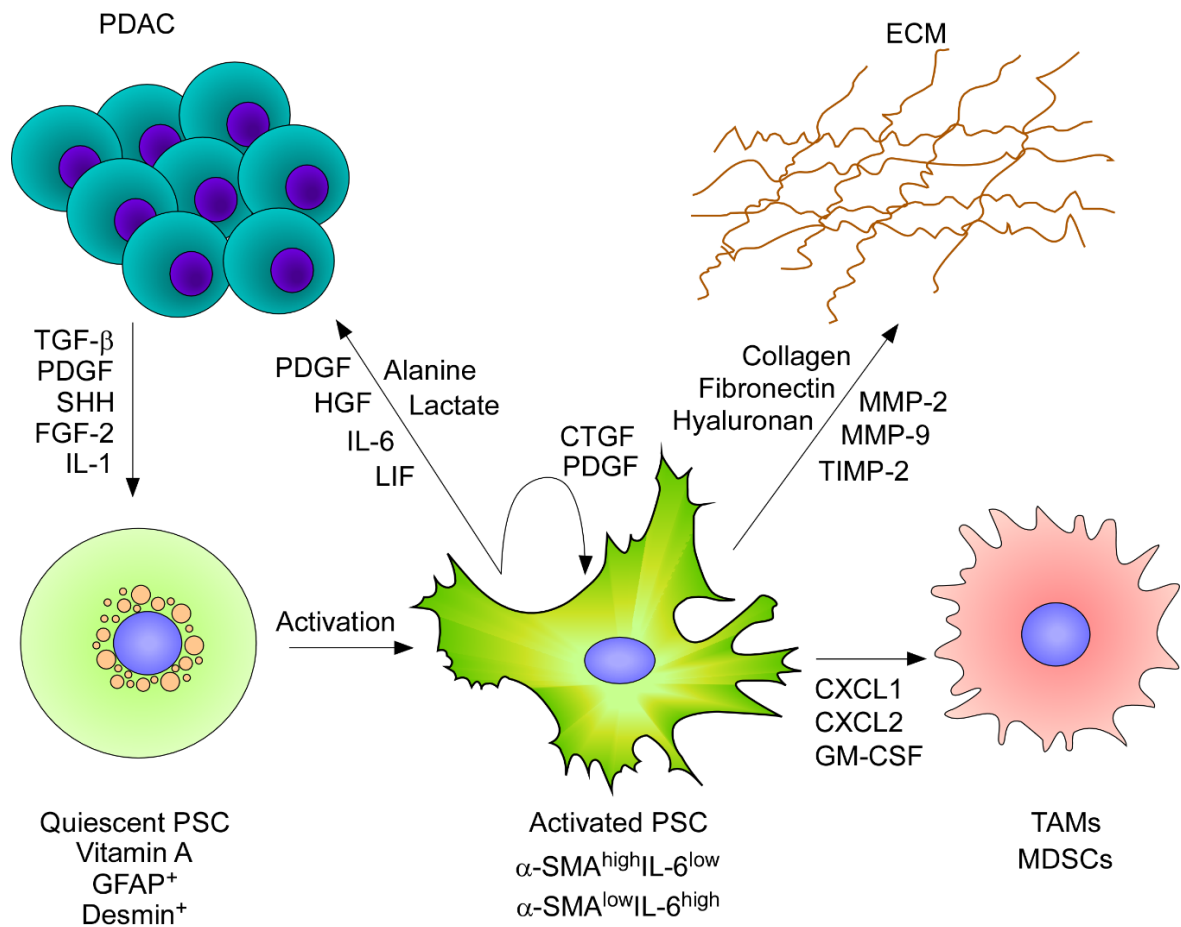
Figure 3. **Pancreatic stellate cell interaction in the tumour microenvironment**. Tumour cells actively secrete several factors that can activate PSCs in the tumour microenvironment. Once activated, PSCs release several factors that affect cancer proliferation, progression, and metabolism. Activated PSCs can also secrete self-stimulating factors in an autocrine manner. Activated PSCs can secrete several chemokines to recruit TAMs, favouring immunosuppressive phenotypes. The ECM is remodelled by activated PSCs by the release of several ECM degrading enzymes and by synthesizing large quantities of ECM components. Adapted from Habisch et al., 2010 (Habisch et al., 2010).

1.2 Hyaluronan

HA is part of a group of negatively-charged, long chain polysaccharides called glycosaminoglycans (GAGs), which are composed of repeating disaccharide units and are present in most tissues (Afratis et al., 2012). HA formed from two glucose derived precursor sugars conjugated to uridine diphosphate (UDP), UDP-glucuronic acid (UDP-GlcUA) and UDP-N-acetylglucosamine (UDP-GlncNAc) (**Figure 4**), which are processed by a hyaluronan synthase (HAS) into a linear polysaccharide composed of multiple disaccharide repeats of glucuronic acid and N-acetyl glucosamine linked by β1-4 and β1-3 glycosidic bonds [β1,4-GlcUA-β1,3-GlcNAc-]$_n$ (Toole, 2004). Hyaluronan differs from other types of GAGs because it is unbranched, lacks additional sulphate groups and is completely devoid of peptide core (Fraser, Laurent and Laurent, 1997). Hyaluronan is ubiquitously present in different human tissues mainly found forming part of the ECM, in synovial fluid of the joints, and in the skin, with the highest concentrations found in the umbilical cord and the vitreous body of the eye (Laurent and Fraser, 1992). It can also be found as an extracellular coating around cells or even located intracellularly associated to the mitotic spindle (Evanko and Wight, 1999; Monslow, Govindaraju and Pure, 2015; Toole, 2004). The number of disaccharides that compose it can vary, ranging from 2000 to 25000 units, which adds up to a molecular weight of approximately 10^6 to 10^7 Da. Another important difference from other GAGs is their synthesis pathway. Most GAGs are mainly synthesized in the Golgi apparatus while hyaluronan is synthesized by plasma membrane bound enzymes known as hyaluronan synthases.

One of the most prominent physical properties of HA is the ability to retain water. HA can retain up to 1000 times its weight (Kultti et al., 2012) at around 15 water molecules per disaccharide unit (Jouon et al., 1995). This allows HA to be an integral part of the ECM, adding viscosity to the tissue, maintaining hydration and controlling water homeostasis. HA also confers structure to the ECM as the large molecules act like a scaffold for hyaluronan binding proteins (hyaladherins) that can interconnect HA with other large proteoglycans adding extra support to the ECM (Abatangelo et al., 2020; Kultti et al., 2012).

HA turnover is a process that varies among tissues, with rapid turnover rates in the blood, from minutes to 2-3 days in most tissues (Fraser, Laurent and Laurent, 1997). With this high turnover rate, it is believed that around a third of HA is degraded and replaced daily (Monslow, Govindaraju and Pure, 2015). In tissues there is a local turnover rate of about 20-30% of HA, the rest is processed systemically as HA is drained from tissues through the lymphatic system where turnover is mainly processed by endothelial cells in the liver and to some degree in lymphatic nodules, therefore it is usual to find low levels of circulating HA in the blood (Fraser, Laurent and Laurent, 1997; Mochizuki et al., 2009). HA is usually found in healthy tissues as a high molecular weight polymer (H-HA), participating in tissue maintenance and protection, however under tissue injury or disease HA suffers fragmentation. These fragments can act as signalling molecules that affect numerous processes such
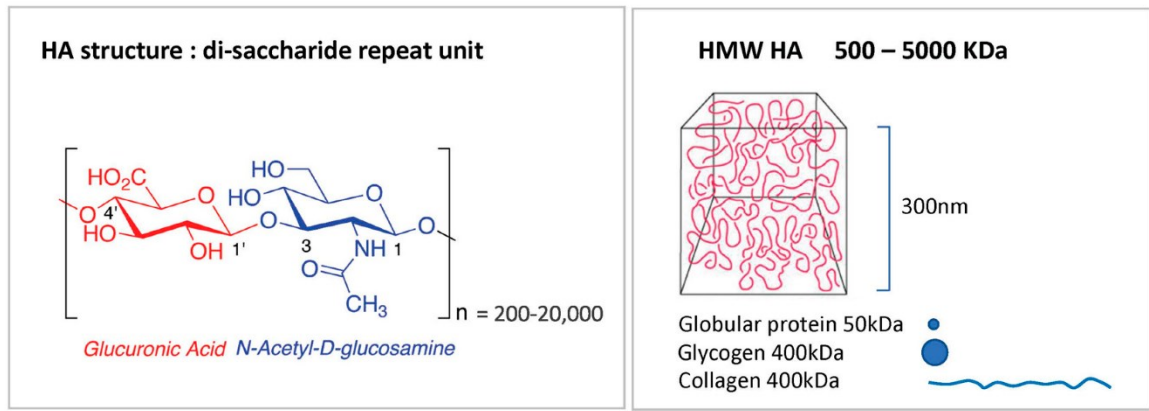
Figure 4. Hyaluronan is a large hydrophilic polysaccharide. HA is formed of repeating disaccharides glucuronic acid and N-acetyl glucosamine. It can form large macromolecules of nearly 20000 disaccharide units. It is highly hydrophobic, holding up to 15 molecules of water per disaccharide units occupying large volumes. Adapted from Johnson et al., 2021 (Johnson and Jackson, 2021).

as cell proliferation, migration, immune activation, and angiogenesis among several others (Stern, Asari and Sugahara, 2006).

1.2.1 Hyaluronan Synthases

In humans, there are three isoenzymes capable of hyaluronan synthesis, hyaluronan synthase 1, 2 and 3 (HAS1, HAS2 and HAS3) encoded by their respective genes located in different chromosomes (Itano and Kimata, 2002). In humans, HAS1 is located on chromosome 19q13.3 – q13.4, HAS2 is on chromosome 8q24.12 and HAS3 is located on chromosome 16q22.1 (Spicer et al., 1997). These enzymes have a shared sequence similarity between 55-70% but they differ in their functions and the output of HA (Itano et al., 1999). Structurally HAS has 7 membrane spanning domains, with both the C- and N-terminal facing the cytosol (Itano and Kimata, 2002). The HAS are special enzymes as they can use four substrates (two sugar-nucleotides and two UDP bound precursors), with two glycosyltransferase activities in the same protein (highly unusual), and they can generate two different types of glycosidic linkages in two different sugars (Itano and Kimata, 2002; Rilla et al., 2005). There are two proposed mechanism for how HA is transferred extracellularly, the first is that it can be translocated or extruded through a pore like structure within HAS as it is being synthesized (**Figure 5**), and the second is that it may be translocated by an unknown ABC transporter (Philipson and Schwartz, 1984; Weigel and DeAngelis, 2007). Their enzymatic properties can vary according to the different isoforms, as shown by *in vitro* experiments using recombinant HAS proteins transfected into rat fibroblasts, and where the size of hyaluronan produced was measured (Itano et al., 1999). These measurements indicated that HA produced by HAS1 ranged from 200-2000 kDa, HAS2 >2000 kDa and HAS3 from 100-1000 kDa (Itano et al., 1999). The difference in hyaluronan molecular weight produced by these enzymes could indicate that there may be a physiological mechanism regulating enzyme expression and therefore the size of hyaluronan that is being synthesized. In knockout mouse models, the HAS2 knockout mice die during gestation due to heart failure (Camenisch et al., 2000). This highlights the importance of HAS2 as it is critical during embryogenesis, while HAS1 and HAS3 knockouts did not present these abnormalities and mice were born without issues and remained fertile (Itano et al., 2002; Itano and Kimata, 2002).

The most common molecule used to inhibit HA synthesis by HAS is a coumarin derivative named 4-methylumbeliferone (4-MU) (Nagy et al., 2015). The proposed mechanism for the inhibitory effect of 4-MU is that it functions as a competitive substrate. The pathway for HA synthesis involves the generation of the UDP-conjugated precursors by a UDP-glucuronosyltransferase (UGT), 4-MU can be used as a substrate by UGT which then conjugates 4-MU to glucuronic acid, depleting the cytoplasmic pool of UDP-GlcUA used in HA synthesis which leads to inhibition (Kakizaki et al., 2004; Kultti et al., 2009) (**Figure 5**).
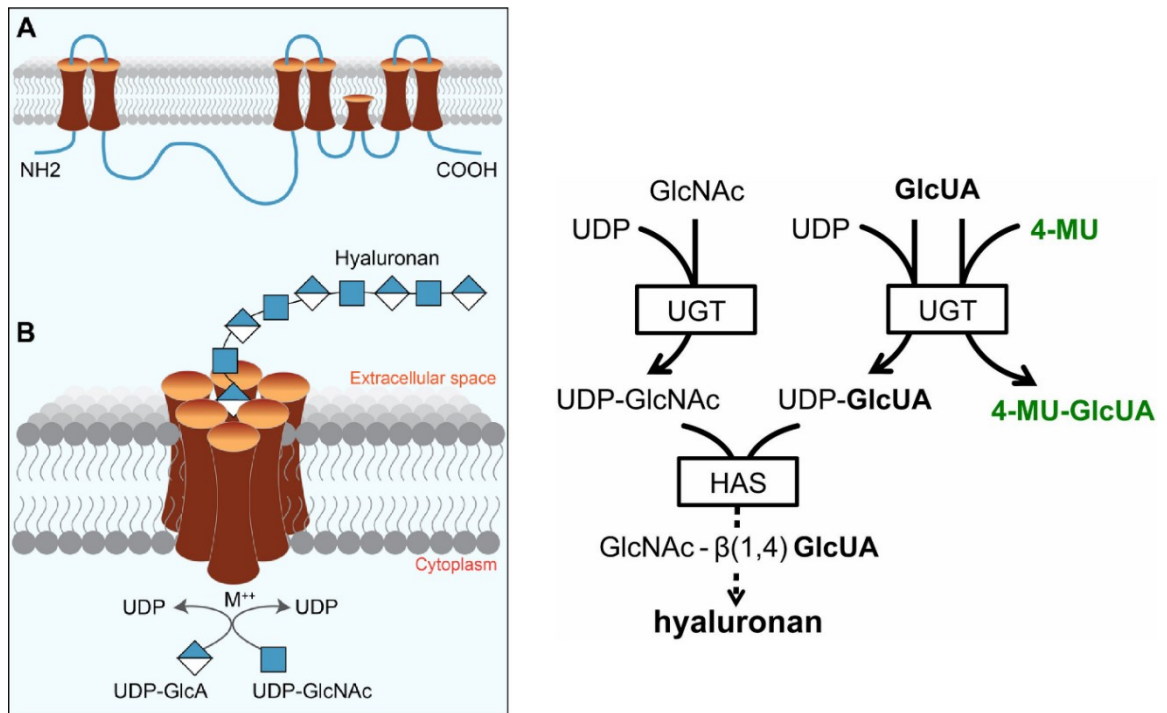
Figure 5. Synthesis of hyaluronan. a) HA is synthesized at the membrane by HAS and is extruded to the extracellular space as it is being synthesized. **b)** Mechanism of action of the HA synthesis inhibitor 4-MU. GlcUA is conjugated to 4-MU reducing the intracellular pool of GlcUAI, leading to synthesis inhibition. Adapted from Kuipers, 2016 (Kuipers et al., 2016) and Passi 2019 (Passi et al., 2019).

1.2.2 Hyaluronidases

One of the important components of HA turnover is HA degradation, which is carried out by a group of enzymes named hyaluronidases, which are hydrolases capable of cleaving β-1-4 glycosidic linkage in HA. There are six hyaluronidases (HYALs) in humans codified by genes clustered in groups of three in two different chromosome locations, *HYAL1, HYAL2* and *HYAL3* are located on chromosome 3p21.3 and *HYAL4*, *PH20 (also known as SPAM1)* and *HYALP1 (non-coding pseudogene)* located on chromosome 7q31.3 (Csoka, Scherer and Stern, 1999). Their activity is pH dependent, acidic HYAL1-4 are active at pH 3-4 and neutral PH20 is active at pH 5-8 (Stern et al., 2007). HYAL1, HYAL2 and PH20 are reported to have hyaluronidase activity, while HYAL3 has no hyaluronidase activity reported. HYLA4 has chondroitinase but not hyaluronidase activity and the HYALP1 pseudogene does not encode a functional enzyme (Csoka, Frost and Stern, 2001). HYAL1 and HYAL2 are the most important enzymes for HA turnover. HYAL1 is primarily located in lysosomes (Puissant et al., 2014) while HYAL2 is located at the cell membrane as a GPI-anchored protein (Andre et al., 2011; Rai et al., 2001). They appear to work together in a concerted action where HYAL2 degrades HA into 20 kDa fragments at the membrane, which are then sequestered by an HA receptor like CD44, followed by the formation of an endocytic vesicle which then fuses with lysosomes where further HA degradation occurs by HYAL1 that can degrade HA of any size (**Figure 6**) (Csoka, Frost and Stern, 2001; Harada and Takahashi, 2007; Tammi et al., 2001). PH20 has a more localized function as it is expressed mainly in the sperm where it aids in the fertilization process by degrading the cumulus ECM of the oocyte (Cherr, Yudin and Overstreet, 2001).

In addition to these hyaluronidases, two other proteins exhibit hyaluronidase-like activity. The KIAA1199/CEMIP (Cell Migration Inducing Hyaluronidase 1), found located intracellularly and on the plasma membrane, induced HA depolymerization generating 10-100 kDa fragments (Yoshida et al., 2013). However, this process was dependent on the cleavage of endo-β-N-acetylglucosamine bonds and occurred via the clathrin-coated pit pathway. The second protein discovered to have hyaluronidase activity is transmembrane protein 2 (TMEM2). This protein is located in the cell membrane and is reported to have calcium dependent hyaluronidase activity and degrades HA into 5 kDa fragments (Yamamoto et al., 2017). Information on these new enzymes with hyaluronidase activity is limited, therefore more studies are needed to assess their function in HA turnover.

1.2.3 Hyaluronan receptors

Hyaluronan can bind to different receptors on the cell surface triggering intracellular signalling that can affect several cellular processes such as cell proliferation, migration, angiogenesis, inflammation and cell survival (Stern, Asari and Sugahara, 2006). The most recognized receptors are cluster of differentiation 44 (CD44) and receptor for HA-mediated motility (RHAMM). These two receptors share a common hyaluronan binding motif (B(X7)B) that is essential for their ability to bind to HA (Yang et al., 1994).
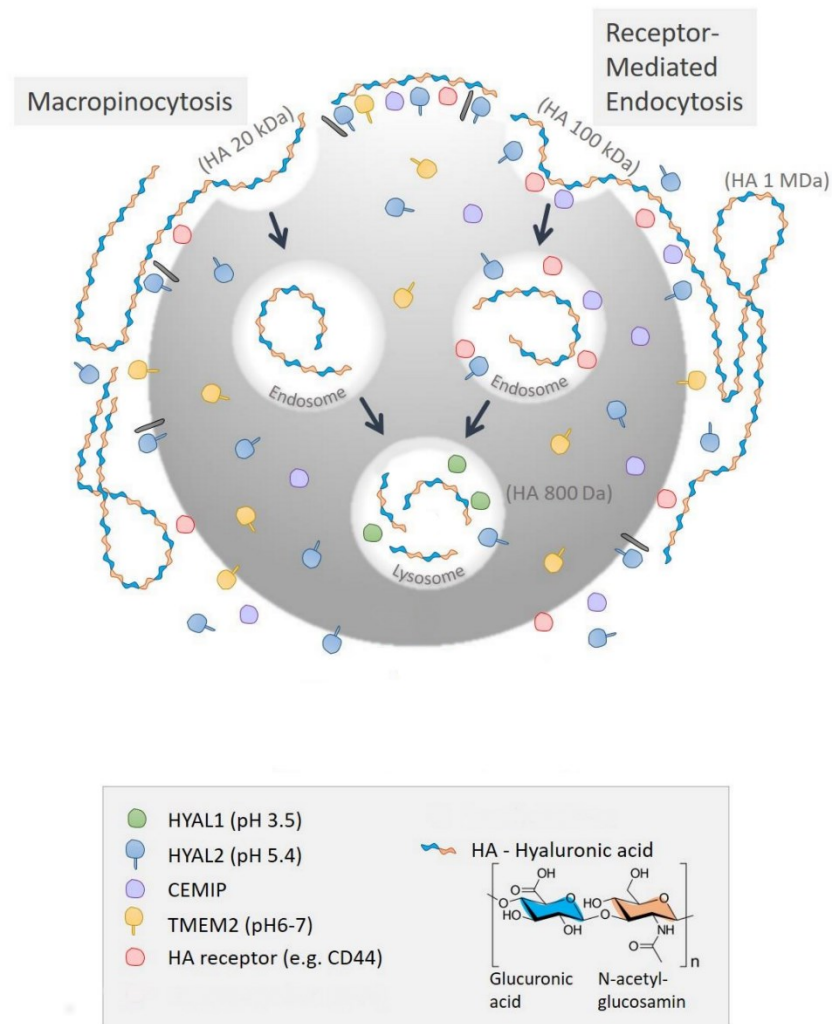
Figure 6. Representation of the proposed mechanism for HA turnover. HA can be internalized by macropinocytosis or receptor-mediated endocytosis. HA binds to HA receptors (CD44) and is initially degraded at the membrane by HYAL2, TMEM2 or CEMIP. Fragmented HA is then internalised by endocytosis and fused with lysosomes where further degradation occurs by HYAL1. Adapted from Zadnikova et al., 2022 (Zadnikova et al., 2022).

CD44: The receptor CD44 is a transmembrane glycoprotein comprised of an extracellular ligand binding domain, a juxtamembrane variable domain, a transmembrane domain and a cytoplasmic tail (Naor et al., 2002). It is encoded by a gene located on chromosome 11p13 (Iczkowski, 2010). The genetic sequence of CD44 has 19 exons, of which 10 remain constant and 9 exons can be variably expressed (Naor et al., 2002). The standard form of CD44 (CD44s) is formed by the 10 constant exons and the variant isoforms (CD44v) are formed by the 10 exons plus alternative splicing of 9 extra exons, affecting only the sequence of the variable juxtamembrane domain (**Figure 7a**). In addition, the variable extracellular domain has glycosylation sites for heparan sulfate and chondroitin sulfate that can alter the affinity of the ligand binding domain(Bennett et al., 1995). CD44s is the most common isoform that is found in most tissue, while CD44v is associated with expression in proliferating epithelial cells and activated T lymphocytes (Naor, Sionov and Ish-Shalom, 1997; Ponta, Sherman and Herrlich, 2003). CD44 does not only bind to HA but to several different ligands as well, other glycosaminoglycans, collagen, fibronectin, periostin among others (Chen et al., 2018). The cytoplasmic tail of CD44 does not have any active sites per se but has a binding motif that allows interaction with cytoplasmic proteins to transmit signals (Ponta, Sherman and Herrlich, 2003). Cytoskeletal proteins such as ankyrin can bind to the cytoplasmic tail of CD44 and regulate cell adhesion, proliferation and calcium signalling (Singleton and Bourguignon, 2004). CD44 can directly interact with the ezrin, radixin and moesin family of proteins (ERM) that are known for regulating cell shape and migration by linking the actin cytoskeleton to CD44 (Cywes and Wessels, 2001; Mori et al., 2008). Upon HA binding, CD44 undergoes conformational changes that can activate different signalling pathways inside the cells such as RhoGTPases, PI3K-Akt, MAPK-Ras-Erk1/2 (Bourguignon et al., 2003; Lv et al., 2016; Yang et al., 2020). The molecular weight of HA can also alter intracellular signalling when binding to CD44. For example, H-HA is associated with promoting cell quiescence by inducing cell cycle arrest in a CD44-HA dependent manner whereas low molecular weight (L-HA) stimulates growth by binding to CD44 inducing ERK activation (Kothapalli et al., 2008; Morrison et al., 2001). On the other hand L-HA induces a proinflammatory phenotype in macrophages while H-HA induces an M2 phenotype (Rayahin et al., 2015).

RHAMM: The receptor for HA-mediated motility, RHAMM (also known as CD168), is a protein with intracellular and extracellular functions (Hinneh et al., 2022). RHAMM is encoded by the *HMMR* gene located on chromosome 5q33.2 (Hardwick et al., 1992). The *HMMR* gene is formed by 18 exons and 2 start codons, which can produce several splice variants (**Figure 7b)** (Lin et al., 2021; Ogiya et al., 2019; Schutze et al., 2016). It is a helicoidal hydrophilic protein found intracellularly or in the cell membrane, however, it lacks a transmembrane domain or a signal peptide, instead, it is thought to be glycosylphosphatidylinositol-anchored (GPI-anchored) to the cell membrane where it can bind to HA (Entwistle, Hall and Turley, 1996). On the membrane, it can interact with CD44 to control cell motility, promote angiogenesis, and modify intracellular cell signalling (Maxwell, McCarthy and Turley, 2008; Misra et al., 2015; Park et al., 2012). Intracellularly RHAMM can bind to microtubules of the mitotic spindle providing structural stability and integrity supporting growth (Maxwell et al., 2003; Tolg et al., 2010). RHAMM can interact with other proteins on the membrane, for example it can form a

complex with CD44 that can promote motility in a Src/Raf-1/MEK-1/ERK1/2 dependent manner (Misra et al., 2015). Several other proteins can interact which include PDGF receptor, TGF-β1 receptor, and FGF-2 receptor (Tolg et al., 2014). RHAMM as CD44 can also bind HA of different molecular sizes generating different outputs, for example in a fibrosarcoma cell line L-HA increased adhesion by activation of ERK1/2-FAK pathway in a RHAMM dependent manner, which was inhibited when exposed to H-HA (Kouvidi et al., 2011).

There are additional HA receptors/binding proteins that are present on the cell membrane which are less studied and appear to be reduced to more specific tissues and functions. One of these receptors is hyaluronan receptor for endocytosis (HARE) also known as stabilin-2 (STAB2) (Zhou et al., 2000). HARE is mainly found in sinusoidal endothelial cells, lymph nodes, spleen and bone marrow (Qian et al., 2009). Its main function is the systemic clearance of HA in the liver and lymph nodes (Harris and Baker, 2020). HARE not only binds to HA but also to other GAGs derived from chondroitin sulphate and heparin (Harris and Baker, 2020).

1.2.4 Other HA receptors

The second receptor is the lymphatic vessel endothelial receptor-1 (LYVE-1), as inferred from its name, is the main HA receptor in lymphatic endothelial cells. LYVE-1 has a sequence similarity of 41% with CD44 (Banerji et al., 1999). The sequence with the highest homology between the two receptors is the HA binding domain. LYVE-1 is thought to participate in the clearance of HA in the lymphatic system, however, one of its more studied functions is its role in leucocyte trafficking in the lymphatic system (Jackson, 2019). The mechanism for leucocyte trafficking is based on the endogenous HA synthesis of a pericellular coating around leucocytes, to which LYVE-1 is recognized and binds, facilitating cell adhesion and transport of cells across the lymphatic endothelium (Johnson et al., 2017; Lawrance et al., 2016).
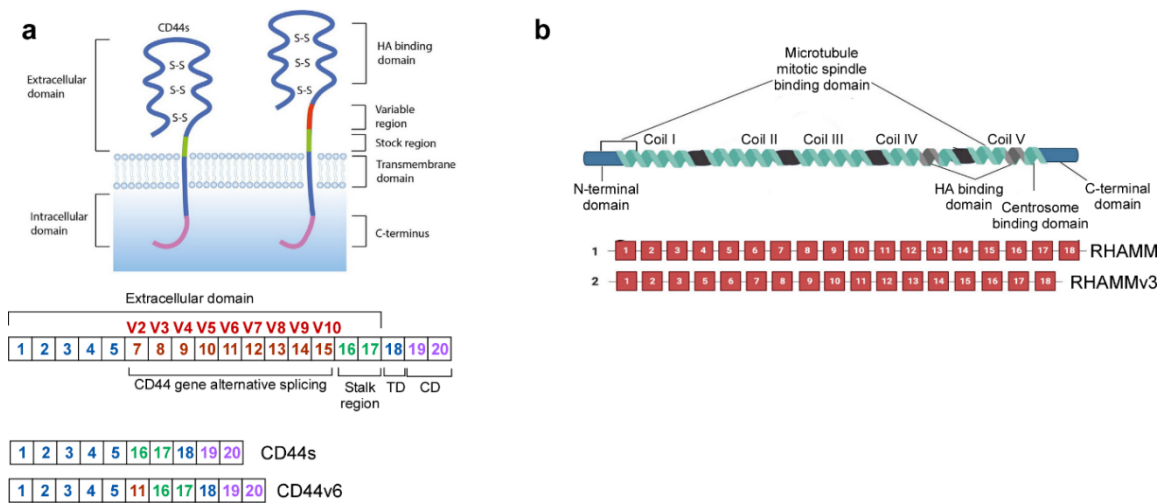
Figure 7. **Structure of hyaluronan receptor CD44 and RHAMM. a)** CD44 is a transmembrane protein with an intracellular C-terminal domain, a transmembrane domain, a variable region and the HA binding domain. The variable region can give rise to multiple variants, of which CD44v6 is commonly found in cancer associated with a malignant phenotype. **b)** RHAMM is a multi-coiled protein with an HA binding domain and a mitotic spindle binding domain. RHAMM can act extracellularly binding to HA or intracellularly stabilizing the mitotic spindle. Adapted from Hinneh et al., 2022 (Hinneh et al., 2022) and adapted from (Weng et al., 2022)

1.3 Hyaluronan in Cancer

HA deposits vary in different types of cancer and are found in the tumour stroma of 25-30% of all tumours (Jacobetz et al., 2013), but it is usually associated with poor prognosis and poor survival. This has been seen in head and neck cancers, where high HA content was related to poor survival (Hendawy et al., 2017). In breast cancer similar results were observed, while stromal staining intensity for HA increased, survival decreased and staining was associated with less differentiated cells (Auvinen et al., 2013; Wu et al., 2020). Analysis of cancers from the digestive system show a prominent HA staining of the surrounding tumour stroma and some HA positive cells invading the muscular wall (Wang et al., 1996). The same has also been reported in some lung carcinomas (Gong et al., 2022; Pirinen et al., 2001) ovarian cancer (Anttila et al., 2000) and prostate cancer (Aaltomaa et al., 2002) where stronger HA staining is an indicator of poor prognosis and higher local invasion of cancer cells. In all the above studies, there is also some degree of HA staining on cancer cells themselves, but the results are inconsistent with some higher-grade carcinoma cells having low staining and others having high staining. What remains most consistent is that stromal HA in cancer is much higher than in normal tissue (Tammi et al., 2008).

Serum HA levels in healthy patients are low but have been found to increase in diseases like cancer which is why it has been proposed as a biomarker for detecting high-risk groups for cancer (Aghcheli et al., 2012). This is the case for upper gastrointestinal tumours where HA blood levels were found to be increased in cancer patients compared to non-cancerous patients (Aghcheli et al., 2012). Similar studies in breast cancer patients have also found increased HA serum levels in cancer patients compared to non-cancerous patients, with even higher serum HA levels in patients with metastasis compared to non-metastatic (Delpech et al., 1990; Wu et al., 2020). L-HA specifically has been shown to increase in the serum of patients with nodal metastasis (Wu et al., 2015). In leukaemia patients, serum HA was increased, and patients in relapse showed higher HA serum levels than patients in remission (Anagnostopoulou et al., 2017). Higher serum levels of HA have also been reported in mesothelioma (Grigoriu et al., 2009; Hotta et al., 2004) oral cancer (Xing et al., 2008) and pancreatic cancer patients (Chen et al., 2020). HA has also been found at higher levels in the urine of patients with higher-grade bladder cancer compared to the urine of patients with low-grade bladder cancer or normal bladder and proposed as a prognostic marker (Lokeshwar et al., 1997; Morera et al., 2017).

In the TME of cancerous tissue, HA can serve multiple functions. TAMs seem to require higher HA deposits as it improves their distribution by serving as a binding structure. As shown in a study on mononuclear leukocytes, they can adhere to HA structures through the HA binding receptor CD44 (de la Motte et al., 2003). There is evidence that tumour derived HA can activate monocytes and polarize them to the M2 immunosuppressive pro-tumorigenic phenotype (Kuang et al., 2007) and that the amount of M2 macrophages in breast cancer tissue correlates with the amount of HA (Zhang et al., 2016). In both studies, the polarization of monocytes to the M2 phenotype was dependent on

the binding of CD44 with HA since blocking CD44-HA binding significantly decreased the population of M2 macrophages (Zhang et al., 2016).

1.3.1 HA receptors in cancer

The expression of different variants of CD44 have been associated with a wide array of functions in cancer cells. Depending on the type of cancer cell, it can affect migration, proliferation, chemoresistance, metastasis, and epithelial mesenchymal transition (EMT) among others (Chen et al., 2018). For example, in an *in vitro* coculture system myofibroblast derived HGF induces activation of the HGF receptor c-Met in prostate cancer cells, stimulating HA-CD44v9 signalling. The activation of CD4v9 results in increased proliferation, migration and HA synthesis and prostate cancer cell lines (Ghatak et al., 2010). It is important to note that a recent meta-analysis of CD44 expression as a prognostic factor in advanced cancer concluded that in patients submitted to chemotherapy or radiotherapy, the expression CD44v9 was specifically associated with poor 5-year cancer specific survival (Han et al., 2019). In lung cancer, CD44v expression is associated with poor overall survival (Nagashima et al., 2020). A study in gallbladder reported conflicting data regarding the role of CD44s and CD44v, CD44s was associated with increased invasiveness but decreased tumorigenicity, while CD44v9 had the opposite phenotype (Miwa et al., 2017). Despite these differences, both CD44s and CD44v9 were associated with poor survival. In lung tumours, CD44v5-6 and CD44v8-9 were significantly increased in tumours but not CD44s (Zhao et al., 2013). One issue that is important to point out in studies related to CD44s and CD44v is that the effect of HA whether it be endogenous or exogenous is not always studied along with the function of CD44, which could explain some discrepancies found in the literature.

Studies in colorectal cancer have shown that inhibition of RHAMM reduces cell migration by at least 50% in vitro whereas in vivo RHAMM knockdown slowed down tumour growth, reduced its size and inhibited metastasis (Mele et al., 2017). In tumour samples from patients with colorectal cancer RHAMM positive cells progressively increase from a primary tumour, nodal metastasis to liver metastasis (Mele et al., 2017). In human urothelial transitional cell cancer of the bladder RHAMM mRNA expression levels were increased in infiltrating tumours compared to non-invasive and higher RHAMM expression was associated with decreased survival in a completely independent manner from other prognostic markers (Niedworok et al., 2013). This was also seen by immunohistochemistry in tumour tissue samples where the percentage of RHAMM positive areas increased with the tumour stage and was higher in invasive tumour samples (Niedworok et al., 2013).

1.3.2 HAS and HYALs in cancer

The functional role of HASs and HYALs vary in different types of cancer. In breast cancer cell lines *in vitro* HAS2 was overexpressed as well as in invasive duct cancer (Li et al., 2015). The knockdown of HAS2 resulted in decreased proliferation and migration of breast cancer cells. Furthermore, when studied *in vivo*, the knockdown of HAS2 decreased the tumorigenicity of breast cancer cells (Li et al., 2015). Another study knocking down HAS2 found a decreased invasion of

breast cancer cells which was correlated to a decrease in FAK/PI3K/AKT signalling (Bernert, Porsch, & Heldin, 2011). In a model of rat colon carcinoma, cells with overexpressed HAS2 showed increased growth and higher tumour development when transplanted *in vivo* (Jacobson et al., 2002). On the contrary, overexpressing HYAL1 had the opposite effect, reducing tumour growth *in vitro* and *in vivo*. In prostate cancer cell lines *in vitro,* the overexpression or suppression of HYAL1 resulted in growth inhibition, therefore a tight control of expression is needed to sustain proliferation (Lokeshwar et al., 2005). In endometrial carcinoma despite finding HA accumulation surrounding the tumour, HASs were not overexpressed but HYALs were downregulated (Nykopp et al., 2010). HAS and HYAL expression in cancer cells still lack sufficient studies to understand its role, since it seems highly dependent on the type of cancer where it has been studied.

As previously established, the molecular weight of HA has different effects on cells (Stern, Asari and Sugahara, 2006). Experiments *in vitro* using different breast cancer cell lines showed that inhibiting HA degradation with dextran sulphate (DSS), a hyaluronidase inhibitor, decreased CD44 and HAS expression, with no changes in cell proliferation (Udabage et al., 2004). Further studies by the same group demonstrated that HAS2, HYAL2 and CD44 expression is associated with breast cancer cell lines with higher invasive potential (Udabage et al., 2005). Interestingly, they also established that in these cell lines, pericellular HA retention was associated with HAS2 and not HAS3. One key finding is that following HA synthesis and extracellular extrusion of 10000 kDa in size, HA was rapidly degraded by HYALs into low molecular weight fragments of 10, 20, 40 kDa up to 500 kDa (Udabage et al., 2005). Another study using breast cancer cell lines established that L-HA (>50 kDa) produced by HAS2, and likely degraded by HYAL1 and HYAL2, is important for cell migration and invasion (**Figure 8**). Blocking the degradation of HA with DSS decreases both migration and invasion (Wu et al., 2015). In a study using gastric cell lines, ultra-low HA (UL-HA) induced cells to adopt a "hummingbird" phenotype characterized by high cellular motility (Amorim et al., 2020). This process was mediated by the RHAMM and activation ERK1/2-AKT pathway. Given that HA in the cancer microenvironment can vary in size, it is an important factor to take into consideration since it can exert different effects on cancer cells and non-cancerous cells.

1.3.3 HA in the naked mole rat and resistance to cancer.

One intriguing study involves the naked mole rat which has a surprising resistance to generating cancer (Tian et al., 2013). In this study, the resistance is attributed to the fact that the fibroblasts of this rodent can synthesize HA of ultra-high molecular weight than what is usually found in humans, 6000-12000 kDa vs the 500-2000 kDa. Overexpression of HAS2 is responsible for synthesizing HA in the naked mole rat. Analysing the sequence for HAS2 there were two asparagines replaced by serines which might explain why the naked mole rat can synthesize HA of such a large size (Tian et al., 2013). Further experiments established that HA produced contact inhibition inducing cell cycle arrest, a process partially mediated by CD44. One interesting point was that treating isolated cells from the naked mole rate with hyaluronidase, abrogated contact inhibition (Tian et al., 2013). This was replicated by overexpression of HYAL2 *in vitro* and *in vivo.* This highlights the importance

	HOMEOSTASIS		DISEASE		
	vH-HA naked mole rat 12000-6000 kDa	**H-HA** 6000-1000 kDa	**M-HA** 1000-250 kDa	**L-HA** 250 – 10 kDa	**UL-HA** 10-0.01 kDa
Stromal / Mesenchymal	Facilitates cell contact inhibition	Increased cell migration Enhanced barrier function Reduced apoptosis	Reduced apoptosis Increased cell differentiation Enhanced ECM remodelling Increased Cytokine release		Inhibited synovial apoptosis Increased cytokine release
Endothelial	Unknown	Enhanced angiogenesis	Inhibited angiogenesis		Enhanced tube formation Increased EC proliferation Increased cytokine release
Immune / Inflammatory	Unknown	Inhibited cell recruitment Reduced cytokine release Enhanced immunosuppression	Increases apoptosis Altered macrophage polarization Pro and anti inflammatory Increased leukocyte mobilization		Monocyte / DC maturation Increased cytokine release Increased trans-migration
Cancer	Tumour resistant	Inhibited cell migration Inhibited tumour growth	Increased immune cell apoptosis Pro and anti proliferative Enhanced adhesion and migration Enhanced tumour immunity		Increased apoptosis Enhanced drug sensitivity Enhanced migration/invasion Increased tumour growth
Pathological Significance	Unknown Increased lifespan	Facilitates development Enhanced wound contraction Reduced scarring Inhibited vascular injury	Increased defence to pathogens in the gut Attenuated or exacerbated lung injury Pro and ant wound healing		Increased aortic remodelling Enhanced skin healing Inhibits vascular injury

Figure 8. The multiple actions of Hyaluronan of different molecular weights. HA can be classified by its molecular weight, with each molecular weight associated with different functions. Adapted from Monslow et al., 2015 (Monslow, Govindaraju and Pure, 2015).

of HYALs in cancer progression, as the balance of HA turnover in the TME might determine the tumorigenicity of HA.

A recent response to the initial study of HA in the naked mole rat (Tian et al., 2013) questioned the statement that cells from the naked mole rat were resistant to oncogenic transformation by SV40LT and HRAS[G12V] (Hadi et al., 2020). This study showed that the oncogenic transformation of naked mole rat cells was possible by lentiviral expression of SV40LT and HRAS[G12V]. These results could cast doubt on the role of ultra-high molecular weight HA in the induction of cancer resistance by contact inhibition. However, this study did not address the role of ultra-high molecular weight HA, CD44 signalling, HAS2 or HYAL2 in these transformed naked mole rat cells, therefore this remains to be elucidated. In addition, another study has shown physical differences between HA from the naked mole rat and mice (Kulaberoglu et al., 2019). The authors found that HA in the naked mole had a unique morphology with highly folded structures that were dependent on the type of tissue, indicating a much more complex role which is not yet understood.

1.4 Hyaluronan in Pancreatic Cancer

In pancreatic cancer, the stromal compartment compromises almost 90% of the total tumour volume, a mixture of large amounts of ECM proteins, glycosaminoglycans and a cellular component formed by CAFs, PSCs, vascular cells, TAMs and other immune cells all of which contribute in different ways to support tumour growth (Cutsem et al., 2018). HA accumulation is a key characteristic as it occurs in more than 80% of PDAC (Jacobetz et al., 2013). The PSCs are one the most important components of the stroma in pancreatic cancer, as their activity is essential in supporting tumour growth, progression and invasion. PSCs have been deemed responsible for the large amounts of HA present in the pancreatic cancer associated stroma (Apte et al., 2004) and elevated levels of HA can promote cancer progression (Li et al., 2018; Theocharis et al., 2000). Analysis of tissue samples from pancreatic cancer patients demonstrated that high staining for HA was correlated with poor survival. The level of desmoplasia observed in primary pancreatic tumours is also seen in pancreatic metastasis to the liver, lung and peritoneal cavity (Whatcott et al., 2015). These results were recently replicated in another group of PDAC tumours, where HA deposits were associated with poor overall survival (Tahkola et al., 2021). Additionally, this study also showed a low immune response with a low presence of T lymphocytes. The vast accumulation of hyaluronan can confer unique properties to PDAC tumours, such as abnormal collapsed blood and lymphatic vessels (Provenzano et al., 2012). This is produced by increased interstitial fluid pressure due to the high capacity of HA to retain water. This generates hypoxia and limits the access of molecules through the bloodstream which complicates therapeutic actions in pancreatic cancer and is one of the main reasons for the lower overall survival seen in most PDAC patients (Jacobetz et al., 2013). As mentioned previously, efforts to remove the excess deposits of HA with recombinant PEGPH20 hyaluronidase have failed in clinical trial settings as no improvement was seen by depleting HA from the tumours followed by chemotherapy (Van Cutsem et al., 2020).

There are a reduced number of studies on HA receptors in PDAC. One study analysing CD44 expression in PDAC tissue reported that CD44s and CD44v6 expression is higher in PDAC tissue, but only high CD44s expression is associated with poor overall survival (Li et al., 2014). Applying a CD44s blocking antibody (H4C4) in a PDAC xenograft model caused a reduction in growth, metastasis, and post radiation recurrence. In another study, CD44v6 and CD44v2 were also found to be increased in PDAC tumours compared to the normal pancreas, and the higher expression was associated with poor overall survival (Gotoda et al., 1998). The HA receptor RHAMM was found to be expressed in several PDAC cell lines. It had a higher expression in PDAC tumours compared to normal tissue and was associated with poor survival (Cheng et al., 2015).

There are far fewer studies investigating the role of HA on PDAC cells compared to the number of studies in other types of cancer, such as breast cancer. Among the few *in vitro* studies in pancreatic cancer cell lines, one study demonstrated that L-HA (25-75 kDa) increased cell migration in Boyden chamber assays, and in some cells lines, H-HA (400-600 kDa) also increased migration to a lesser extent (Cheng et al., 2016). Migration experiments inhibiting HA synthesis with 4-MU showed a decreased migration, as opposed to PMA (12-O-tetradecanoyl-phorbol-13-acetate) a stimulator of HA synthesis which showed increased migration. When PDAC cell lines were co-cultured with primary CAFs from pancreatic cancer tissue in a Boyden chamber, migration increased compared to monocultures. One interesting finding in this report is that mRNA for HAS2 was higher than HAS1 and HAS3 in most PDAC cells analysed. For hyaluronidases, HYAL1 mRNA was higher in most PDAC cells while HYLA2 mRNA was lower, it was fairly consistent among all cell lines (Cheng et al., 2016). However, this report has several observable issues in the migration assays and in the use of PMA, as it is known to be a tumour promotor on its own through the activation of PKC (Ron and Kazanietz, 1999; Taniuchi, Yokotani and Saibara, 2012). Inhibition of HA by using 4-MU a hyaluronan synthase inhibitor showed that proliferation, migration and invasion were reduced in MIA PaCa-2 pancreatic cancer cell line (Nagase et al., 2017). In a study of PDAC cells *in vitro* HA induced motility and migration through the Src-PI3K-Akt signalling pathway, since applying PI3k inhibitor wortmannin, reduced motility and migration were observed (Teranishi et al., 2009).

In xenografts models using BXPC-3 pancreatic cancer cell lines with forced overexpression of HAS2 and HAS3, there was an increase in HA content compared to non-overexpressing cells (Kultti et al., 2014). This was accompanied by a loss of E-cadherin, accumulation of cytoplasmic β-catenin and a decrease in apoptotic markers (Kultti et al., 2014). When these tumours were treated with the recombinant human hyaluronidase PEGPH20, there was a decrease in HA content which was accompanied by a reduction in tumour volume and hypoxic markers, a recovery of E-cadherin and membrane β-catenin, and an increase in apoptotic markers. This could indicate the possibility of HA promoting tumour growth, inducing EMT, generating hypoxia and favouring HIF-1α nuclear translocation and protection from apoptosis (Kultti et al., 2014).

HA plays an important part in PDAC, from promoting tumour growth, migration and metastasis to participating in the chemoresistance of PDAC as a component of the desmoplastic

reaction. However, the effects of HA in PDAC cells are limited and more information is needed to understand the characterises of HA turnover in PDAC and the effects that it can have on different cancer hallmarks.

Hypothesis

One of the most predominant characteristics of PDAC is extensive fibrosis of the tumour stroma called the desmoplastic reaction. Activated PSCs are responsible for the synthesis of excessive amounts of numerous macromolecules that are deposited into the tumour causing dense fibrosis that limits access of immune cells to the tumour and collapses blood vessels resulting in chemoresistance. Among these macromolecules is HA which can be found in more than 80% of PDAC tumour tissue and has been associated with poor survival. We hypothesized that HA can directly interact with HA receptors on PDAC cells *in vitro* and by doing so, it can regulate important cancer hallmarks such as proliferation and migration.

Aims

General aim

Analyse PDAC cell proliferation and migration *in vitro* under treatment with conditioned media containing HA produced by activated PSCs, with exogenous HA and endogenous HA produced by PDAC cells.

Specific aim 1

Establish an HA-producing PSC phenotype by activating PSC using cytokines TGF-β and PDGF to obtain conditioned media that will be applied to PDAC cells in proliferation and migration experiments. This includes standardizing the conditions of serum type and glucose concentration for optimal HA synthesis and moderate growth of PDAC cells.

Specific aim 2

Determine the effects of PSC-derived HA on PDAC cell growth and *migration*. This will be achieved using conditioned media from activated PSCs and by adding exogenous HA to the culture media. To understand the role of different components participating in HA turnover, a series of inhibitors will be used to block HA synthesis, HA degradation by hyaluronidases and HA receptors to block HA binding.

Specific aim 3

Determine the role of PDAC cell derived HA on PDAC cell proliferation and migration. This will be achieved by stripping the HA pericellular coating with hyaluronidase and inhibiting HA synthesis with the inhibitor 4-MU or by knocking down HAS with siRNA.

Chapter 2   Methodology

2.1 Cell culture

The PDAC cell lines MIA PaCa-2 and PANC1 cells were purchased from the American Type Culture Collection (ATCC). The BXPC3 cell line was a kind gift from Dr Ayse Latif (University of Manchester). MIA PaCa-2 and PANC1 cells were cultured in Dulbecco's modified Eagle's media (DMEM, Cat.#D5796, Cat.#D6064, Sigma) containing 25 mM glucose or 10 mM glucose, supplemented with 1% streptomycin/penicillin (Cat.#P0781, Sigma) and 10% foetal bovine serum (FBS, Cat.#F9665, Corning) or 10% NU-Serum (NU-S) (Cat.#355500, Corning). Human PSCs (hPSCs) were a kind gift from Professor David I. Yule from the University of Rochester. hPSCs were grown in DMEM supplemented with 1% streptomycin/penicillin and 25 or 10 mM with either 10% FBS or 10% NU-S, for a maximum of 9 or 10 passages. All cells were cultured in a humidified incubator at 37°C with 5% CO_2. Cells were subcultured between 80-90% confluence, washed with Dulbecco's phosphate buffer saline (DPBS, Cat.#D8537, Sigma), followed by a 5-10 min trypsinisation, depending on the cell type, with 0.25% Trypsin-EDTA (Cat.#T4174, Sigma). Then fresh media was added and cells in suspension were centrifuged at 900 RPM for 4 min at room temperature (U-32R centrifuge, BOECO Germany). The pellets were re-suspended in fresh media and transferred to T75 flasks. PDAC cells were used for a maximum of 30 passages.

2.2 hPSC activation standardization.

hPSCs were seeded onto 12 mm glass coverslips in 24 well plates at a density of $5x10^4$ cells per well and cultured in DMEM supplemented with 25 or 10 mM glucose with either 10% FBS or 10% NU-S. hPSCs were allowed to attach for 24 h and then the media was changed to serum free media with 0.1% Bovine Serum Albumin (BSA, Cat.#A9647, Sigma) (as a carrier protein) and activated with 1-10 ng/ml of TGF-β (Cat.#PHG9214, Gibco), 10 ng/ml of PDGF (Cat.#PHG9204, Gibco) or a combination of both according to each experiment. hPSCs were left in activation media for 24 h and then fixed in 4% paraformaldehyde (PFA, Cat.#P6148, Sigma) for immunofluorescence or left for a further 48 h and then fixed in 4% PFA according to each experiment.

2.3 Immunofluorescence

Cells were seeded onto 12 mm glass coverslips in 24 well plates at a density of $5x10^4$ cells per well. After the experimental treatment cells were fixed in 4% PFA prepared in HEPES buffer (15 mM HEPES, 135 mM NaCl, 5 mM KCl, 1.8 mM $CaCl_2$, 0.8 mM $MgCl_2$, pH 7.4) for 20-30 minutes at room temperature. Fixed cells were washed with HEPES buffer and permeabilized with Triton X-100 (Cat.#X100, Sigma) for 5 min. The cells were then washed in HEPES buffer and blocked in blocking buffer (5% BSA in HEPES buffer) for 30 minutes. The blocked cells were incubated with primary antibodies (Table 1) prepared in blocking buffer overnight at 4°. Then the cells were washed in HEPES buffer and incubated with secondary antibodies prepared in blocking buffer, for 1 h at room

temperature. The cells were washed and incubated for 7 min in Hoechst 33342 at 300 ng/ml (Cat.#3570, Invitrogen), then cells were washed again and mounted onto glass slides using ProLongTM Gold antifade (Cat.#P36934, Thermo Fisher Scientific).

Immunofluorescence for HYAL2 followed the same protocol except for the permeabilization step which was done with saponin (#47036, Sigma) 0.1% in HEPES buffer, which selectively permeabilizes cholesterol-enriched plasma membrane zones.

2.3.1 Hyaluronan detection by fluorescence

Cells were seeded onto 12 mm glass coverslips in 24 well plates at a density of 5×10^4 cells per well. After the experimental treatment cells were fixed in 4% PFA prepared in HEPES. Fixed cells were washed with HEPES buffer and permeabilized with Triton X-100 for 5 min. The cells were then washed in HEPES buffer and blocked with an avidin-biotin block (Cat.#R37628, Thermo Scientific) for 10 min. The cells were washed in HEPES buffer and blocked in 5% BSA in HEPES buffer for 30 min. Then we used a biotinylated HA binding protein (HABP, Cat.# AMS.HKD-BC41, AMSBIO) a recombinant protein corresponding to the versican G1 HA binding domain that exclusively binds HA and no other GAG. The HABP was incubated overnight at 4°C. The cells were washed in HEPES buffer and incubated for 1 h with FITC-conjugated streptavidin (Cat.#SA-5001, Vector Labs) that binds to the biotin on the HABP. The cells were then washed and incubated for 7 min in Hoechst and then washed and mounted onto glass slides using ProLongTM Gold antifade.

Target	Host	Clonality	Isotype	Dilution	Supplier	Reference
Primary antibodies						
α-SMA	Rabbit	Monoclonal	IgG	1/200	Cell Signalling	19245
CD44	Mouse	Monoclonal	IgG	1/200	Cell Signalling	E7K2Y
RHAMM	Rabbit	Polyclonal	IgG	1/200	Cell Signalling	55463
HYAL2	Rabbit	Polyclonal	IgG	1/200	Proteintech	51148-1-AP
HAS2 [4E7]	Mouse	Monoclonal	IgG	1/200	Abcam	Ab140671
Secondary antibodies						
Anti-mouse Alexa Fluor 488	Goat	Polyclonal	IgG	1/400	Thermo Scientific	A11029
Anti-rabbit Alex Fluor 488	Goat		F(ab')2	1/400	Cell Signalling	4412S
Anti-mouse Alexa Fluor 594	Goat		F(ab')2	1/400	Cell Signalling	8890S

Table 1 Primary and secondary antibodies used for Immunofluorescence.

2.3.2 Immunofluorescence image analysis of hPSC activation

Two strategies to quantify hPSC activation were adopted, the first strategy was to count the total number of α-SMA+ cells as a percentage of total Hoechst stained cells. This strategy was used when hPSCs were at relatively low density, as cell boundaries were easily visible.

The second strategy was to measure the total α-SMA+ fluorescent area which was then normalized by the total number of cells, which were counted by counting the nuclei stained with Hoechst. This second strategy was used when cells were highly confluent and cell boundaries were much more difficult to distinguish, which made accurate counting of individual α-SMA+ cells almost impossible.

2.3.3 Immunofluorescence image analysis of PDAC cells treated with HAdase and 4-MU

In MIA PaCa-2 cells, to evaluate HA fluorescence after treatments with either HAdase or 4-MU, a line profile of fluorescent intensity was traced using FIJI/ImageJ. This intensity profile will show a high peak of fluorescence intensity indicating pericellular HA. If treatments with HAdase or 4-MU reduce pericellular HA this will be reflected by the loss of the intensity peaks.

For BXPC3 cells a qualitative analysis was done by plotting fluorescence intensity as a 3D surface plot. The fluorescent pixel intensity is represented in a colour temperature scale, with low intensity peaks in colour blue to high intensity peaks in red colour.

2.3.4 Immunofluorescence Imaging

Images were collected on a [Zeiss Axioimager.D2] upright microscope using a 20x / 0.5 EC Plan-neofluar, or the 63x / 1.4 Plan Apochromat (Oil, DIC) objectives and captured using a Coolsnap HQ2 camera (Photometrics) through Micromanager software v1.4.23. Specific band pass filter sets for DAPI and FITC were used to prevent bleed through from one channel to the next. Images were then processed and analysed using [Fiji ImageJ (http://imagej.net/Fiji/Downloads)].

2.4 Cell treatments

2.4.1 Conditioned media collection from PDAC cells

MIA PaCa-2, PANC1 and BXPC3 cells were seeded at a density of 40000 cells/cm^2 and grown in T75 culture flasks in 10 ml of the appropriate media. They were grown to 70-80 % confluency and then the media was changed to serum free media. Cells were incubated for 24, 48 or 72 h according to experimental conditions. The conditioned media (CM) was collected and centrifuged at 500 RPM to eliminate cell debris. Cells left on the flask were trypsinised and an aliquot was taken for cell counting, the rest of the cells were saved to prepare protein lysates for protein quantification.

2.4.2 Activated and non-Activated PSC conditioned media collection.

hPSCs were 40,000 cells/cm^2 and grown in T75 culture flasks in 10 ml of DMEM supplemented with 25 or 10 mM glucose with either 10% FBS or 10% NU-S. Cells were grown to 80% confluency and then the media was replaced with serum free media supplemented with 0.1% BSA containing 5 ng/ml of TGF-β. For the non-activated media on serum free DMEM with 0.1%, BSA was added to the media. hPSCs were activated for 24 h and then the media was replaced with fresh serum free DMEM. hPSCs were left for a further 24, 48 or 72 h according to each experiment. The CM was collected and centrifuged at 500 RPM to eliminate cell debris. Cells left on the flask were trypsinised and an aliquot was taken for cell counting, the rest of the cells were saved to prepare protein lysates for protein quantification.

2.4.3 Filtered activated and non-activated PSC conditioned media.

For filtered hPSC CM the same process was followed as mentioned above. After the centrifuge step eliminating cell debris, the 10 ml of CM was loaded on 15 ml 3kDa Amicon filters (Amicon® Ultra-15 Centrifugal Filter Unit, Cat.#UFC9003, Millipore) and centrifuged at 3850 g for 60 min. The media that was retained in the upper chamber of the filter was retained and the filtrate was discarded. The concentrated media was then diluted in 10 ml of fresh DMEM with 10% FBS or NU-S and either 10 or 25 mM glucose.

2.5 Hyaluronan Enzyme-Linked Immunosorbent Assay

HA in PDAC conditioned media was detected using the Hyaluronan Enzyme-Linked Immunosorbent Assay Kit (K-1200, Echelon Biosciences Inc). This is a competitive ELISA, where the signal detected is inversely proportional to the amount of HA present in the sample. A standard curve was included to determine the concentration of HA. Briefly, samples and the standard curve (K-1202) were loaded on yellow U-bottom plates and incubated with the HA detector (K-1203) for 1 h at 37°C. Then, controls and samples were moved to a detection plate and incubated for 30 min at 4°C. The detection plates were washed with wash buffer (K-PBST3) 3 times and then the plates were inverted and tapped dry on absorbent tissue. Later, a working Enzyme (K-1206) was added to the wells, and the plate was incubated for 30 min at 37°C. Plates were washed as described before and then incubated in the dark at room temperature with Substrate solution (K-1208). 30 minutes later, absorbance was measured at 405 nm using a plate reader (Synergy HT, BioTEK). The reaction was stopped by adding Stop solution to the plate. Quantification of the samples was done by interpolation from the standard curve.

2.6 Hyaluronan

HA of four different molecular weights (R&D Systems®, Inc.) were used for proliferation and migration assays. Ultra low molecular weight HA (UL-HA, 4.66 kDa, Cat.#GLR003), low molecular weight HA (L-HA, 33 kDa, Cat.#GLR001), medium molecular weight HA (M-HA, 205 kDa, Cat.#GLR004) and

high molecular weight HA (H-HA, 1500 kDa, Cat.#GLR002). Each HA was dissolved in PBS at a concentration of 5 mg/ml, aliquoted and stored at -20°C.

2.7 Cell counting kit-8 viability assay (WST-8)

Cell proliferation was measured with Cell Counting Kit-8 (CK04, Dojindo Molecular Technologies) an assay that uses WST-8 [2-(2-methoxy-4-nitrophenyl)-3-(4-nitrophenyl)-5-(2,4-disulfophenyl)-2H-tetrazolium, monosodium salt] a water soluble tetrazolium salt to quantify the number of live cells that reduce WST-8 producing an orange formazan dye (WST-8 formazan) in the presence of an electron donor. The WST-8 solution was added to each well and the plate was incubated for 2 h in a humidified incubator at 37°C. Absorbance was measured at 450 nm using a plate reader (Synergy HT, BioTEK).

2.7.1 Proliferation assays with the cell counting kit-8

PDAC cells were seeded onto a 96 wells plate at a density of 2500 or 5000 cells according to the experimental conditions. Cells were allowed to attach for 24 h, then the media was replaced according to each treatment. The cells were left to grow for up to 96 h. Every 24 h a plate was processed by adding 10 μl of WST-8 solution to each well. The plate was incubated for 2 h in a humidified incubator. After 2 h, absorbance was measured at 450 nm using a plate reader (Synergy HT, BioTEK).

2.7.2 WST-8 proliferation assay for standardization of serum and glucose concentration

For proliferation assays standardizing serum and glucose concentration, 2500 or 5000 cells were seeded in 96 well plates. Cells were allowed to attach for 24 h, then the media was replaced with DMEM supplemented with 0, 1, and 10% NU-S with 5, 8, 10, 15, and 25 mM glucose. Proliferation was measured every 24 h by the WST-8 assay.

2.7.3 WST-8 proliferation assay with hPSC conditioned media

For proliferation assays using hPSC CM 2500 cells were seeded onto 96 well plates. After 24 h the media was changed to either activated or non-activated hPSC CM with 10% NU-S and 10 mM glucose or to filtered activated or non-activated hPSC CM with 10% NU-S and 10 mM glucose. Proliferation was measured every 24 h by the WST-8 assay.

2.7.4 WST-8 proliferation with hyaluronan

For proliferation assays using HA of different molecular weights, cells were seeded onto 96 well plates. After 24 h the media was changed to DMEM with 10% NU-S and 10 mM glucose supplemented with either UL-HA, L-HA, M-HA or H-HA at concentrations of 30, 100, and 300 μg/ml. Proliferation was measured every 24 h by the WST-8 assay.

2.7.5 WST-8 proliferation with HAdase treatment and 4-MU

For proliferation assays using 4-Methylumbelliferone (4-MU, Cat.#M1381, SIGMA) and hyaluronidase from bovine testes type I-S (HAdase, Cat.#H3506, Sigma) cells were seeded onto 96 well plates. After 24 h the media was changed to serum free media with 0.1% BSA and incubated with 800 µg/ml or media 10% NU-S and 10 mM glucose accordingly. Cells were then washed in DPBS and fresh media with 10% NU-S and 10 mM glucose supplemented with 1-100 µM 4-MU and 300 µg/ml of UL-HA, L-HA, M-HA, or H-HA accordingly. Proliferation was measured every 24 h by the WST-8 assay.

2.7.6 Cytotoxicity assay for dextran sulphate using the cell counting kit-8

PDAC cells were seeded at 5×10^4 cells per well and allowed to attach for 24 h. The media was then replaced with media containing 0.1-1000 µg/ml of DSS (Dextran sulfate Cat.#D8906, Sigma) and the cells were left to incubate for 48 h. The WST-8 solution was added to each well and the plate was incubated for 2 h in a humidified incubator at 37°C. Absorbance was measured at 450 nm using a plate reader (Synergy HT, BioTEK).

2.8 Sulforhodamine B protein (SRB) assay protein quantification method

The SRB assay is used to determine cell density based on the measurement of protein components of cells adhered to a cell culture surface. This is possible due to the ability of SRB to bind cellular protein content that has been fixed by TCA (Trichloroacetic acid, Cat.#T6399, Sigma). The binding of SRB to proteins is stoichiometric, which means that the amount of dye is proportional to the amount of protein present and is therefore proportional to cell mass.

Briefly, cells were seeded on a 96 well plate, and after 24-96 h days, cells were fixed by adding 10% w/w TCA and incubating them for 1 h at 4°C. Fixed cells were washed and dried at room temperature. Then cells were stained with 0.057% w/v SRB solution for 30 min. Cells are then quickly rinsed with 1% v/v acetic acid to remove unbound dye. The cells were left to dry at room temperature. Later 10 mM Tris base solution was added and the plate was incubated on a shaker for 5 min to solubilize the protein bound to the dye. Absorbance was measured at 540 nm using a plate reader (Synergy HT, BioTEK) to quantify the protein content.

2.8.1 SRB proliferation assay for standardization of serum and glucose concentration

For proliferation assays standardizing serum and glucose concentration, 2500 or 5000 cells were seeded in 96 well plates. Cells were allowed to attach for 24 h, then the media was replaced with DMEM supplemented with 0, 1, and 10% NU-S with 5, 8, 10, 15, and 25 mM glucose. Proliferation was measured every 24 h by the SRB assay.

2.8.2 SRB proliferation assay with hPSC conditioned media

For proliferation assays using hPSC CM 2500 cells were seeded onto 96 well plates. After 24 h the media was changed to either activated or non-activated hPSC CM with 10% NU-S and 10 mM glucose or to filtered activated or non-activated hPSC CM with 10% NU-S and 10 mM glucose. Proliferation was measured every 24 h by the SRB assay.

2.8.3 SRB proliferation with hyaluronan

For proliferation assays using HA of different molecular weights, cells were seeded onto 96 well plates. After 24 h the media was changed to DMEM with 10% NU-S and 10 mM glucose supplemented with either UL-HA, L-HA, M-HA, or H-HA at concentrations of 30, 100, and 300 µg/ml. For proliferation analysis in HA coated plates, the day before seeding cells, 96 well plates were incubated with UL-HA, L-HA, M-HA, or H-HA at concentrations of 300 µg/ml in DPBS for 24 h at 4°C. Proliferation was measured every 24 h by the SRB assay.

2.8.4 SRB proliferation with HAdase treatment and 4-MU

For proliferation assays using 4-MU and HAdase, cells were seeded onto 96 well plates. After 24 h the media was changed to serum free media with 0.1% BSA supplemented with or without 800 µg/ml of HAdase. Cells were treated for 1 h at 37°C. Cells were then washed in DPBS and incubated in fresh media with (10% NU-S and 10 mM glucose) with or without 1-100 µM 4-MU and 300 µg/ml of UL-HA, L-HA, M-HA, or H-HA according to experimental conditions. Proliferation was measured every 24 h by the SRB assay.

2.9 Gap closure assays

2.9.1 Gap closure assays for migration

The gap closure assay performed in these experiments uses 2-chamber silicone Ibidi inserts (Cat.#80209, Ibidi) which are based on the principle of area exclusion by generating a cell free space through physical exclusion, in this case, the silicone divider of the Ibidi inserts. PDAC cells were seeded into each side of the chamber at 40000-50000 cells per side of the insert in 12 or 24-well culture plates. For the assay to work properly, a high confluence must be achieved >95%. The cells were allowed to attach for 24 h, after which fresh media was added supplemented with 2 µg/ml of mitomycin C previously standardized(Sritangos et al., 2020) (Cat.#3258, Tocris). Mitomycin C is used as a proliferation inhibitor at non-lethal concentrations to ensure the cell free area is occupied by migrating cells. The cell free gaps were imaged at 0, 24, 36, and 48 h for MIA PaCa-2 cells. Brightfield images were acquired using an Olympus IX83 inverted microscope using a 4x / 0.13 LUC PlanFL N objective and captured using an Orca ER camera (Hamamatsu) using CellSens software (Olympus). BXPC3 cells were imaged every 15 min for up to 22 h. Brightfield images were acquired on an Eclipse Ti inverted microscope (Nikon) using a 4x Plan Fluor (PhLDL) objective. Imaging software NIS

Elements AR.46.00.0. Point visiting was used to allow multiple positions to be imaged within the same time course and cells were maintained at 37°C and 5% CO2. The images were collected using a Retiga R6 (Q-Imaging). Images were analysed and processed using FIJI ImageJ. The percentage of gap closure was calculated according to the following formula:

$$Gap\ closure\ \% = \left(\frac{A_{t=0} - A_{t=\Delta}}{A_{t=0}}\right) \times 100,$$

Where ($A_{t=0}$) is the area of the gap at time 0 and ($A_{t=\Delta}$) is the area of the gap at any given time point. The migration rate in µm/h was calculated using the Wound_healing_size_tool (Suarez-Arnedo et al., 2020) and the following formula

$$R_M = \frac{W_i - W_f}{t}$$

where W_i is the average of the initial gap width, W_f is the average of the final gap width, both in µm, and t is a time point of the assay in h. For MIA PaCa-2 and PANC1 cells, t was 24 h and for BXPC3 cells t was the time at which 50% of the gap was closed.

2.9.2 Gap closure assay with hPSC conditioned media

For gap closure assays using hPSC CM cells were seeded into Ibidi inserts at 4000-50000 per side of the insert. The cells were allowed to attach for 24 h the media. The media was then replaced with filtered or non-filtered hPSC CM, from activated or non-activated cells supplemented with 2 µg/ml of mitomycin C. Images of the gap were captured according to the main protocol.

2.9.3 Gap closure assay with exogenous Hyaluronan

For gap closure assays using HA, cells were seeded into Ibidi inserts at 4000-50000 per side of the insert. The cells were allowed to attach for 24 h the media. The media was then replaced with fresh media (10% NU-S and 10 mM glucose) with 2 µg/ml of mitomycin C supplemented with 300 µg/ml of UL-HA, L-HA, M-HA, or H-HA. For gap closure assay involving coated HA, the day before seeding cells 24 well plates were incubated with UL-HA, L-HA, M-HA, or H-HA at concentrations of 300 µg/ml in DPBS for 24 h at 4°C. The inserts were then placed inside the HA coated wells followed by cell seeding. Images of the gap were captured according to the main protocol.

2.9.4 Gap closure assay with Hyaluronidase treatment and 4-MU

For gap closure assays using 4-MU and HAdase, cells were seeded into Ibidi inserts at 4000-50000 per side of the insert. The cells were allowed to attach for 24 h the media. For experiments including 4-MU alone, fresh media was added (10% NU-S and 10 mM glucose) with 2 µg/ml of mitomycin C supplemented with 1-100 µM 4-MU. For experiments including HAdase, the media was changed to serum free media with 0.1% BSA supplemented with 200, 400 or 800 µg/ml and treated for 1 h at 37°C, according to each experiment. Cells were then washed in DPBS and fresh media was added

(10% NU-S and 10 mM glucose) with 2 µg/ml of mitomycin C supplemented with 100 µM 4-MU and 300 µg/ml of UL-HA, L-HA, M-HA, or H-HA according to each experiment. Images of the gap were captured according to the main protocol.

2.9.5 Gap closure with HAS2 siRNA

For gap closures assays using HAS2 siRNA, 50000 BXPC3 cells were seeded into each side of the Ibidi inserts that were preloaded with a mix of 25 nM of HAS2 siRNA and TurboFect Transfection Reagent (Cat.#R0531, Thermo Scientific). After 36 h the inserts were removed, and fresh media was added (RPMI with 10% NU-S and 10 mM glucose) with 2 µg/ml of mitomycin C. For experiments including HAdase, the media was changed to serum free media with 0.1% BSA supplemented with 800 µg/ml of HAdase and treated for 1 h at 37°C. Cells were then washed in DPBS and fresh media was added (10% NU-S and 10 mM glucose) with 2 µg/ml of mitomycin C. Depending on experimental conditions the media was also supplemented with 300 µg/ml of H-HA. Images of the gap were captured according to the main protocol.

2.10 CD44 Neutralising antibody

Anti-CD44 antibody KM81 (Cat.#ab112178, Abcam) was used to target the HA binding domain of CD44. The antibody was applied to PDAC cells in migration assays (as described before) at concentrations of 1, 5 and 10 µg/ml.

2.11 Protein preparation and detection

2.11.1 Protein lysate preparation

Cells were harvested using Lysis buffer containing 50 mM Tris Base, 40 mM sodium pyrophosphate, 100 mM sodium fluoride, 150 mM sodium chloride, 0.5 M EDTA and 0.5 M EGTA, supplemented with protease and phosphatase inhibitors: cOmplete EDTA-free protease inhibitor cocktail (Cat.#11873580001, Sigma) and PhosSTOPT phosphatase Inhibitor (Cat.#4906837001, Sigma). Cell lysates were sonicated (Soniprep 150 Ultrasonic disintegrator, MSE) on ice at amplitude 7-8 and 6 seconds intervals 5 times. Then samples were incubated on ice for 30 minutes, and later centrifuged at 13000 rpm (PRISMR centrifuge, Lab International Inc.) at 4°C, for 10 minutes. Lysate supernatant was collected and stored at -20°C until further use.

2.11.2 Membrane protein extraction

Membrane proteins were extracted and enriched from adherent cell culture using the Mem-PER plus kit (Thermo scientific, 89842) following manufacturer instructions. This is a detergents-based kit that permeabilises cells allowing the release of soluble cytosolic proteins and solubilises the membrane proteins. Briefly, cells were scraped and resuspended in cell culture media and centrifuged at 300 g for 5 min. The cell pellet was washed with the cell washing solution and centrifuged at 300 g for 5 min

twice. The cell pellet was resuspended with Permeabilization buffer and vortexed to obtain a homogeneous cell suspension. Cells were incubated at 4°C for 10 min with frequent mixing. Permeabilized cells were centrifuged at 16000 g for 15 min. The supernatant containing cytosolic proteins was transferred to a new tube. A solubilization buffer was added to the pellet, and it was resuspended by pipetting. The mixture was incubated at 4°C for 30 min with constant mixing. Later, it was centrifuged at 16000 g for 5 min and the supernatant containing membrane proteins was transferred to a new tube. Cytosolic and membrane samples were stored at -20°C until further use.

2.11.3 SDS-PAGE and Western blot

Cell lysates were prepared in NuPAGE LDS Loading buffer (Invitrogen, NP0007) and denatured for 5 - 20 min at 95°C. Denatured samples were loaded onto a NuPAGE 4 to 12%, Bis-Tris Protein Gel (Cat.#NP0321, Cat.#NP0336, Invitrogen) with a protein ladder (Precision Plus Protein Dual Color Standards Cat.#1610374 Bio-Rad). Gels were run in a mini gel tank (Cat.#A25977, ThermoFisher Scientific) between 100-200 V with an electrophoresis power supply (E831 electrophoresis power supply, Consort) for 45-90 min in NuPAGE MOPS SDS running buffer (Cat.#NP0001, Invitrogen).

For immunoblotting, the proteins were transferred with Transblot Turbo transfer buffer to PVDF membranes (Trans-Blot Turbo RTA Mini 0.2 µm PVDF Transfer Kit. Cat.# 1704272, Bio-Rad) using the TransBlot® Turbo and transfer system (1.3 Amps constant, up to 25 V, 15 minutes; Bio-Rad). The membranes were washed with Tris-buffer saline with 0.1% Tween 20 (TBST) and then blocked for 1 h in 5% BSA TBST. Later, membranes were incubated overnight with primary antibodies (Table 2) in orbital agitation. On the following day, membranes were washed 3 times for 10 min with TBS-Tween. Membranes were incubated with secondary antibodies conjugated to HRP diluted in 5% BSA TBST (Table 2) for 1 h at room temperature in orbital agitation. Membranes were washed in TBST and incubated for 3 min in Clarity Western ECL substrate (Cat.# 170-5060, Bio-Rad). Images were acquired using a ChemiDoc XRS+ (Bio-Rad). Analysis and editing of the images were done on Image Lab Standard Edition v6.0.1 software (Bio-Rad).

Target	Host	Clonality	Isotype	Dilution	Supplier	Reference
Primary Antibodies						
B-actin	Mouse	Monoclonal	IgG	1/50000	Sigma	A3854
Cyclophilin A	Rabbit	Polyclonal	IgG	1/1000	Cell Signalling	2175S
Cyclophilin B	Rabbit	Monoclonal	IgG	1/1000	Cell Signalling	43603S
HAS2	Mouse	Monoclonal	IgG	1/2000	Abcam	ab140671
HYAL2	Rabbit	Polyclonal	IgG	1/2000	Proteintech	51148-1AP
Secondary Antibodies						
Rabbit IgG HRP	Goat	Purified		1/1000 1/8000	Cell Signalling	7074S
Mouse IgG-HRP	Goat	Purified		1/8000	Cell Signalling	7076S

Table 2 Primary and secondary antibodies used for Immunoblotting.

2.12 Expression knockdown by siRNA

The expression of HAS2 and HYAL2 was knocked down using 10-50 nM of ON-TARGETplus SMARTpool siRNA targeting HAS2 mRNA (siHAS2; L-0112053-02-0010) or HYAL2 mRNA (siHYAL2; L-013689-01-0010). Non-targeting scrambled siRNA (siSCR; D-001810-10-05) was used as a control. Knockdown conditions were performed using serval transfection reagents 0.1-0.2% DharmaFect1 (D1), D DharmaFect2 (D2), Dharmafect4 (D4) (Dharmacon), Turbofect, (Cat.# R0531, ThermoFisher), JetPEI (Cat.# 101-10N, Polyplus-Transfection) and Fugene (Cat.#Promega). All target sequences for ON-TARGETplus SMARTpool siRNA used in knockdown experiments are listed below in Table 3.

Target gene	ON-TARGETplus Reference	Target Sequence
HAS2	L-0112053-02-0010	GGGUGUGUUCAGUGCAUUA
		GGAUUAAAGUUGUCAUGGU
		CCAAACGGAUAAUUACUAU
		GGUUUGUGAUUCAGACACU
HYAL2	L-013689-01-0010	AGAUGUGUAUCGCCGGUUA
		UGCUGGAGACACUGCGUUA
		GCUCAGUUGGGCCGACAUU
		UAGUCAAACAGGCACAAUA
Non-Targeting scrambled	D-001810-10-05	UGGUUUACAUGUCGACUAA
		UGGUUUACAUGUUGUGUGA
		UGGUUUACAUGUUUUCUGA
		UGGUUUACAUGUUUUCCUA

Table 3 Dharmacon gene targeting sequences of ON-TARGETplus SMARTpool siRNA.

2.13 Statistical Analysis

Prism 9 software (GraphPad) was used for generating graphs and statistical analysis. Error bars are presented as mean ± SEM (error bars). Data Normality was checked by Shapiro-Wilk test. Statistical significance for comparing two groups was determined by unpaired t-test with parametric distribution and Mann-Whitney for non-parametric distribution. Two-way ANOVA with Tukey's post hoc test for multiple comparisons was used when comparing 2 or more factors in 3 or more groups. One-way ANOVA with Dunnett's post hoc test was used to compare every mean against a control mean. Statistical significance was defined as $p < 0.05$.

Chapter 3   Optimization of pancreatic stellate cell activation and collection of stellate cell conditioned media

3.1 Activation of human pancreatic stellate cells.

In pancreatic cancer tissue, human PSCs (hPSCs) are present in an activated state. These activated hPSCs have been linked to pancreatic tumour progression, by secreting several extracellular matrix proteins and Hyaluronan among others (Li et al., 2018). By activating hPSC cells in culture we attempted to reproduce the interaction they have with PDAC cells *in vivo* by collecting the media in which they grow (conditioned media), to capture the molecules secreted by hPSCs. We aimed to use this hPSC conditioned media (CM) on PDAC cells to study the *in vitro* effects of hPSC-derived HA on the two main cancer hallmarks proliferation, and migration. To accomplish this, we first standardized hPSC activation to obtain the optimal conditions for HA production, controlling for serum type, glucose concentration and activating cytokines using a-SMA as a readout of hPSC activation (Apte et al., 2004). We then measured HA production in these activated stellate cells with an ELISA-like assay that detects HA.

Under *in vitro* conditions, hPSCs have been reported to be contact activated when grown on plastic or glass. The most common marker used to detect activation is α-SMA expression (Apte et al., 1998; Lachowski et al., 2017). We used NU-S to grow hPSC as it has less variation batch to batch, less overall protein that can interfere with secreted molecules and maintains consistency with future proliferation assays in PDAC cells. hPSCs were grown first in T75 flasks for 1-2 weeks in DMEM supplemented with 10% NU-S and 10 or 25 mM glucose. hPSC Cells were seeded on glass coverslips and allowed to attach and grow for 24 h. Then the media was changed to either serum free, 1% or 10% Nu-serum with 10 mM or 25 mM glucose. After 48 h they were fixed in 4% PFA and incubated with an α-SMA antibody detected with Alexa 488 conjugated secondary antibody (**Figure 9a**).

We used two strategies to quantify hPSC activation, the first strategy was to count the total number of cells and α-SMA$^+$ cells to obtain the percentage of α-SMA$^+$ cells. The second strategy was to measure the α-SMA$^+$ fluorescent area and normalize this by the total number of cells. The second strategy was used when individual α-SMA$^+$ cells were not possible to count due to high cell density and unclear cell borders.

When hPSC activation was quantified by the number of α-SMA$^+$ cells the overall activation was very low (**Figure 9c**), however when hPSC activation was quantified by fluorescent area, hPSCs grown in 10% NU-S and 25 mM glucose showed a statistically significant higher activation than cells grown in 10 mM glucose (**Figure 9d**).
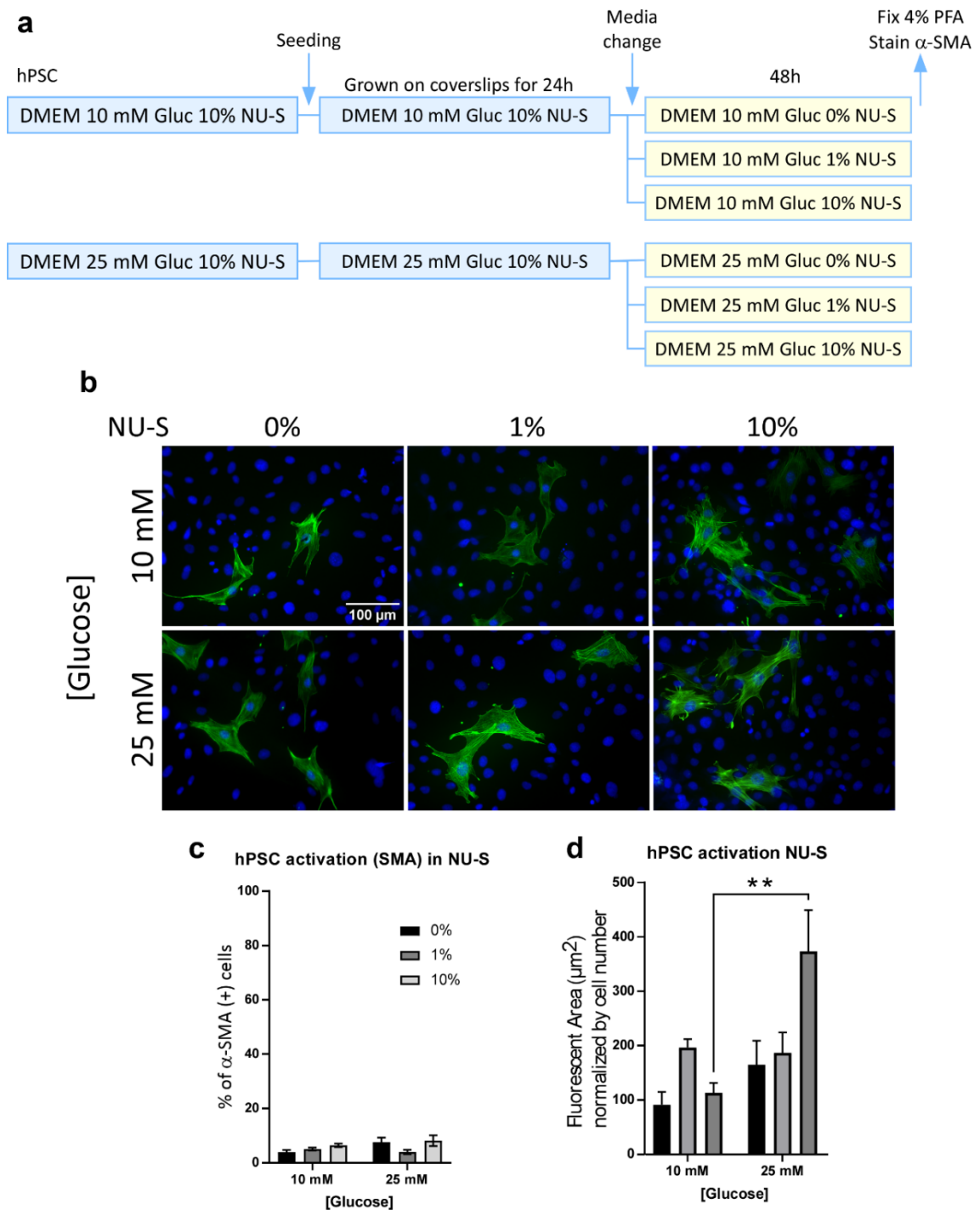
Figure 9. Low Activation of hPSC in NU-S. a,b) hPSC were grown on coverslips for 24 h in DMEM supplemented with 0%, 1% or 10% NU-S and 10 or 25 mM glucose. Cells were fixed in PFA and stained α-SMA antibody detected with an Alex 488 conjugated secondary antibody (green). All nuclei were stained with Hoechst to determine the total number of cells (blue). Epifluorescence images were collected on a Zeiss Axioimager and analysed with ImageJ. **c,d)** α-SMA positive cells were quantified by cell number and fluorescent area (μm^2). Two-way ANOVA using Tukey´s multiple comparison test was used for analysis (**p<0.005) (n=5).
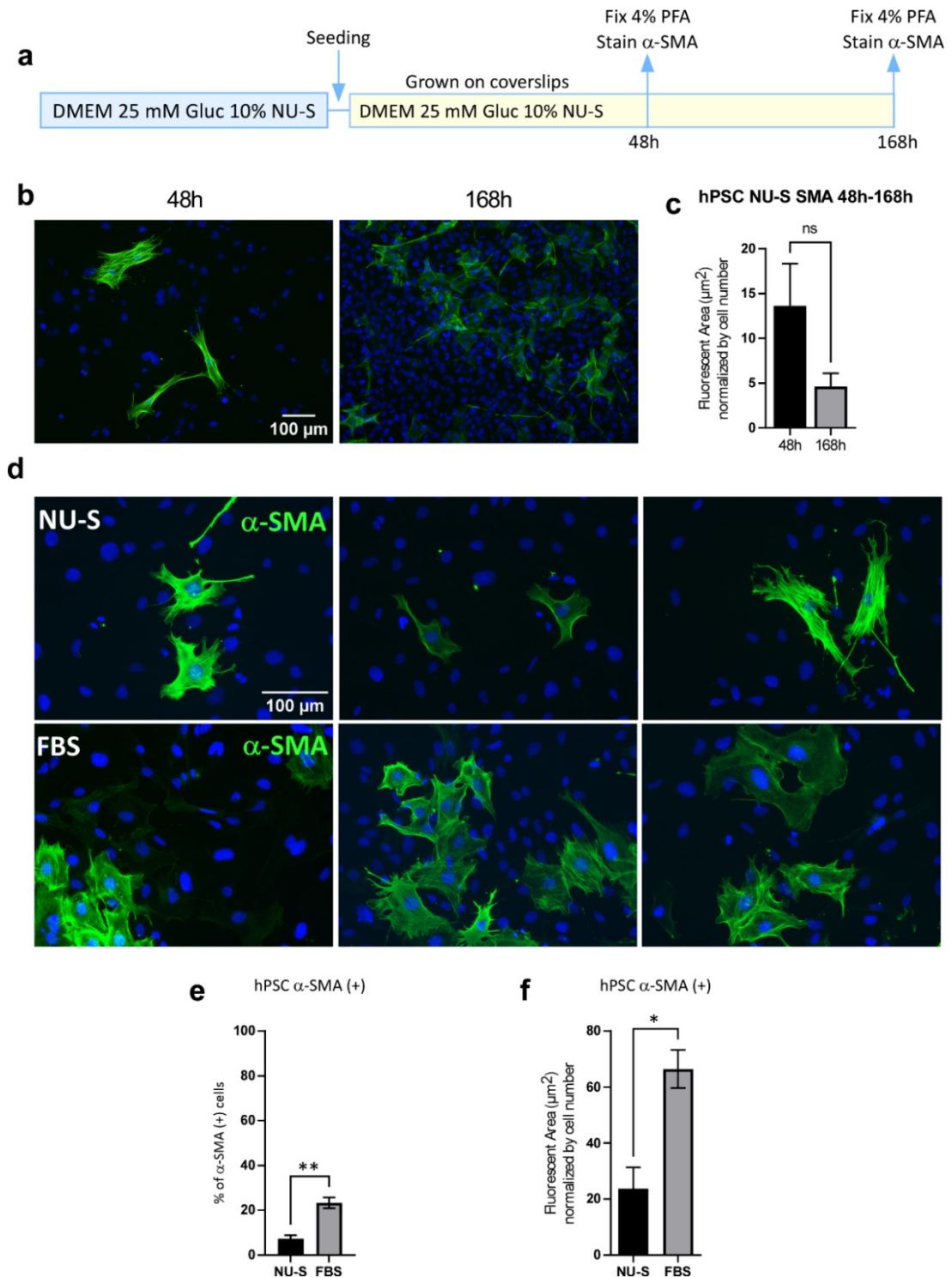
Figure 10. hPSC activation in NU-S remains low over time but is higher in FBS cultured cells.
a) hPSC were seeded on coverslips and cultured in DMEM supplemented with NU-S and 25 mM for 48 to 168 h. **b)** Fluorescent images were taken of α-SMA positive hPSC (green) at 48 and 168 h and were analysed with ImageJ. **c)** Flourescent area quantification. **d)** hPSC were grown in DMEM supplemented with NU-S or FBS with 25 mM glucose for 48 h. Fluorescent images were taken of α-SMA positive hPSC at 48 h and were analysed with imageJ. **e,f)** α-SMA positive cells were quantified by cell number and fluorescent area (μm^2) Mann Whitney´s test was used for analysis (*p<0.05 and **p<0.005) (n=5).

Time has also been suggested as a factor for the activation of hPSC in vitro (Apte et al., 1998; Bachem et al., 1998). We therefore seeded cells in DMEM with 10% NU-S and 25 mM glucose for 168 h (**Figure 10a**). Cells continued to show a low level of activation overall. At 168 h individual cells are impossible to count due to unclear cell borders (**Figure 10b**), so a fluorescent area was used to quantify the level of activation. No significant difference in hPSC activation was observed between 48 and 168 h. Despite a visual increase of α-SMA[+] fluorescent area, when this was normalized by cell number there was no difference in the level of hPSC activation between 48 and 168 h (**Figure 10c**).

Due to the overall low activation of hPSCs grown in NU-S, we compared them to hPSCs cultured in FBS (**Figure 10d**). Cells grown in FBS showed a significant 2.8-fold increase in hPSC activation compared to cells grown in NU-S (**Figure 10e**), but activation was still low at 20% of α-SMA^{+} cells**.**

To further investigate this difference and to achieve the highest level of activation possible we incorporated two known activators of hPSCs, PDGF and TGF-β (Apte et al., 1999; Bachem et al., 1998). We seeded hPSCs on coverslips cultured with FBS or NU-S and supplemented with 10-or 25-mM glucose for 24 h. To activate the cells we used cytokines PDGF (1 ng/ml) and TGF-β (1 ng/ml) which have been reported to induce the activation of hPSCs (Apte et al., 1999). hPSCs were incubated with each cytokine separately and with a combination of both for 24 h. A group of cells were then fixed and stained for α-SMA to analyse the state of activation after 24 h incubation **(Figure 11a).** The remaining cells were kept in culture, the media was replaced with fresh media supplemented with FBS or NU-S and 10 or 25 mM glucose accordingly and incubated for a further 48 h. As shown in **Figure 11c** after the activation period cells grown in FBS showed a significant level of activation compared to cells grown in NU-S, even when the cells were treated with PDGF and TGF-β.

This difference is maintained at 48 h and maximum activation was achieved when cells were grown in FBS treated with TGF-β regardless of whether PDGF was included (**Figure 11d**). Therefore, we selected TGF-β in DMEM supplemented with 10% FBS as the activator to use in subsequent experiments.

To optimize the concentration of TGF-β, cells were grown first in 10% FBS and 25 mM glucose and then treated with increasing concentrations from 0.5 ng/ml to 10 ng/ml of TGF-β. Cells were activated for 24 h in serum free DMEM with 0.1% BSA and 25 mM glucose. After 24 h a group of cells were fixed in 4% PFA and stained for α-SMA. Another group of cells were left for a further 48 h in serum free DMEM supplemented with 25 mM glucose to evaluate if activation was sustained in time (**Figure 12a**).

hPSCs reached a significantly increased activation when treated with either 5 or 10 ng/ml (**Figure 12c**). hPSC activation was sustained in time and did not reverse during this period (**Figure 12d**). However, there were no significant differences in activation between 5 and 10 ng/ml TGF-β.
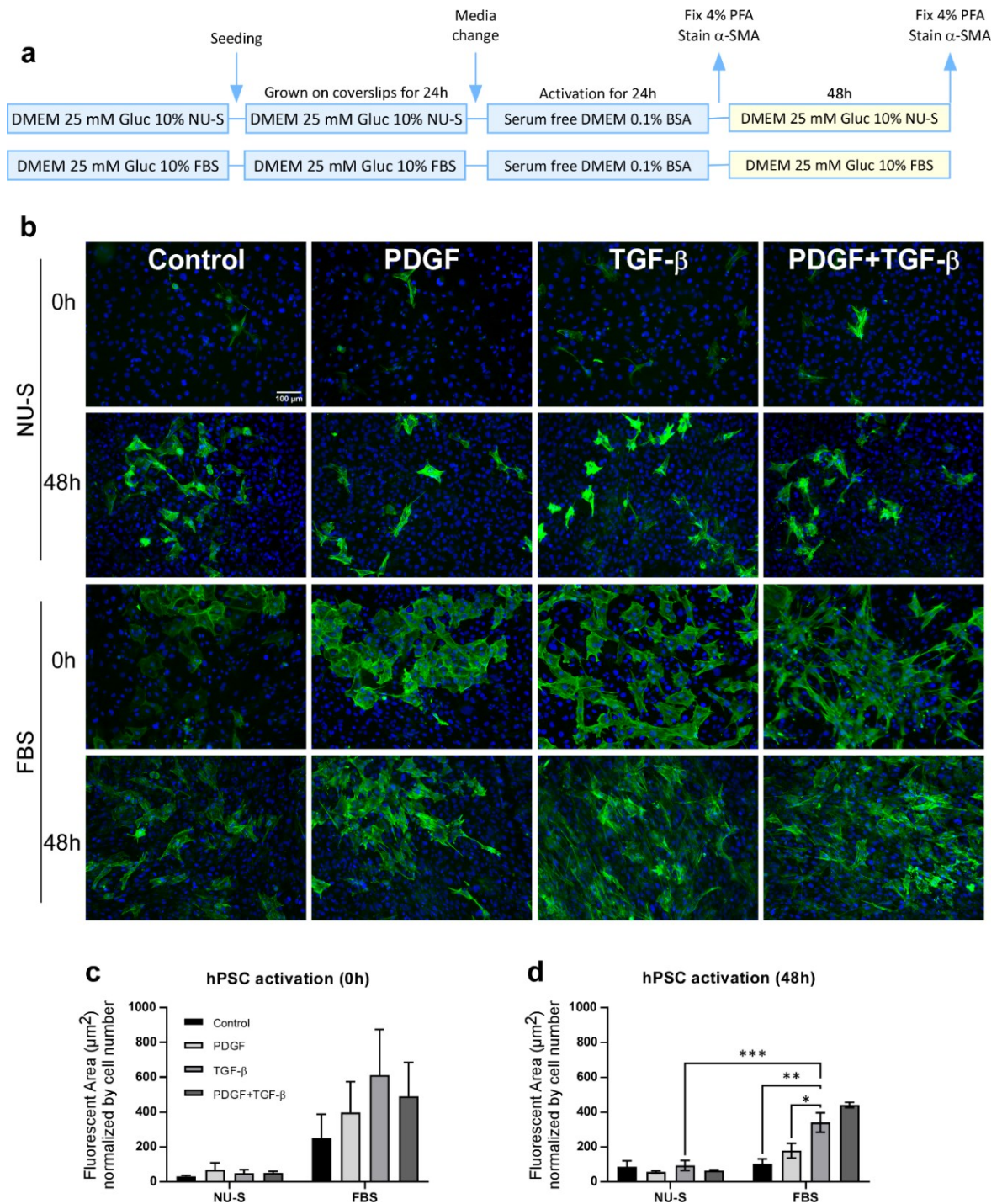
Figure 11. **hPSC activation is increased in cells grown in FBS and activated with TGF-β. a)** hPSC were cultured in DMEM supplemented with either NU-S or FBS with 25 mM glucose. Cells were activated for 24 h in 0.1% BSA serum free DMEM supplemented with 1 ng/ml of TGF-β or 10 ng/ml of PDGF or a mix of the TGF-β + PDGF. **b)** Cells were fixed and stained for α-SMA (green) and nuclei with Hoescht staining (blue) at 0 h after activation and 48 h after activation. Fluorescent images were collected and analysed in ImageJ. **c,d)** hPSC activation was quantified by α-SMA positive fluorescent area (μm^2). Two-way ANOVA using Tukey´s multiple comparison test was used for analysis (*p<0.05, **p<0.005, *** p<0.005) (n=5).
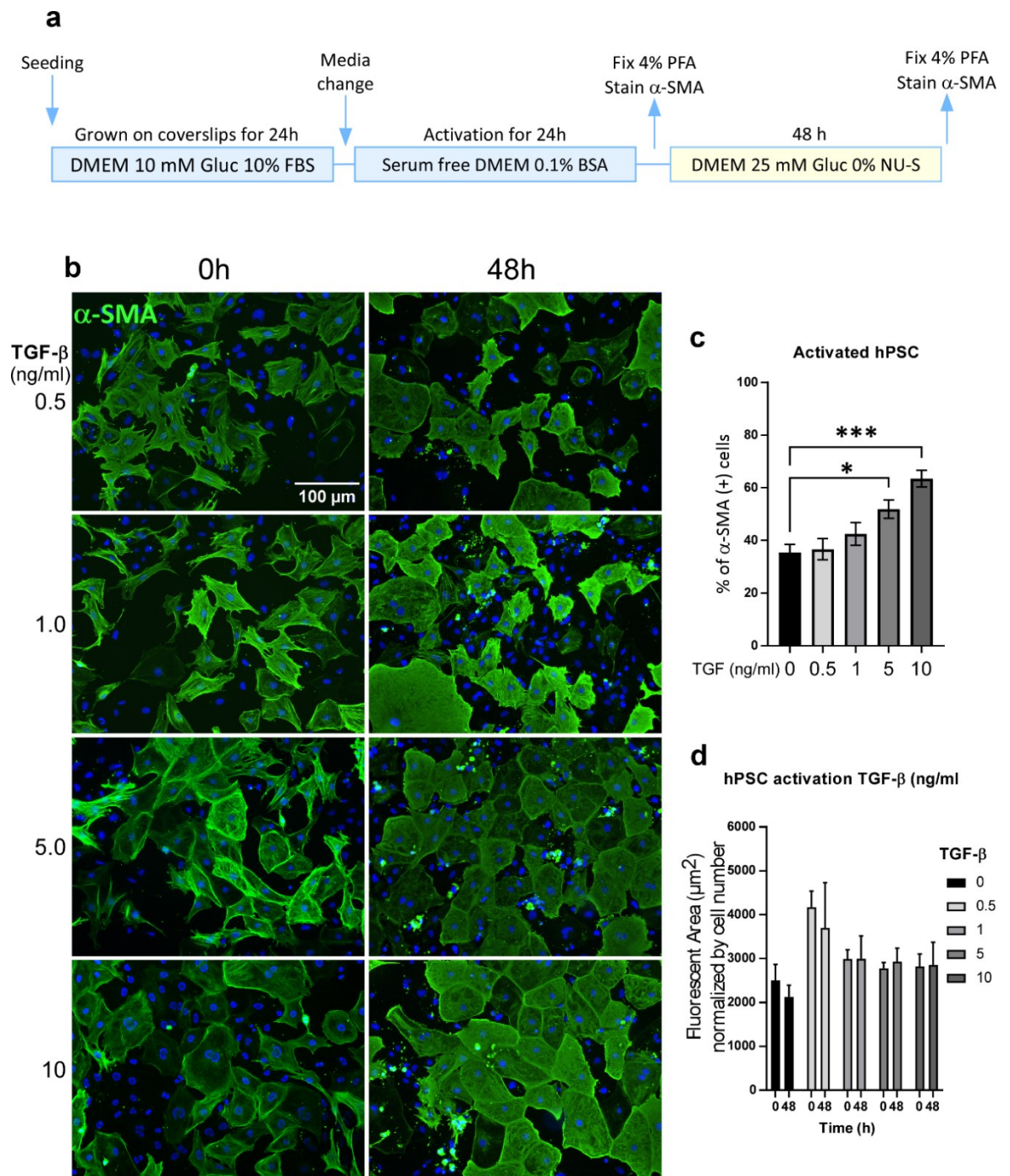
Figure 12. Concentration-dependent hPSC activation is reached by 5 or 10 ng/ml of TGF-β and cells remain activated in serum free DMEM after 48 h. a) hPSC were grown in DMEM supplemented with 10% FBS and 25 mM glucose. Cells were activated for 24 h in 0.1% BSA serum free DMEM with increasing concentrations of TGF-β 0.5, 1, 5 and 10 ng/ml. **b)** Cells were fixed stained for α-SMA (green) and Hoescht staining for nuclei (blue) at 0 h and 48 h after activation. **c, d)** α-SMA positive cells were quantified by cell number and fluorescent area (µm^2). Two-way ANOVA using Tukey´s multiple comparison test was used for analysis (*p<0.05, ***p<0.0005) (n=5).

Given these results, 5 ng/ml was selected for subsequent experiments and the generation of conditioned media from activated hPSC.

In addition, it is also important to note that the reason no FBS was added during the 48 h period post activation was to test the conditions that were used in subsequent experiments where the conditioned media was collected and applied to PDAC cell proliferation. These experiments included media supplement with NU-S therefore if the conditioned media contained any traces of FBS then this may have interfered with the assay.

3.2 Measurement of Hyaluronan in conditioned media

Hyaluronan production was measured with an ELISA based assay using a Hyaluronan binding protein (versican G2 domain) which can detect Hyaluronan independent of its molecular weight. This Echelon kit was used to detect Hyaluronan in conditioned media of TGF-β-activated hPSCs cultured in 10- or 25-mM glucose for 24-72 h (**Figure 13a-b**). MIA PaCa-2 cells received the same treatment and were used as a control as it has been reported that these PDAC cells release low levels of HA to the media (Kudo et al., 2019). hPSCs released more than 10-fold of HA to the media compared to MIA PaCa-2 cells (**Figure 13c**). HA had a time-dependent accumulation reaching ~1.5 µg/ml in hPSC CM collected at 72 h. Surprisingly, when comparing conditions of activated hPSCs the HA concentration was higher in activated hPSC cultured in 10 mM glucose compared to 25 mM glucose (**Figure 13c**). When hyaluronan concentration was normalized to cell number or protein concentration to control for potential differences in cell growth under the different conditions, the differences in HA concentration or patterns of HA production between conditions did not change significantly (**Figure 13d-e**). Due to the small difference in Hyaluronan concentration between 48 and 72 h in hPSCs grown in 10 mM glucose, the 48 h HA accumulation timepoint was selected for the collection of conditioned media. This was mainly to avoid excessively long periods without serum, excessive nutrient deprivation, or metabolite accumulation, each with potentially confounding effects as we have previously seen in the lab. We determined the glucose concentration in the hPSC CM (**Figure 13f**), which decreased by 50% when used at a concentration of 25 mM and 75% when used at a 10 mM concentration. This allowed us to replenish glucose in the hPSC CM for subsequent experiments to eliminate glucose deprivation as a confounding variable in proliferation or migration studies.
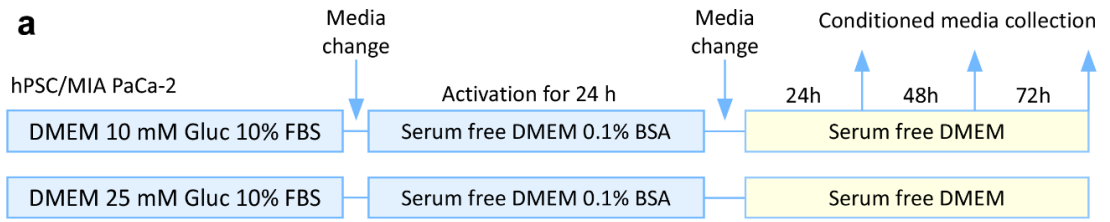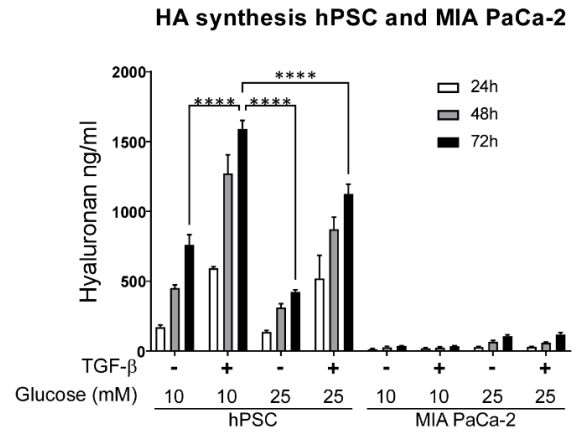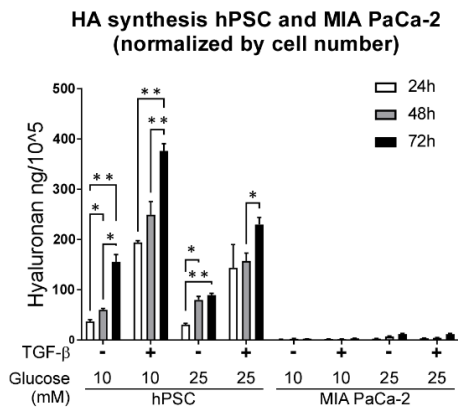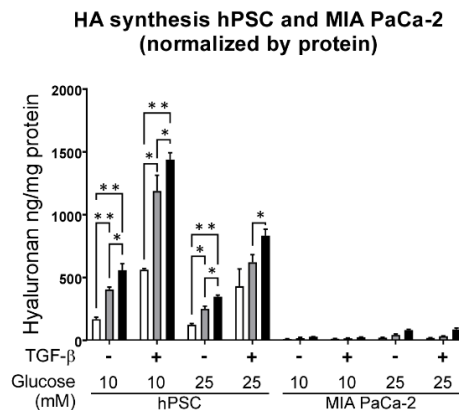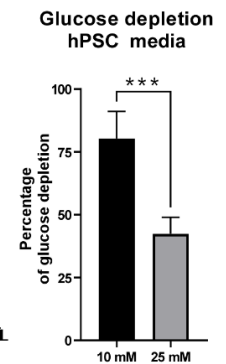
Figure 13. Activated hPSC secrete the highest concentration of HA when cultured in 10 mM glucose. a,b) Conditioned media was prepared from hPSC and MIA PaCa culturing cells in DMEM supplemented with 10% FBS with either 10 or 25 mM glucose. Both hPSCs and MIA PaCa cells were activated for 24 h in serum free media 0.1% BSA with 5 ng/ml TGF-β. After activation, the cells were left for 48 h in serum free media with 10 or 25 mM glucose and conditioned media was collected. **c-e)** An ELISA-based assay for HA was used to measure the concentration of HA in the conditioned media collected. Absorbance was measured after 30 min incubation at 405nm and HA concentration was calculated from a standard curve. HA concentrations were normalized to cell number and mg of protein to determine whether growth, which is faster in MIA PaCa cells, might be an independent variable. **f)** Glucose concentration was measured in the media of hPSC at 48h. Two-way ANOVA using Tukey´s multiple comparison test was used for analysis (*p<0.05, **p<0.005) (n=2). Two-tailed unpaired t-test was used for analysis of glucose depletion (***p<0.0005) (n=3).

3.3 Standardization of proliferation conditions of MIA PaCa-2 cells

To standardize proliferation conditions for MIA PACa-2 cells it was necessary to determine the optimum growth in glucose and serum. Most culture conditions use high glucose and high serum which maximises cell growth and could potentially be at its maximum rate and a non-physiological condition. Therefore, we used NU-S, a commercial formulation with 25% of FBS that has less variability in each batch. We tested several concentrations of glucose and NU-S to find the optimal conditions that did not oversaturate cell growth factors but still supported cell proliferation.

Two assays were used to study proliferation, the WST-8 assay, is based on the reduction of a water-soluble tetrazolium salt by cellular dehydrogenases into a yellow formazan dye that is also water-soluble. The second assay uses sulforhodamine B (SRB), which is a dye that binds to basic amino acid residues. This binding of the dye is stoichiometric which means that the amount of bound dye is directly proportionate to the amount of protein and thus to cell mass (Vichai and Kirtikara, 2006).

The conditions for PDAC proliferation assays were standardized by cell density and glucose concentration for optimal proliferation of cells, sufficient to maintain cell growth rate but at a submaximal rate so that any experimental condition has the potential to further increase or decrease cell growth. We applied these two assays to analyse the growth curves of MIA PaCa-2 cells grown in DMEM with different concentrations of NU-S (0%, 1% and 10%) and glucose (10 and 25 mM).

Cells were seeded at a density of 5000 cells per well in 96 well plates and proliferation was measured every 24 h up to 72 h. Concentrations of NU-S lower than 10% did not appear to support cell proliferation and glucose concentration did not affect cell growth assessed by either WST-8 or SRB (**Figure 14a-b**). We then extended the proliferation time frame to 96 h. For the extended time frame, we standardized glucose concentration and cell density. Glucose concentrations of 5, 8, 10, 15 and 25 mM and cell densities of 2500 and 5000 cells/well were analysed. With the WST-8 assay, MIA PaCa-2 cells showed a significant decrease in signal at 96 h when cells were cultured in 5-8 mM glucose and seeded at a density of 2500 per well (**Figure 14c**). However, this reduced signal when assessed using SRB was not apparent suggesting that this may be a fundamental difference in how these assays report cell growth (**Figure 14d**). For example, the WST-8 assay may report a sudden drop in cellular redox state independent of cell growth that would not be detected by SRB. Likewise, a change in cell adherence may affect the SRB assay, due to the vigorous washing step that would lose non-adherent or loosely adherent cells, but not the WST-8 assay. When the cell density was 5000 cells per well this decrease in signal was observed up to a concentration of 15 mM glucose (**c**) but not at the highest glucose concentration (25 mM). Overall, the WST-8 assay together with the SRB assay showed that seeding cells at a density of 2500 per well combined with a concentration of 10 or 25 mM glucose were the optimal conditions. However, to avoid hyperglycaemic conditions and use concentrations closer to an *in vivo* we chose to use 10 mM glucose since proliferation was not significantly different between 10 + 25 mM glucose at the 96 h time point.
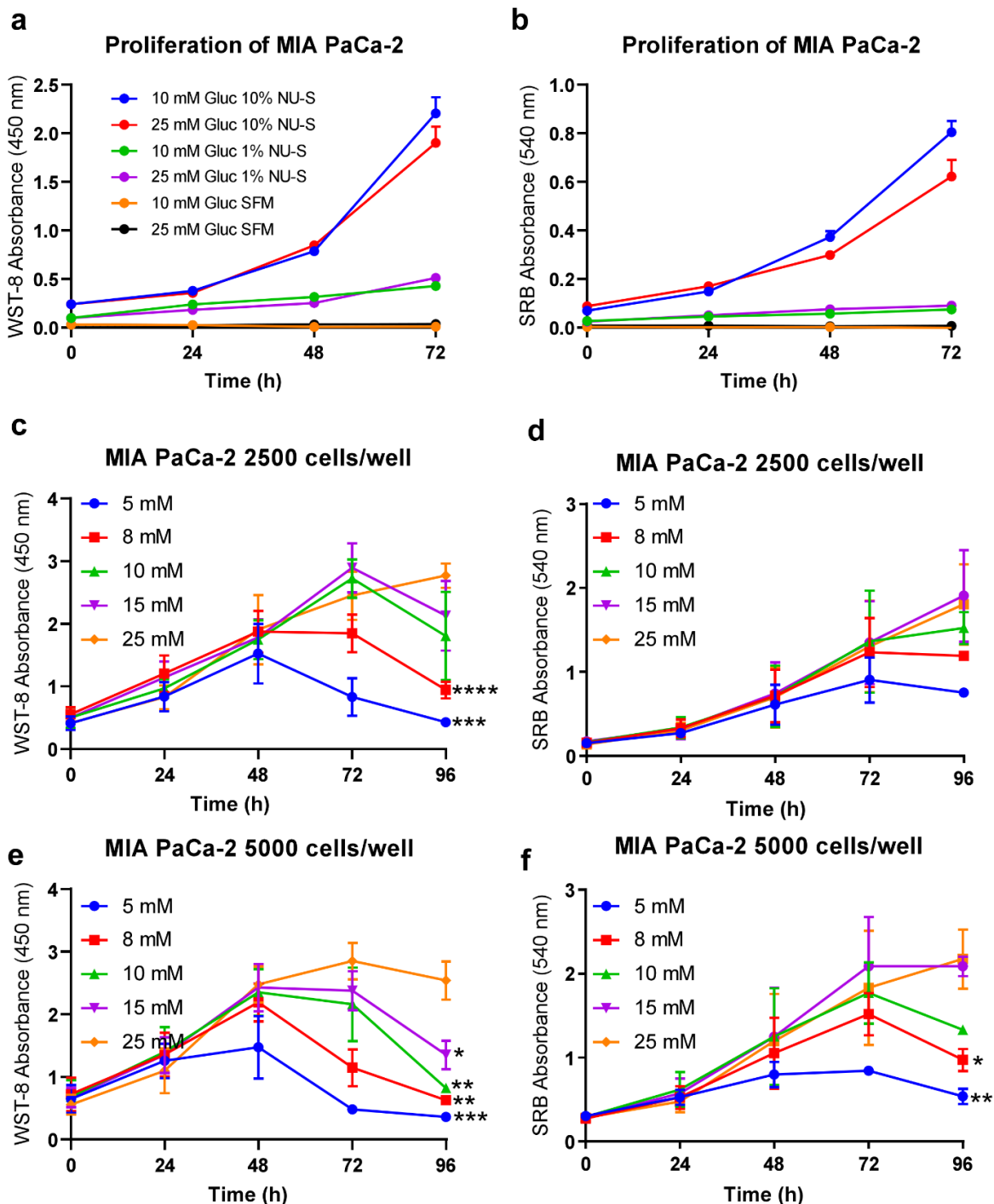
Figure 14. Optimization of MIA PaCa-2 cell growth. a,b) MIA PaCa-2 cells were seeded at a density of 5000 cells per well in DMEM supplemented with 0%, 1% or 10% FBS. Cell proliferation was measured every 24 h up to 72 h. **c,d)** MIA PaCa-2 cells were seeded at a density of 2500 cells per well in DMEM supplement with 10% NU-S with increasing concentrations of glucose of 5, 8, 10, 15 and 25 mM. **e,f)** MIA PaCa-2 cells were seeded at a density of 5000 cells per well in DMEM supplement with 10% NU-S with increasing concentrations of glucose of 5, 8, 10, 15 and 25 mM. Proliferation was measured with the WST-8 and SRB assays. Two-way ANOVA using Tukey´s multiple comparison test was used for analysis (*p<0.05, **p<0.005, ****p<,00001) (n=3).

3.4 Discussion

To truly investigate the role of hPSC-derived HA on PDAC cells, it was necessary to characterise and optimise the activation of hPSCs and conditions for collecting CM. hPSCs when grown in vitro are highly dependent on external stimulation by TGF-β or PDGF. This was evidenced when hPSCs were grown in media supplemented with NU-S, in which the overall level of activation, assessed by α-SMA⁺ staining was only partial at best despite being cultured for up to 168 h. This somewhat conflicts with previous reports in which sufficient activation was achieved by simply growing cells on plastic and glass for 48 hrs (Apte et al., 1998). One explanation for this difference could be that our batch of primary hPSCs is not pure but contaminated by other types of cells therefore the number of α-SMA⁺ cells is fewer because there are fewer total bona fide hPSCs within the population. Initially, NU-S was used as it is a more standardized serum with less variation from batch to batch, and with fewer proteins that can interfere with proteins and macromolecules secreted to the CM. However, when PSCs were grown in the commonly used FBS, the number of α-SMA⁺ increased. This suggests that FBS may contain a high repertoire of cytokines that can activate the hPSCs compared to simply growing on plastic or glass. This is supported by the fact that FBS is known to contain TGF-β (10-20 ng/ml), one of the main activators of PSC (Oida and Weiner, 2010). The composition of NU-S according to the manufacturer (Corning™) is 25% FBS plus several growth factors and hormones with less difference from batch to batch compared to FBS. This would indicate that NU-S has only 25% of the required TGF-β necessary to activate PSCs.

In line with previous studies, TGF-β induced more α-SMA⁺ cells than PDGF which is known to have a greater effect on proliferation–(Apte et al., 1999; Luttenberger et al., 2000). We observed maximum activation with TGF-β at 5 ng/ml, with no further statistical increase at 10 ng/ml. This activation was sustained over time and did not reverse. Interestingly, even after reaching maximum activation, there was still close to 40% of hPSC that did not show any staining for α-SMA and did not respond to TGF-β mediated activation. Populations of α-SMA^{low} PSCs have been previously reported in a mouse model of PDAC (Biffi et al., 2019; Ohlund et al., 2017). These two populations of PSCs are characterized as myCAFs (α-SMA^{high}IL-6^{low}) and iCAFs (α-SMA^{low}IL-6^{high}) because they respond to different stimuli secreted by PDAC cells. The myCAF phenotypes respond to TGF-β and turn into a fibrogenic hPSC with increased synthesis of ECM, while the iCAF phenotypes respond to IL-1 and transform into an inflammatory PSC that secretes IL-6 among other cytokines. Therefore, it is likely that the cells in our culture are a heterogenous mix of fibrogenic and inflammatory PSCs.

Activated hPSCs synthesized higher quantities of HA compared to non-activated PSCs and PDAC cell line MIA PaCa-2. The concentration of HA released to the media was almost 40-fold higher compared to HA released by MIA Paca-2. This was in line with previous studies where higher concentrations of HA were measured in the media of activated PSCs compared to PDAC cells.(Junliang et al., 2019; Kim et al., 2021). However, in terms of raw concentrations, these differ between our study and the two studies mentioned, 2 fold less than Kim et al., and.70 fold higher than in Junliang et al. This could be because different kits were used for measuring HA in each study and

the overall protocol was also different. Another important point is that neither study mentioned the level of activation of the PSCs that were used to measure HA released to the media which could explain some of the differences seen.

Interestingly when hPSCs, were grown in lower glucose concentrations (10 mM) the quantity of HA released to the media, was higher than that of hPSCs grown in high glucose concentrations (25 mM). This response may seem counterintuitive and is at odds with previous research showing that HA synthesis is not affected by either high or low glucose concentrations in a model of cardiac fibroblasts (Gorski et al., 2019). However, in this study HA synthesis did not change when fibroblasts were activated with TGF-β which differs from our findings. In another study, mesangial cells increased HA synthesis when exposed to high glucose concentrations (25.6 mM) (Wang and Hascall, 2004). A similar effect was seen in vascular smooth muscle cells when grown in hyperglycaemic conditions (25 mM), there was an upregulation of HAS2 accompanied by increased HA synthesis (Sainio et al., 2010). One critical regulator of HAS2 activity is AMPK (adenosine monophosphate-activated protein kinase), which inhibits HAS2 activity by phosphorylation of Thr-110 (Vigetti et al., 2011). This supports the notion of higher HA synthesis in high glucose environments as AMPK is down regulated by high glucose concentration (Jiang et al., 2021) this could in turn release HAS2 from inhibition and allow synthesis of HA.

One important piece of data is that when we measured glucose in the media of activated PSC after 48 h, there was a higher glucose depletion in PSCs grown in 10 mM glucose (80%) compared to 25 mM (40%). Although in raw quantities cells grown in 25 mM consumed nearly 10 mM while cells grown in 10 mM consumed 8 mM of glucose. To understand the results of this conflicting data more studies are needed to understand how PSC controls glucose metabolism and HA synthesis to explain our findings.

Standardizing the growth conditions for our cell model was key for the experiments that followed. MIA PaCa-2 cells have a high growth rate and high glycolytic phenotype as previously established in our lab (Ahlam thesis). We wanted to determine the optimum conditions of growth such that growth is not too fast nor too slow. This is important to not mask any experimental increase or decrease when applying hPSC-derived CM (containing hPSC-derived HA) or exogenous HA. It is also important to assess optimum glucose concentrations and assess glucose depletion over the long time course of these proliferation experiments (96 h). Controlling for cell density was also key for the long 96 h growth experiments, as higher densities (5000 cell/well) glucose depletion becomes evident from 48 h by a decline in growth at lower glucose concentrations with WST-8 and SRB. At cell densities of 2500 cells/well there is a sharp decrease in WST-8 signal at 5-8 mM glucose which was not seen in the SRB assay. This is probably due to glucose deprivation, which is known to induce oxidative stress (Spitz et al., 2000). This could affect the readings for WST-8 assays as it depends on con the redox state of the cell to produce a signal, but not affect the SRB assay, which is what we observed. According to the data obtained the optimum growth conditions for 96 h proliferation assays in MIA PaCa-2 cells are 2500 cells/well in 10 mM glucose. PDAC tumour tissue is characterized by

nutrient depletion including lower glucose concentrations (Kamphorst et al., 2015), therefore we used the lowest glucose concentrations possible that could sustain growth but not affect the cells (10 mM), avoiding extremely hyperglycaemic concentrations (25 mM).

Chapter 4   Effect of pancreatic stellate cell conditioned media and exogenous hyaluronic acid on PDAC cells

4.1 PDAC cell proliferation and migration in filtered and non-filtered hPSC conditioned media

After standardizing the conditions for hPSC activation, CM collection and PDAC cell proliferation, we studied the effects of CM from activated and non-activated hPSC on PDAC cell proliferation and migration. Cells were seeded at a density of 2500 cells/well and grown for 96 h hPSC CM supplemented with 10% NU-S (**Figure 15a-b,e-f**) or FBS (**Figure 15c-d,g-h**) and the glucose was replenished to 10 (**Figure 15a-d**) or 25 mM (**Figure 15e-h)** to compensate for glucose deprivation. These were the optimum conditions defined in Chapter 3. Proliferation was quantified every 24 h with the WST-8 and SRB assays. There were no measurable effects on cell proliferation when cells were grown in CM. Neither activation, serum type nor glucose concentrations had any significant effects (**Figure 15a-h**). Although there was considerable variability in these data, we hypothesised that HA secreted by hPSCs in CM may be responsible for any potential increase in cell proliferation. However, nutrient depletion, metabolite accumulation or both may have confounding and counteracting effects in reducing cell proliferation.

To eliminate any confounding variables from nutrient depletion and metabolite accumulation we filtered the hPSC CM using 3 kDa amicon filters. Through this procedure, we can filter out molecules smaller than the 3kDa cut-off and are left with a small volume of media (~500 µl) containing molecules over 3 kDa in size. This concentrated hPSC CM was then resuspended in fresh DMEM supplemented with 10% NU-S and 10 mM glucose. Nevertheless, when this filtered CM from either activated or non-activated hPSC was tested on PDAC cell proliferation there were no differences when compared to the corresponding non-filtered control (**Figure 16a-b**). These proliferation experiments were only carried out in MIA PaCa-2 cells.

We then used the same strategy and tested filtered and non-filtered CM on cell migration by using a gap closure assay. In this assay, cells are seeded in a monolayer into silicone inserts with 2 wells separated by a silicone divide. This assay is based on generating a cell free space by physical exclusion, in this case, the silicone divider. When the insert is removed, migration can then be assessed as cells migrate into the cell free space. In addition, to avoid measuring space occupation due to cell proliferation, the anti-proliferation drug mitomycin C (Vang Mouritzen and Jenssen, 2018) was added to the culture media. Mitomycin C is a drug from *Streptomyces caespitosus* that causes crosslinking of CpG areas in the DNA, limiting cell division (Tomasz, 1995). This drug was previously standardized for its use in this assay and a concentration of 1-2 µg/ml was found to be sufficient to block cell proliferation without any toxic effects to induce cell death (Sritangos, 2019).
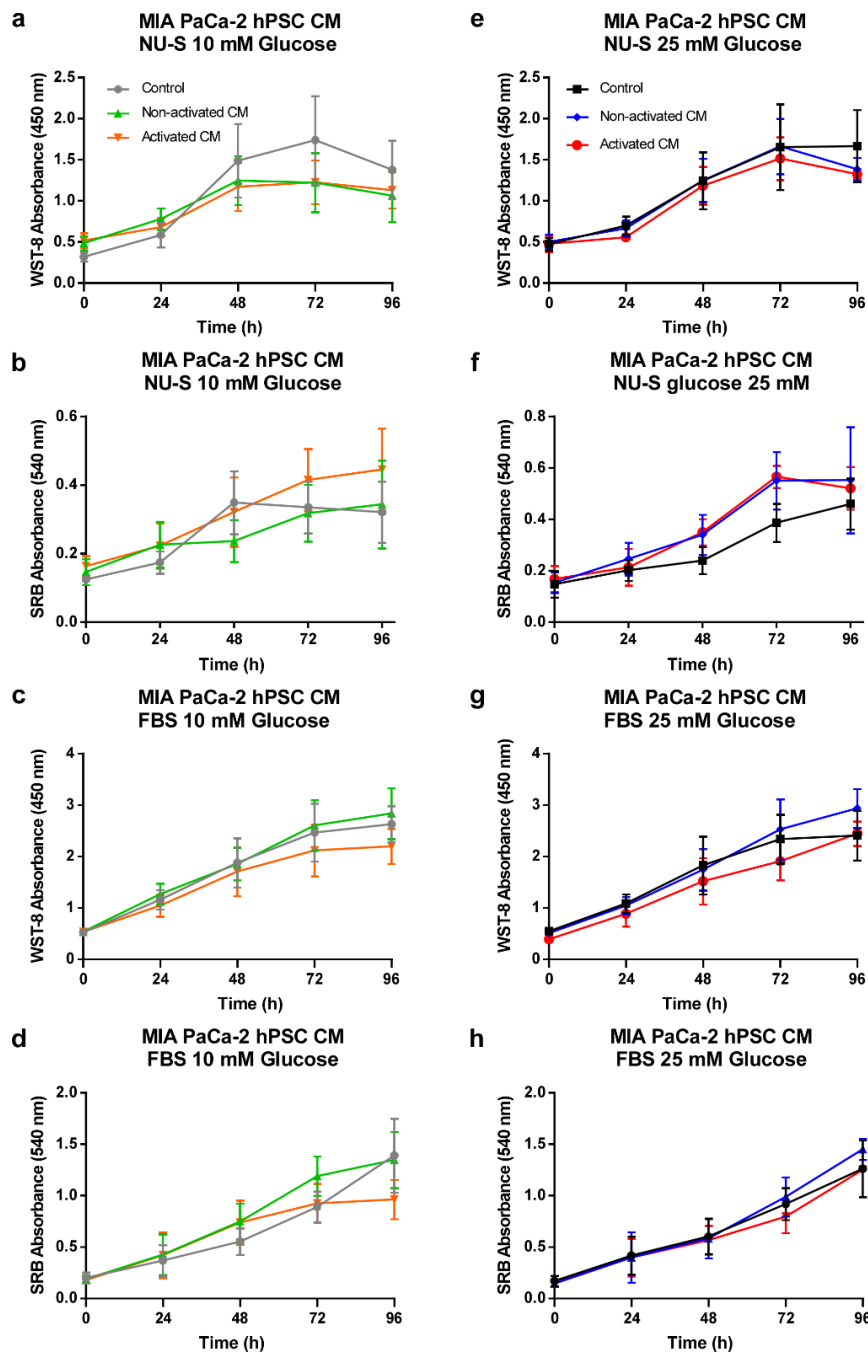
Figure 15. Conditioned media from activated hPSC does not affect MIA PaCa-2 cell proliferation measured by the WST-8 and SRB assay. a,b) CM was obtained from hPSC activated for 24 h with TGF-β 5 ng/ml for 24 h. CM was supplemented with either 10% NU-S or 10% FBS and glucose was replenished to 10 mM or 25 mM. MIA PaCa-2 cells were seeded onto 96 well plates and incubated in the CM collected. **a,b)** MIA PaCa-2 cells were grown in activated or non-activated hPSC CM supplemented with 10% NU-S and 10 mM glucose. **c,d)** MIA PaCa-2 cells were grown in activated or non-activated hPSC CM supplemented with 10% FBS and 10 mM glucose. **e.f)** MIA PaCa-2 cells were grown in activated or non-activated hPSC CM supplemented with 10% NU-S and 25 mM glucose. **g,h)** MIA PaCa-2 cells were grown in activated or non-activated hPSC CM supplemented with 10% FBS and 25 mM glucose. Proliferation was measured every 24 h for 96 h by the WST-8 and SRB assay. Two-way ANOVA using Tukey´s multiple comparison test was used for analysis. (n=3).
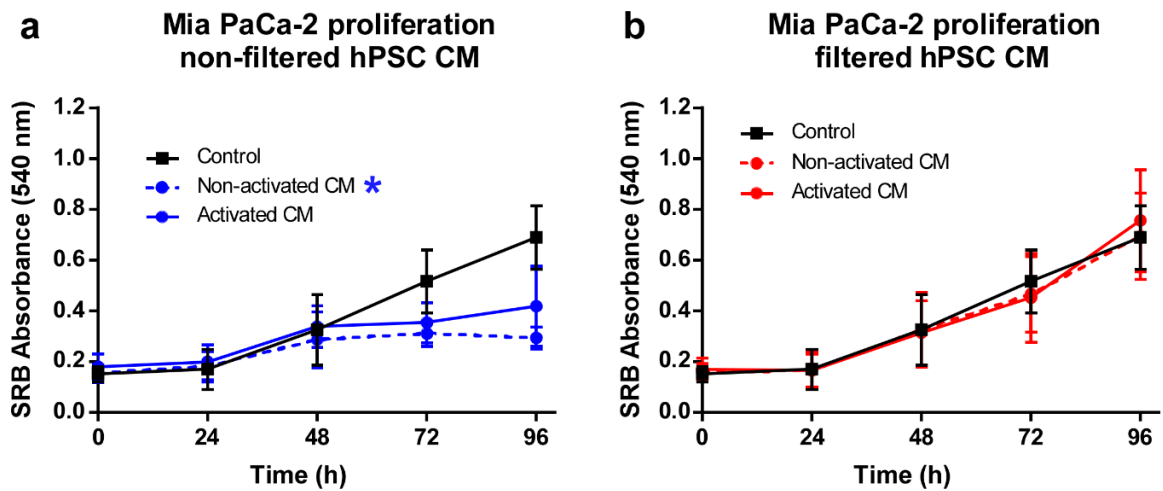
Figure 16. Filtered conditioned media from activated hPSC does not affect MIA PaCa-2 cell proliferation. a,b) hPSC were activated with 5 ng/ml TGF for 24 h. Serum free DMEM was added and after 48 h the conditioned media was collected. The conditioned media was processed in 2 separate paths. The first was supplemented with 10% NU-S and 10 mM glucose and the second included a filtration step with 3 kDa Amicon filters. All molecules above 3 kDa were kept and resuspended in fresh DMEM supplemented with 10% NU-S and 10 mM glucose. MIA PaCa-2 cells were incubated in DMEM 10% NU-S 10 mM glucose, non-activated hPSC conditioned media and activated conditioned media. Proliferation was measured every 24 h up to 96 h by the SRB assay. Two-way ANOVA using Tukey's multiple comparison test was used for analysis (*$p < 0.05$) (n=3).

MIA PaCa-2 cells were seeded into wells containing the silicone inserts and allowed to attach for 24 h to the culture plate. The inserts were then removed, and the cells were incubated in optimised CM (e.g. NU-S, glucose replenished) containing Mitomycin. The gap closure measures the occupation of a cell free area over time. The percentage of gap closure can then calculate using the following equation

$$Gap\ closure\ \% = \left(\frac{A_{t=0} - A_{t=\Delta}}{A_{t=0}}\right) \times 100,$$

where ($A_{t=0}$) is the area of the gap at time 0 and ($A_{t=\Delta}$) is the area of the gap at any given time point.

The migration rate in µm/h was calculated using the Wound_healing_size_tool (Suarez-Arnedo et al., 2020) and the following formula

$$R_M = \frac{W_i - W_f}{t}$$

where **W_i** is the average of the initial gap width, **W_f** is the average of the final gap width both in µm and **t** is a time point of the assay in h. For MIA PaCa-2 and PANC1 cells, **t** was 24 h and for BXPC3 cells **t** was the time at which 50% of the gap was closed.

We then compared migration by the gap closure assay in all three PDAC cells (MIA PaCa-2, PANC1 and BxPC3) in activated hPSC CM (5 ng/ml TGF-β) vs non-activated hPSC CM, that was either filtered or non-filtered. There were marked differences in the migration between the PDAC cell lines. In the control cells, MIA PaCa-2 cells exhibited a slow migration, with a linear phase between 12-36 h after which migration began to slow down (**Figure 17a,d**). PANC1 control cells showed a faster linear migration up to 24 h but then slowed down as the gap began closing between 36 and 48 h (**Figure 17b,e**). BXPC3 control cells rapidly migrated between 6 to 12 h closing the gap at approximately 15-18h (**Figure 17c,f**). When we analysed the migration with non-filtered hPSC CM (activated or unactivated) there were no significant differences in migration (**Figure 17a-c**). Analysing the gap closure in filtered hPSC CM there was a significant increase in migration in MIA PaCa-2 cells treated with activated filtered hPSC CM (**Figure 17d**). However, there were no significant differences in migration between activated and non-activated filtered hPSC CM (**Figure 17d**). Therefore, the only determining factor increasing migration was the hPSC CM independently of activation (**Figure 17d**). Neither PANC1 nor BXPC3 cells showed a significant increase in migration (**Figure 17e,f**).

We also measured the migration rate (µm/h). This was measured by calculating the average distance migrated at 24 h for the MIA PaCa-2 cells, and at the time point of 50% gap closure for the BXPC3 cells (more data was available for BXPC3 cells because images were taken every 15 min due to the very fast migration). Only in MIA PaCa-2 cells the activated filtered hPSC CM induced a significant increase in migration (**Figure 17g**). Representative images of the gap closure assay for MIA PaCa-2 cells are shown in **Figure 17k**.
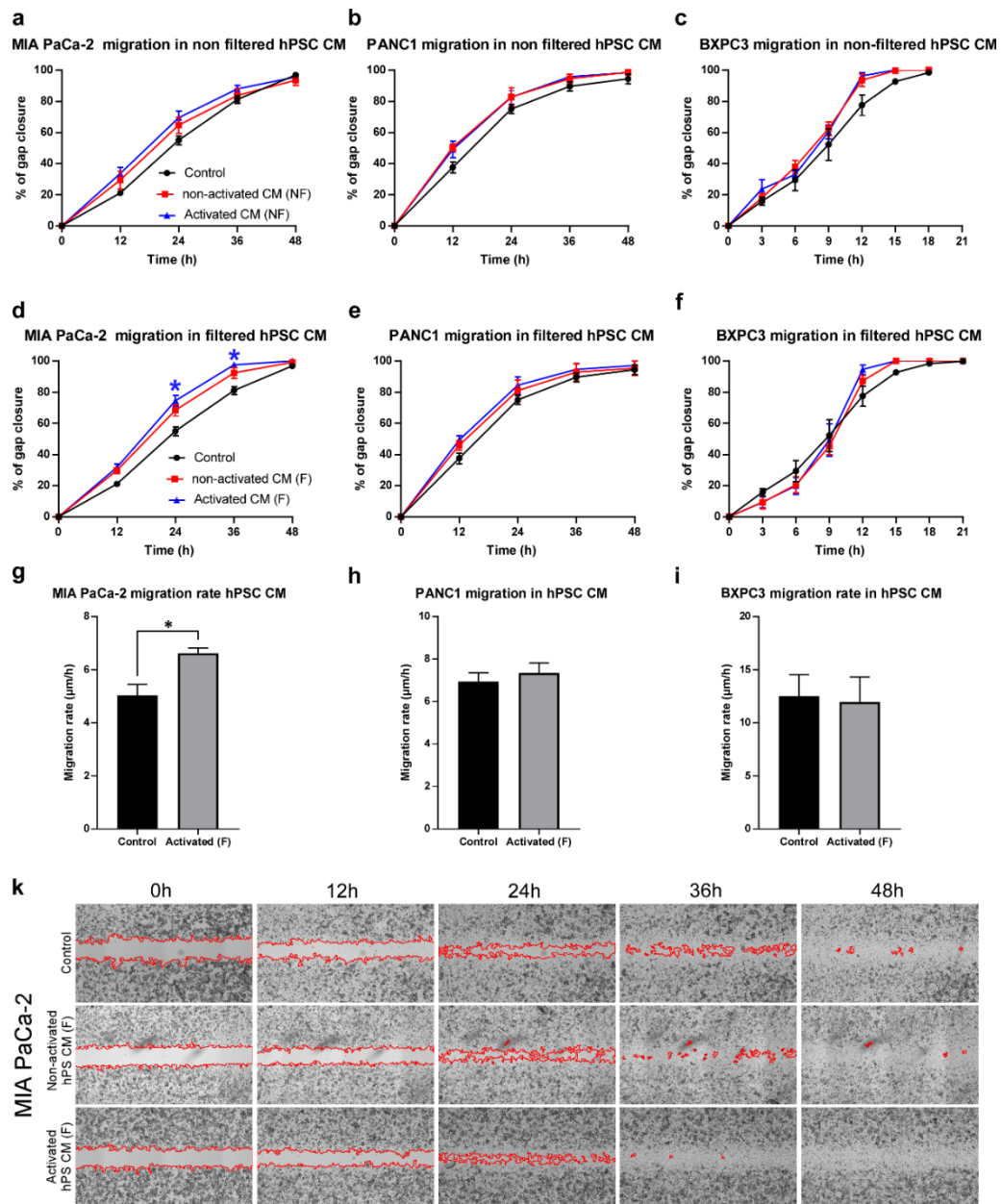
Figure 17. hPSC conditioned media increases MIA PaCa-2 migration but not PANC1 or BXPC3 cell migration. a-c) MIA PaCa-2, PANC1 and BXPC3 cells were seeded into IBIDI 2-well silicone inserts for 24 h. The insert was removed, and the media was changed to non-filtered hPSC CM, either non-activated or activated hPSC CM with 10% NU-S, glucose replenished to 10 mM, supplemented with mitomycin C (2 µg/ml). **d-f)** MIA PaCa-2, PANC1 and BXPC3 cells were seeded into IBIDI 2-well silicone inserts for 24 h. The insert was removed, and the media was changed to filtered hPSC CM, either non-activated or activated hPSC CM resuspended in 10% NU-S, 10 mM glucose, supplemented with mitomycin C (2 µg/ml). Images were taken every 12 h for MIA PaCa-2 and Panc1 cells. For Bxpc3 cells, images were taken every 15 min for up to 16 h. Analysis of gap closure was processed in Fiji ImageJ. **g-i)** The migration rate (µM/h) of PDAC cells in hPSC CM was calculated from the average gap width at 0 h, minus the average gap width at 24 h for MIA PaCa-2 and PANC1 cells. For BXPC3 cells the migration rate was calculated at 50% gap closure. **k)** Representative images of gap closure of MIA PaCa-2 cells treated with control media and filtered, activated hPSC CM. Gap is delimited by the red lines. Two-way ANOVA using Tukey's multiple comparison test was used for analysis of % of gap closure (*p<0.05). Two-tailed unpaired t-test was used for analysis of migration rate(*p<0.05) (n=3).

4.2 Characterization of HA receptors in the effect of exogenous HA in PDAC cells

To better understand PDAC cell behaviour we investigated the presence of HA receptors in our PDAC cell lines. Immunoblotting and immunofluorescence were carried out to detect the two most common HA receptors, CD44 and RHAMM. All PDAC cell lines expressed CD44 and RHAMM by immunofluorescence. CD44 was located in the cell membrane, including in filopodia-like membrane projections, in all cell lines (**Figure 18a-c**). RHAMM did not have a clear membrane pattern but more of a punctate pattern (**Figure 18d-f**). However, in BXPC3 cells it appeared to be located on the leading edge of a lamellipodia-type projection and in PANC1 cells at the tip of membrane projections (**Figure 18f**). In MIA PaCa-2 cells there was mainly a punctate pattern more than a membrane pattern and some cells display higher intensities than others (**Figure 18d**).

In the immunoblotting assays, the expected band of 80 kDa for CD44 standard (CD44s) was present in whole cell lysates of MIA PaCa-2 and PANC1 cells, but only a light and thin band was present in BXPC3 whole cell lysates (**Figure 18g**). In BXPC3 cell lysates there was an additional higher molecular band close to 150 kDa that could correspond to CD44 variants (CD44v) as previously reported (Zhao et al., 2016). When BXPC3 lysate bands were exposed separately from the other cell lines, these double bands were more evident (**Figure 18h**). When RHAMM protein was detected, a band at the expected molecular weight of 85 kDa was present in MIA PaCa-2 and PANC1 cell lines. However, there were two separate smaller bands between 50 and 40 in BXPC3 lysates **Figure 18i**), similar to a 45 kDa band for RHAMM that has been reported in a fibrosarcoma cell line (Kouvidi et al., 2011).
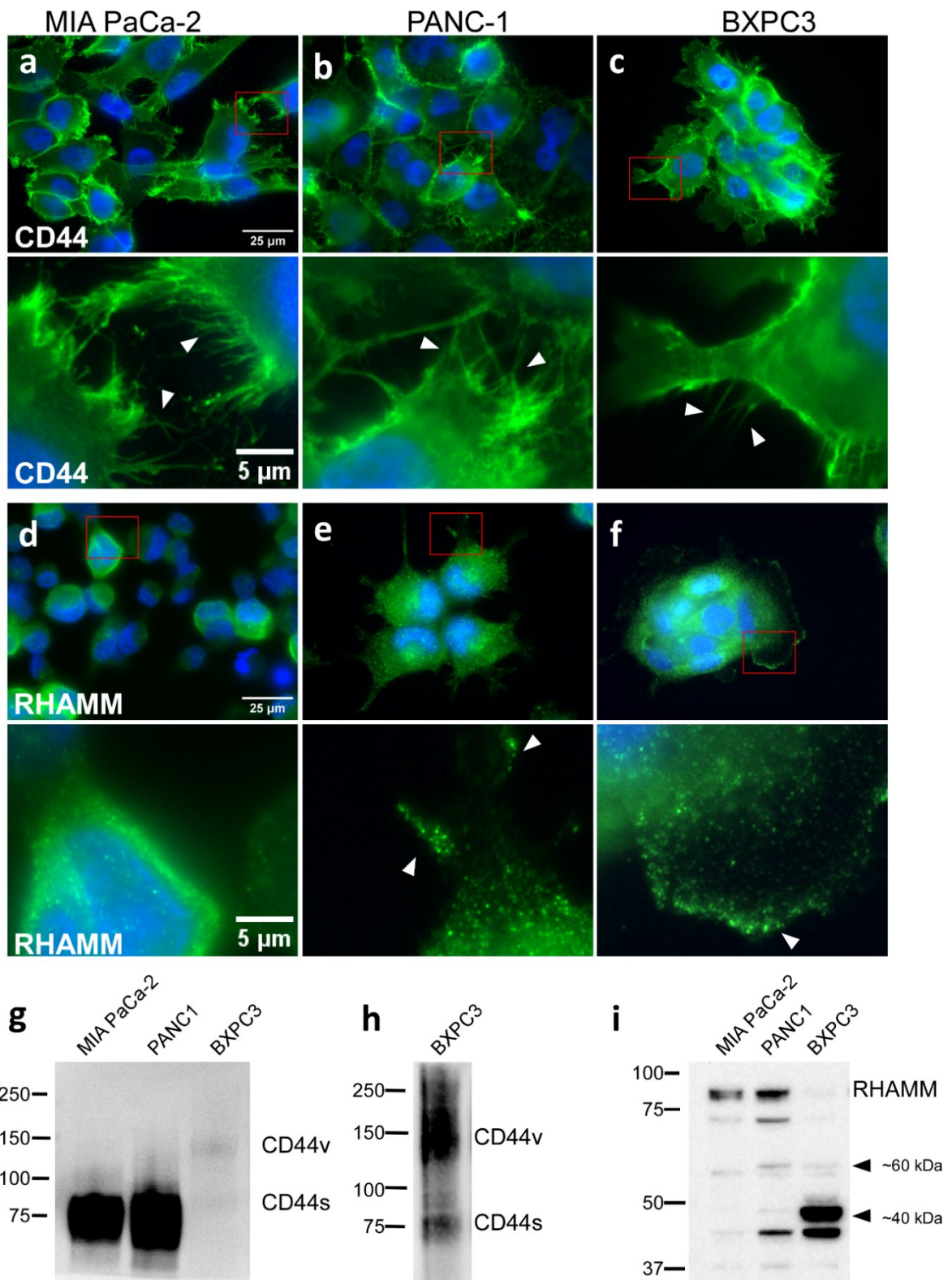
Figure 18. PDAC cells express HA receptors in vitro. a-c) Immunocytochemistry in MIA PaCa-2, PANC1 and BXPC3 cells of HA receptors using anti-CD44 and **d-f)** anti-RHAM antibodies detected with Alexa 488 conjugated secondary antibody. In the close-up images, the staining of CD44 can be appreciated on membrane protrusions (white arrowheads). **g-h)** Immunoblotting for CD44 and **i)** RHAMM using whole cell lysates of MIA PaCa-2, PANC1 and BXPC3 cells.

4.3 Proliferation and migration of PDAC cell lines treated with exogenous HA

Although there were some effects of hPSC CM on PDAC cells, there were no drastic changes in PDAC cell proliferation or migration. Therefore, we studied how PDAC cells responded to the addition of exogenous HA to the culture media. We used commercially produced HA (R&D systems) at 4 different molecular weights, UL-HA at 4.66 kDa, L-HA at 33 kDa, M-HA at 205 kDa and H-HA at >1520 kDa and three concentrations were tested 30, 100 and 300 ug/ml of HA. Cells were grown for up to 96 h in DMEM supplemented with 10% NU-S 10 mM glucose and proliferation was measured every 24 h. Due to the variability seen in previous growth experiments, we focused on using only the SRB assay to measure proliferation in these experiments.

There were no significant changes in cell proliferation (**Figure 19a-l**) with any of the exogenous HAs of different molecular weights in any of the PDAC cell lines, which is at odds with previous reports that show HA can increase PDAC cell proliferation (Kim et al., 2021). Oppositely, H-HA has been shown to inhibit cancer cell proliferation (Amorim et al., 2020; Enegd et al., 2002; Mueller et al., 2010). We also assessed proliferation by coating the cell culture plates with HA at 300 µg/ml instead of adding HA to the culture media. Similarly, there were no significant effects on cell proliferation under these conditions either (**Figure 20**).

We then assessed the effect of exogenous HA, of different molecular weights on cell migration. The system used to assess the migration of hPSC conditioned media was also used in these experiments. Similar to the proliferation assays, we studied HA in two ways, by coating cell culture plates with HA and by adding HA to the culture media (**Figure 21**). Coating the plates with H-HA did not affect cell migration in any cell line (**Figure 21a,c,e**). The same negative effect was observed when HA was added to the media on MIA PaCa-2 or PANC1 cells (**Figure 21b,d**). However, there was a significant increase in migration in BXPC3 cells with H-HA added to the media (**Figure 21f**). To see this effect more clearly H-HA treated BXPC3 cells were plotted separately in **Figure 22a**. Representative images of migration of BXPC3 cells treated with H-HA show the degree of gap closure over time (**Figure 22c**). This becomes more evident when analysing the migration rate (µm/h) which shows a 2-fold increase in migration rate compared to the control (**Figure 22b**). This result was somewhat surprising considering that the reported data generally shows that H-HA is associated with the inhibition of cell proliferation and UL-HA with the promotion of proliferation, therefore we decided to further investigate these inconsistencies.
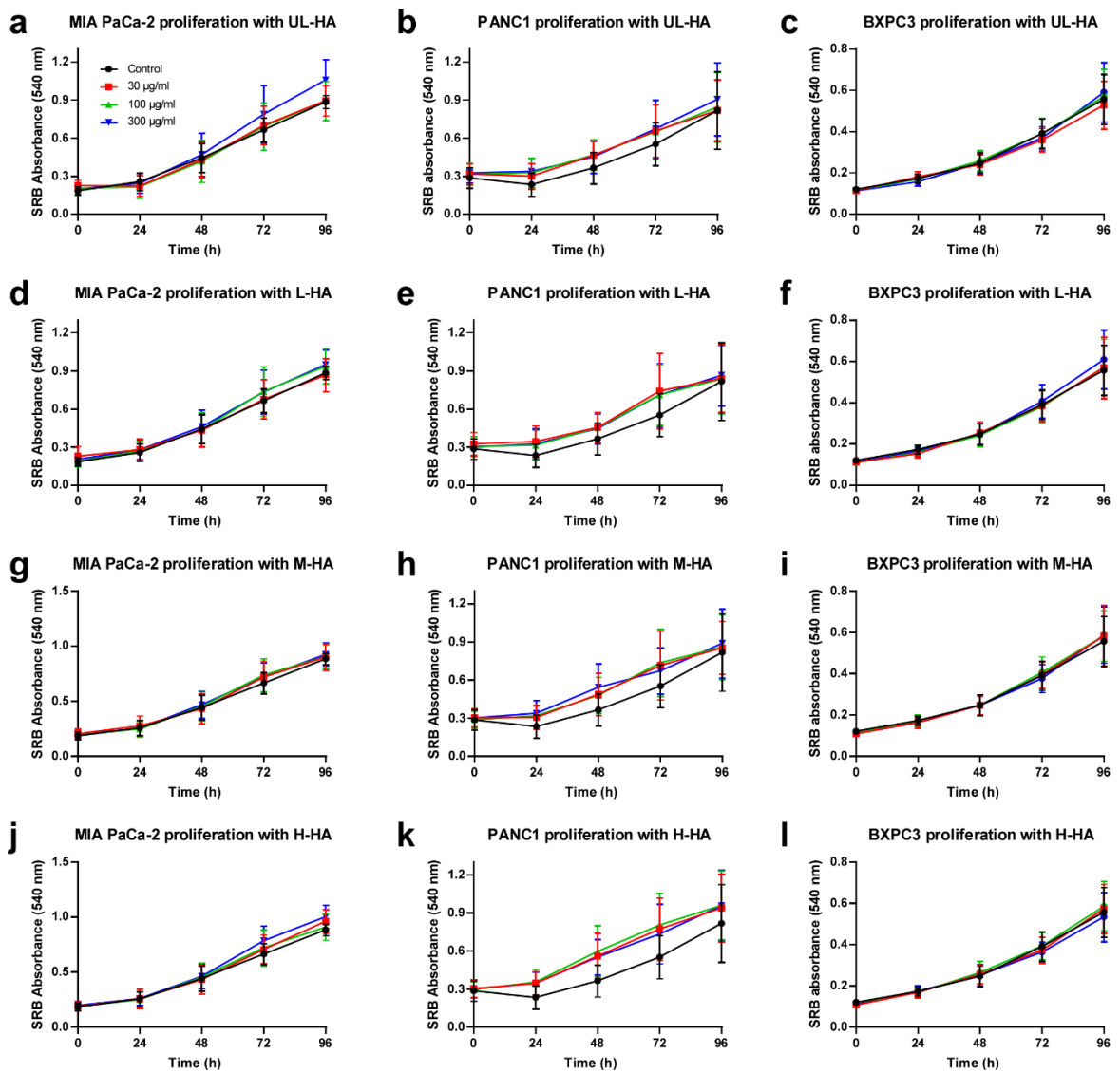
Figure 19. HA does not affect proliferation independent of its molecular weight. MIA PaCa-2, PANC1 and BXPC3 cells were cultured for 96 h and proliferation was measured by the SRB assay every 24 h. The cells were cultured in DMEM with 10% NU-S, and 10 mM glucose supplemented with HA of different molecular weights at a concentration of 30 µg/ml (**red line**), 100 µg/ml (**green line**) and 300 g/ml (**blue line**). **a-c)** PDAC cells were incubated with UL-HA (4.66 kDa). **d-f)** PDAC cells were incubated with L-HA (33 kDa). **g-i)** PDAC cells were incubated with M-HA (205 kDa). **j-l)** PDAC cells were incubated with H-HA (1500 kDa).

a

MIA PaCa-2 proliferation on coated HA

SRB absorbance (540 nm)

- ● Control
- ■ UL-HA
- ▲ L-HA
- ▼ M-HA
- ♦ H-HA

Time (h)

b

PANC1 proliferation on coated HA

SRB absorbance (540 nm)

Time (h)
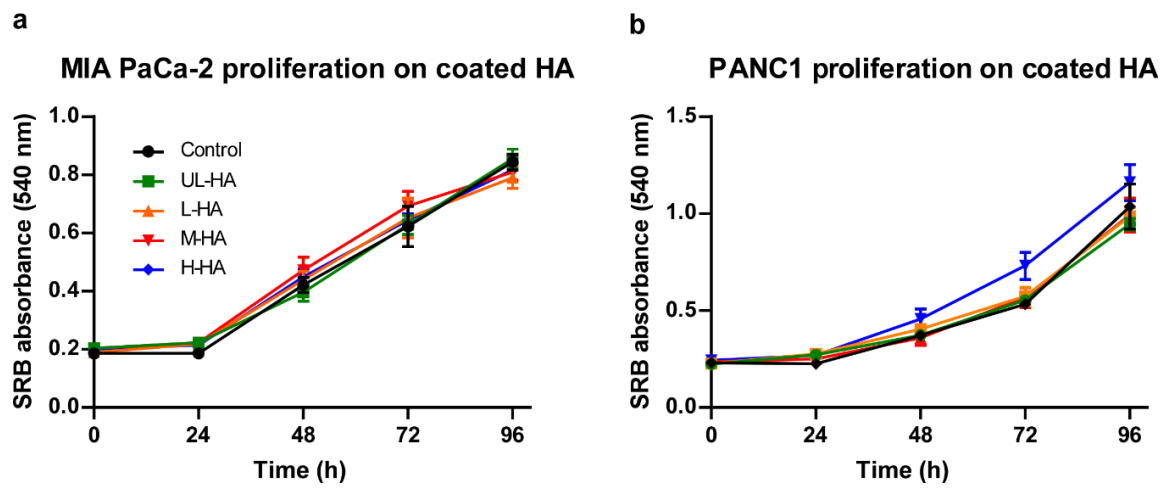
Figure 20. Coating plates with HA does not affect PDAC cell proliferation. Culture plates were coated with HA of different molecular weights (UL, L, M and H) at 300 µg/ml for 24 h at 4°C. MIA PaCa-2 and PANC1 cells were seeded on the prepared HA coated plates and cell proliferation was measured every 24 h up to 96 h using the SRB assay.
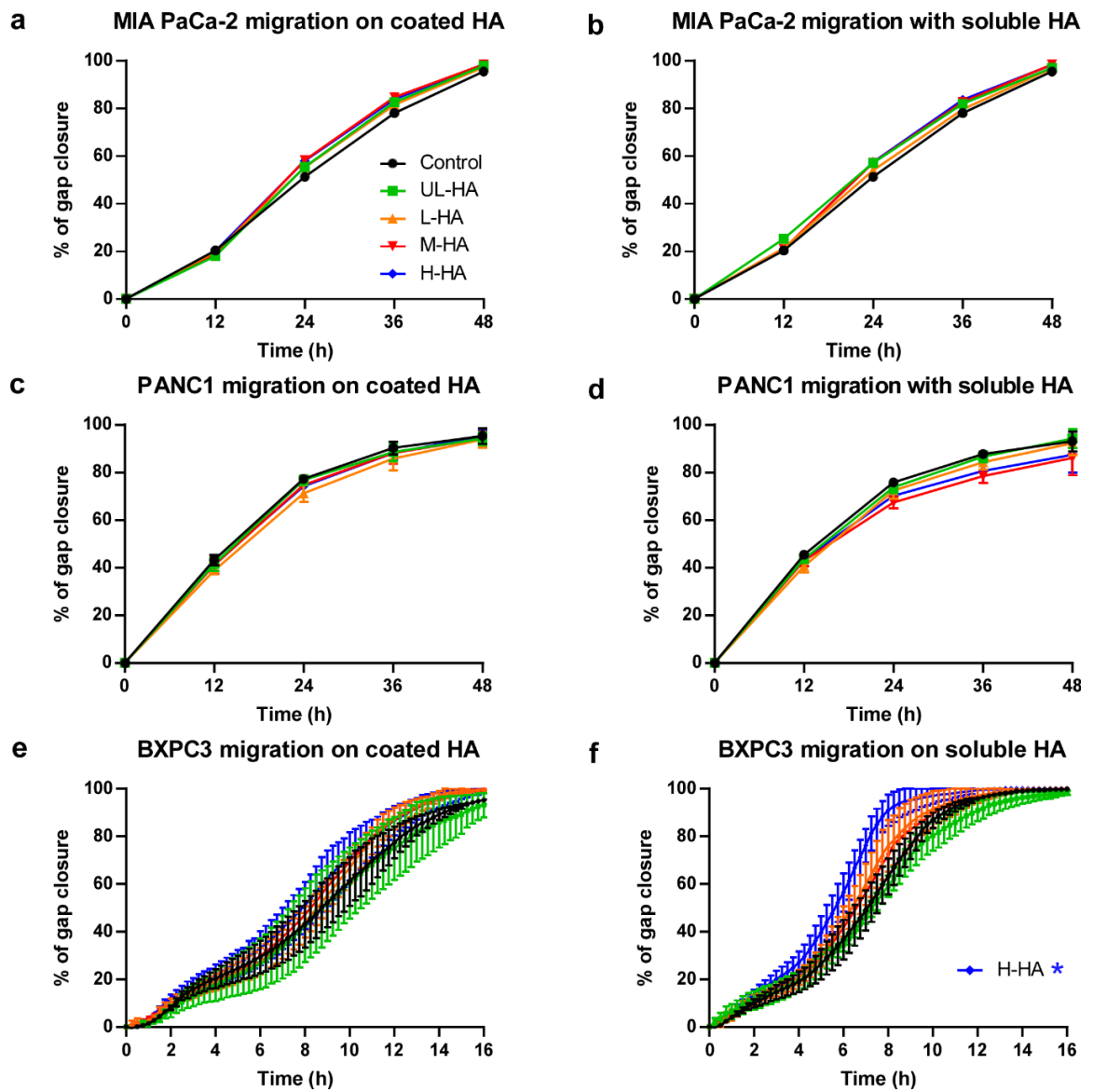
Figure 21. H-HA increases migration of BXPC3 cells but not MIA PaCa-2 or PANC1 cells. MIA PaCa-2, PANC1 and BXPC3 cells were seeded into IBIDI 2-well silicone inserts for 24 h. The insert was removed, and the media was changed to DMEM 10% NU-S 10 mM glucose supplemented with mitomycin C (2 µg/ml) and HA of different molecular weights (UL, L, M, H) at 300 µg/ml. **a, c, e)** PDAC cells grown on culture plates precoated with HA. **b, d, f)** PDAC cells were treated with soluble HA. Images were taken every 12 h for MIA PaCa-2 and PANC1 cells. For BXPC3 cells, images were taken every 15 min for up to 16 h. Analysis of gap closure was processed in Fiji ImageJ. Two-way ANOVA using Tukey's multiple comparison test was used for analysis (*$p < 0.05$) (n=3).
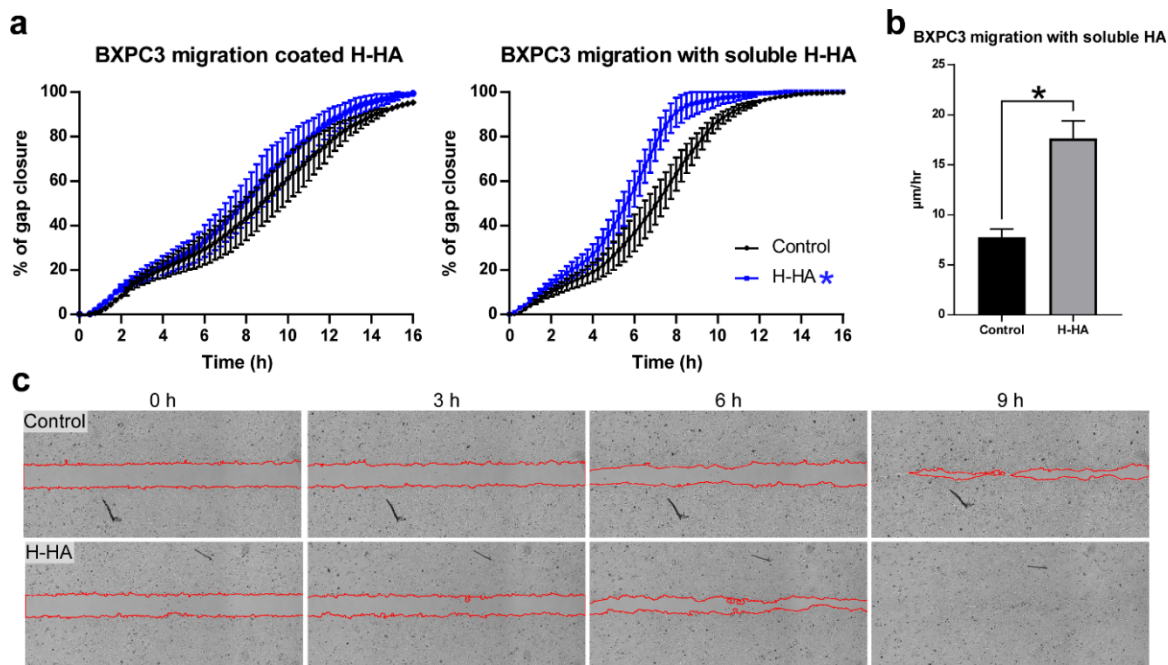
Figure 22. The migration rate increases in H-HA treated BXPC3 cells. a) Migration represented by the percentage of gap closure over a 16 h period. **b)** Migration in µm/hr was calculated by measuring the width at 0 h minus the width at 50% of gap closure in control versus H-HA treated BXPC3 cells. **c)** Representative images of the gap closure assay in BXPC3 cells. Gap is delimited by the red lines. Two-way ANOVA using Tukey's multiple comparison test was used for analysis of % of gap closure (*p<0.05). Two-tailed unpaired t-test was used for analysis of migration rate(*p<0.05) (n=3).

4.4 Discussion

Following the characterisation and optimisation for activation of hPSCs for hPSC-derived HA production and the subsequent collection of hPSC CM, we next wanted to test the effect of this optimised hPSC CM on PDAC cell proliferation and migration, two key cancer hallmark responses. Our results showed no major changes in cell proliferation in PDAC cells treated with hPSC CM from either TGF-β activated or non-activated PSC. Even when the hPSC CM was filtered to capture macromolecules above 3 kDa and resuspended in fresh media to control for nutrient depletion and metabolite accumulation, no increase or decrease in cell proliferation was observed. This suggests that hPSC-derived HA in the conditioned media, despite the high levels of HA produced by hPSC cells, nor any other hPSC-derived macromolecules, had any effects on PDAC cell growth. This is despite attempts to control for any confounding effects of nutrient depletion/metabolite accumulation within the hPSC CM and optimization of PDAC cell growth conditions so that any changes could be appropriately observed. These findings conflict with previous reports, as increased proliferation was observed in PDAC cells MIA PaCa-2 and PANC1 when incubated with CM from PSCs (Vonlaufen et al., 2008). This proliferation was in part mediated by PDGF, since using neutralizing antibodies against PDGF decreased MIA PaCa-2 cell proliferation. However, the protocol used to collect hPSC CM was not specified, therefore we cannot determine the main differences with our study other than the outcome. TGF-β activated hPSC CM increased migration but only in MIA PaCa-2 cells, consistent with the previous study by (Vonlaufen et al., 2008). Nevertheless, there was no corresponding increase in migration with hPSC-CM on PANC1 or BXPC3 cells in the present study, which is at variance with the study by Vonlaufsen et al (2008) who showed that PSC CM increased PANC1 migration. It is important to mention that in this study even though hPSCs were assessed for α-SMA, there is no mention of the percentage of α-SMA$^+$ cells which could have important effects on the outcome of the experiments.

In a different study CM from PSCs also increased proliferation in the PDAC cell lines BXPC3 and PANC1, however in this case the CM was prepared differently (Hwang et al., 2008). In this study hPSCs that were more than 95% positive for α-SMA were used to obtain hPSC CM. The hPSC CM was also processed differently, it was concentrated using filters and then this concentrated CM was applied to the PDAC cells. This differs from our approach in which we added back the filtered CM to fresh media at the equivalent concentration (i.e., filtration condenses the volume to 10%, so this is added back to fresh media 1 in 10 dilutions) to not influence the results. Furthermore, our hPSC in culture only reached approximately 60% of α-SMA$^+$ cells when activated by TGF-β, even though HA was being synthesized by these cells and released into the CM, this level of activation may have been inadequate to produce enough HA into the CM to increase cell proliferation and thus may explain our observed lack of response. There could also be a mixed population of myCAFs and iCAFs that could be contributing differently to the CM and affecting the outcome. Further studies would be required to dissect the specific mechanism.

We next characterized HA receptors in our PDAC cell lines to determine whether the lack of effect of hPSC CM was due to a lack of HA receptors. CD44 was expressed in all three cell lines mainly associated with the plasma membrane and specifically within filopodia-like structures of the membrane. In a gastric cell line, CD44 has been detected in filopodia, colocalizing with HA (Harkonen et al., 2019). This is also seen in gastroesophageal cancer cell lines, where CD44 and HA colocalize in filopodia (Twarock et al., 2010). However, even though CD44 can be found in filopodia, it is not essential in their development (Kyykallio et al., 2020). Immunostaining for RHAMM revealed a mainly cytoplasmic expression in MIA PaCa-2 cells, while there was a mixed cytoplasmic and membrane expression for RHAMM in PANC1 and BXPC3 cells. RHAMM is known to have a dual function, on the membrane, it can bind to other proteins like CD44 and activate signalling pathways like ERK1/2 and induce tumour cell motility (Hamilton et al., 2007). It can also participate in cell adhesion as seen in a fibrosarcoma cell line (Kouvidi et al., 2011). Intracellularly RHAMM can bind to the centrosome and microtubules in the mitotic spindle adding stability to the mitotic process (Maxwell et al., 2003).

The detection of CD44 revealed that MIA PaCa-2 and PANC1 cells expressed CD44s, while BXPC3 expressed CD44v with only a faint band for CD44s. Previous studies have found this to be the case for BXPC3 cells, as CD44v3 and CD44v6 have both been found in this cell line while CD44s was mostly detected in MIA PaCa-2 and PANC1 cells(Zhao et al., 2016). CD44s have been shown to be the most prominent variant in the EMT phenotype in PDAC cells (Zhao et al., 2016). The CD44v6 variant has recently been found to be highly expressed in PDAC patients with liver metastasis where it can promote liver fibrosis and is associated with poor survival (Xie et al., 2022). Detection of RHAMM protein revealed three variants of different molecular weights with varying levels of intensity among the three PDAC cell lines (~80, ~60 and ~40 kDa). The 80 kDa band was the predominant variant found in MIA PaCa-2 and PANC1 lysates while the lower 40 kDA band was most prominent in BXP3 lysates. These three variants have been found in several studies (Hamilton et al., 2007; Kouvidi et al., 2011; Lin et al., 2021). The 40 kDa variant could associate with ERK1/2 while the 80 and 60 kDa were found to associate with CD44 (Hamilton et al., 2007). As we previously mentioned the interaction between CD44 and RHAMM has been shown to promote cell motility (Hamilton et al., 2007).

Due to the lack of effects of hPSC CM despite the presence of HA receptors, we next tested the effects of exogenously applied HA (of varying molecular weight), to control the concentration of exogenous HA more effectively. Results show that none of the exogenously applied HAs, of any molecular weight, whether added to the media or coating the plates had any effect on cell proliferation in any of the three PDAC cell lines (MIA PaCa-2, PANC1 or BxPC3). There is limited evidence regarding proliferation by HA but most studies suggest that H-HA induces proliferation. In a study using vascular smooth muscle cells, they showed opposite effects for HA depending on their molecular weight (Cuff et al., 2001). This study showed that L-HA (of undisclosed molecular weight) stimulated cell proliferation while H-HA (of undisclosed molecular weight) decreased proliferation. Both effects were mediated by CD44, this was corroborated by using a neutralizing anti-CD44

antibody and CD44 knockout cells. This was reproduced in two more studies of the same group (Kothapalli et al., 2008; Kothapalli et al., 2007). On the contrary, two studies in breast cancer cells showed increased proliferation with H-HA (~1000 kDa and 500 kDa) (Bourguignon et al., 2003; Bourguignon, Xia and Wong, 2009). In a human oral squamous carcinoma cell line, the same group also saw increased growth when cells were treated with H-HA (500 kDa) (Bourguignon et al., 2006). In a study in a human leukemic cell H-HA (1500-1800 kDa) also induced proliferation (Lompardia et al., 2013). An important detail lacking in all these studies is the effect that endogenous hyaluronidases can have on exogenous HA, as they can be present in the cell membrane degrading HA (Udabage et al., 2005; Wu et al., 2015).

Our analysis of cell migration revealed interesting differences among PDAC cell lines. BXPC3 cells migrated the fastest followed by PANC1 cells and MIA PaCa-2 cells migrated the slowest. BXPC3 were the only cells that responded to incubation with HA, specifically with H-HA, which induced a 50% increase in the migration rate compared to the untreated control. This is partially in line with the only study of PDAC cell migration treated with exogenous HA. In this previous report there was an almost universal increase in migration with L-HA (25-75 kDa) in the 8 PDAC cell lines tested. When PDAC cell lines were incubated with H-HA (400-600 kDa), migration only increased in 4 out of the 8 cell lines tested. Interestingly, BXPC3 cells were among the cell lines that showed an increase in migration (Cheng et al., 2016). However, this migration was measured using the Boyden chamber assay, which measures the migration of cells through a porous membrane while the assay used in our study measures cells migrating into a cell-free area, so there are intrinsic differences in these assays that could explain some disparity. One other important point to note is that exogenous HA used in these studies can largely vary in molecular weight and origin. There is no standardized classification of the use of exogenous HA which makes comparisons more difficult.

Chapter 5   Autocrine effect of endogenous hyaluronic acid on PDAC cells

5.1 Characterization of HA in PDAC cells

The effect of exogenously applied HA of different molecular weights on PDAC cell proliferation and migration was unexpectedly minimal. Only BXPC3 cells exhibited an increase in migration in response to H-HA. A similar increase in cell migration has been reported in breast cancer and hepatoma cell lines (Bourguignon et al., 2010; Fuchs et al., 2013). However, this effect seems to be cell specific since H-HA (of unspecified molecular weight) has also been reported to inhibit migration in a fibrosarcoma cell line (Berdiaki et al., 2009). Due to the conflicting data reported, we first attempted to fully characterise the endogenous location and synthesis of HA in our PDAC cell lines and determine whether this may influence the effects or lack of effect of exogenously applied HA. This was achieved using a recombinant HA binding protein (Versican G1 domain) conjugated to biotin that can be detected using streptavidin conjugated to FITC (HABP/FITC-streptavidin).

MIA PaCa-2, PANC1 and BXPC3 all showed positive staining for HA; however, its cellular localisation was different for each cell line (**Figure 23a-c**). MIA PaCa-2 and PANC1 cells showed a pericellular staining mixed with an intracellular staining pattern, while BXPC3 exhibited a predominantly punctate intracellular staining (**Figure 23c**) rather than pericellular staining seen with MIA PaCa-2 and PANC1 cells (**Figure 23a**-b). We grew all PDAC cells in serum free media for 48 hrs and collected the media to examine the concentration of HA present in the media using an ELISA-based assay (**Figure 23d**). This also revealed differences between cell lines where PANC1 released nearly 600 ng/ml of HA into the media, BXPC3 cells more than 200 ng/ml and MIA PaCa-2 secreted the lowest at around 40 ng/ml. Given the marked pericellular staining in MIA PaCa-2 cells, we investigated this further to see if there was any association with HA receptors. MIA PaCa-2 cells double labelled against CD44 and HA (**Figure 23e**), show a close relationship between the presence of CD44 and HA as seen by the overlap of the fluorescence intensity profiles between CD44 and HA. When the labelling of CD44 is negative so is the labelling of HA as seen in the fluorescence intensity profile (**Figure 23f**).

Altogether these results show that these cell lines have different mechanisms of HA turnover which could impact how they respond to exogenously added HA. It has been recently shown that endogenously synthesized HA can fuel pancreatic cancer cell growth (Kim et al., 2021). Based on the heterogeneity of HA staining within the different PDAC cells we further investigated other components of HA turnover. We focused on two important mechanisms in HA turnover this includes HASs responsible for the synthesis of HA and HYALs responsible for the degradation of H-HA into smaller fragments.
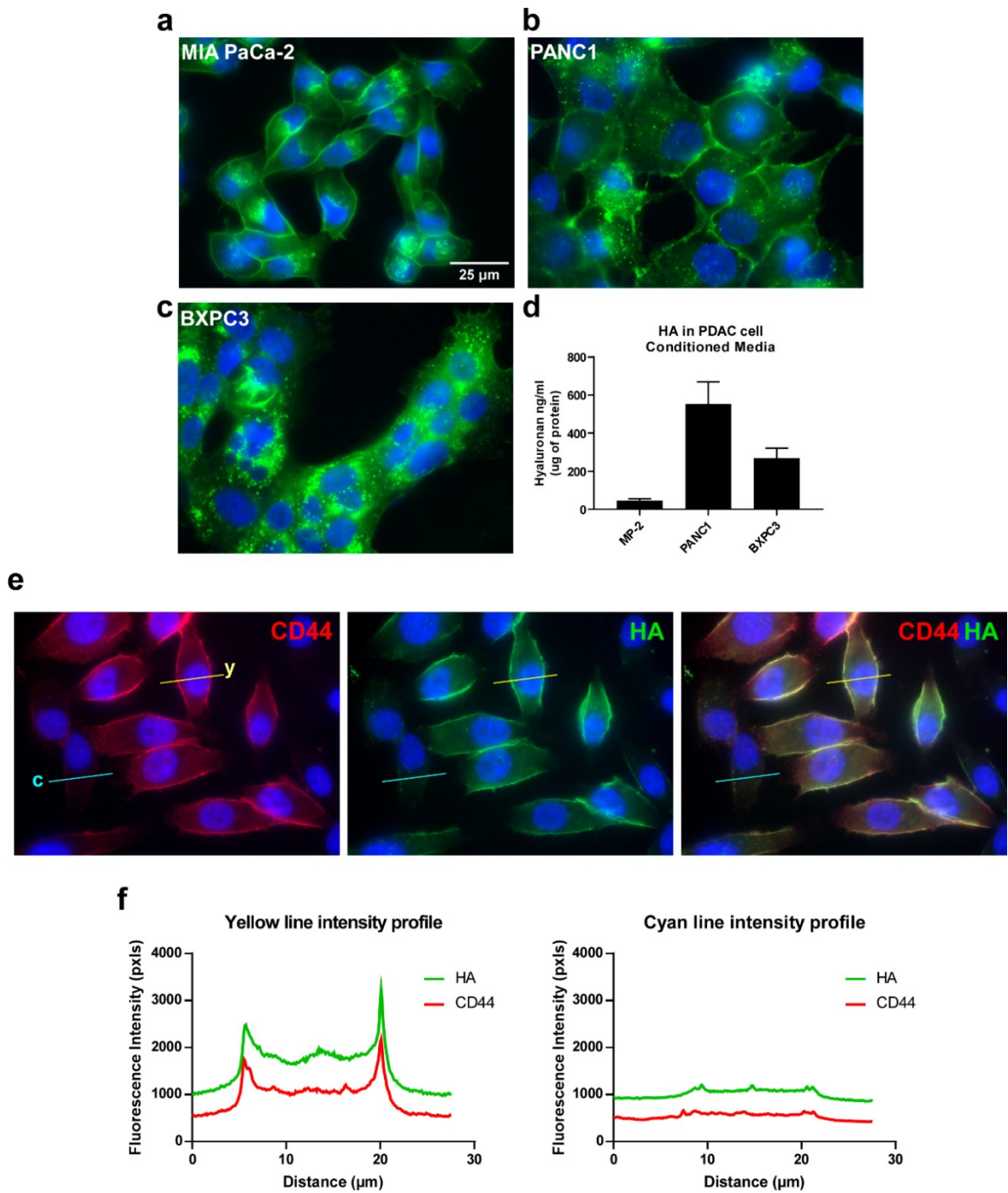
Figure 23. Characterization of HA in PDAC cells. **a-c)** PDAC cells were fixed in PFA and the presence of HA was analysed using a biotinylated HA binding protein (Versican G2 binding domain) that was detected with FITC-conjugated streptavidin (HABP/FITC-streptavidin). **d)** PDAC cells were seeded in T75 flasks. After 24 h the media was replaced with serum free media and the cells were incubated for a further 48 h. PDAC cell CM was collected and an HA ELISA-based assay was used to detect HA in the PDAC cell CM. **e)** MIA PaCa-2 cells were labelled with CD44-Alexa 594 and HABP/FITC-streptavidin. Line intensity profiles were traced in positive cells (y, yellow line) and negative cells (c, cyan line). **f)** Intensity profile plots for CD44 and HA.

5.2 Characterization of HAS2 and HYAL2 in PDAC cells

HASs are an important component of HA turnover, they are a family of transmembrane enzymes responsible for the synthesis of HA from two precursors UDP-GlcUA and UDP-GlcNAc. We focused on Hyaluronan synthase 2 (HAS2) as it has been extensively shown to be associated with several types of cancer including breast, colorectal and ovarian cancer and has been known to promote invasion, tumour cell survival and contribute to several characteristics of malignant phenotypes (Kim et al., 2019; Riecks et al., 2022; Sheng et al., 2021).

Several HYALs can break down HA, however, we focused on HYAL2 (McAtee, Barycki and Simpson, 2014). HYAL2 is an extracellular facing, GPI-anchored, lipid raft associated enzyme (Andre et al., 2011) that can breakdown HA into 20 kDa fragments which can then be internalized by endocytosis or micropinocytosis (Greyner et al., 2010; Tammi et al., 2001). Increased HYAL2 expression has been associated with malignant melanoma (Siiskonen et al., 2013) and when overexpressed in the cancer resistance mole rat they become susceptible to cancer (Tian et al., 2013). We chose to investigate the role of HYAL2 in PDAC due to its membrane localization and association with cancer.

We hypothesized that endogenously produced H-HA by HAS2 within PDAC cells was subsequently cleaved into smaller fragments by endogenously expressed HYAL2. This facilitates the interaction of these fragments with HA receptors such as CD44 and RHAMM. Therefore, inhibition of either HYAL2 or HAS2 might be expected to inhibit PDAC cancer hallmarks responses if they have any role in this response.

Both HAS2 and HYAL2 were expressed by all PDAC cell lines (**Figure 24a**) as assessed by standard western blotting of whole cell lysates. However, because HAS2 is a transmembrane protein and HYAL2 is an exofacial plasma membrane-tethered enzyme we sought to determine their cellular location using two different membrane enrichment kits to separate membrane proteins from cytosolic proteins. The Mem-PER Plus kit from Pierce™ is a detergent based extraction kit, through several centrifugation steps a lysate is obtained, enriched in integral membrane proteins and membrane associated proteins. Western blotting of these lysates showed HYAL2 almost exclusively associated with cell membranes compared to HAS2 which was mostly in the cytosol with some detection in the membrane fraction (**Figure 24b**). In addition, we used the Cell Surface Protein Biotinylation and Isolation Kit from Pierce™ which is based on the biotinylation of cell surface proteins followed by a detergent based lysis of the cells and subsequent capture of biotinylated proteins with Neutravidin. This Neutravidin can later be removed, and lysates processed through western blotting. These lysates also showed HYAL2 present in the membrane of all three cell lines (**Figure 24c**). HAS2 was also detected with the cell surface biotinylation, with faint bands in MIA PaCa-2 cells and prominent bands in PANC1 and BXPC3 lysates (**Figure 24c**).
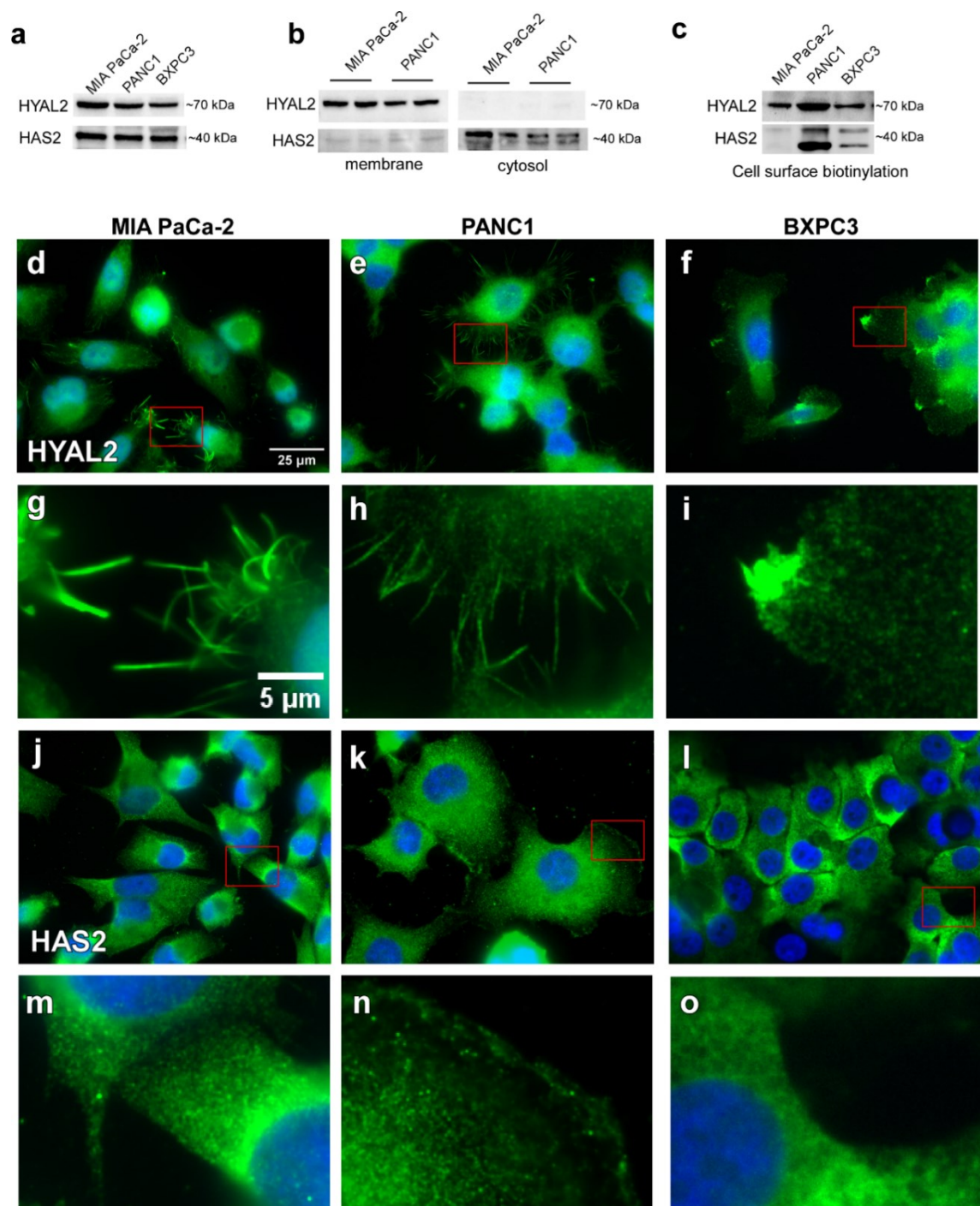
Figure 24. Characterization of HAS2 and HYAL2 in PDAC cells. a) Immunoblotting of whole cell lysates was used to detect HAS2 and HYAL2. **b)** Membrane and cytosol fractions of PDAC cells were prepared using the Mem-PER Plus Membrane Protein Extraction Kit from Pierce™, followed by immunoblotting for HAS2 and HYAL2 detection. **c)** The cell Surface Protein Biotinylation and Isolation Kit from Pierce™ was used to enrich membrane proteins, followed by immunoblotting for HYAL2. **d, e, f)** Immunofluorescence using an anti-HYAL2 antibody (green) in PDAC cells. **g, h, i)** Closeup images of HYAL2 staining in PDAC cells. **j, k, l)** Immunofluorescence using an anti-HAS2 antibody (green) in PDAC cells. **m, n, o)** Closeup images of HAS2 staining in PDAC cells. All immunofluorescence was stained with Hoechst for nuclei detection. Images were processed in FIJI/ImageJ.

Immunofluorescence assays were also used to further study the location of HYAL2 and HAS2 in PDAC cells (**Figure 24d-f**). Because HYAL2 is associated with lipid rafts, we used saponin as a permeabilizing agent because it can remove cholesterol that is enriched in lipid rafts (Simons and Ehehalt, 2002). This improved our visualization of HYAL2 on the cell membrane when using immunofluorescence. In MIA PaCa-2 and PANC1 cells exhibited HYAL2 staining in filopodia-like membrane protrusions (**Figure 24g,h**). These protrusions were more prominent in MIA PACa-2 cells than in PANC1 cells (**Figure 24g**). BXPC3 cells showed a different HYAL2 staining pattern, mainly on the tip of membrane protrusions that resembled lamellipodia. HAS2 showed a more diffuse punctate pattern, with mainly a cytosolic location (**Figure 24i**).

We next wanted to determine the effect of inhibiting hyaluronidases on PDAC cell cancer hallmark responses: proliferation and migration. HYAL2 has been reported to be involved in an autocrine chemokinetic motility system in HeLa cells. This occurs by breaking down H-HA into smaller fragments that promote cell motility (Saito et al., 2011). We used a known inhibitor of HYALs, DSS (Udabage et al., 2004). We first tested DSS for cytotoxicity by incubating PDAC cells for 48h under increasing concentrations of DSS (0.1-1000 µg/ml) (**Figure 25a,b**). Cytotoxicity can also be measured with the WST-8 and SRB assays. This requires a change in the protocol used for proliferation by seeding cells at a much higher density and then applying the treatment for a fixed period of time, usually 24 or 48 h. For MIA PaCa-2 cells, there was an increase in WST-8 signal starting from 1 µg/ml of DSS (**Figure 25a**). However, there are no corresponding changes in the SRB signal at the same concentrations (**Figure 25b**). This suggests that the sharp increase in signal is likely an alteration of the redox state of MIA PaCa-2 cells caused by DSS. In the SRB assay, there is a slight reduction in signal with DSS concentrations greater than 30 µg/ml (**Figure 25b**). This could suggest that DSS could be slightly cytotoxic causing either cell death, growth inhibition or reduction of cell adherence. On the contrary BXPC3 cells showed no signs of cytotoxicity in both WST-8 and SRB assays and did not seem affected by DSS as they maintained a constant signal in all concentrations (**Figure 25a,b**). Even though there was a slight cytotoxic effect of DSS on MIA PACa-2 cells we then studied the effects of DSS (50-400 µg/ml) on cell migration using the gap closure assay. This caused a marked decrease in cell migration of MIA PaC-2 cells reducing migration by approximately 60% (**Figure 25c**). On the other hand, DSS had minimal effects on BXPC3 cell migration (**Figure 25d**).

We next wanted to determine whether exogenously applied HA could reverse the inhibitory effect of DSS. Given that DSS is reported to inhibit HYAL2 (Udabage et al., 2004). According to our hypothesis that HYAL2 cleaves synthesized H-HA into smaller L-HA fragments, we expected that L-HA could reverse the effects of DSS. However, the addition of HA of any molecular weight did not reverse the effects of DSS, at least in MIA PaCa-2 cells (**Figure 26a-d**). The effect of DSS and the subsequent addition of exogenous HA on BXPC3 cells was very different. There was no effect with UL-HA L-HA or M-HA **Figure 26e-g**). We previously showed in Chapter 4 that the addition of

exogenous H-HA increases the migration of BXPC3 cells, when exogenous H-HA was added in combination with DSS, the increase in migration was abolished (**Figure 26h**).

To see these effects more clearly of H-HA and DSS treated BXPC3 cells, those curves were plotted separately (**Figure 27a).** When the migration rate (µm/h) was measured there was a tendency to decrease cell migration in BXPC3 cells treated with H-HA and DSS, even though this decrease was not statistically significant (**Figure 27b**). However, the combined treatment was also not significantly different from the control.

We then studied another component of HA turnover, the HA receptor CD44. This receptor plays an important role in tumour cells that range from proliferation to adhesion, migration, and invasion (Chen et al., 2018; Zoller, 2011). As most of the effects of HA were seen in migration, we studied the effects of blocking the CD44 receptor in gap closure assays. We used the anti-CD44 antibody (KM81) that specifically binds to the HA binding site of the CD44 receptors and blocks its interaction with HA.

Previous reports have shown that KM81 reduces cell migration and invasion (Uchino et al., 2010). We incubated MIA PaCa-2 and BXPC3 cells with concentrations of 1, 5, and 10 µg/ml of anti-CD44 antibody for the complete duration of the gap closure assay. The incubation with the anti-CD44 antibody showed no decrease in the migration of MIA PaCa-2 or BXPC3 cells **(Figure 28a,b).** When MIA PaCa-2 cells were incubated with non-activated and activated hPSC CM in the presence of the KM81 antibody no decrease in migration was observed for the non-activated or activated hPSC CM (**Figure 28c,d**). These results could imply that HA effects on PDAC cells may not be mediated by CD44 or that the blocking of CD44 by the KM81 antibody is not functional in these cell models. To corroborate these results multiple antibodies that block the HA binding site on CD44 should be tested. The next step was to study the last component of HA turnover, HA synthesis. To accomplish this, we used a known blocker of HA synthesis 4-Methylumbelliferone (4-MU) (Kakizaki et al., 2004). HA is a long polysaccharide formed of multiple repeats of a single disaccharide of glucuronic acid (GlcUA) and N-acetylglucosamine (GlcNAc). HAS synthesizes this disaccharide from two precursors, UDP-glucuronic acid (UDP-GlcUA) and UDP-N-Acetylglucosamine (UDP-GlcNAc) which are generated by a UDP-glucuronyltransferase. The mechanism of action of this inhibitor is based on the conjugation of 4-MU to GlcUA generating 4-MU-GlcUA and thereby depleting the pool of UDP-GlcUA and inhibiting synthesis of HA by the low availability of one of its precursors as shown in **Figure 5** (Kakizaki et al., 2004; Kuipers et al., 2016).
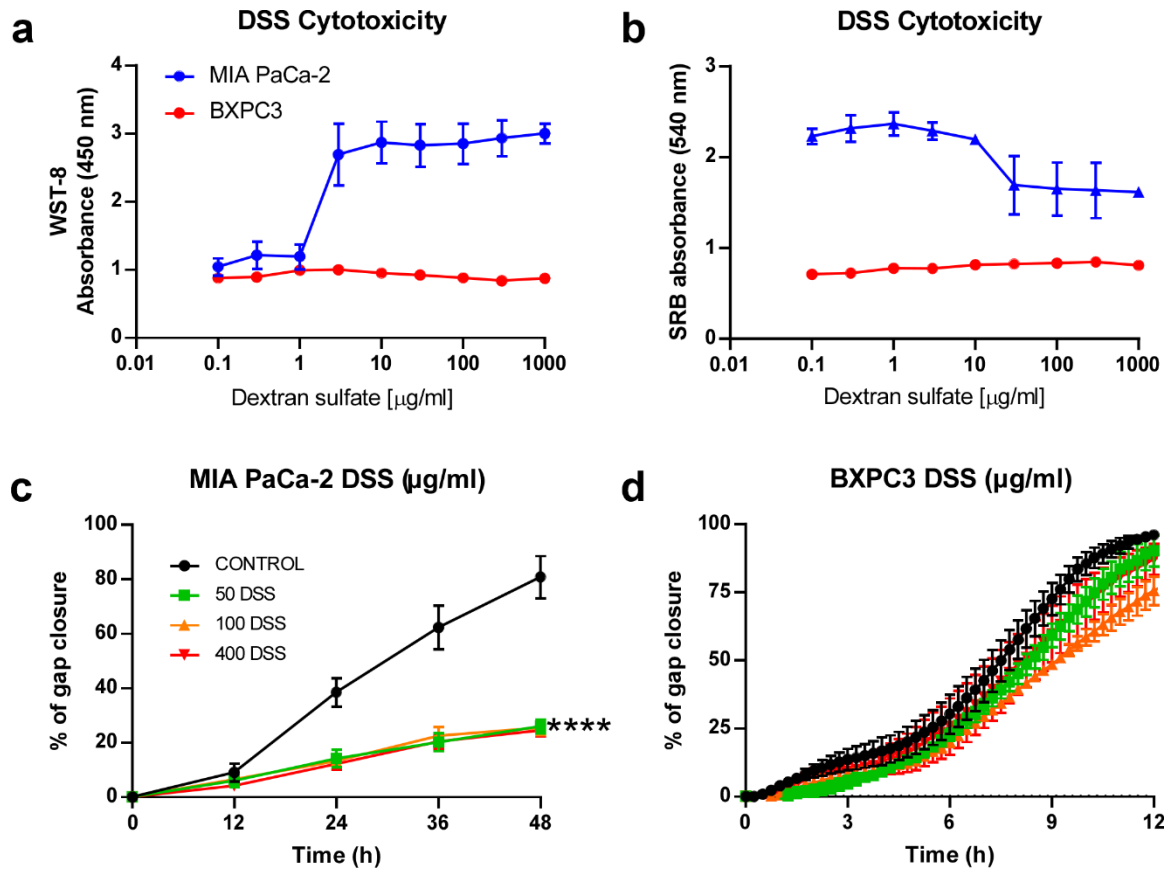
Figure 25. Cytotoxicity and migration effects of hyaluronidase inhibitors. a, b) The hyaluronidase inhibitor DSS was tested to evaluate cytotoxicity using the WST-8 and SRB assays. Cells were seeded for 24 h and later treated with the DSS in increasing concentrations (0.1-1000 µg/ml) for 48 h. **c, d**) Cells were seeded in silicone inserts which were removed after 24 h. Cells were treated with DSS (50, 100, 400 µg/ml) in media containing 2 µg/ml of mitomycin. Images of MIA PaCa-2 cells were taken every 12 h for 24 h. Images of BXPC3 cells were taken every 15 min for 22 h Gap closure was analysed and quantified using Fiji/ImageJ. Two-way ANOVA using Tukey´s multiple comparison test was used for analysis (**** $p < 0.0001$) (n=3).
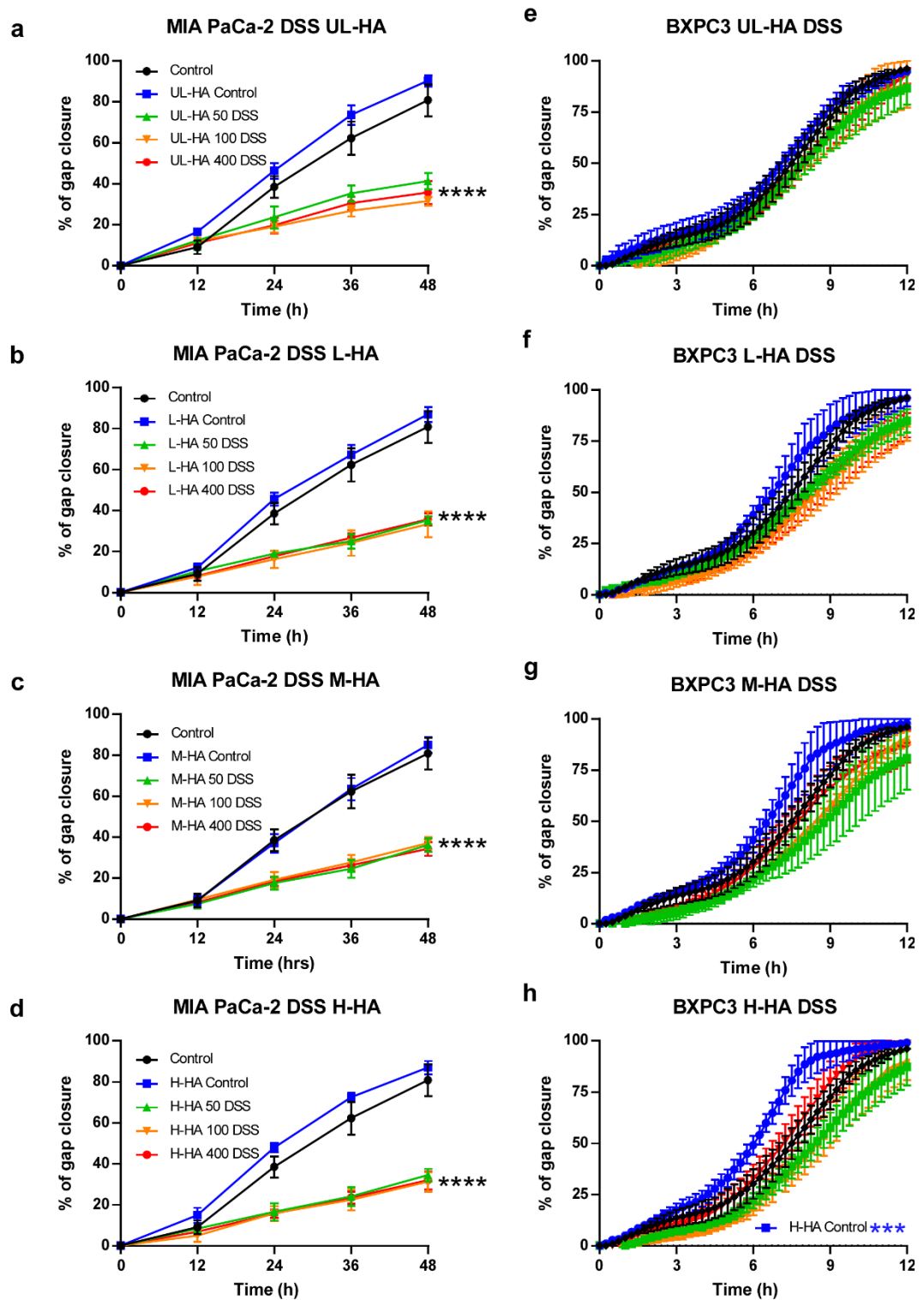
Figure 26. Differential effect of DSS on PDAC cell migration. Cells were seeded into silicone inserts. After 24 h the insert was removed and cells were treated with HA of different molecular weights (UL, L, M, H at 300 µg/ml) and DSS (50,100, 400 µg/ml) in media containing 2 µg/ml of mitomycin. **a-d)** Percentage of gap closure calculated from images of MIA PaCa-2 cells taken every 12 h for 24 h. **e-h)** Percentage of gap closure calculated from images of BXPC3 cells taken every 15 min for 22 h. Gap closure was analysed and quantified using Fiji/ImageJ. ANOVA using Tukey´s multiple comparison test was used for analysis (***p<0.0005, **** p<0.0001) (n=3).
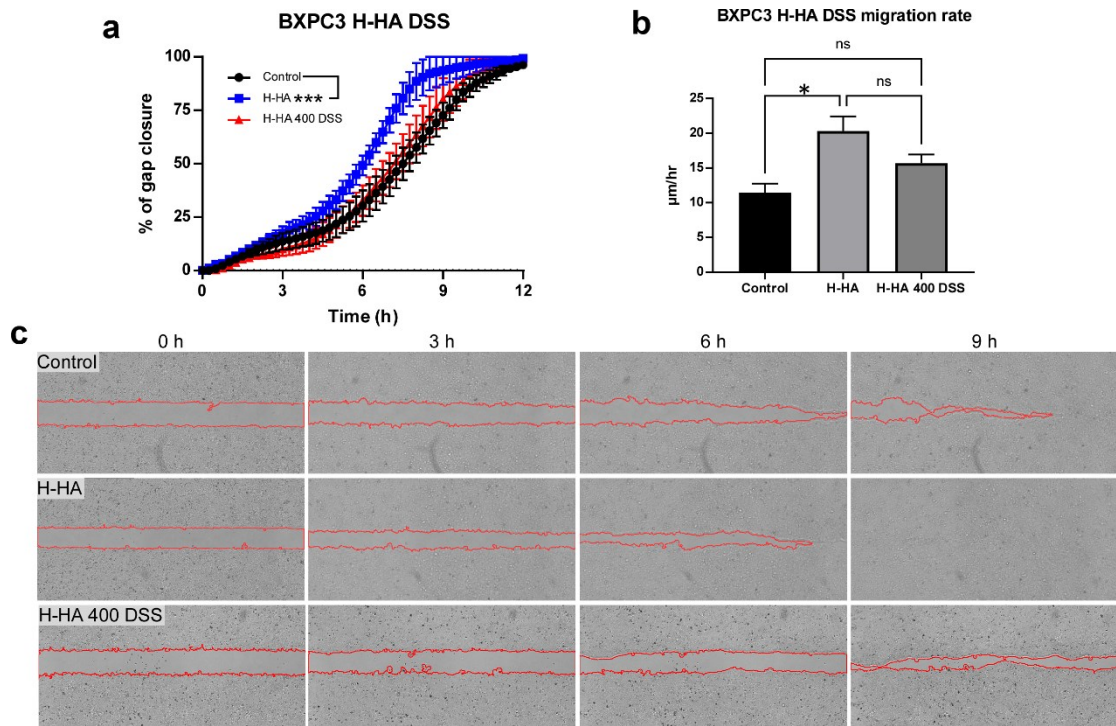
Figure 27. **DSS inhibits the increase in migration by H-HA. a)**. Quantification of gap closure of BXPC3 cells treated with H-HA and DSS. **b)** Migration rate in µm/hr of BXPC3 cell treated with H-HA and DSS **c)** Representative images of the gap closure assay of BXPC3 treated with HA and DSS. Two-way ANOVA using Tukey's multiple comparisons test was used for analysis of % of gap closure (***p<0.0005). One-way ANOVA using Tukey´s multiple comparison test was used for analysis of migration rate (*p<0.05) (n=3).
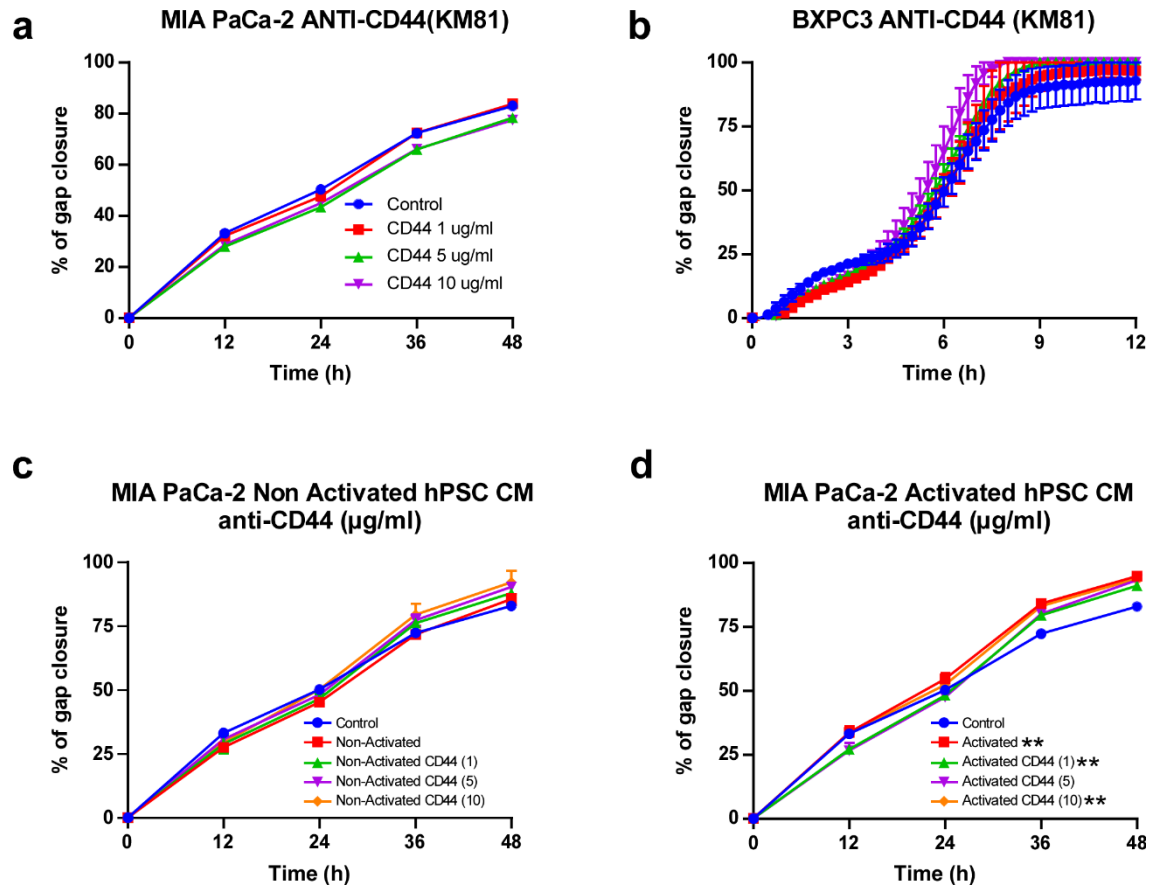
Figure 28. CD44 neutralizing antibody KM81 does not affect cell proliferation or migration in PDAC cells. a,b) Migration was assessed in MIA PaCa-2 and BXPC3 cells by gap closure assays. Cells were incubated in media containing mitomycin C and increasing concentrations of anti-CD44 antibody (KM81) at 1, 5 and 10 µg/ml. **c,d)** Migration was assessed in cell incubated in non-activated or activated hPSC CM containing mitomycin C and increasing concentrations of CD44 as previously mentioned. Two-way ANOVA using Tukey's multiple comparisons test was used for analysis of % of gap closure (**$p<0.005$) (n=3).

We studied the effects of 4-MU on proliferation and migration in MIA PaCa-2 and BXPC3 cells. MIA PaCa-2 cell proliferation was affected showing a 2-fold decrease using the WST-8 assay (**Figure 29a**). However, when the SRB was analysed, the data showed a different situation. There were no significant changes to SRB absorbance (**Figure 29c**). Therefore, 4-MU may be causing an alteration to the redox state of the cell. This could mainly be due to the depletion of NADPH which is a key component of the cell's redox system and the functional basis of how the WST-8 assay measures cell viability/proliferation. NADPH is an important cofactor in the synthesis cascade of HA, especially in the mechanism of action of 4-MU by the conjugation of 4-MU to GlcUA. There were no major effects of 4-MU on BXPC3 cell proliferation at 100 µM 4-MU (**Figure 29b, d**). When gap closure was examined 4-MU did not affect MIA PaCa-2 cell migration (**Figure 29e**) but it reduced migration in BXPC3 cells at 100 µM 4-MU (**Figure 29f**). These results indicate a possible involvement of endogenously synthesized HA in BXPC3 cell migration. We next analysed the effects of 4-MU on HA distribution in PDAC cells by immunofluorescence-like assays with HABP/FITC-streptavidin. MIA PaCa-2 cells showed a decrease in pericellular HA which was clearly observed by plotting a line intensity profile (**Figure 29g**). In BXPC3 cells changes were less obvious as the staining of HA is diffuse with punctate intracellular staining (**Figure 29h**). Analysing cells using 3D surface plots of fluorescence no clear observation could be made, apart from a slight decrease in overall fluorescence in 4-MU treated BXPC3 cells (**Figure 29h**).

5.3 Strategies for removing endogenous pericellular hyaluronic acid from PDAC cells.

From experiments shown previously in this chapter, we established that PDAC cell lines synthesize HA endogenously (**Figure 30a-c**), however, each cell line exhibited different locations throughout the cell, with spotty or punctate patterns in the cytoplasm or a pericellular distribution. We next wanted to know if the endogenous pericellular HA coating had any functional role in PDAC, for example through activation of HA receptors. Firstly, bovine testes hyaluronidase (HAdase) was used to remove the pericellular HA coating. This enzyme can degrade HA and has previously been demonstrated as a successful method of removing HA from cells in culture by removing extracellular HA from a breast cancer cell line (Sullivan et al., 2018). Using the same methodology, we used HAdase to remove HA from MIA PaCa-2 cells. The cells were incubated at 37°C for 1, 2, 3 or 4 h with 200, 400, or 800 µg/ml of HAdase prepared in serum free DMEM with 0.1% BSA. After the HAdase treatment cells were fixed in 4% PFA and HA was detected using the biotinylated HABP/FITC-streptavidin system. Fluorescent images were taken of control cells and HAdase treated cells. These images show the distinct pericellular distribution of HA in MIA PaCa-2 cells in the controls at all 4-time points (**Figure 30b**). On the other hand, in all the different concentrations of HAdase and different incubation time points, the pericellular distribution was lost and only cytoplasmic staining could be seen (**Figure 30b**). This proved the effectiveness of the HAdase in degrading HA and removing the extracellular coating. Higher incubation times with the HAdase had no further effect on removing HA therefore the lowest incubation time of 1 h was used for the following experiments.
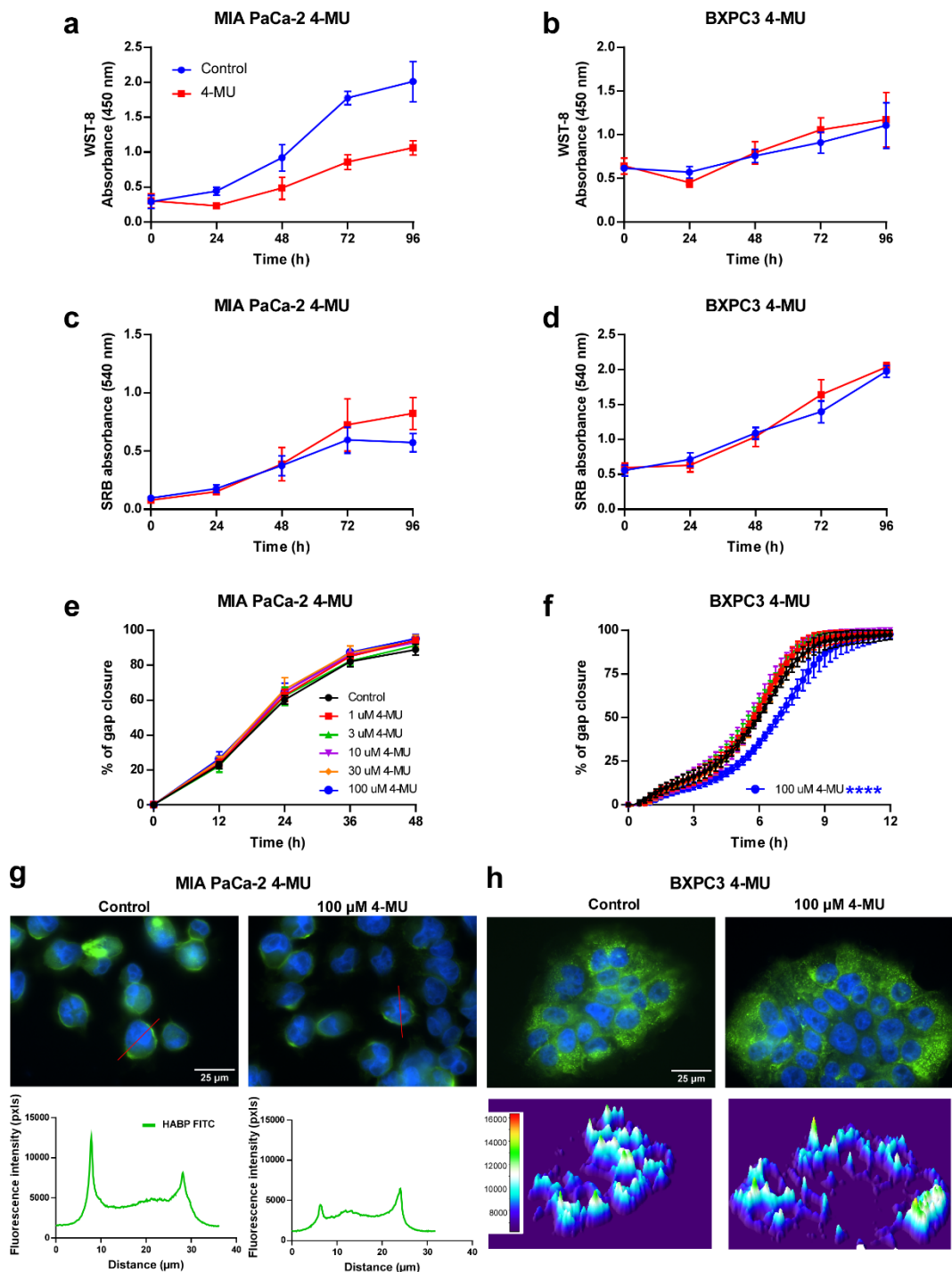
Figure 29. The HAS inhibitor 4-methylumbeliferone differentially decreases migration but not proliferation of PDAC cells. a-d) Cells were grown media with 10% NU-S and 10 mM glucose, supplemented with 100 µM 4-MU for up to 96 h. Proliferation was measured every 24 hrs with the WST-8 and SRB assays. **e, f)** Gap closure assay was used to assess migration of MIA PaCa-2 and BXPC3 cells incubated in media supplemented with mitomycin C and increasing concentrations of 4-MU (1, 3, 10, 30, 100 µM). **g)** The effects of 4-MU on endogenous HA were studied by staining HA with HABP/FITC-streptavidin in MIA PaCa-2 cells. The pericellular HA was studied by line profiles of fluorescence intensity generated in FIJI ImageJ. **h)** The effects of 4-MU on endogenous HA were studied by staining HA with HABP/FITC-streptavidin in BXPC3 cells.). Pseudo-coloured fluorescence intensity 3D surface plots were generated in FIJI ImageJ to study fluorescence distribution in BXPC3 cells. Two-way ANOVA using Tukey's multiple comparisons test was used for analysis of % of gap closure (****p<0.0001) (n=3).
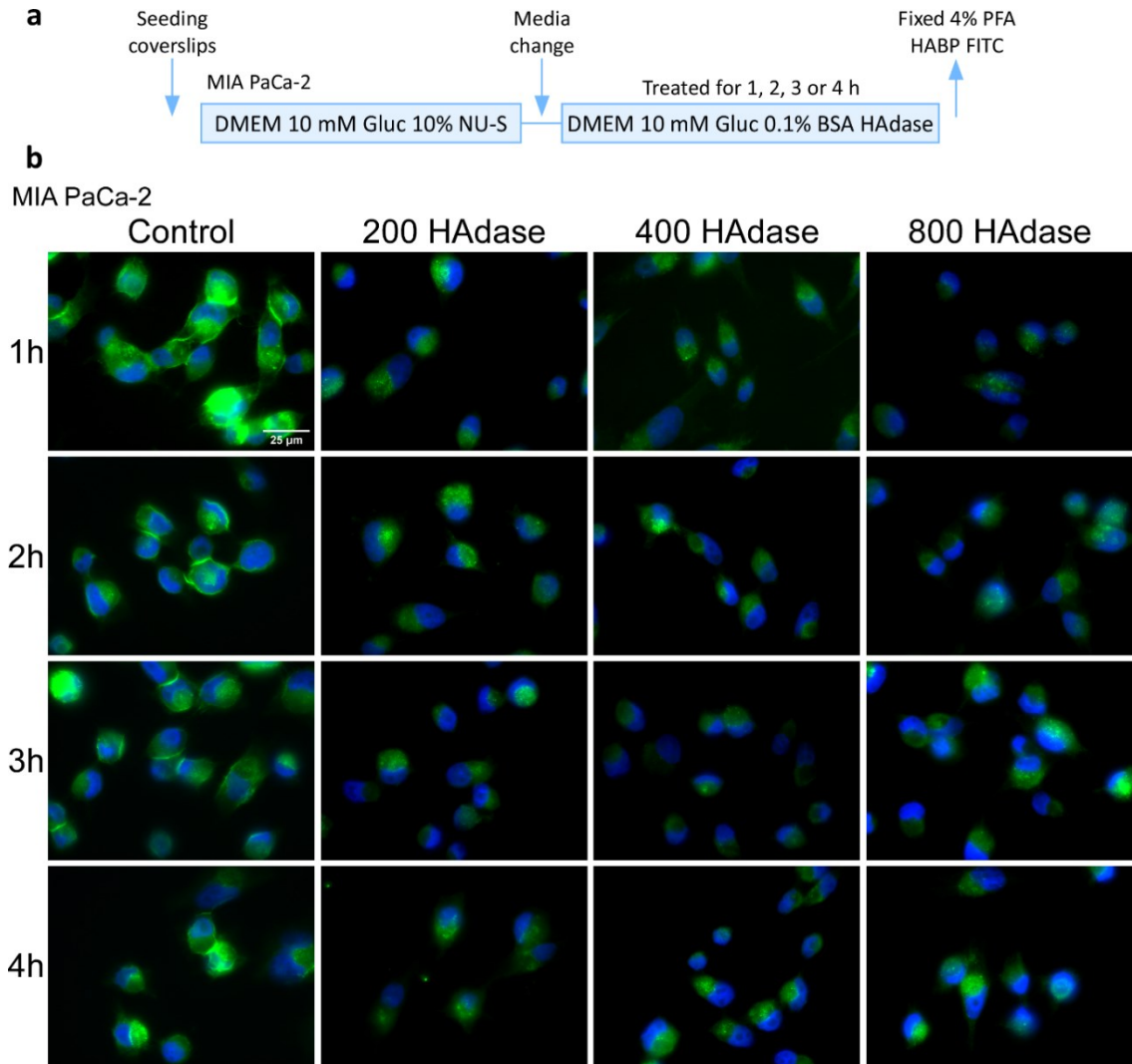
Figure 30. Bovine hyaluronidase removes pericellular hyaluronic acid from MIA PaCa-2 cells.
a) Schematic illustrating the experimental design. MIA PaCa-2 cells were seeded on coverslips and incubated for 24 hrs. The cells were treated with different concentrations (200, 400 and 800 μg/ml) of bovine hyaluronidase (HAdase). The treatments were applied for 1, 2, 3, or 4 hours. **b)** An immunofluorescence-type assay was used to detect HA with HABP/FITC-streptavidin.

Although the removal of HA proved to be effective, we did not know if the cells were able to resynthesize this extracellular coating over time. To explore this, we treated MIA PaCa-2 and BXPC3 cells for 1 h with HAdase at a concentration of 100, 200, 400 and 800 µg/ml and fixed cells immediately after treatment and the remaining cells were washed in PBS and cultured for a further 24 h in normal media. HA was detected in the fixed samples using the same HABP/FITC-streptavidin. The fluorescent images taken of MIA PaCa-2 cells show that HA synthesis did not come back after 24 h at the high concentration of HAdase (200, 400 and 800 µg/ml) (**Figure 31b)** but a faint signal was detected at 24 h in cells treated with 100 µg/ml of HAdase (**Figure 31b**). When we analysed fluorescence using an intensity profile graph (Figure 9c) we corroborated that with 100 µg/ml, the pericellular coating is starting to recover (**Figure 31c, red arrows**).

BXPC3 cells show a different distribution of HA within the cell, mainly consisting of a cytoplasmic location and the pericellular location is not as evident as seen on MIA PaCa-2 cells. When the cells were treated with hyaluronidase for 1 h there was not a clear decrease in fluorescent intensity for HA that would indicate its removal (**Figure 32b**). We could observe that in HAdase treated cells starting from 200 and up to 800 µg/ml there are vesicle-like structures in the cell displaying high fluorescent intensity (**Figure 32b**). To overcome this issue, fluorescent intensity 3d surface plots were generated in FIJI (Figure 10c). Presenting fluorescent intensity data in this way allowed us to observe that the overall pixel intensities were reduced in HAdase treated cells (**Figure 32c).** Interestingly at 400 and 800 µg/ml, we can observe high intensity peaks that coincide with the vesicle-like structures previously observed (**Figure 10c).** We speculate that these vesicle-like structures could be the result of accumulation through endocytosis of degraded HA from the use of HAdase. Even though the presence of a pericellular coating is not evident we could see a loss of HABP-FITC fluorescence by treatment with HAdase in BXPC3 cells. This could indicate the presence of pericellular HA obscured by intracellular staining due to epifluorescence imaging, which is characterized by out of focus light. After 24 h HA fluorescence showed a slight recovery that is more evident after treatment with 100 HAdase (**Figure 32d,e**).

After establishing that HAdase removes HA from PDAC cells, we wanted to study the effects that this could have on the proliferation and migration of PDAC cells. Cells for proliferation assays were seeded at double density than for previous experiments due to some loss of cells from the HAdase treatment. For all experiments, we used 800 µg/ml of HAdase and treated the cells for 1 h followed by a wash in PBS to remove any remnants of the enzyme that could interfere with the assays. Due to the extended lengths of these assays (96 h), we used the highest concentration of HA to ensure the removal of as much HA as possible. PDAC cells were then further grown in DMEM or RPMI accordingly in 10% NU-S and 10 mM glucose as was done for previous proliferation assays. The WST-8 and SRB assays were used to measure proliferation every 24 h up to 96 h. The removal of HA did not affect the proliferation of PDAC cells measured by WST-8 or SRB (**Figure 33b-e**).
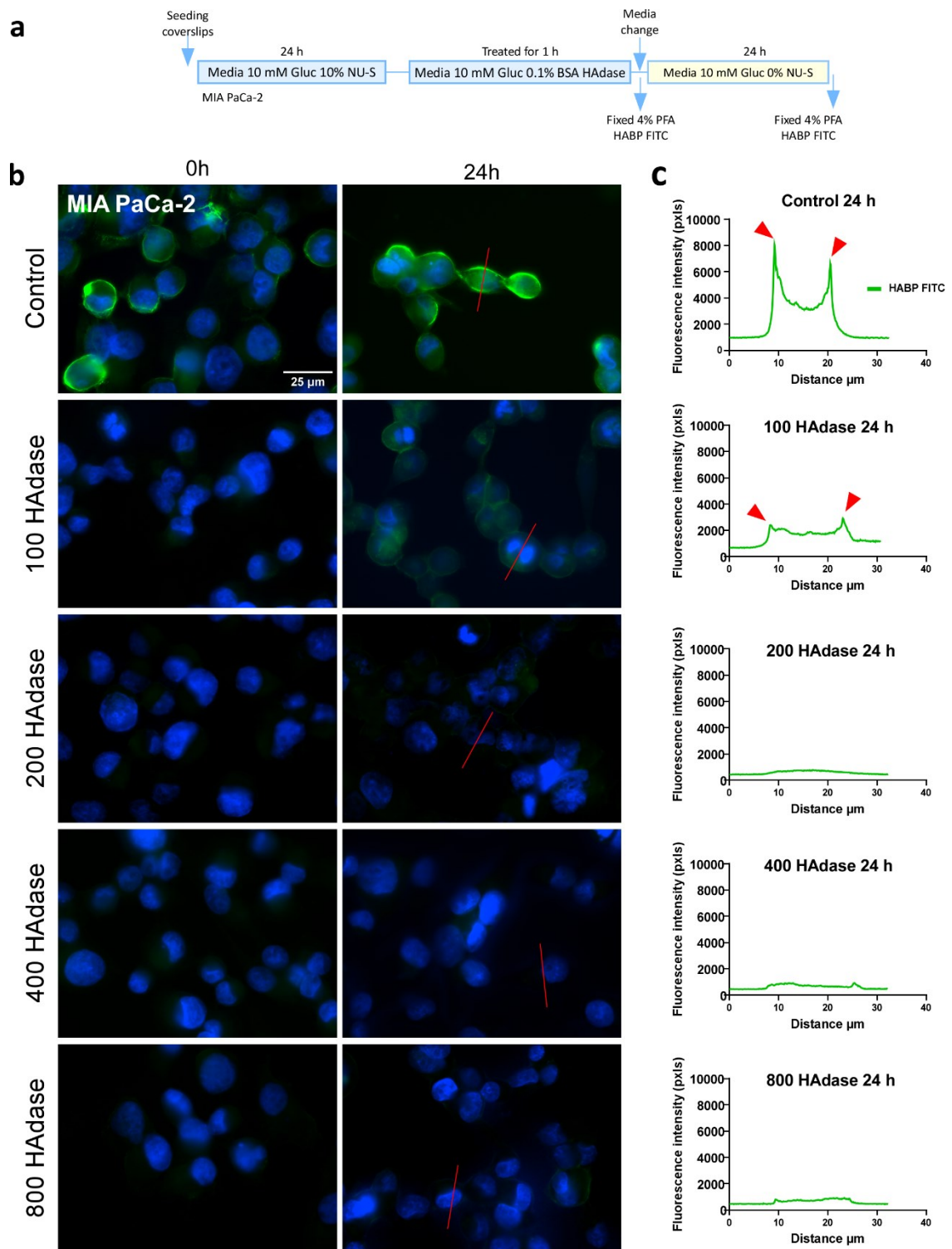
Figure 31. Pericellular hyaluronic acid removed by bovine hyaluronidase is not resynthesized after 24 hrs. a) Schematic illustrating the experimental design. MIA PaCa-2 cells were seeded on glass coverslips and incubated for 24 hrs. Cells were treated with increasing concentrations (100, 200, 400, 800 µg/ml) of bovine hyaluronidase (HAdase) for 1 h. A first batch of cells was fixed in 4% PFA and another batch was incubated for a further 24 hrs before being fixed in 4% PFA. **b)** Representative images of HABP/FITC-streptavidin labelled (green) cells and Hoechst nuclei stain (blue). **c)** Line profiles of fluorescence intensity were generated in FIJI ImageJ. The red arrows indicate the pericellular HA of MIA PaCa-2 cells. d,f) HA was detected in HAdase treated BXPC3 cells as in (b). e, g) Pseudocolored fluorescence intensity 3D surface plots were generated in FIJI.
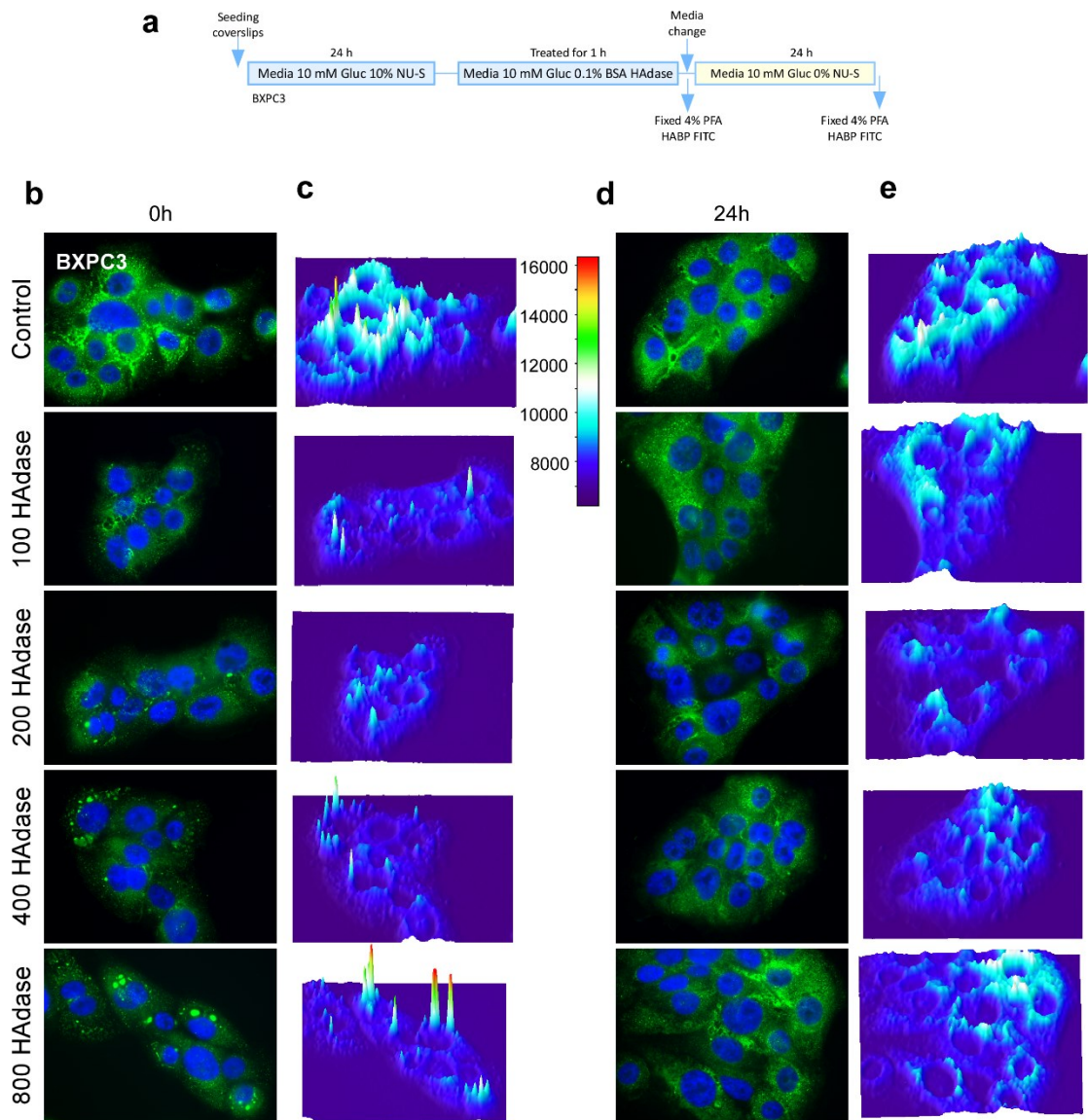
Figure 32. Pericellular hyaluronic acid is removed by bovine hyaluronidase in BXPC3 cells. a) Schematic illustrating the experimental design. BXPC3 cells were seeded on glass coverslips and incubated for 24 hrs. Cells were treated with increasing concentrations (100, 200, 400, 800 µg/ml) of bovine hyaluronidase (HAdase) for 1 h. A first batch of cells was fixed in 4% PFA and another batch was incubated for a further 24 hrs before being fixed in 4% PFA. **b,c)** Representative images at 0 h after treatment of HA detected with HABP/FITC-streptavidin labelled (green) and Hoechst nuclei stain (blue). **c)** Pseudocoloured fluorescence intensity 3D surface plots at 0 h after treatment. **d)** Representative images at 24 h after treatment of HA detected with HABP/FITC-streptavidin labelled (green) and Hoechst nuclei stain (blue).**e)** Pseudocoloured fluorescence intensity 3D surface plots at 0 h after treatment.
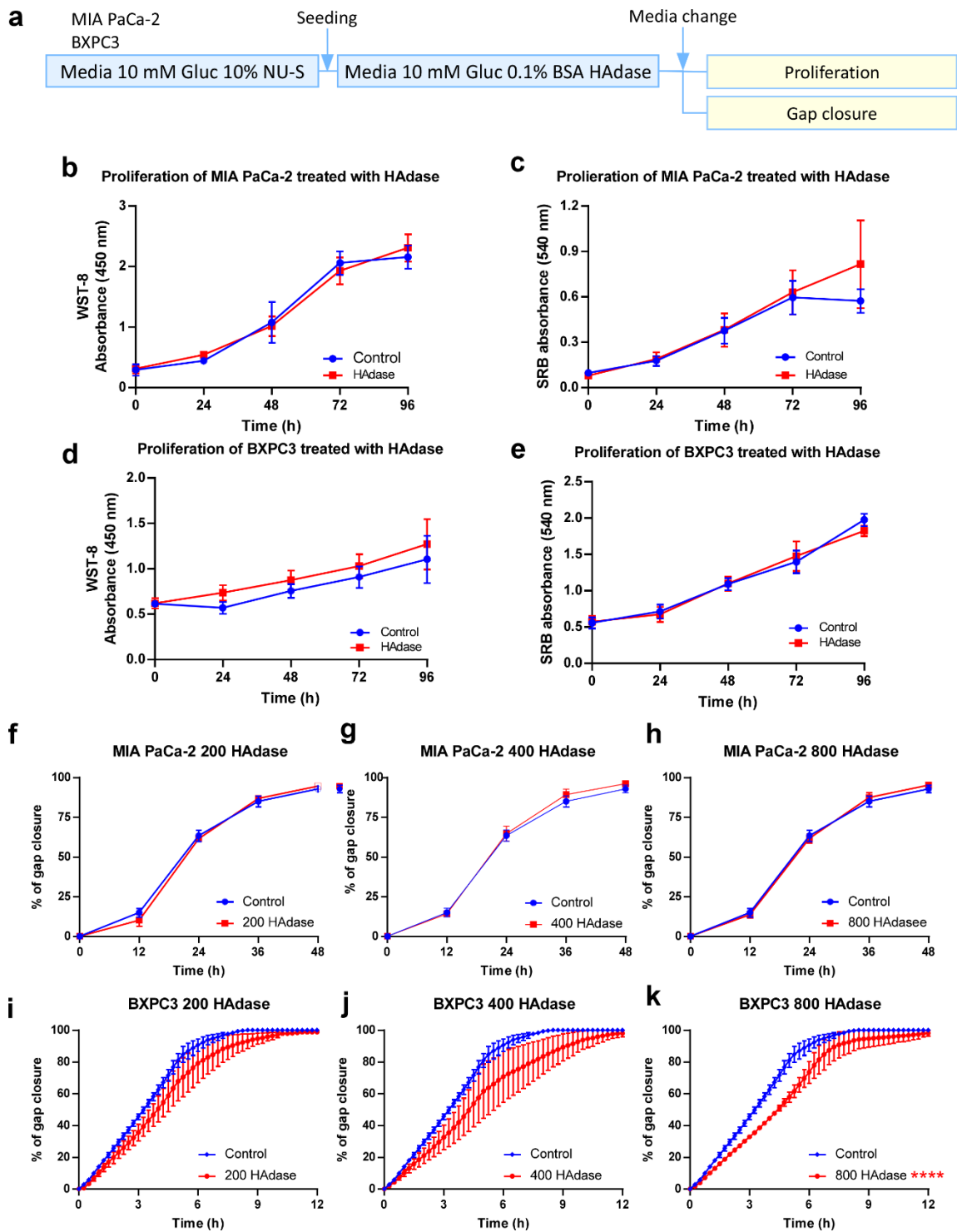
Figure 33. Treatment with bovine hyaluronidase affects migration only in BXPC3 cells and does not affect the proliferation of PDAC cells. a) MIA PaCa-2 and BXPC3 cells were seeded for proliferation and gap closure assays. Cells were treated for 1 h with bovine hyaluronidase in serum free media with 0.1% BSA at a concentration of 800 µg/ml for proliferation assays and 200, 400 and 800 µg/ml for gap closure assays. **b-e)** Cell proliferation was assessed with the WST-8 and SRB assays every 24 h up to 96 h. **f-k)** Cell migration was assessed by the gap closure assay using silicone inserts. Images of the gap were taken every 12 h up to 48 h for MIA PaCa-2 cells and every 15 min for BXPC3 cells up to 12 h. Two-way ANOVA using Tukey's multiple comparisons test was used for analysis of % of gap closure (****p<0.0001) (n=3).

Migration assays followed the same process as previously mentioned with the added extra step of treating the cells with HAdase at 200, 400 or 800 µg/ml after the silicon inserts were removed. The cells were washed with PBS to remove any leftover enzyme and were incubated in media supplemented with mitomycin C (2 µg/ml). Migration of MIA PaCa-2 cells was completely unaffected by HAdase treatment (**Figure 33f-h**), however, BXPC3 cells showed a slight decrease in cell migration when the cells were treated with 800 µg/ml of HAdase (**Figure 33k**). These assays together with what was observed previously in this chapter, show that BXPC3c cells are sensitive to disruption of endogenous pericellular HA. Therefore, we could continue to exploit this feature by a combination of synthesis inhibition with 4-MU and removal of extracellular HA with HAdase. Combining hyaluronic acid synthesis inhibition with 4-MU and hyaluronic acid removal with HAdase to study proliferation and migration in PDAC cells.

5.4 Disruption of endogenous HA with a combined treatment with HAdase and 4-MU

We have shown that disrupting endogenous HA through synthesis inhibition with 4-MU or extracellular removal with HAdase can differentially affect PDAC cells. However, despite the effectiveness of HAdase in removing pericellular HA, there could still be resynthesis of the pericellular coating of HA. Therefore, to prevent recoating of pericellular HA we used a combined approach by degrading the pericellular HA with HAdase, followed by synthesis inhibition with 4-MU.

The first step was to analyse through fluorescence microscopy the presence of HA in cells treated with the combination of 4-MU at 100 µM and HAdase at 800 at µg/ml. These concentrations were chosen because they independently decreased migration in BXPC3 cells. For this assay, PDAC cells were seeded onto coverslips and incubated for 24 h. The cells were then treated with 800 µg/ml of HAdase for 1 h. The cells were washed and then continued incubation in either DMEM or RPMI supplemented with 100 µM of 4-MU for 24, 48 and 72 hrs. HA was detected using the HABP/FITC-streptavidin. Fluorescent images show that the pericellular HA distribution exhibited by untreated control MIA PaCa-2 cells (**Figure 34a**) is lost in cells treated with HAdase-4-MU (**Figure 34b**). There is no sign of recovery of pericellular HA up to the 72 h timepoint studied as seen in the fluorescence intensity line profiles (**Figure 34c**).

Given that both 4-MU and HAdase separately reduced migration in BXPC3 cells within 12 h from starting the assay, we only aimed to analyse the effects of the combined treatment in the first 24 h, as it is well within the timeframe that migration occurs (6-12 h). BXPC3 cells treated with HAdase-4-MU exhibited a very localized high fluorescence intensity (**Figure 35a**) exhibited as high intensity peaks in the 3D surface intensity plots, compared to control cells that exhibit a more diffuse but high intensity (**Figure 35b**). These high intensity peaks resemble those seen previously immediately after HAdase treatment and are probably due to the accumulation of extracellular HA degraded by HAdase.
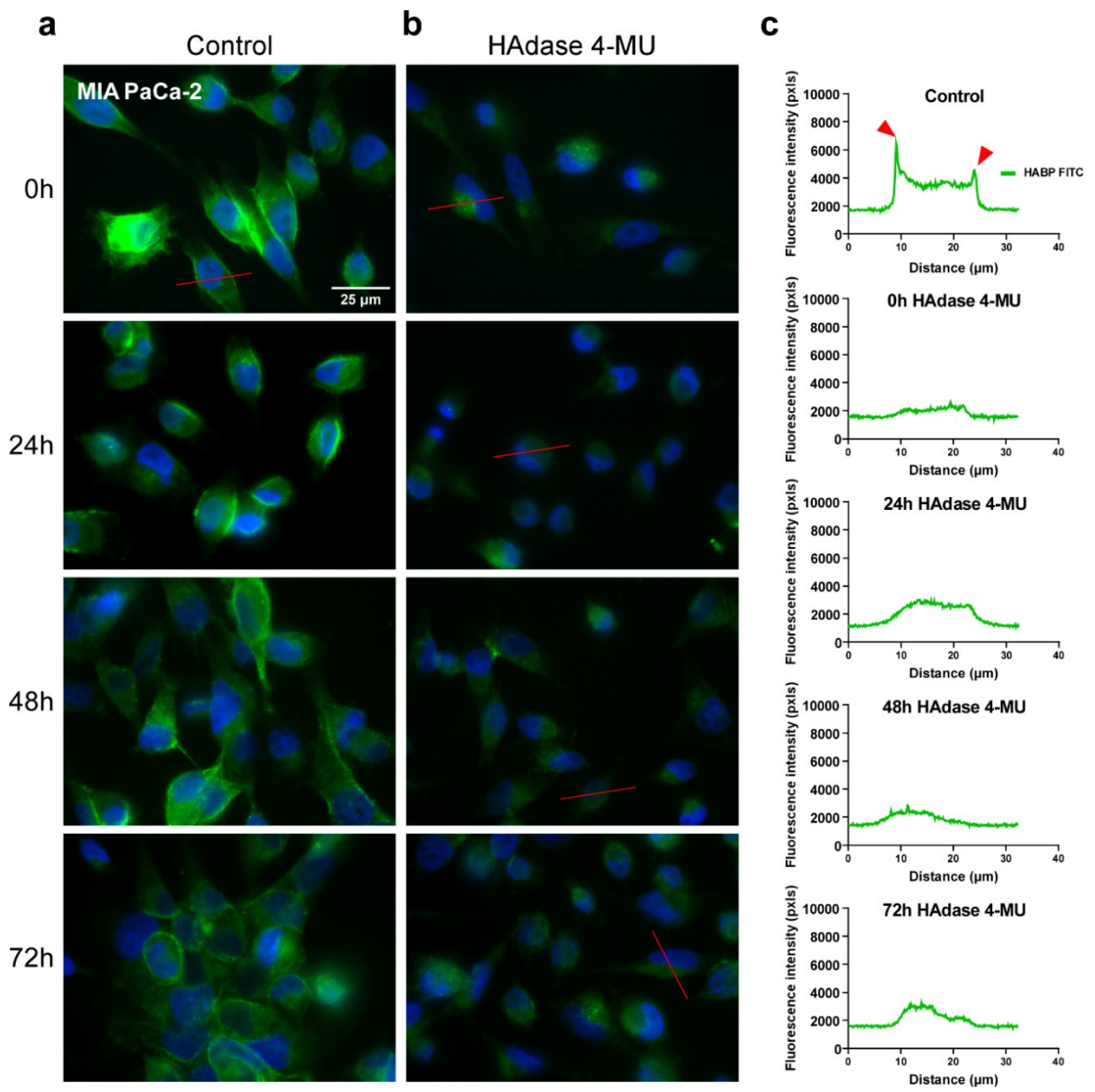
Figure 34. Treating cells with a combination of bovine hyaluronidase and 4-methylumbeliferone maintains hyaluronic acid levels low in MIA PaCa-2 cells. **a)** MIA Paca-2 cells were treated with bovine hyaluronidase at a concentration of 800 µg/ml for 1 h. The cells were fixed in 4% PFA at different time points starting from 0 h, immediately after treatment with hyaluronidase. The cells after 0 h were incubated in media containing 100 µM of 4-MU for 24, 48 and 72 h. **b)** HA was detected by the HABP/ FITC-streptavidin (green), nuclei were stained with Hoechst (blue) and fluorescent images were obtained. **c)** From the images line profiles of fluorescence intensity were generated, processed, and analysed using FIJI. In control cells, high fluorescence intensity peaks (red arrows) correspond to pericellular HA.
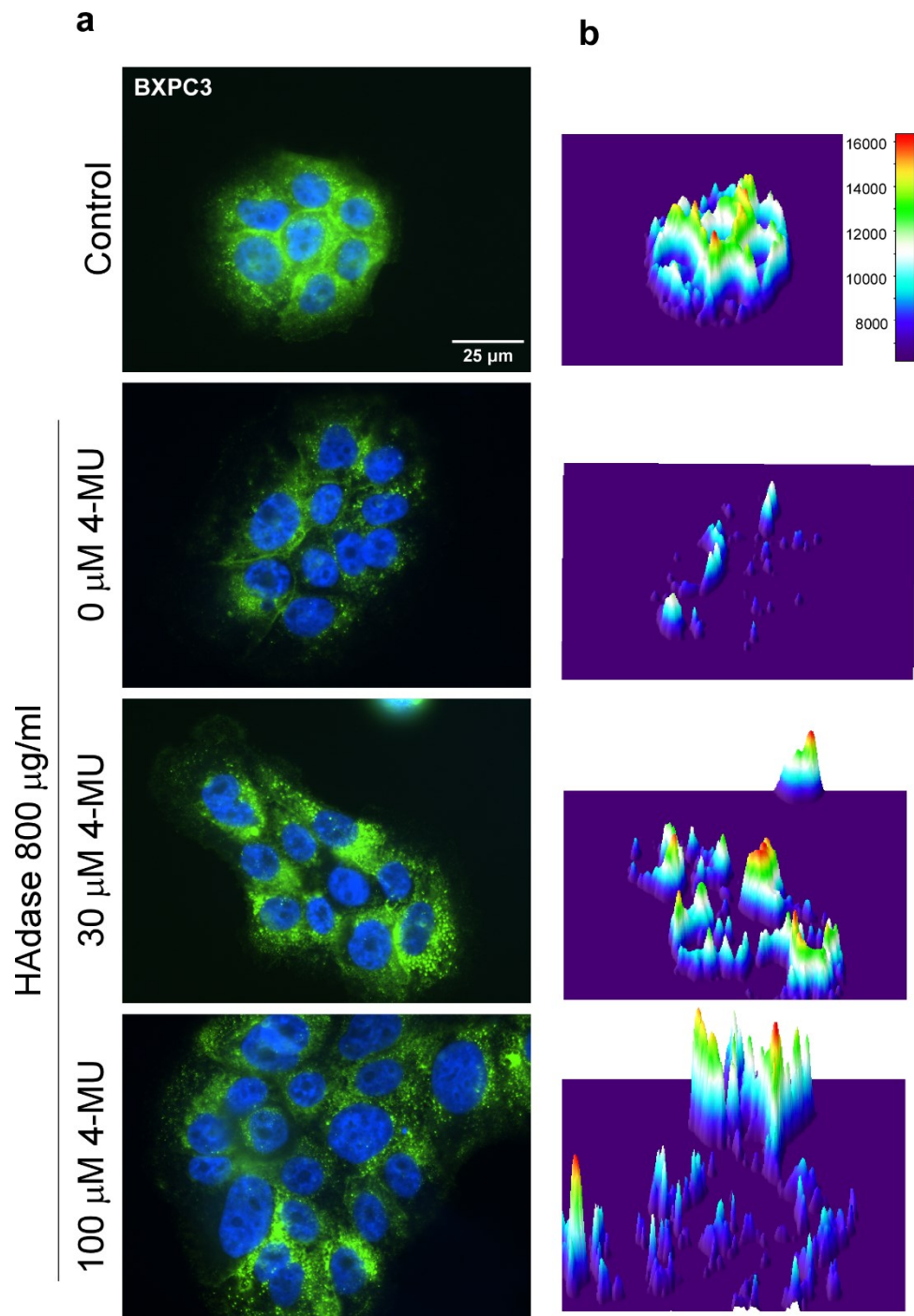
Figure 35. Treating cells with a combination of bovine hyaluronidase and 4-methylumbeliferone maintains hyaluronic acid levels low in BXPC3 cells a) BXPC3 cells were treated with bovine hyaluronidase at a concentration of 800 µg/ml for 1 h. After, the cells were incubated in media containing 100 µM of 4-MU for 24 h and then fixed in 4% PFA. HA was detected by the biotinylated HABP and FITC-streptavidin and fluorescent images were obtained. **b)** Fluorescent intensity 3D surface plots were generated using FIJI.

After establishing the decrease of HA by the combined treatment of HAdase-4-MU we wanted to study how this could affect proliferation. In addition, we added exogenous HA of different molecular weights to observe if there was any change in cell behaviour when treated with HAdase-4-MU. PDAC cells were seeded onto culture plates and left to grow for 24 h. The cells were then treated with 800 µg/ml of HAdase for 1 h. Cells were washed and left to grow in either DMEM or RPMI supplemented with 10% NU-S, 10 mM glucose, and 100 µM 4-MU for up to 96 h. We assessed proliferation using the WST-8 and SRB assays every 24 h. As previously seen in MIA PaCa-2 cells (**Figure 29a**) when 4-MU is added to the media the WST-8 shows a decrease in signal (**Figure 36a**) but when cells were analysed by the SRB (fig) there was no change compared to the control (**Figure 36e**). Adding HA of different molecular weights had no effect in any of the conditions studied and MIA PaCa-2 cells remained completely unresponsive to these changes when analysed by the SRB assay (**Figure 36e-h**). It is important to note that MIA PaCa-2 cells with the combined treatment (HAdase/4-MU) showed a tendency to increase cell proliferation at 96 h with the SRB assay, however, this does not have any statistical significance (**Figure 36e-h**).

In BXPC3 cells there was no decrease in signal when 4-MU was added to the media compared to MIA PaCa-2 cells (**Figure 37a-d**). Moreover, in both assays measuring proliferation there was no difference compared to the control, and cells remain unresponsive to the combined treatment of HAdase-4-MU (**Figure 37a-h**). There were also no changes when exogenous HA was added to the media (**Figure 37a-h**).

We studied MIA PaCa-2 and BXPC3 cell migration by the gap closure assay using the combined treatment of HAdase-4-MU. Similar to the previous assays, after the silicon inserts were removed the cells were treated with 800 µg/ml of HAdase for 1 h in serum free media. The HAdase was removed, and the cells were washed with PBS to remove any remnants of the enzyme. The cells were further incubated in media supplemented with mitomycin C (µg/ml) and exogenous HA of different molecular weights. Images of the gap were taken every 12 h for MIA PaCa-2 cells and every 15 min for up to 12 h for BXPC3 cells.

The percentage of gap closure did not change in MIA PACa-2 cells incubated with the HAdase-4-MU combination when compared to control cells (**Figure 38a-d**). The addition of exogenous HA to the media also did not affect migration (**Figure 38a-d**). This was reflected when the migration rate (µm/h) was measured, showing no significant differences from the control in any of the conditions studied (**Figure 38j**). Interestingly, BXPC3 cell migration was affected with the combined treatment of HAdase-4-MU, significantly reducing migration in treated cells compared to the control (**Figure 38i**). However, the addition of exogenous HA could not recover the decrease in migration (**Figure 38e-h**). Analysing the migration rate (µm/h) of treated BXPC3 cells there is approximately a 40% decrease in the migration rate in cells treated with HAdase, 4-MU or the combination of HAdase-4-MU (**Figure 38k**).

Taken together, these results show that endogenous HA seems to play a critical role in BXPC3 cells, but not MIA PaCa-2 cells, as a disruption of cell surface HA by HAdase and synthesis inhibition by 4-MU cause a drastic reduction in the migration capabilities of BXPC3 cells. The rapid migratory phenotype of BXCP3 cells seems to be partially dependent on the synthesis of endogenous HA and the formation of a pericellular coating.
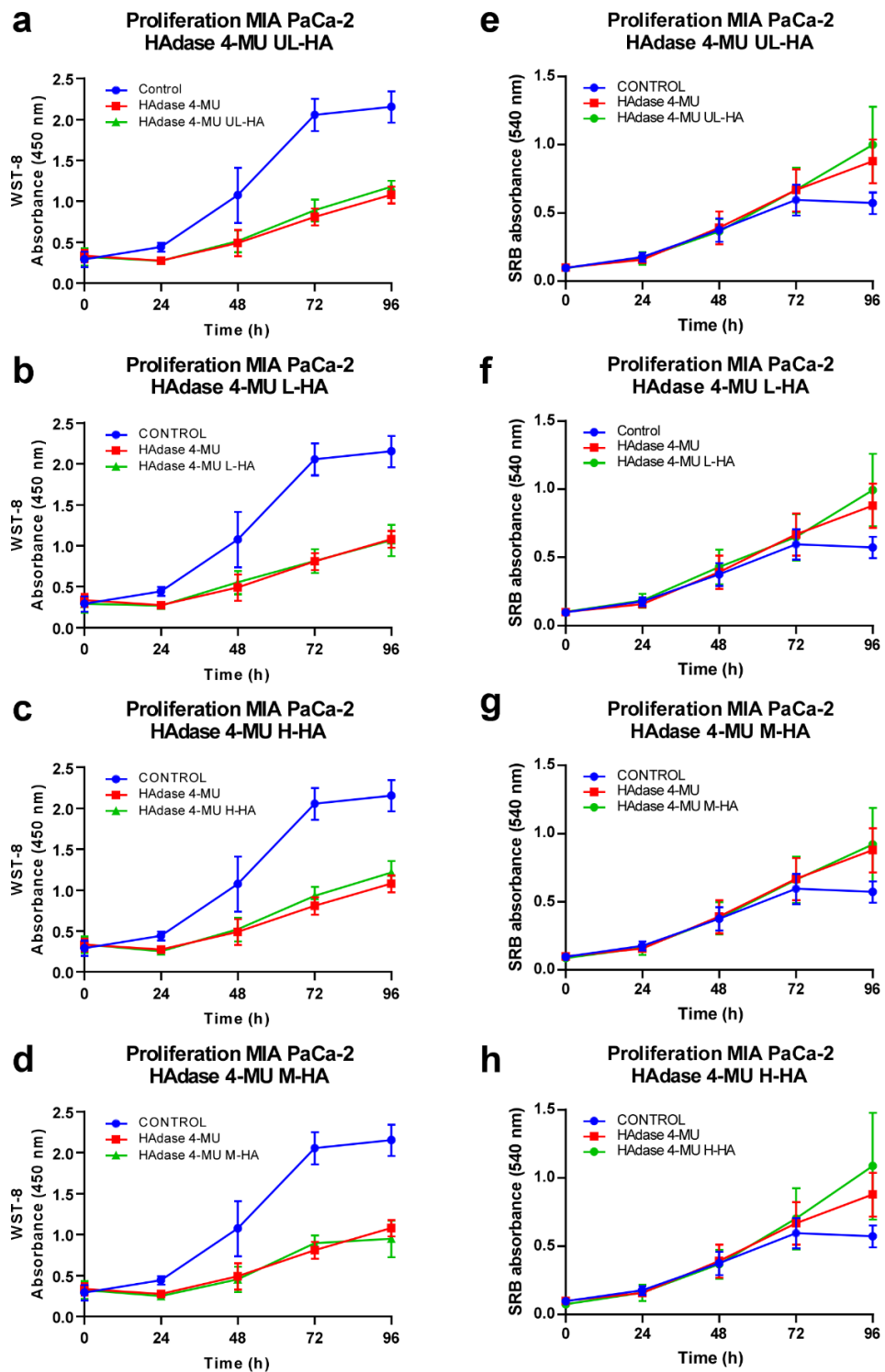
Figure 36. Treatment with bovine hyaluronidase and 4-methylumbeliferone does not affect MIA PaCa-2 cell proliferation even after the addition of exogenous hyaluronic acid. MIA PaCa-2 and BXPC3 cells were seeded for proliferation assays. Cells were treated for 1 h with bovine hyaluronidase in serum free media with 0.1% BSA at a concentration of 800 μg/ml. Then the cells were incubated in media containing 100 μM of 4-MU supplemented with HA of different molecular weights at a concentration of 300 μg/ml (UL, L, M, H) for 24, 48, 72 and 96 h. **a-d)** Cell proliferation was assessed at each time point with the WST-8 assay. **e-h)** Cell proliferation was assessed at each time point with the SRB assays (n=3).
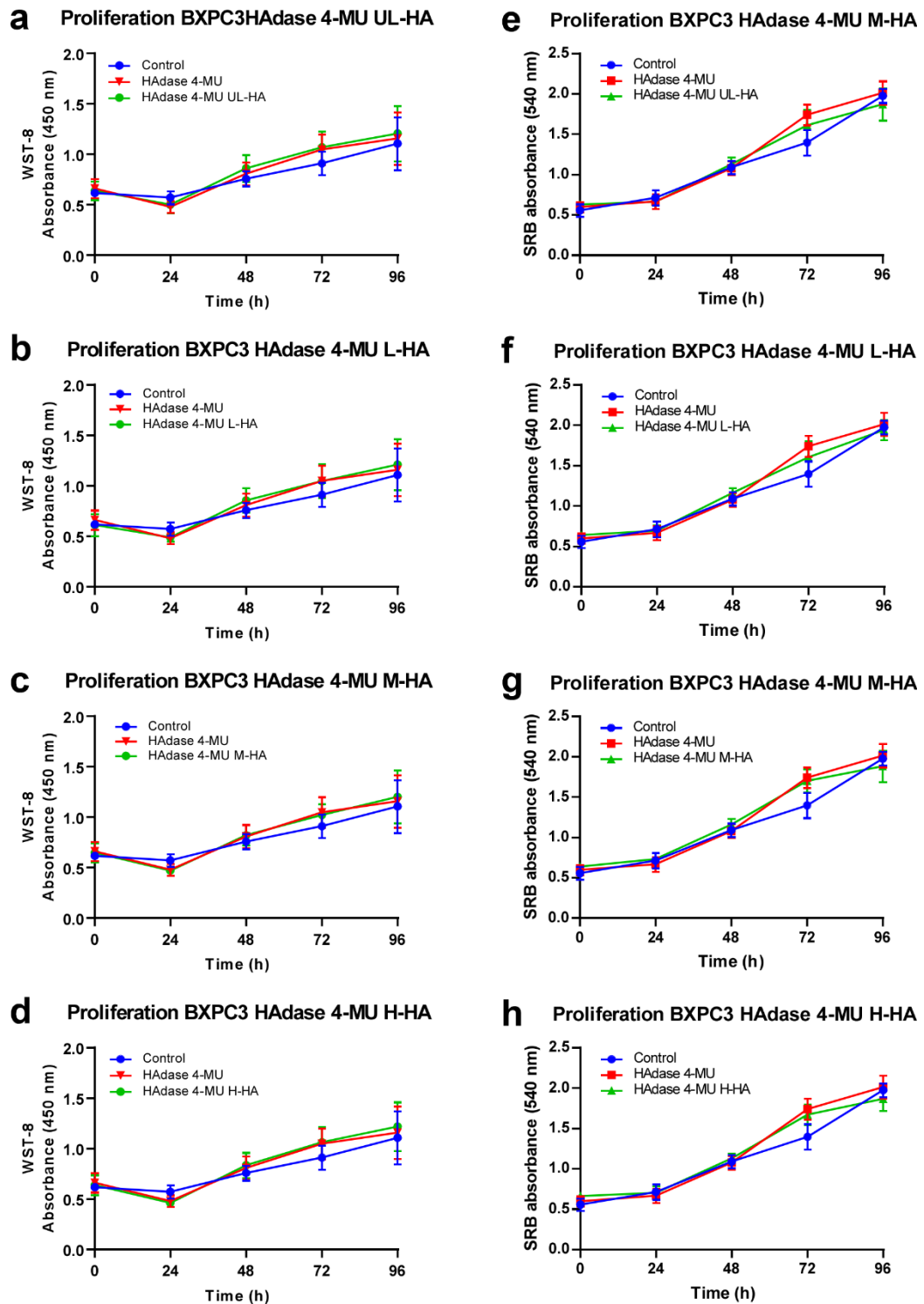
Figure 37. Treatment with bovine hyaluronidase and 4-methylumbeliferone does not affect BXPC3 cell proliferation even after the addition of exogenous hyaluronic acid. BXPC3 cells were seeded for proliferation assays. Cells were treated for 1 h with bovine hyaluronidase in serum free media with 0.1% BSA at a concentration of 800 µg/ml. Then the cells were incubated in media containing 100 µM of 4-MU supplemented with HA of different molecular weights at a concentration f 300 µg/ml (UL, L, M, H) for 24, 48, 72 and 96 h. **a-d)** Cell proliferation was assessed at each time point with the WST-8 assay. **e-h)** Cell proliferation was assessed at each time point with the SRB assay (n=3).
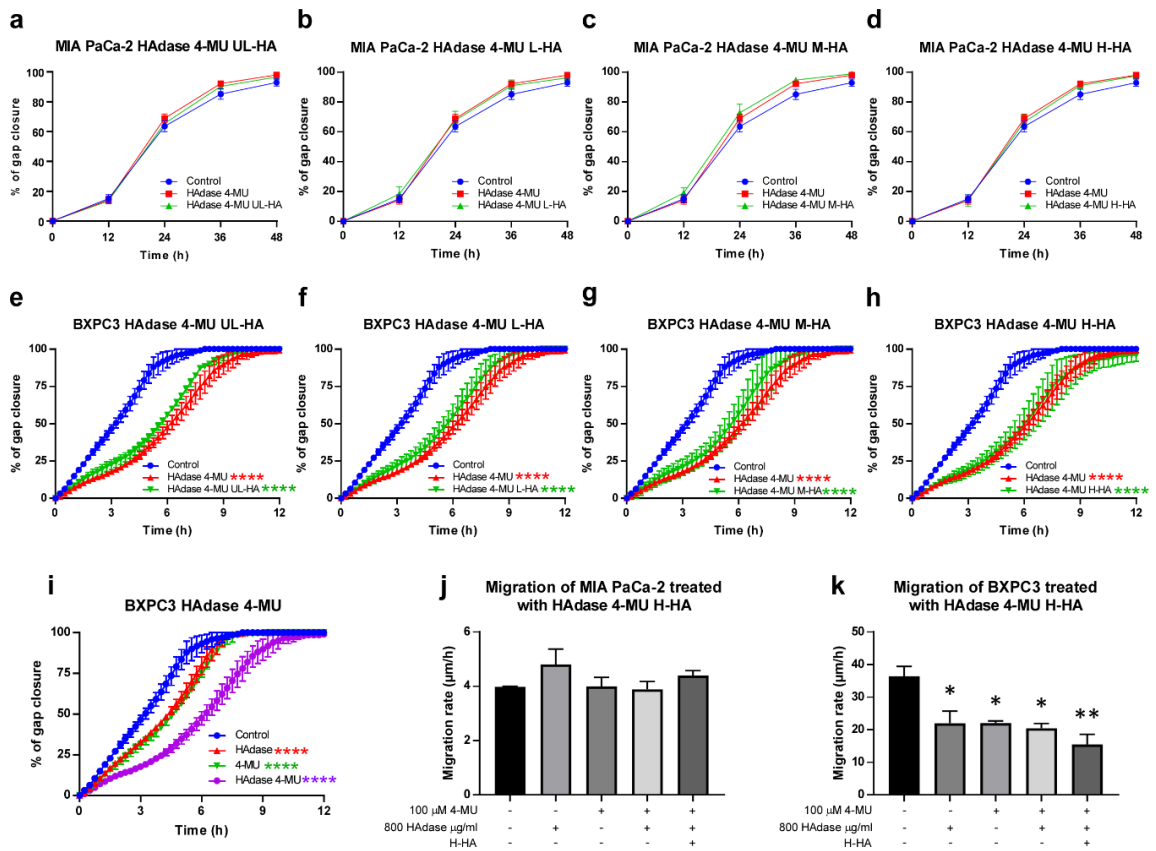
Figure 38. **Treatment with bovine hyaluronidase and 4-methylumbeliferone decreases migration in BXPC3 cells but not MIA PaCa-2 cells and this decrease is not recovered by exogenous hyaluronic acid. a-h)** MIA PaCa-2 and BXPC3 cells were seeded into silicone inserts for gap closure assays for 24 h. The cells were then treated for 1 h with bovine hyaluronidase in serum free media with 0.1% BSA at a concentration of 800 µg/ml. Next, the cells were incubated in media containing 100 µM of 4-MU for up to 48 h for MIA PaCa-2 cells and up to 12 h for BXPC3 cells. Images of the gap were taken every 12 h up to 48 h for MIA PaCa-2 cells and every 15 min for BXPC3 cells up to 12 h. Gap closure images were analysed and processed using FIJI. **i)** BXPC3 cell migration treated with 800 µg/ml, 100 µM of 4-MU or a combination of both. **j,k**) From the gap closure images the migration rate (µm/h) was calculated at the 24 h timepoint for MIA PaCa-2 cells and 50% gap closure for the BXPC3 cells. Two-way ANOVA with Tukey's post hoc test was used for statistical analysis of % of gap closure (**p<0.005, ****p<0.0001). One-way ANOVA with Dunnett's post hoc test was used for statistical analysis of migration rate (*p<0.05, **p<0.005) (n=3).

5.5 Standardization of hyaluronic acid synthase-2 and hyaluronidase-2 knockdown with siRNA

We established that endogenous HA turnover is an important characteristic of PDAC cells, and in some causing its disruption with inhibitors (DSS, 4-MU) or directly removing extracellular HA with HAdase can have an effect on cell behaviour. To further understand endogenous HA turnover the next logical step was to knock down the expression of key proteins involved in this process. We chose to knock down HYAL2, hyaluronidase present on the membrane that is likely the main target of inhibitor DSS. Our migration experiments indicated that blocking hyaluronidases with DSS drastically reduces migration of MIA PaCa-2 cells and reduces the H-HA induced migration in BXPC3 cells. Therefore, HYAL2 could be a critical enzyme for PDAC cell migration and knocking it down could reveal more important information.

The synthesis of HA is another important component of HA turnover, and its inhibition by 4-MU showed that it can reduce migration in BXPC3 cells. However, the potential non-specific effects of 4-MU cannot be completely ruled out Therefore, interrupting HA synthesis by knocking down the enzymes involved in the process was a critical way of understanding the role HA synthesis can have in PDAC cells. We focused on HAS2 as it is one of the most important enzymes that synthesize HA and is involved in cancer progression.

For the knockdown of HYAL2 and HAS2, we used a mix of 4 different siRNAs (Dharmacon) to increase our chances of a knockdown. The recommended transfection agent, Dharmafect 1, was produced by the same manufacturer. This transfection agent was previously standardized in the lab for its use in PDAC cells (Sritangos et al., 2020), where the optimal concentration for the transfection agent was 0.1% -0.2%. Concentrations of 10, 25 and 50 nM were tested for both siRNAs for a period of 24, 48 and 72 hrs. A siRNA based on scrambled sequences of RNA was used as an experimental control. To verify protein knockdown whole lysates from transfected cells were used. Cyclophilin A and B (CYPA and CYPB) were used as a loading control. A decrease in band intensity would indicate a successful knockdown, however, there was no decrease in band intensity for both siRNAs (**Figure 39a**). Continued testing of other available transfection agents from the same company, Dharmafect 2 (D2) and Dharmafect 4 (D4) showed the same result, no successful transfection even after 120 h (**Figure 39b-d**).
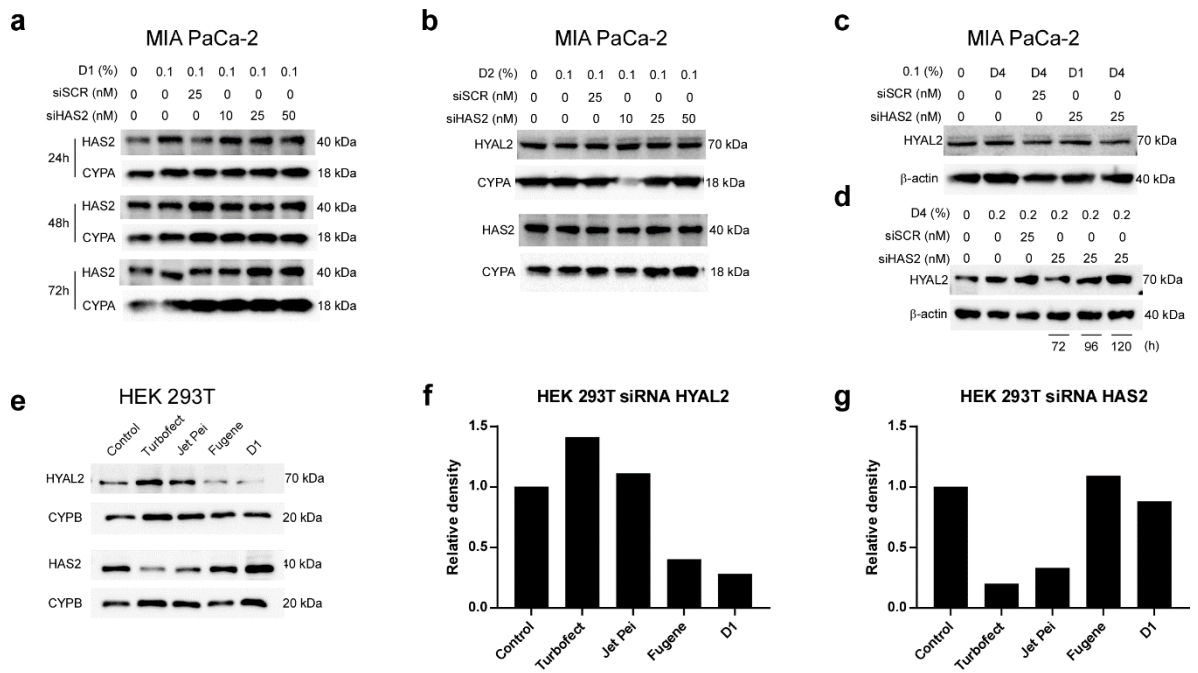
Figure 39. Standardization of HAS2 and HYAL2 knockdown by siRNA. **a-d**) MIA PaCa-2 cells were transfected with siRNAs for HAS2 or HYAL2 and a scrambled (SCR) siRNA was used as a control (Dharmacon). Cells were transfected with different concentrations (10, 25 and 50 nM) using several transfection agents from the same manufacturer. These included Dharmafect 1 (D1), Dharmafect 2 (D2) and Dharmafect 4 (D4). Transfection times were tested from 24 to 120 h. Silencing of HAS2 and HYAL2 proteins was evaluated by western blotting of whole cell lysates obtained from MIA PaCa-2 cells. **e)** HEK 293T cells were transfected with the 25 nM of siHAS2 or siHYAL2 mix using four different transfecting agents that included Turbofect, JetPEI, Fugene and Dharmafect 1 for 48 hrs. Western blotting of whole cell lysates was used to evaluate protein silencing. **f-g)** Relative density HYAL2 and HAS2 bands were quantified using Image Lab software from BioRad (each western blot n=1).

PDAC cells as well as other cancer lines can sometimes be proven difficult to transfect, therefore we used a common and easy-to-transfect cell line to test the effectiveness of the siRNA in generating a knockdown. HEK293T cells were transfected with four different transfection agents including, Turbofect, JetPEI, Fugene and D1. In HEK293T cells HYAL2 was effectively knocked down using Fugene and D1 by 60% and 70% respectively (**Figure 39e-g**). On the other hand, the most effective transfection agent for HAS2 knockdown was Turbofect which decreased band intensity by 80% (**Figure 39e-g**).

After establishing that the siRNAs did induce knockdowns in HEK293T cells, we tested the same conditions in MIA PaCa-2 and BXPC3 cells. Application of siHYAL2 yielded no effective knockdowns in both cell lines (**Figure 40a,d**). In MIA PaCa-2 siHAS2 decreased band intensity by 40%, much less than what we obtained in HEK293T cells (**Figure 40b**). In the case of BXPC3 cells, the decrease in band intensity was closer to 60% (**Figure 40e**). Given the higher decrease in band intensity and the fact that HA synthesis inhibition had effects only in BXPC3 cells, we chose to continue with this cell line for further experiments.

Once the optimal transfection conditions for HAS2 were found, we tested the effects of HAS2 knockdown in BXPC3 cell migration. The cells were seeded into the silicon inserts containing the transfection mix, transfection agent (Turbofect) and siHAS2. During this process, the transfection occurs while cells are settling down and attaching to the culture plate. The cells were left transfecting for 36 h before removing the silicon insert. After this, and depending on the experimental conditions, siHAS2 cells were subsequently treated with HAdase and H-HA. In these experiments, the knockdown of HAS2 only reached 50% of gap closure at the 12 h timepoint compared to nearly 90% for the control with siSCR (**Figure 40g**). In cells treated with HAdase in addition to siHAS2, cell migration decreased by around 75% at the 12 h timepoint (**Figure 40h**). On the other hand, the addition of H-HA could not recover the migration of the cells transfected with siHAS2, including the cells treated with HAdase. These experiments reinforce our previous findings that endogenous HA synthesis is critical for the migration of BXPC3 cells.
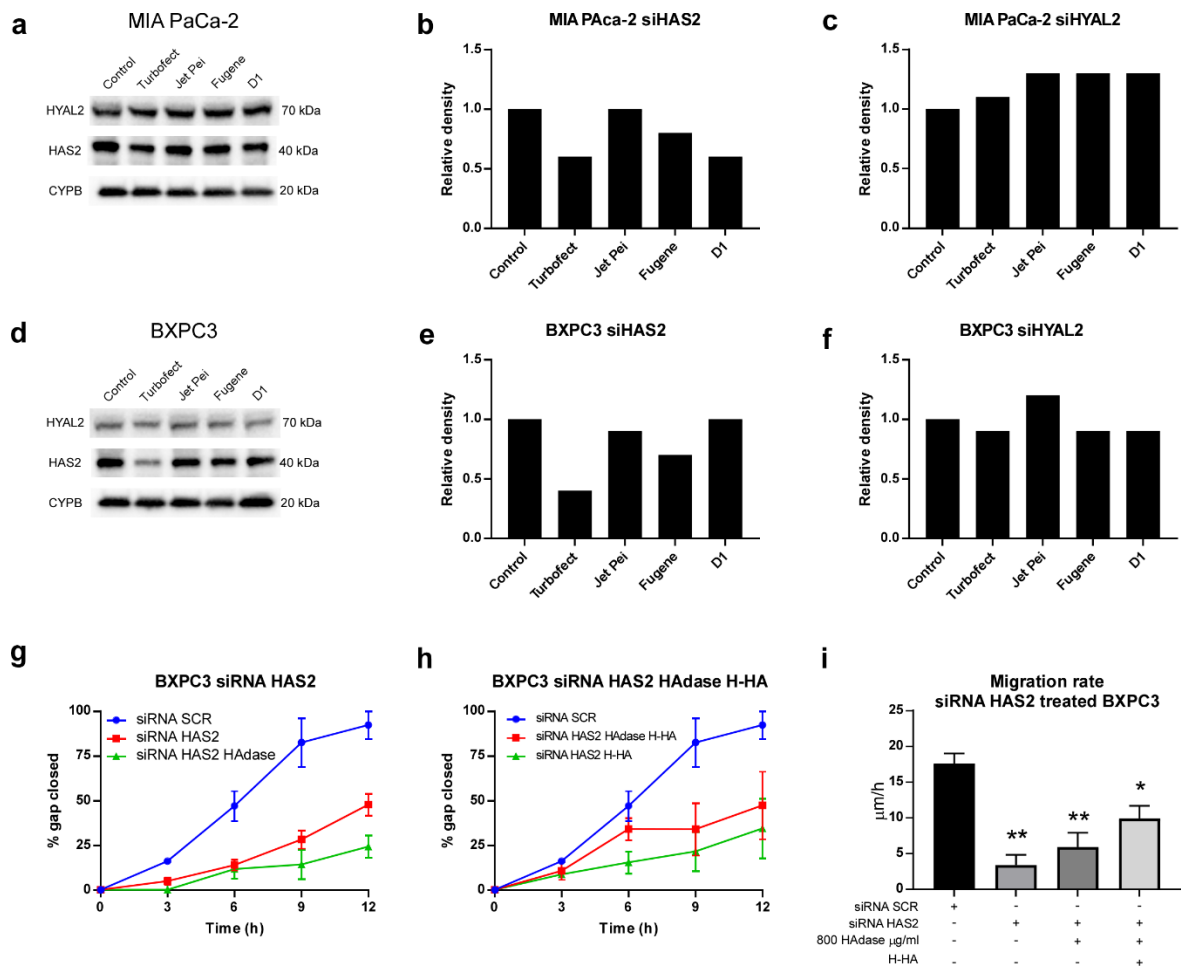
Figure 40. Knockdown of HAS2 by siRNA decreases BXPC3 cell migration. **a, d)** MIA PaCa-2 and BXPC3 cells were transfected with the HAS2 or HYAL2 siRNA mix using four different transfecting agents that included Turbofect, JetPEI, Fugene and Dharmafect 1 for 48 hrs. Western blotting of whole cell lysates was used to evaluate protein following respective RNA silencing. Cyclophilin B (CYPB) was used as a loading control. **b, c, e, f)** Relative density for western blot bands was quantified using Image Lab software from BioRad. **g, h)** BXPC3 cells were seeded into silicone inserts containing siRNA for HAS2 or scrambled. Cells were incubated for 36 h before removing the insert. Gap closure was evaluated by taking images every 3 h for up to 12 hrs. Images were processed and analysed using FIJI. Statistical analysis. One way ANOVA was used for statistical analysis (*p<0.05, **p<0.005) (western blots n=1, gap closures n=3, migration rate n=3).

5.6 Discussion

The overall lack of response with HA-containing hPSC CM and exogenous HA (H-HA-induced increase in BxPC3 cell migration notwithstanding) led us to investigate the autocrine effect of endogenous HA turnover in PDAC cells. This involved investigating HA localisation, the expression of enzymes involved in HA synthesis (HAS2) and HA breakdown (HYAL2), and strategies for functionally inhibiting these processes on PDAC cell proliferation and migration. All three PDAC cell lines showed positive staining for endogenous HA. The fluorescent pattern observed in MIA PaCa-2 and PANC1 cells was characterised by an intense pericellular fluorescence while BXCP3 cells showed mainly a punctate pattern intracellularly with faint fluorescence on the cell membrane. The pericellular coating is thought to be an important feature of metastasizing cells as it can offer protection from immune cells as well as allow adherence to endothelial cells through HA receptors like LYVE-1(Toole, 2004). PDAC cells release HA to the culture media in different quantities, MIA PaCa-2 releasing very small quantities. This feature has been observed in several types of cancer cells, becoming an intrinsic feature for some cells (Cheng et al., 2016; Li et al., 2007; Udabage et al., 2005). Intracellular HA is usually associated with endocytic vesicles where HA is destined to be degraded by HYAL1 (McAtee et al., 2015; Puissant et al., 2014). HYAL1 is an important mechanism proposed for HA turnover that begins with HA tethered to CD44 that is fragmented into smaller fragments by HYAL2 in the membrane where subsequent endocytosis occurs and it is finally degraded by HYAL1 in these endocytic vesicles (Kobayashi, Chanmee and Itano, 2020). The intracellular HA staining observed in BXPC3 cells could indicate that these cells have a high turnover rate for HA. It's also important to emphasise that despite the relative lack of plasma membrane HA staining and abundant intracellular HA staining within BxPC3 cells, does not necessarily mean that HA at the plasma membrane is not exerting an important functional response.

We determined that PDAC cells express HYAL2 in the membrane and not intracellularly. On the membrane immunofluorescence assays showed that HYAL2 was located on filopodia-like structures in MIA PaCa-2 and PANC-1 but on BXPC3 cells HYAL2 seem to be located in a morphologically different membrane structure at the leading edge, characteristic of lamellipodia (Olson and Sahai, 2009). This appears to be a novel finding as to this date there is no report indicating the presence of HYAL2 associated with these membrane structures. HAS2 was expressed in all cell lines in accordance with previous reports (Cheng et al., 2016; Junliang et al., 2019; Nagase et al., 2017). HAS2 is the most important isoform of the three HASs in adult tissue (Caon et al., 2021) and has been associated with the proliferation, migration, invasion and tumorigenicity of cancer cells (Bernert, Porsch and Heldin, 2011; Jacobson et al., 2002; Li et al., 2015). Although HAS2 plays an important role in tumour progression, it is important to note that the majority of HA associated with the desmoplastic reaction in PDAC is thought to be synthesized by PSCs (Apte et al., 2004).

To better understand HA turnover in PDAC cells we targeted different components of this system. Blocking HYALs with dextran sulphate sodium (DSS) generated striking inhibitory effects in MIA PaCa-2 cell migration but not on other cell lines. Moreover, DSS did not affect cell proliferation

in any PDAC cell line. A similar finding also showed that DSS could decrease migration, however, the cell line used was BXPC3, that in our experiments was only minimally affected by DSS treatment (Kohi et al., 2016). These discrepancies could be due to the type of assay used, Boyden chamber versus gap closure and the DSS used in these experiments which were not specified in Kohi et. al. Migration decrease by DSS has also been reported in gastric cancer cells (Xu et al., 2018) and breast cancer cells (Udabage et al., 2005; Wu et al., 2015). Interestingly it was shown that DSS decreased the generation of L-HA fragments by inhibiting HYALs in breast cancer cell lines and that L-HA was responsible for the decrease in migration (Wu et al., 2015). However, in our cell model, MIA PaCa-2 is characterized by releasing low levels of HA which might not fit with this proposed model, as adding exogenous L-HA did not recover migration. The effects of DSS might thus be related to the location of HYAL2 in filopodia-like structures, where it might have a function in stabilizing these structures (Jacquemet, Hamidi and Ivaska, 2015) that are important for cell migration (Xue, Janzen and Knecht, 2010). Interestingly DSS abolished the increase in migration seen by H-HA In BXPC3 cells which seem to express HYAL2 within lamellipodia-like structures, which could implicate HYAL-dependent migration when exposed to exogenous HA, aligning with the model proposed by Wu et. al (2005).

HA synthesis by HASs has been associated with the migration and proliferation of cancer cells, therefore its inhibition can reveal the level of participation of HA in these cellular processes. Treatment with 4-MU slightly decreased proliferation but not migration in MIA PaCa-2 cells, but slightly decreased BXPC3 cell migration without any effect on cell proliferation. These differences seen among the two cell lines could be related to their intrinsic characteristics, MIA PaCa-2 have a high proliferation rate while BXPC3 proliferate slower. This is reflected in our experiments since BXPC3 cells need to be seeded in double the density of MIA PaCa-2 cells to reach similar growth curves. On the contrary, BXPC3 cells migrate 4 to 5 times faster than MIA PaCa-2 cells. A discrepancy was seen in the outcomes of the two assays used to quantify the proliferation of MIA PaCa-2 cells, the WST-8 assay showed a marked decrease in signal while the SRB assay showed a slight decrease in signal. One explanation for this is related to how the WST-8 assay works, it relies on the redox state of the cell. The treatment with 4-MU could be increasing the oxidative stress of the cells, an effect seen in fibrosarcoma cells (Saga et al., 2021), and therefore altering the readout of the assay. MIA PaCa-2 cells have a highly glycolytic phenotype (Sritangos et al., 2020)which added to the depletion of the cytoplasmic pool of UDP-GlcUA (Kakizaki et al., 2004) could explain the apparent decrease in proliferation observed.

The HA receptor CD44 is commonly found in PDAC cells and has been associated with migration, proliferation, and invasion. Blocking CD44 with neutralizing antibodies have shown to decrease proliferating PDAC cells and reduce invasion (Li et al., 2014). Specifically, the anti-CD44 KM81 antibody induced a decrease in proliferation and migration in MIA PaCa-2 cells (Nagase et al., 2017). We did not see any of these effects in MIA PaCa-2 or BXPC3 cells treated with HA-containing hPSC CM. These results are puzzling and difficult to reconcile but they could be due to intrinsic differences in the cells, due to the expression of CD44 variants in PDAC.

Tumour cells express HASs that can synthesize a pericellular coating of HA (Aaltonen et al., 2022; Brett et al., 2018; Kainulainen et al., 2022; Rilla et al., 2008). This pericellular coating of HA is thought to be tethered to the membrane by CD44, as the absence of CD44 decreases the amount of HA on the membrane (Harkonen et al., 2019). In MIA PaCa-2 cells, we observed a similar phenomenon as HA was only localized in cells expressing CD44 on the membrane. Removing this pericellular coating with HAdase was very effective as there was no measurable membrane HA at high concentrations of the HAdase. In BXPC3 cells it was much more difficult to observe a clear-cut membrane HA staining, and any consequent removal of membrane HA staining following HAdase treatment, due to predominant and extensive intracellular staining for HA. One of the reasons for this could be that in capturing a single plane with epifluorescence imaging, any HA staining out of focus, either above or below the focal plane may also be captured in the image In addition, to exacerbate this problem, BXPC3 cells have a rounder voluminous shape, whereas MIA PaCa-2 cells are much flatter and by definition produce a sharper image with less out of focus light and a clearly defined membrane staining. However, by analysing the overall fluorescence in the 3D surface plots, a decrease in HA staining after HAdase treatment could be appreciated, thus the presence of pericellular HA could be expected. The resynthesis of HA appears to be a slow process as HA staining was maintained at a low level and did not recover to the control levels at 24 h after the treatment. The delay in synthesis could be due to the low levels of HAS2 seen in the membrane enrichment immunoblots or to the loss of CD44 signalling by internalization, which could lead to a decrease in HA synthesis by HASs (Yang et al., 2020).

The pericellular coating of HA seen in many cells is synthesized by HASs (Evanko et al., 2007; Kultti et al., 2014). This pericellular HA has been associated with facilitating cell proliferation (Itano et al., 2002; Kultti et al., 2014) by overcoming contact inhibition (Itano et al., 2002). However, the loss of the pericellular coating did not affect the proliferation of MIA PaCa-2 or BXPC3 cells. One possibility for this lack of response is that endogenous HA synthesis was not completely inhibited and thus HA was still able to engage with the HA receptor and activate downstream signalling. The other possibility is that proliferation is mainly driven by mutations in the genes *KRAS2, CDKN2A/INK4, TP53* or *DPC4/SMAD* and are less affected by HA signalling.

The synthesis of HA has been associated with migration in several types of cancer cells (Cheng et al., 2016; Kim et al., 2019) (Li et al., 2015). Removing the pericellular coating of HA differentially affects PDAC cells. In BXPC3 cells a decrease in migration could be observed while MIA PaCa-2 cells were unaffected. This indicates HA metabolism plays an active role in this cell line as it also responds to exogenous HA by increasing migration and to HA synthesis inhibition by decreasing migration. This has been alluded to in a recent report where a classification of PDAC cells was determined by the activity of HA metabolism based on the expression of several proteins that included the synthase HAS2, HAS3, and the hyaluronidases HYAL1, CEMIP (Kudo et al., 2019). PDAC cell lines express 4 proteins that are used to classify cells into having an HA activated-metabolism

phenotype (HAMP), which, in a small sample of PDAC patients (n=4) is associated with poor survival. (Kudo et al., 2019).

To eliminate the possibility of HA resynthesizing after treatment with HAdase, we used a combined treatment of HAdase for the removal of pericellular HA plus 4-MU to inhibit the resynthesis of HA. After 72 h no resynthesis of pericellular HA was observed in MIA PaCa-2 cells. We used this combination of HAdase and 4-MU to analyse PDAC cell proliferation. Both cells had no response to the treatment, and adding exogenous HA did not result in any increase or decrease in proliferation. In MIA PaCa-2 cells we observed the same effect seen with 4-MU alone, where there is a decrease in the signal of WST-8 that does not correlate with the results from the SRB assays. This was probably due to the redox-altering effects of 4-MU inducing a decrease in signal for WST-8 (Saga et al., 2021), rather than any real effect on cell proliferation as the same was not observed with SRB. These experiments sustain the fact that HA does not seem to have an important role in the proliferation of PDAC cells.

Analysing migration with the combined use of HAdase and 4-MU affected only BXPC3 cells. An additive/synergistic effect could be seen in BXPC3 cells where the combined effect of HAdase and 4-MU produced a greater decrease in migration compared to each treatment on their own. When the migration rate was measured (µm/h) there was a 40% decrease in migration rate with the combined treatment while no changes were observed in MIA PaCa-2 cells. One important thing to note is that adding exogenous HA along with 4-MU in HAdase treated cells did not recover the decrease in migration. One reason for this could be related to HA receptor CD44, as reports have shown that HA can bind to CD44 which is then internalized (Spadea et al., 2019). However, CD44 is critical for the function of HYALs on the membrane, as their activity decreases in the absence of CD44 (Harada and Takahashi, 2007). The internalization of CD44 would decrease HYAL activity which we know is crucial for the action of exogenous HA since blocking HYALs with DSS abolishes the action of exogenous HA. This highlights the importance that HA turnover has in the BXPC3 cells. Given the differences between these two cell lines, further studies exploring their characteristics could give a better understanding of HA turnover in the context of cancer.

We attempted to replicate these findings by inhibiting HA synthesis through a knockdown of the HAS2 with siRNA in BxPC3 cells. This was particularly important to remove any confounding non-specific effects of HAS2 inhibition by 4-MU. We observed a 50% decrease in migration in the HAS2 knockdown cells and a further decrease when treatment with HAdase was added. This replicates the findings observed in previous experiments with combined treatment (HAdase 4-MU). Adding exogenous HA produced a partial recovery up to 6 h and then was lost. These findings show a similar pattern observed in breast cancer cells where HAS2 knockdown produced a decrease in both migration and invasion (Bernert, Porsch and Heldin, 2011; Li et al., 2015; Porsch et al., 2013). Similar findings have been seen in colorectal cancer cells (Kim et al., 2019). Taken together these data provide evidence that HA turnover within PDAC cells; HA synthesis by HAS2 and HA breakdown by HYAL have an important role in cell migration. This is especially true in BXPC3 cells with a high HA

116

turnover rate and high migratory phenotype. Given the differences in HA turnover among PDAC cells, a similar phenomenon could be happing in a tumour setting. This could explain the failure of the clinical trial using PEGPH20 to degrade the stromal HA, as this could generate HA fragments that could be captured by tumours with high HA turnover and therefore promote the malignant phenotype.

Chapter 6   Conclusions and Future work

6.1 Conclusions

The desmoplastic reaction is one of the most defining characteristics of PDAC. The high level of fibrosis surrounding the tumour produces a collapse of blood vessels due to abnormally high interstitial pressure. This is one of the many challenges for successful treatments as it limits the access of chemotherapeutic drugs to the tumour (Olive et al., 2009). The difficulty in overcoming this barrier has led PDAC to be among the cancers with the lowest overall survival rates of all types of cancer.

HA is a main component of this extensive fibrosis and the culprit of the high interstitial pressure typically observed in PDAC tumours. Several experimental treatments have been developed to deplete the tumour stroma from HA (Provenzano et al., 2012). These are based on the use of a recombinant hyaluronidase that degrades the HA in the tumour stroma, which decreases the interstitial pressure and recovers the collapsed blood vessels allowing access to chemotherapeutic drugs. Despite the efforts, these treatments have failed at the clinical trial stage, therefore further studies are needed to understand the role that HA has in PDAC (Van Cutsem et al., 2020).

In the tumour microenvironment, the PSCs are responsible for synthesizing large quantities of ECM proteins and glycosaminoglycans (GAGs), and HA in particular. Studies have shown extensive crosstalk between PSC and PDAC cells that support tumour growth and progression. PSC can become activated by signals from PDAC cells and in response, PSCs secrete several cytokines and growth factors that directly support tumour progression. PSCs can also contribute to metabolic coupling with PDAC cells supplying tumour cells with metabolites to support growth. In this study, we attempted to investigate the role that PSC-derived HA could have on two classic cancer hallmarks: proliferation and migration. Our studies found that the CM from activated PSCs did not have any effects on proliferation but did increase migration in one of the studied PDAC cell lines (MIA PaCa-2 cells). Although when these experiments were done in the presence of blocking antibodies against the most common HA receptor CD44, this increase in migration by PSC CM was not affected. These results indicated that the migration induced by PSC CM was independent of CD44 signalling, which could imply that HA does not have a role in this process. However, MIA PaCa-2 cells also express another HA receptor, RHAMM, that we did not address in this work and could be participating in this process. In addition, since our activated hPSC cell culture did not reach 100% activation, as assessed by α-SMA, this could also have confounding effects on our results.

Recent studies have demonstrated that one of the two building blocks of HA, GlcNAc can be used to fuel the hexosamine biosynthetic pathway and promote tumour growth (Kim et al., 2021). Other studies have found that HA can promote migration (Cheng et al., 2016; Teranishi et al., 2009) and *in vivo* tumour growth (Kultti et al., 2014). However, the number of studies addressing the functional role of HA on PDAC is limited. Therefore, we attempted to further investigate the role of

HA in the proliferation and migration of PDAC cells using exogenous HA of different molecular weights. Our experiments found that HA did not affect proliferation in any of the PDAC cells studied. When we analysed migration, only H-HA increased the migration, and this effect was only seen in BXPC3 cells.

Several studies have reported that some types of tumour cells have an active HA metabolism, expressing several proteins that participate in HA turnover (Amorim et al., 2020; Bernert, Porsch and Heldin, 2011; Li et al., 2015). HAS can produce endogenous HA in PDAC cells, while HYALs can degrade HA into smaller fragments and HA receptors CD44 and RHAMM can bind HA activating intracellular signalling in PDAC cells, promoting proliferation and migration. This study focused on the expression of HAS2, HYAL2, CD44 and RHAMM. We found that the three PDAC cell lines studied expressed all four proteins. But we found some key differences, BXPC3 cells expressed variants of both HA receptors CD44 and RHAM. One important finding is that expression of HYAL2 was associated with membrane protrusions resembling filopodia in MIA PaCa-2 cells and lamellipodia in BXPC3 cells. The location of HYAL2 seems to be a novel finding that has not been reported in previous studies.

When analysing the role of HYAL2 in migration, we used the HYAL blocker DSS (Udabage et al., 2004) to inhibit HYAL2. We found a marked decrease in the migration of MIA PACa-2 cells, which was not replicated in other PDAC cell lines. Previous studies have reported that HYAL2 is a key protein in the migration of breast cancer cells (Udabage et al., 2005), therefore this could highlight the importance of HYAL2 in the migration capacity of MIA PaCa-2 cells. The role of HYAL2 in migration could be related to its cellular location that we demonstrated is associated with membrane protrusions (filopodia) that are important for cell migration (Arjonen, Kaukonen and Ivaska, 2011).

The HA receptor CD44 is overexpressed in several types of cancer, and it has been implicated in cancer cell migration and invasion (Hamilton et al., 2007; Harkonen et al., 2019; Udabage et al., 2005). Blocking the HA receptor CD44 did not produce any significant effects on migration in MIA PaCa-2 or BXPC3 cells, therefore there is a possibility that any effects of endogenous HA on PDAC cell migration may not be mediated by CD44 signalling. Furthermore, when we blocked HA synthesis in PDAC cells using 4-MU, proliferation was not affected and only BXPC3 cell migration slightly decreased. Previous studies have shown this to be the case for other cell lines as well, where HA synthesis inhibition with 4-MU also decreased the migration of several PDAC cell lines (Cheng et al., 2016).

Endogenous HA synthesis in cell lines cultured *in vitro* is usually exhibited as a pericellular coating synthesized by HASs (Evanko et al., 2007; Harkonen et al., 2019; Rilla et al., 2008). In this study, we analysed the role that this endogenous pericellular HA could play in the migration of PDAC cells. By using a bovine HAdase, we removed this pericellular coating from MIA PaCa-2 and BXPC3 cells. The removal of the pericellular HA slightly decreased migration in BXPC3 cells, but MIA PaCa-2 cells were unaffected. Furthermore, we used a combined treatment of HAdase for pericellular HA

removal and 4-MU for HA synthesis inhibition. When these two treatments were combined, there was an additive effect decreasing migration in BXPC3 cells more than each treatment applied separately. We were able to replicate these results by inhibiting HA synthesis through the knock-down of HAS2 in combinate with pericellular HA removal. This also produced a decrease in migration even more drastic than in the previous experiments. These experiments highlighted the importance of endogenous HA in the migration of BXPC3 cells.

The migration experiments in this study produced an intriguing result. Migration could not be rescued by exogenous HA when any decreases occurred by blocking HYALs, inhibiting HAS or removing pericellular HA. In previous reports studying colon carcinoma cell invasion, inhibiting HA synthesis by knocking down HASs decreased invasion, which could eventually be recovered by the addition of exogenous HA (Kim et al., 2004). One possible explanation for the lack of recovery with exogenous HA after treatments with HAdase could be the possibility of HA receptor internalization (Spadea et al., 2019; Yang et al., 2020).

Studies involving exogenous HA present several difficulties as there is no standard classification regarding the molecular weight of HA. Other issues arise in reporting the effects of HA as it exists in a range of molecular weights, therefore studies should include the molecular weight of HA used, a very important detail that is not always included. The range of molecular weights falls within a very high range, for example, H-HA can vary from 500 kDa to over 1000 kDa, while L-HA can range between over 30 kDa and up to 100 kDa. This adds another layer of difficulty when comparing different studies, as there is no agreed-upon classification for the use of HA in cancer biology studies. Even more so, when reporting the effects of HA on *in vitro* cell line cultures the presence of HYALs is not always considered, so for example the effects of H-HA could be due to the breakdown into smaller fragments rather H-HA per se. There is an urgent need for some sort of standardization to improve the knowledge of the role that HA has in cancer biology.

The main outcome of our experiments highlighted key differences in migration between two PDAC cell lines MIA PaCa-2 and BXPC3. MIA PaCa-2 cells did not respond to exogenous HA or changes in endogenous HA. Only when DSS was used to block HYALs we saw a drastic fall in MIA PaCa-2 cell migration. BXPC3 cells on the other hand increased migration when exogenous HA was applied, and decreased migration when endogenous HA was disrupted, either by inhibiting HA synthesis or removing pericellular HA. In addition to the difference in migration, how endogenous HA was present also different among these cells. The staining pattern in BXPC3 cells was prominent intracellularly and these cells released moderate quantities of HA to the media, while MIA PaCa-2 were characterized by a noticeable pericellular coating of HA and released low quantities of HA to media. The expression of HA receptors is also different, MIA PaCa-2 cells express RHAMM and CD44s more than CD44v while BXPC3 cells predominantly express low molecular weight RHAMM variants and CD44v. These characteristics suggest that BXPC3 cells have a highly active HA turnover while MIA PaCa-2 cells have a less active HA turnover. This has also been alluded to in a recent study of PDAC cells (Kudo et al., 2019) which supports the results of our study. These differences

may help to explain the intrinsic differences in cell migration; BXPC3 with a fast migratory phenotype and MIA PaCa-2 cells with a slow migratory phenotype.

Many more studies are needed to understand the role of HA in PDAC to understand what caused the failure of the clinical trials targeting HA in the tumour stroma. A further understanding could in the future improve these types of treatments which are desperately in need for patients with PDAC as treatment options are limited.

6.2 Future work

- o Explore the effects of PSC CM from at least two PSC primary cultures. Identify subpopulations by using markers for myCAFs (α-SMA) and iCAFs(IL-6) through flow cytometry to get a more accurate reading.
- o Confocal imaging of pericellular HA for a more detailed analysis.
- o The differential effect of HA on PDAC cells should be investigated by a complete characterization of the HA receptors involved, identifying CD44v that are expressed and what their role is, by knocking down both CD44s and CD44v. Complementing with the knockdown of RHAMM to reveal if it plays a role in exogenous HA induced migration.
- o A complete study of the signalling cascades involved in exogenous HA induced migration by studying the main effectors of HA-receptor interaction such as PI3K, ERK1/2, AKT, and Rho.
- o Identifying the cause of the failure of exogenous HA to recover migration in PDAC cells treated with HAdase by studying the possibility of CD44 or RHAMM receptor internalization.
- o Study the role of other hyaluronidases CEMIP and TMEM2, and their contribution to HA turnover in PDAC cells, through inhibition or knockdown strategies.
- o Study the effects of HA of different molecular weights on invasion using the Boyden chamber assay with Matrigel supplemented with HA.
- o Investigate the role of HYAL2 in membrane protrusions by knocking down HYAL2 and measuring any changes in protrusion length and number.
- o Use several more CD44 blocking antibodies to elucidate the role of CD44 in HA turnover in PDAC cells.
- o PDAC cell invasion assays with HA of different molecular weights and knockdown of HYALs.
- o Test the effects of PDAC-hPSC co-cultures on PDAC migration and proliferation (differentially express each cell type with RFP vs GFP) then knockout HAS2/HYAL2 and determine the effect on cell migration/proliferation.

- Cell proliferation could be assessed using flow cytometry (or imaging) of RFP+ vs GFP+ cells.
- Gap closure could still be used to monitor cell migration of the co-culture but with comparisons made between control co-cultures with stable knock-down of hPSC HAS2 vs HYAL2 compared to knock-down of PDAC HAS2 vs HYAL2.
- Alternatively, particle tracking software could be used to assess the migration of RFP+ vs GFP+ cells within a co-culture.
- In vivo models – xenograft vs orthotopic of PDAC cells implanted compared to PDAC-hPSC co-culture implanted with or without stable HAS2/HYAL2 knockdown/overexpression in either PDAC cells or hPSCs.

Chapter 7   References

Aaltomaa, S., et al. (2002). 'Strong Stromal Hyaluronan Expression Is Associated with PSA Recurrence in Local Prostate Cancer', *Urol Int*, 69(4), pp. 266-72. doi: 10.1159/000066123.

Aaltonen, N., et al. (2022). 'MCF10CA Breast Cancer Cells Utilize Hyaluronan-Coated EV-Rich Trails for Coordinated Migration', *Front Oncol*, 12(p. 869417. doi: 10.3389/fonc.2022.869417.

Abatangelo, G., et al. (2020). 'Hyaluronic Acid: Redefining Its Role', *Cells*, 9(7). doi: 10.3390/cells9071743.

Afratis, N., et al. (2012). 'Glycosaminoglycans: key players in cancer cell biology and treatment', *FEBS J*, 279(7), pp. 1177-97. doi: 10.1111/j.1742-4658.2012.08529.x.

Aghcheli, K., et al. (2012). 'Serum hyaluronic acid and laminin as potential tumor markers for upper gastrointestinal cancers', *Eur J Intern Med*, 23(1), pp. 58-64. doi: 10.1016/j.ejim.2011.07.018.

Al-Ismaeel, Q., et al. (2019). 'ZEB1 and IL-6/11-STAT3 signalling cooperate to define invasive potential of pancreatic cancer cells via differential regulation of the expression of S100 proteins', *Br J Cancer*, 121(1), pp. 65-75. doi: 10.1038/s41416-019-0483-9.

Amorim, S., et al. (2020). 'Hyaluronic Acid of Low Molecular Weight Triggers the Invasive "Hummingbird" Phenotype on Gastric Cancer Cells', *Adv Biosyst*, 4(11), p. e2000122. doi: 10.1002/adbi.202000122.

Anagnostopoulou, E., et al. (2017). 'Serum Hyaluronic Acid Levels Are Altered in Acute Leukemia Patients: Potential Prognostic Implications', *Acta Haematol*, 138(1), pp. 44-51. doi: 10.1159/000477574.

Andre, B., et al. (2011). 'Hyal2 is a glycosylphosphatidylinositol-anchored, lipid raft-associated hyaluronidase', *Biochem Biophys Res Commun*, 411(1), pp. 175-9. doi: 10.1016/j.bbrc.2011.06.125.

Anttila, M. A., et al. (2000). 'High levels of stromal hyaluronan predict poor disease outcome in epithelial ovarian cancer', *Cancer Res*, 60(1), pp. 150-5.

Apte, M. V., et al. (1998). 'Periacinar stellate shaped cells in rat pancreas: identification, isolation, and culture', *Gut*, 43(1), pp. 128-33. doi: 10.1136/gut.43.1.128.

Apte, M. V., et al. (1999). 'Pancreatic stellate cells are activated by proinflammatory cytokines: implications for pancreatic fibrogenesis', *Gut*, 44(4), pp. 534-41. doi: 10.1136/gut.44.4.534.

Apte, M. V., et al. (2004). 'Desmoplastic reaction in pancreatic cancer: role of pancreatic stellate cells', *Pancreas*, 29(3), pp. 179-87. doi: 10.1097/00006676-200410000-00002.

Arina, A., et al. (2016). 'Tumor-associated fibroblasts predominantly come from local and not circulating precursors', *Proc Natl Acad Sci U S A*, 113(27), pp. 7551-6. doi: 10.1073/pnas.1600363113.

Arjonen, A., Kaukonen, R. and Ivaska, J. (2011). 'Filopodia and adhesion in cancer cell motility', *Cell Adh Migr*, 5(5), pp. 421-30. doi: 10.4161/cam.5.5.17723.

Armstrong, T., et al. (2004). 'Type I collagen promotes the malignant phenotype of pancreatic ductal adenocarcinoma', *Clin Cancer Res*, 10(21), pp. 7427-37. doi: 10.1158/1078-0432.CCR-03-0825.

Auvinen, P., et al. (2013). 'Increased hyaluronan content and stromal cell CD44 associate with HER2 positivity and poor prognosis in human breast cancer', *Int J Cancer*, 132(3), pp. 531-9. doi: 10.1002/ijc.27707.

Bachem, M. G., et al. (1998). 'Identification, culture, and characterization of pancreatic stellate cells in rats and humans', *Gastroenterology*, 115(2), pp. 421-32. doi: 10.1016/s0016-5085(98)70209-4.

Bachem, M. G., et al. (2005). 'Pancreatic carcinoma cells induce fibrosis by stimulating proliferation and matrix synthesis of stellate cells', *Gastroenterology*, 128(4), pp. 907-21. doi: 10.1053/j.gastro.2004.12.036.

Bailey, J. M., et al. (2008). 'Sonic hedgehog promotes desmoplasia in pancreatic cancer', *Clin Cancer Res*, 14(19), pp. 5995-6004. doi: 10.1158/1078-0432.CCR-08-0291.

Banerji, S., et al. (1999). 'LYVE-1, a new homologue of the CD44 glycoprotein, is a lymph-specific receptor for hyaluronan', *J Cell Biol*, 144(4), pp. 789-801. doi: 10.1083/jcb.144.4.789.

Bardeesy, N., et al. (2006). 'Both p16(Ink4a) and the p19(Arf)-p53 pathway constrain progression of pancreatic adenocarcinoma in the mouse', *Proc Natl Acad Sci U S A*, 103(15), pp. 5947-52. doi: 10.1073/pnas.0601273103.

Basturk, O., et al. (2015). 'A Revised Classification System and Recommendations From the Baltimore Consensus Meeting for Neoplastic Precursor Lesions in the Pancreas', *Am J Surg Pathol*, 39(12), pp. 1730-41. doi: 10.1097/PAS.0000000000000533.

Bayne, L. J., et al. (2012). 'Tumor-derived granulocyte-macrophage colony-stimulating factor regulates myeloid inflammation and T cell immunity in pancreatic cancer', *Cancer Cell*, 21(6), pp. 822-35. doi: 10.1016/j.ccr.2012.04.025.

Bennett, K. L., et al. (1995). 'CD44 isoforms containing exon V3 are responsible for the presentation of heparin-binding growth factor', *J Cell Biol*, 128(4), pp. 687-98. doi: 10.1083/jcb.128.4.687.

Berchtold, S., et al. (2015). 'Collagen type V promotes the malignant phenotype of pancreatic ductal adenocarcinoma', *Cancer Lett*, 356(2 Pt B), pp. 721-32. doi: 10.1016/j.canlet.2014.10.020.

Berdiaki, A., et al. (2009). 'bFGF induces changes in hyaluronan synthase and hyaluronidase isoform expression and modulates the migration capacity of fibrosarcoma cells', *Biochim Biophys Acta*, 1790(10), pp. 1258-65. doi: 10.1016/j.bbagen.2009.06.013.

Bernert, B., Porsch, H. and Heldin, P. (2011). 'Hyaluronan synthase 2 (HAS2) promotes breast cancer cell invasion by suppression of tissue metalloproteinase inhibitor 1 (TIMP-1)', *J Biol Chem*, 286(49), pp. 42349-42359. doi: 10.1074/jbc.M111.278598.

Biffi, G., et al. (2019). 'IL1-Induced JAK/STAT Signaling Is Antagonized by TGFbeta to Shape CAF Heterogeneity in Pancreatic Ductal Adenocarcinoma', *Cancer Discov*, 9(2), pp. 282-301. doi: 10.1158/2159-8290.CD-18-0710.

Blando, J., et al. (2019). 'Comparison of immune infiltrates in melanoma and pancreatic cancer highlights VISTA as a potential target in pancreatic cancer', *Proc Natl Acad Sci U S A*, 116(5), pp. 1692-1697. doi: 10.1073/pnas.1811067116.

Bourguignon, L. Y., et al. (2006). 'Hyaluronan-CD44 interaction with leukemia-associated RhoGEF and epidermal growth factor receptor promotes Rho/Ras co-activation, phospholipase C epsilon-Ca2+ signaling, and cytoskeleton modification in head and neck squamous cell carcinoma cells', *J Biol Chem*, 281(20), pp. 14026-40. doi: 10.1074/jbc.M507734200.

Bourguignon, L. Y., et al. (2003). 'Hyaluronan-mediated CD44 interaction with RhoGEF and Rho kinase promotes Grb2-associated binder-1 phosphorylation and phosphatidylinositol 3-kinase signaling leading to cytokine (macrophage-colony stimulating factor) production and breast tumor progression', *J Biol Chem*, 278(32), pp. 29420-34. doi: 10.1074/jbc.M301885200.

Bourguignon, L. Y., et al. (2010). 'Hyaluronan-CD44 interaction promotes c-Src-mediated twist signaling, microRNA-10b expression, and RhoA/RhoC up-regulation, leading to Rho-kinase-associated cytoskeleton activation and breast tumor cell invasion', *J Biol Chem*, 285(47), pp. 36721-35. doi: 10.1074/jbc.M110.162305.

Bourguignon, L. Y. W., Xia, W. and Wong, G. (2009). 'Hyaluronan-mediated CD44 interaction with p300 and SIRT1 regulates beta-catenin signaling and NFkappaB-specific transcription activity leading to MDR1 and Bcl-xL gene expression and chemoresistance in breast tumor cells', *J Biol Chem*, 284(5), pp. 2657-2671. doi: 10.1074/jbc.M806708200.

Brett, M. E., et al. (2018). 'In vitro elucidation of the role of pericellular matrix in metastatic extravasation and invasion of breast carcinoma cells', *Integr Biol (Camb)*, 10(4), pp. 242-252. doi: 10.1039/c7ib00173h.

Camenisch, T. D., et al. (2000). 'Disruption of hyaluronan synthase-2 abrogates normal cardiac morphogenesis and hyaluronan-mediated transformation of epithelium to mesenchyme', *J Clin Invest*, 106(3), pp. 349-60. doi: 10.1172/JCI10272.

Cao, F., et al. (2015). 'HES 1 is essential for chemoresistance induced by stellate cells and is associated with poor prognosis in pancreatic cancer', *Oncol Rep*, 33(4), pp. 1883-9. doi: 10.3892/or.2015.3789.

Caon, I., et al. (2021). 'Cell Energy Metabolism and Hyaluronan Synthesis', *J Histochem Cytochem*, 69(1), pp. 35-47. doi: 10.1369/0022155420929772.

Chen, C., et al. (2018). 'The biology and role of CD44 in cancer progression: therapeutic implications', *J Hematol Oncol*, 11(1), p. 64. doi: 10.1186/s13045-018-0605-5.

Chen, I. M., et al. (2020). 'Clinical value of serum hyaluronan and propeptide of type III collagen in patients with pancreatic cancer', *Int J Cancer*, 146(10), pp. 2913-2922. doi: 10.1002/ijc.32751.

Chen, Y. W., et al. (2014). 'SMAD4 loss triggers the phenotypic changes of pancreatic ductal adenocarcinoma cells', *BMC Cancer*, 14(p. 181. doi: 10.1186/1471-2407-14-181.

Cheng, X. B., et al. (2016). 'Hyaluronan stimulates pancreatic cancer cell motility', *Oncotarget*, 7(4), pp. 4829-40. doi: 10.18632/oncotarget.6617.

Cheng, X. B., et al. (2015). 'Receptor for Hyaluronic Acid-Mediated Motility is Associated with Poor Survival in Pancreatic Ductal Adenocarcinoma', *J Cancer*, 6(11), pp. 1093-8. doi: 10.7150/jca.12990.

Cherr, G. N., Yudin, A. I. and Overstreet, J. W. (2001). 'The dual functions of GPI-anchored PH-20: hyaluronidase and intracellular signaling', *Matrix Biol*, 20(8), pp. 515-25. doi: 10.1016/s0945-053x(01)00171-8.

Colicelli, J. (2004). 'Human RAS superfamily proteins and related GTPases', *Sci STKE*, 2004(250), p. RE13. doi: 10.1126/stke.2502004re13.

Collaborators, G. B. D. P. C. (2019). 'The global, regional, and national burden of pancreatic cancer and its attributable risk factors in 195 countries and territories, 1990-2017: a systematic analysis for the Global Burden of Disease Study 2017', *Lancet Gastroenterol Hepatol*, 4(12), pp. 934-947. doi: 10.1016/S2468-1253(19)30347-4.

Conroy, T., et al. (2018). 'Unicancer GI PRODIGE 24/CCTG PA.6 trial: A multicenter international randomized phase III trial of adjuvant mFOLFIRINOX versus gemcitabine (gem) in patients with resected pancreatic ductal adenocarcinomas', *Journal of Clinical Oncology*, 36(18_suppl), pp. LBA4001-LBA4001. doi: 10.1200/JCO.2018.36.18_suppl.LBA4001.

Csoka, A. B., Frost, G. I. and Stern, R. (2001). 'The six hyaluronidase-like genes in the human and mouse genomes', *Matrix Biol*, 20(8), pp. 499-508. doi: 10.1016/s0945-053x(01)00172-x.

Csoka, A. B., Scherer, S. W. and Stern, R. (1999). 'Expression analysis of six paralogous human hyaluronidase genes clustered on chromosomes 3p21 and 7q31', *Genomics*, 60(3), pp. 356-61. doi: 10.1006/geno.1999.5876.

Cuff, C. A., et al. (2001). 'The adhesion receptor CD44 promotes atherosclerosis by mediating inflammatory cell recruitment and vascular cell activation', *J Clin Invest*, 108(7), pp. 1031-40. doi: 10.1172/JCI12455.

Cutsem, E. V., et al. (2018). 'More than a Gel & Hyaluronic Acid, a Central Component in the Microenvironment of Pancreatic Cancer', *European Oncology & Haematology*, 14(1), p. 40. doi: 10.17925/eoh.2018.14.1.40.

Cywes, C. and Wessels, M. R. (2001). 'Group A Streptococcus tissue invasion by CD44-mediated cell signalling', *Nature*, 414(6864), pp. 648-52. doi: 10.1038/414648a.

Dawson, D. W., et al. (2013). 'High-fat, high-calorie diet promotes early pancreatic neoplasia in the conditional KrasG12D mouse model', *Cancer Prev Res (Phila)*, 6(10), pp. 1064-73. doi: 10.1158/1940-6207.CAPR-13-0065.

de la Motte, C. A., et al. (2003). 'Mononuclear leukocytes bind to specific hyaluronan structures on colon mucosal smooth muscle cells treated with polyinosinic acid:polycytidylic acid: inter-alpha-trypsin inhibitor is crucial to structure and function', *Am J Pathol*, 163(1), pp. 121-33. doi: 10.1016/s0002-9440(10)63636-x.

Delpech, B., et al. (1990). 'Serum hyaluronan (hyaluronic acid) in breast cancer patients', *Int J Cancer*, 46(3), pp. 388-90. doi: 10.1002/ijc.2910460309.

Detlefsen, S., et al. (2005). 'Pancreatic fibrosis associated with age and ductal papillary hyperplasia', *Virchows Arch*, 447(5), pp. 800-5. doi: 10.1007/s00428-005-0032-1.

Drifka, C. R., et al. (2016). 'Highly aligned stromal collagen is a negative prognostic factor following pancreatic ductal adenocarcinoma resection', *Oncotarget*, 7(46), pp. 76197-76213. doi: 10.18632/oncotarget.12772.

Drifka, C. R., et al. (2015). 'Periductal stromal collagen topology of pancreatic ductal adenocarcinoma differs from that of normal and chronic pancreatitis', *Mod Pathol*, 28(11), pp. 1470-80. doi: 10.1038/modpathol.2015.97.

DuFort, C. C., et al. (2016). 'Interstitial Pressure in Pancreatic Ductal Adenocarcinoma Is Dominated by a Gel-Fluid Phase', *Biophys J*, 110(9), pp. 2106-19. doi: 10.1016/j.bpj.2016.03.040.

Eguchi, D., et al. (2013). 'Hypoxia enhances the interaction between pancreatic stellate cells and cancer cells via increased secretion of connective tissue growth factor', *J Surg Res*, 181(2), pp. 225-33. doi: 10.1016/j.jss.2012.06.051.

Ene-Obong, A., et al. (2013). 'Activated pancreatic stellate cells sequester CD8+ T cells to reduce their infiltration of the juxtatumoral compartment of pancreatic ductal adenocarcinoma', *Gastroenterology*, 145(5), pp. 1121-32. doi: 10.1053/j.gastro.2013.07.025.

Enegd, B., et al. (2002). 'Overexpression of hyaluronan synthase-2 reduces the tumorigenic potential of glioma cells lacking hyaluronidase activity', *Neurosurgery*, 50(6), pp. 1311-8. doi: 10.1097/00006123-200206000-00023.

Entwistle, J., Hall, C. L. and Turley, E. A. (1996). 'HA receptors: regulators of signalling to the cytoskeleton', *J Cell Biochem*, 61(4), pp. 569-77. doi: 10.1002/(sici)1097-4644(19960616)61:4<569::aid-jcb10>3.0.co;2-b.

Erkan, M., et al. (2008). 'The activated stroma index is a novel and independent prognostic marker in pancreatic ductal adenocarcinoma', *Clin Gastroenterol Hepatol*, 6(10), pp. 1155-61. doi: 10.1016/j.cgh.2008.05.006.

Evanko, S. P., et al. (2007). 'Hyaluronan-dependent pericellular matrix', *Adv Drug Deliv Rev*, 59(13), pp. 1351-65. doi: 10.1016/j.addr.2007.08.008.

Evanko, S. P. and Wight, T. N. (1999). 'Intracellular localization of hyaluronan in proliferating cells', *J Histochem Cytochem*, 47(10), pp. 1331-42. doi: 10.1177/002215549904701013.

Farrow, B., Berger, D. H. and Rowley, D. (2009). 'Tumor-derived pancreatic stellate cells promote pancreatic cancer cell invasion through release of thrombospondin-2', *J Surg Res*, 156(1), pp. 155-60. doi: 10.1016/j.jss.2009.03.040.

Felsenstein, M., et al. (2018). 'IPMNs with co-occurring invasive cancers: neighbours but not always relatives', *Gut*, 67(9), pp. 1652-1662. doi: 10.1136/gutjnl-2017-315062.

Firuzi, O., et al. (2019). 'Role of c-MET Inhibitors in Overcoming Drug Resistance in Spheroid Models of Primary Human Pancreatic Cancer and Stellate Cells', *Cancers (Basel)*, 11(5). doi: 10.3390/cancers11050638.

Fraser, J. R., Laurent, T. C. and Laurent, U. B. (1997). 'Hyaluronan: its nature, distribution, functions and turnover', *J Intern Med*, 242(1), pp. 27-33. doi: 10.1046/j.1365-2796.1997.00170.x.

Fuchs, K., et al. (2013). 'Opposing effects of high- and low-molecular weight hyaluronan on CXCL12-induced CXCR4 signaling depend on CD44', *Cell Death Dis*, 4(10), p. e819. doi: 10.1038/cddis.2013.364.

Furukawa, T. (2022). 'Mechanisms of development and progression of pancreatic neoplasms', *Pathol Int*, 72(11), pp. 529-540. doi: 10.1111/pin.13272.

Gabrilovich, D. (2004). 'Mechanisms and functional significance of tumour-induced dendritic-cell defects', *Nat Rev Immunol*, 4(12), pp. 941-52. doi: 10.1038/nri1498.

Gabrilovich, D. I., Ostrand-Rosenberg, S. and Bronte, V. (2012). 'Coordinated regulation of myeloid cells by tumours', *Nat Rev Immunol*, 12(4), pp. 253-68. doi: 10.1038/nri3175.

Ghatak, S., et al. (2010). 'Stromal hyaluronan interaction with epithelial CD44 variants promotes prostate cancer invasiveness by augmenting expression and function of hepatocyte growth factor and androgen receptor', *J Biol Chem*, 285(26), pp. 19821-32. doi: 10.1074/jbc.M110.104273.

Gieniec, K. A., et al. (2019). 'Cancer-associated fibroblasts-heroes or villains?', *Br J Cancer*, 121(4), pp. 293-302. doi: 10.1038/s41416-019-0509-3.

Gong, J., et al. (2022). 'Tumor hyaluronan as a novel biomarker in non-small cell lung cancer: A retrospective study', *Oncotarget*, 13(pp. 1202-1214. doi: 10.18632/oncotarget.28304.

Gorski, D. J., et al. (2019). 'Cardiac fibroblast activation and hyaluronan synthesis in response to hyperglycemia and diet-induced insulin resistance', *Sci Rep*, 9(1), p. 1827. doi: 10.1038/s41598-018-36140-6.

Gotoda, T., et al. (1998). 'Expression of CD44 variants and its association with survival in pancreatic cancer', *Jpn J Cancer Res*, 89(10), pp. 1033-40. doi: 10.1111/j.1349-7006.1998.tb00493.x.

Grant, T. J., Hua, K. and Singh, A. (2016). 'Molecular Pathogenesis of Pancreatic Cancer', *Prog Mol Biol Transl Sci*, 144(pp. 241-275. doi: 10.1016/bs.pmbts.2016.09.008.

Greyner, H. J., et al. (2010). 'Inducible macropinocytosis of hyaluronan in B16-F10 melanoma cells', *Matrix Biol*, 29(6), pp. 503-10. doi: 10.1016/j.matbio.2010.06.004.

Grigoriu, B., et al. (2009). 'Serum mesothelin has a higher diagnostic utility than hyaluronic acid in malignant mesothelioma', *Clin Biochem*, 42(10-11), pp. 1046-50. doi: 10.1016/j.clinbiochem.2009.03.007.

Guo, J., Xie, K. and Zheng, S. (2016). 'Molecular Biomarkers of Pancreatic Intraepithelial Neoplasia and Their Implications in Early Diagnosis and Therapeutic Intervention of Pancreatic Cancer', *Int J Biol Sci*, 12(3), pp. 292-301. doi: 10.7150/ijbs.14995.

Haber, P. S., et al. (1999). 'Activation of pancreatic stellate cells in human and experimental pancreatic fibrosis', *Am J Pathol*, 155(4), pp. 1087-95. doi: 10.1016/S0002-9440(10)65211-X.

Habisch, H., et al. (2010). 'Interaction of stellate cells with pancreatic carcinoma cells', *Cancers (Basel)*, 2(3), pp. 1661-82. doi: 10.3390/cancers2031661.

Habtezion, A., Edderkaoui, M. and Pandol, S. J. (2016). 'Macrophages and pancreatic ductal adenocarcinoma', *Cancer Lett*, 381(1), pp. 211-6. doi: 10.1016/j.canlet.2015.11.049.

Hadi, F., et al. (2020). 'Transformation of naked mole-rat cells', *Nature*, 583(7814), pp. E1-E7. doi: 10.1038/s41586-020-2410-x.

Hamilton, S. R., et al. (2007). 'The hyaluronan receptors CD44 and Rhamm (CD168) form complexes with ERK1,2 that sustain high basal motility in breast cancer cells', *J Biol Chem*, 282(22), pp. 16667-80. doi: 10.1074/jbc.M702078200.

Han, S., et al. (2019). 'Prognostic Value of CD44 and Its Isoforms in Advanced Cancer: A Systematic Meta-Analysis With Trial Sequential Analysis', *Front Oncol*, 9(p. 39. doi: 10.3389/fonc.2019.00039.

Hanahan, D. and Weinberg, R. A. (2000). 'The hallmarks of cancer', *Cell*, 100(1), pp. 57-70. doi: 10.1016/s0092-8674(00)81683-9.

Hanahan, D. and Weinberg, R. A. (2011). 'Hallmarks of cancer: the next generation', *Cell*, 144(5), pp. 646-74. doi: 10.1016/j.cell.2011.02.013.

Harada, H. and Takahashi, M. (2007). 'CD44-dependent intracellular and extracellular catabolism of hyaluronic acid by hyaluronidase-1 and -2', *J Biol Chem*, 282(8), pp. 5597-607. doi: 10.1074/jbc.M608358200.

Hardwick, C., et al. (1992). 'Molecular cloning of a novel hyaluronan receptor that mediates tumor cell motility', *J Cell Biol*, 117(6), pp. 1343-50. doi: 10.1083/jcb.117.6.1343.

Harkonen, K., et al. (2019). 'CD44s Assembles Hyaluronan Coat on Filopodia and Extracellular Vesicles and Induces Tumorigenicity of MKN74 Gastric Carcinoma Cells', *Cells*, 8(3). doi: 10.3390/cells8030276.

Harris, E. N. and Baker, E. (2020). 'Role of the Hyaluronan Receptor, Stabilin-2/HARE, in Health and Disease', *Int J Mol Sci*, 21(10). doi: 10.3390/ijms21103504.

Hayashi, A., Hong, J. and Iacobuzio-Donahue, C. A. (2021). 'The pancreatic cancer genome revisited', *Nat Rev Gastroenterol Hepatol*, 18(7), pp. 469-481. doi: 10.1038/s41575-021-00463-z.

Hendawy, H. A. E., et al. (2017). 'N-cadherin and hyaluronan expression in head and neck squamous cell carcinoma, relation to patient outcomes', *Journal of Solid Tumors*, 8(1). doi: 10.5430/jst.v8n1p19.

Herting, C. J., Karpovsky, I. and Lesinski, G. B. (2021). 'The tumor microenvironment in pancreatic ductal adenocarcinoma: current perspectives and future directions', *Cancer Metastasis Rev*, 40(3), pp. 675-689. doi: 10.1007/s10555-021-09988-w.

Hidalgo, M. (2010). 'Pancreatic cancer', *N Engl J Med*, 362(17), pp. 1605-17. doi: 10.1056/NEJMra0901557.

Hinneh, J. A., et al. (2022). 'The role of RHAMM in cancer: Exposing novel therapeutic vulnerabilities', *Front Oncol*, 12(p. 982231. doi: 10.3389/fonc.2022.982231.

Hosein, A. N., Brekken, R. A. and Maitra, A. (2020). 'Pancreatic cancer stroma: an update on therapeutic targeting strategies', *Nat Rev Gastroenterol Hepatol*, 17(8), pp. 487-505. doi: 10.1038/s41575-020-0300-1.

Hotta, T., et al. (2004). 'Chemotherapy and serum hyaluronic acid levels in malignant peritoneal mesothelioma', *Hepatogastroenterology*, 51(58), pp. 1073-83.

Hruban, R. H., et al. (2010). 'Update on familial pancreatic cancer', *Adv Surg*, 44(1), pp. 293-311. doi: 10.1016/j.yasu.2010.05.011.

Hruban, R. H., et al. (2000). 'Progression model for pancreatic cancer', *Clin Cancer Res*, 6(8), pp. 2969-72.

Hruban, R. H., Wilentz, R. E. and Kern, S. E. (2000). 'Genetic progression in the pancreatic ducts', *Am J Pathol*, 156(6), pp. 1821-5. doi: 10.1016/S0002-9440(10)65054-7.

Huang, H., et al. (2019). 'Targeting TGFbetaR2-mutant tumors exposes vulnerabilities to stromal TGFbeta blockade in pancreatic cancer', *EMBO Mol Med*, 11(11), p. e10515. doi: 10.15252/emmm.201910515.

Hurwitz, E., et al. (2023). 'Antagonism between Prdm16 and Smad4 specifies the trajectory and progression of pancreatic cancer', *J Cell Biol*, 222(4). doi: 10.1083/jcb.202203036.

Hwang, R. F., et al. (2008). 'Cancer-associated stromal fibroblasts promote pancreatic tumor progression', *Cancer Res*, 68(3), pp. 918-26. doi: 10.1158/0008-5472.CAN-07-5714.

Hwang, R. F., et al. (2012). 'Inhibition of the hedgehog pathway targets the tumor-associated stroma in pancreatic cancer', *Mol Cancer Res*, 10(9), pp. 1147-57. doi: 10.1158/1541-7786.MCR-12-0022.

Hynes, R. O. and Naba, A. (2012). 'Overview of the matrisome--an inventory of extracellular matrix constituents and functions', *Cold Spring Harb Perspect Biol*, 4(1), p. a004903. doi: 10.1101/cshperspect.a004903.

Iacobuzio-Donahue, C. A. (2012). 'Genetic evolution of pancreatic cancer: lessons learnt from the pancreatic cancer genome sequencing project', *Gut*, 61(7), pp. 1085-94. doi: 10.1136/gut.2010.236026.

Iczkowski, K. A. (2010). 'Cell adhesion molecule CD44: its functional roles in prostate cancer', *Am J Transl Res*, 3(1), pp. 1-7.

Itano, N., et al. (2002). 'Abnormal accumulation of hyaluronan matrix diminishes contact inhibition of cell growth and promotes cell migration', *Proc Natl Acad Sci U S A*, 99(6), pp. 3609-14. doi: 10.1073/pnas.052026799.

Itano, N. and Kimata, K. (2002). 'Mammalian hyaluronan synthases', *IUBMB Life*, 54(4), pp. 195-9. doi: 10.1080/15216540214929.

Itano, N., et al. (1999). 'Three isoforms of mammalian hyaluronan synthases have distinct enzymatic properties', *J Biol Chem*, 274(35), pp. 25085-92. doi: 10.1074/jbc.274.35.25085.

Jackson, D. G. (2019). 'Hyaluronan in the lymphatics: The key role of the hyaluronan receptor LYVE-1 in leucocyte trafficking', *Matrix Biol*, 78-79(pp. 219-235. doi: 10.1016/j.matbio.2018.02.001.

Jacobetz, M. A., et al. (2013). 'Hyaluronan impairs vascular function and drug delivery in a mouse model of pancreatic cancer', *Gut*, 62(1), pp. 112-20. doi: 10.1136/gutjnl-2012-302529.

Jacobson, A., et al. (2002). 'Expression of hyaluronan synthase 2 or hyaluronidase 1 differentially affect the growth rate of transplantable colon carcinoma cell tumors', *Int J Cancer*, 102(3), pp. 212-9. doi: 10.1002/ijc.10683.

Jacquemet, G., Hamidi, H. and Ivaska, J. (2015). 'Filopodia in cell adhesion, 3D migration and cancer cell invasion', *Curr Opin Cell Biol*, 36(pp. 23-31. doi: 10.1016/j.ceb.2015.06.007.

Jiang, P., et al. (2021). 'Negative regulation of AMPK signaling by high glucose via E3 ubiquitin ligase MG53', *Mol Cell*, 81(3), pp. 629-637 e5. doi: 10.1016/j.molcel.2020.12.008.

Johnson, L. A., et al. (2017). 'Dendritic cells enter lymph vessels by hyaluronan-mediated docking to the endothelial receptor LYVE-1', *Nat Immunol*, 18(7), pp. 762-770. doi: 10.1038/ni.3750.

Johnson, L. A. and Jackson, D. G. (2021). 'Hyaluronan and Its Receptors: Key Mediators of Immune Cell Entry and Trafficking in the Lymphatic System', *Cells*, 10(8), p. 2061. doi: 10.3390/cells10082061.

Jonckheere, N., Vasseur, R. and Van Seuningen, I. (2017). 'The cornerstone K-RAS mutation in pancreatic adenocarcinoma: From cell signaling network, target genes, biological processes to therapeutic targeting', *Crit Rev Oncol Hematol*, 111(pp. 7-19. doi: 10.1016/j.critrevonc.2017.01.002.

Jouon, N., et al. (1995). 'Hydration of hyaluronic acid as a function of the counterion type and relative humidity', *Carbohydrate Polymers*, 26(1), pp. 69-73. doi: 10.1016/0144-8617(95)98837-7.

Junliang, L., et al. (2019). 'High-molecular-weight hyaluronan produced by activated pancreatic stellate cells promotes pancreatic cancer cell migration via paracrine signaling', *Biochem Biophys Res Commun*, 515(3), pp. 493-498. doi: 10.1016/j.bbrc.2019.05.167.

Kainulainen, K., et al. (2022). 'M1 Macrophages Induce Protumor Inflammation in Melanoma Cells through TNFR-NF-kappaB Signaling', *J Invest Dermatol*, 142(11), pp. 3041-3051 e10. doi: 10.1016/j.jid.2022.04.024.

Kakizaki, I., et al. (2004). 'A novel mechanism for the inhibition of hyaluronan biosynthesis by 4-methylumbelliferone', *J Biol Chem*, 279(32), pp. 33281-9. doi: 10.1074/jbc.M405918200.

Kalluri, R. (2016). 'The biology and function of fibroblasts in cancer', *Nat Rev Cancer*, 16(9), pp. 582-98. doi: 10.1038/nrc.2016.73.

Kamphorst, J. J., et al. (2015). 'Human pancreatic cancer tumors are nutrient poor and tumor cells actively scavenge extracellular protein', *Cancer Res*, 75(3), pp. 544-53. doi: 10.1158/0008-5472.CAN-14-2211.

Karamanos, N. K., et al. (2021). 'A guide to the composition and functions of the extracellular matrix', *FEBS J*, 288(24), pp. 6850-6912. doi: 10.1111/febs.15776.

Khaled, Y. S., Ammori, B. J. and Elkord, E. (2014). 'Increased levels of granulocytic myeloid-derived suppressor cells in peripheral blood and tumour tissue of pancreatic cancer patients', *J Immunol Res*, 2014(p. 879897. doi: 10.1155/2014/879897.

Kim, H. R., et al. (2004). 'Hyaluronan facilitates invasion of colon carcinoma cells in vitro via interaction with CD44', *Cancer Res*, 64(13), pp. 4569-76. doi: 10.1158/0008-5472.CAN-04-0202.

Kim, P. K., et al. (2021). 'Hyaluronic acid fuels pancreatic cancer cell growth', *Elife*, 10(doi: 10.7554/eLife.62645.

Kim, W. Y. and Sharpless, N. E. (2006). 'The regulation of INK4/ARF in cancer and aging', *Cell*, 127(2), pp. 265-75. doi: 10.1016/j.cell.2006.10.003.

Kim, Y. H., et al. (2019). 'Hyaluronic acid synthase 2 promotes malignant phenotypes of colorectal cancer cells through transforming growth factor beta signaling', *Cancer Sci*, 110(7), pp. 2226-2236. doi: 10.1111/cas.14070.

Klein, A. P. (2021). 'Pancreatic cancer epidemiology: understanding the role of lifestyle and inherited risk factors', *Nat Rev Gastroenterol Hepatol*, 18(7), pp. 493-502. doi: 10.1038/s41575-021-00457-x.

Kobayashi, T., Chanmee, T. and Itano, N. (2020). 'Hyaluronan: Metabolism and Function', *Biomolecules*, 10(11), p. 1525. doi: 10.3390/biom10111525.

Koenig, A., et al. (2006). 'Collagen type I induces disruption of E-cadherin-mediated cell-cell contacts and promotes proliferation of pancreatic carcinoma cells', *Cancer Res*, 66(9), pp. 4662-71. doi: 10.1158/0008-5472.CAN-05-2804.

Kohi, S., et al. (2016). 'Increased Expression of HYAL1 in Pancreatic Ductal Adenocarcinoma', *Pancreas*, 45(10), pp. 1467-1473. doi: 10.1097/MPA.0000000000000670.

Kopp, J. L., et al. (2012). 'Identification of Sox9-dependent acinar-to-ductal reprogramming as the principal mechanism for initiation of pancreatic ductal adenocarcinoma', *Cancer Cell*, 22(6), pp. 737-50. doi: 10.1016/j.ccr.2012.10.025.

Kothapalli, D., et al. (2008). 'Differential activation of ERK and Rac mediates the proliferative and anti-proliferative effects of hyaluronan and CD44', *J Biol Chem*, 283(46), pp. 31823-9. doi: 10.1074/jbc.M802934200.

Kothapalli, D., et al. (2007). 'Hyaluronan and CD44 antagonize mitogen-dependent cyclin D1 expression in mesenchymal cells', *J Cell Biol*, 176(4), pp. 535-44. doi: 10.1083/jcb.200611058.

Kouvidi, K., et al. (2011). 'Role of receptor for hyaluronic acid-mediated motility (RHAMM) in low molecular weight hyaluronan (LMWHA)-mediated fibrosarcoma cell adhesion', *J Biol Chem*, 286(44), pp. 38509-38520. doi: 10.1074/jbc.M111.275875.

Kuang, D. M., et al. (2007). 'Tumor-derived hyaluronan induces formation of immunosuppressive macrophages through transient early activation of monocytes', *Blood*, 110(2), pp. 587-95. doi: 10.1182/blood-2007-01-068031.

Kudo, Y., et al. (2019). 'Hyaluronan activated-metabolism phenotype (HAMP) in pancreatic ductal adenocarcinoma', *Oncotarget*, 10(54), pp. 5592-5604. doi: 10.18632/oncotarget.27172.

Kuipers, H. F., et al. (2016). 'Hyaluronan synthesis is necessary for autoreactive T-cell trafficking, activation, and Th1 polarization', *Proc Natl Acad Sci U S A*, 113(5), pp. 1339-44. doi: 10.1073/pnas.1525086113.

Kulaberoglu, Y., et al. (2019). 'The material properties of naked mole-rat hyaluronan', *Sci Rep*, 9(1), p. 6632. doi: 10.1038/s41598-019-43194-7.

Kultti, A., et al. (2012). 'Therapeutic targeting of hyaluronan in the tumor stroma', *Cancers (Basel)*, 4(3), pp. 873-903. doi: 10.3390/cancers4030873.

Kultti, A., et al. (2009). '4-Methylumbelliferone inhibits hyaluronan synthesis by depletion of cellular UDP-glucuronic acid and downregulation of hyaluronan synthase 2 and 3', *Exp Cell Res*, 315(11), pp. 1914-23. doi: 10.1016/j.yexcr.2009.03.002.

Kultti, A., et al. (2014). 'Accumulation of extracellular hyaluronan by hyaluronan synthase 3 promotes tumor growth and modulates the pancreatic cancer microenvironment', *Biomed Res Int*, 2014(p. 817613. doi: 10.1155/2014/817613.

Kyykallio, H., et al. (2020). 'The Density and Length of Filopodia Associate with the Activity of Hyaluronan Synthesis in Tumor Cells', *Cancers (Basel)*, 12(7), p. 1908. doi: 10.3390/cancers12071908.

Lachowski, D., et al. (2017). 'Substrate Rigidity Controls Activation and Durotaxis in Pancreatic Stellate Cells', *Sci Rep*, 7(1), p. 2506. doi: 10.1038/s41598-017-02689-x.

Lankadasari, M. B., et al. (2019). 'TAMing pancreatic cancer: combat with a double edged sword', *Mol Cancer*, 18(1), p. 48. doi: 10.1186/s12943-019-0966-6.

Laurent, T. C. and Fraser, J. R. E. (1992). 'Hyaluronan

1', *The FASEB Journal*, 6(7), pp. 2397-2404. doi: 10.1096/fasebj.6.7.1563592.

Lawrance, W., et al. (2016). 'Binding of Hyaluronan to the Native Lymphatic Vessel Endothelial Receptor LYVE-1 Is Critically Dependent on Receptor Clustering and Hyaluronan Organization', *J Biol Chem*, 291(15), pp. 8014-30. doi: 10.1074/jbc.M115.708305.

Leitinger, B. and Hohenester, E. (2007). 'Mammalian collagen receptors', *Matrix Biol*, 26(3), pp. 146-55. doi: 10.1016/j.matbio.2006.10.007.

Leppanen, J., et al. (2019). 'Tenascin C, Fibronectin, and Tumor-Stroma Ratio in Pancreatic Ductal Adenocarcinoma', *Pancreas*, 48(1), pp. 43-48. doi: 10.1097/MPA.0000000000001195.

Li, L., et al. (2014). 'Antibody against CD44s inhibits pancreatic tumor initiation and postradiation recurrence in mice', *Gastroenterology*, 146(4), pp. 1108-18. doi: 10.1053/j.gastro.2013.12.035.

Li, P., et al. (2015). 'Hyaluronan synthase 2 overexpression is correlated with the tumorigenesis and metastasis of human breast cancer', *Int J Clin Exp Pathol*, 8(10), pp. 12101-14.

Li, X., et al. (2018). 'Parallel Accumulation of Tumor Hyaluronan, Collagen, and Other Drivers of Tumor Progression', *Clin Cancer Res*, 24(19), pp. 4798-4807. doi: 10.1158/1078-0432.CCR-17-3284.

Li, Y., et al. (2007). 'Silencing of hyaluronan synthase 2 suppresses the malignant phenotype of invasive breast cancer cells', *Int J Cancer*, 120(12), pp. 2557-67. doi: 10.1002/ijc.22550.

Lin, A., et al. (2021). 'High levels of truncated RHAMM cooperate with dysfunctional p53 to accelerate the progression of pancreatic cancer', *Cancer Lett*, 514(pp. 79-89. doi: 10.1016/j.canlet.2021.05.011.

Lippi, G. and Mattiuzzi, C. (2020). 'The global burden of pancreatic cancer', *Arch Med Sci*, 16(4), pp. 820-824. doi: 10.5114/aoms.2020.94845.

Lohr, M., et al. (2001). 'Transforming growth factor-beta1 induces desmoplasia in an experimental model of human pancreatic carcinoma', *Cancer Res*, 61(2), pp. 550-5.

Lokeshwar, V. B., et al. (2005). 'HYAL1 hyaluronidase in prostate cancer: a tumor promoter and suppressor', *Cancer Res*, 65(17), pp. 7782-9. doi: 10.1158/0008-5472.CAN-05-1022.

Lokeshwar, V. B., et al. (1997). 'Tumor-associated hyaluronic acid: a new sensitive and specific urine marker for bladder cancer', *Cancer Res*, 57(4), pp. 773-7.

Lompardia, S. L., et al. (2013). 'Human leukemic cell lines synthesize hyaluronan to avoid senescence and resist chemotherapy', *Glycobiology*, 23(12), pp. 1463-76. doi: 10.1093/glycob/cwt074.

Luttenberger, T., et al. (2000). 'Platelet-derived growth factors stimulate proliferation and extracellular matrix synthesis of pancreatic stellate cells: implications in pathogenesis of pancreas fibrosis', *Lab Invest*, 80(1), pp. 47-55. doi: 10.1038/labinvest.3780007.

Lv, L., et al. (2016). 'Upregulation of CD44v6 contributes to acquired chemoresistance via the modulation of autophagy in colon cancer SW480 cells', *Tumour Biol*, 37(7), pp. 8811-24. doi: 10.1007/s13277-015-4755-6.

Maia, A. and Wiemann, S. (2021). 'Cancer-Associated Fibroblasts: Implications for Cancer Therapy', *Cancers (Basel)*, 13(14). doi: 10.3390/cancers13143526.

Maxwell, C. A., et al. (2003). 'RHAMM is a centrosomal protein that interacts with dynein and maintains spindle pole stability', *Mol Biol Cell*, 14(6), pp. 2262-76. doi: 10.1091/mbc.e02-07-0377.

Maxwell, C. A., McCarthy, J. and Turley, E. (2008). 'Cell-surface and mitotic-spindle RHAMM: moonlighting or dual oncogenic functions?', *J Cell Sci*, 121(Pt 7), pp. 925-32. doi: 10.1242/jcs.022038.

McAtee, C. O., Barycki, J. J. and Simpson, M. A. (2014). 'Emerging roles for hyaluronidase in cancer metastasis and therapy', *Adv Cancer Res*, 123(pp. 1-34. doi: 10.1016/B978-0-12-800092-2.00001-0.

McAtee, C. O., et al. (2015). 'Hyaluronidase Hyal1 Increases Tumor Cell Proliferation and Motility through Accelerated Vesicle Trafficking', *J Biol Chem*, 290(21), pp. 13144-56. doi: 10.1074/jbc.M115.647446.

McGuigan, A., et al. (2018). 'Pancreatic cancer: A review of clinical diagnosis, epidemiology, treatment and outcomes', *World J Gastroenterol*, 24(43), pp. 4846-4861. doi: 10.3748/wjg.v24.i43.4846.

Mele, V., et al. (2017). 'The hyaluronan-mediated motility receptor RHAMM promotes growth, invasiveness and dissemination of colorectal cancer', *Oncotarget*, 8(41), pp. 70617-70629. doi: 10.18632/oncotarget.19904.

Messmer, M. N., et al. (2015). 'Tumor-induced myeloid dysfunction and its implications for cancer immunotherapy', *Cancer Immunol Immunother*, 64(1), pp. 1-13. doi: 10.1007/s00262-014-1639-3.

Mews, P., et al. (2002). 'Pancreatic stellate cells respond to inflammatory cytokines: potential role in chronic pancreatitis', *Gut*, 50(4), pp. 535-41. doi: 10.1136/gut.50.4.535.

Midha, S., Chawla, S. and Garg, P. K. (2016). 'Modifiable and non-modifiable risk factors for pancreatic cancer: A review', *Cancer Lett*, 381(1), pp. 269-77. doi: 10.1016/j.canlet.2016.07.022.

Misra, S., et al. (2015). 'Interactions between Hyaluronan and Its Receptors (CD44, RHAMM) Regulate the Activities of Inflammation and Cancer', *Front Immunol*, 6(p. 201. doi: 10.3389/fimmu.2015.00201.

Miwa, T., et al. (2017). 'Isoform switch of CD44 induces different chemotactic and tumorigenic ability in gallbladder cancer', *Int J Oncol*, 51(3), pp. 771-780. doi: 10.3892/ijo.2017.4063.

Mizrahi, J. D., et al. (2020). 'Pancreatic cancer', *Lancet*, 395(10242), pp. 2008-2020. doi: 10.1016/S0140-6736(20)30974-0.

Mochizuki, S., et al. (2009). 'Uptake of enzymatically-digested hyaluronan by liver endothelial cells in vivo and in vitro', *J Biomater Sci Polym Ed*, 20(1), pp. 83-97. doi: 10.1163/156856208X393518.

Monslow, J., Govindaraju, P. and Pure, E. (2015). 'Hyaluronan - a functional and structural sweet spot in the tissue microenvironment', *Front Immunol*, 6(p. 231. doi: 10.3389/fimmu.2015.00231.

Morera, D. S., et al. (2017). 'Hyaluronic acid family in bladder cancer: potential prognostic biomarkers and therapeutic targets', *Br J Cancer*, 117(10), pp. 1507-1517. doi: 10.1038/bjc.2017.318.

Mori, T., et al. (2008). 'Structural basis for CD44 recognition by ERM proteins', *J Biol Chem*, 283(43), pp. 29602-12. doi: 10.1074/jbc.M803606200.

Morrison, H., et al. (2001). 'The NF2 tumor suppressor gene product, merlin, mediates contact inhibition of growth through interactions with CD44', *Genes Dev*, 15(8), pp. 968-80. doi: 10.1101/gad.189601.

Morton, J. P., et al. (2010). 'Mutant p53 drives metastasis and overcomes growth arrest/senescence in pancreatic cancer', *Proc Natl Acad Sci U S A*, 107(1), pp. 246-51. doi: 10.1073/pnas.0908428107.

Mouw, J. K., Ou, G. and Weaver, V. M. (2014). 'Extracellular matrix assembly: a multiscale deconstruction', *Nat Rev Mol Cell Biol*, 15(12), pp. 771-85. doi: 10.1038/nrm3902.

Mueller, B. M., et al. (2010). 'Hyaluronan inhibits postchemotherapy tumor regrowth in a colon carcinoma xenograft model', *Mol Cancer Ther*, 9(11), pp. 3024-32. doi: 10.1158/1535-7163.MCT-10-0529.

Murray, P. J., et al. (2014). 'Macrophage activation and polarization: nomenclature and experimental guidelines', *Immunity*, 41(1), pp. 14-20. doi: 10.1016/j.immuni.2014.06.008.

Nagase, H., et al. (2017). '4-Methylumbelliferone Suppresses Hyaluronan Synthesis and Tumor Progression in SCID Mice Intra-abdominally Inoculated With Pancreatic Cancer Cells', *Pancreas*, 46(2), pp. 190-197. doi: 10.1097/MPA.0000000000000741.

Nagashima, T., et al. (2020). 'Clinical Significance of Tumour CD44v and MIST1 Expression in Patients With Non-small-cell Lung Cancer', *Anticancer Res*, 40(11), pp. 6407-6416. doi: 10.21873/anticanres.14662.

Nagathihalli, N. S., et al. (2016). 'Pancreatic stellate cell secreted IL-6 stimulates STAT3 dependent invasiveness of pancreatic intraepithelial neoplasia and cancer cells', *Oncotarget*, 7(40), pp. 65982-65992. doi: 10.18632/oncotarget.11786.

Nagy, N., et al. (2015). '4-methylumbelliferone treatment and hyaluronan inhibition as a therapeutic strategy in inflammation, autoimmunity, and cancer', *Front Immunol*, 6(123), p. 123. doi: 10.3389/fimmu.2015.00123.

Naor, D., et al. (2002). 'CD44 in cancer', *Crit Rev Clin Lab Sci*, 39(6), pp. 527-79. doi: 10.1080/10408360290795574.

Naor, D., Sionov, R. V. and Ish-Shalom, D. (1997). 'CD44: Structure, Function and Association with the Malignant Process', in Vande Woude, G. F. and Klein, G. (eds.) *Advances in Cancer Research*: Academic Press, pp. 241-319.

Neesse, A., et al. (2015). 'Stromal biology and therapy in pancreatic cancer: a changing paradigm', *Gut*, 64(9), pp. 1476-84. doi: 10.1136/gutjnl-2015-309304.

Neoptolemos, J. P., et al. (2017). 'Comparison of adjuvant gemcitabine and capecitabine with gemcitabine monotherapy in patients with resected pancreatic cancer (ESPAC-4): a multicentre, open-label, randomised, phase 3 trial', *Lancet*, 389(10073), pp. 1011-1024. doi: 10.1016/S0140-6736(16)32409-6.

Neoptolemos, J. P., et al. (2010). 'Adjuvant chemotherapy with fluorouracil plus folinic acid vs gemcitabine following pancreatic cancer resection: a randomized controlled trial', *JAMA*, 304(10), pp. 1073-81. doi: 10.1001/jama.2010.1275.

Niedworok, C., et al. (2013). 'The impact of the receptor of hyaluronan-mediated motility (RHAMM) on human urothelial transitional cell cancer of the bladder', *PLoS One*, 8(9), p. e75681. doi: 10.1371/journal.pone.0075681.

Nykopp, T. K., et al. (2010). 'Hyaluronan synthases (HAS1-3) and hyaluronidases (HYAL1-2) in the accumulation of hyaluronan in endometrioid endometrial carcinoma', *BMC Cancer*, 10(1), p. 512. doi: 10.1186/1471-2407-10-512.

Ogiya, D., et al. (2019). 'Aberrant RHAMM Splicing in Multiple Myeloma (MM) and Its Implications for Immunotherapy', *Blood*, 134(Supplement_1), pp. 1804-1804. doi: 10.1182/blood-2019-131775.

Ohlund, D., et al. (2013). 'Type IV collagen stimulates pancreatic cancer cell proliferation, migration, and inhibits apoptosis through an autocrine loop', *BMC Cancer*, 13(p. 154. doi: 10.1186/1471-2407-13-154.

Ohlund, D., et al. (2017). 'Distinct populations of inflammatory fibroblasts and myofibroblasts in pancreatic cancer', *J Exp Med*, 214(3), pp. 579-596. doi: 10.1084/jem.20162024.

Oida, T. and Weiner, H. L. (2010). 'Depletion of TGF-beta from fetal bovine serum', *J Immunol Methods*, 362(1-2), pp. 195-8. doi: 10.1016/j.jim.2010.09.008.

Olivares, O., et al. (2017). 'Collagen-derived proline promotes pancreatic ductal adenocarcinoma cell survival under nutrient limited conditions', *Nat Commun*, 8(p. 16031. doi: 10.1038/ncomms16031.

Olive, K. P., et al. (2009). 'Inhibition of Hedgehog signaling enhances delivery of chemotherapy in a mouse model of pancreatic cancer', *Science*, 324(5933), pp. 1457-61. doi: 10.1126/science.1171362.

Olson, M. F. and Sahai, E. (2009). 'The actin cytoskeleton in cancer cell motility', *Clin Exp Metastasis*, 26(4), pp. 273-87. doi: 10.1007/s10585-008-9174-2.

Opitz, F. V., et al. (2021). 'Tumor Microenvironment in Pancreatic Intraepithelial Neoplasia', *Cancers (Basel)*, 13(24). doi: 10.3390/cancers13246188.

Orth, M., et al. (2019). 'Pancreatic ductal adenocarcinoma: biological hallmarks, current status, and future perspectives of combined modality treatment approaches', *Radiat Oncol*, 14(1), p. 141. doi: 10.1186/s13014-019-1345-6.

Ostuni, R., et al. (2015). 'Macrophages and cancer: from mechanisms to therapeutic implications', *Trends Immunol*, 36(4), pp. 229-39. doi: 10.1016/j.it.2015.02.004.

Ozdemir, B. C., et al. (2015). 'Depletion of Carcinoma-Associated Fibroblasts and Fibrosis Induces Immunosuppression and Accelerates Pancreas Cancer with Reduced Survival', *Cancer Cell*, 28(6), pp. 831-833. doi: 10.1016/j.ccell.2015.11.002.

Park, D., et al. (2012). 'Hyaluronic acid promotes angiogenesis by inducing RHAMM-TGFbeta receptor interaction via CD44-PKCdelta', *Mol Cells*, 33(6), pp. 563-74. doi: 10.1007/s10059-012-2294-1.

Paron, I., et al. (2011). 'Tenascin-C enhances pancreatic cancer cell growth and motility and affects cell adhesion through activation of the integrin pathway', *PLoS One*, 6(6), p. e21684. doi: 10.1371/journal.pone.0021684.

Passi, A., et al. (2019). 'Dissecting the role of hyaluronan synthases in the tumor microenvironment', *FEBS J*, 286(15), pp. 2937-2949. doi: 10.1111/febs.14847.

Perez-Mancera, P. A., et al. (2012). 'What we have learned about pancreatic cancer from mouse models', *Gastroenterology*, 142(5), pp. 1079-92. doi: 10.1053/j.gastro.2012.03.002.

Petitjean, A., et al. (2007). 'Impact of mutant p53 functional properties on TP53 mutation patterns and tumor phenotype: lessons from recent developments in the IARC TP53 database', *Hum Mutat*, 28(6), pp. 622-9. doi: 10.1002/humu.20495.

Philipson, L. H. and Schwartz, N. B. (1984). 'Subcellular localization of hyaluronate synthetase in oligodendroglioma cells', *J Biol Chem*, 259(8), pp. 5017-23. doi: 10.1016/S0021-9258(17)42948-6.

Phillips, P. A., et al. (2003). 'Rat pancreatic stellate cells secrete matrix metalloproteinases: implications for extracellular matrix turnover', *Gut*, 52(2), pp. 275-82. doi: 10.1136/gut.52.2.275.

Piersma, B., Hayward, M. K. and Weaver, V. M. (2020). 'Fibrosis and cancer: A strained relationship', *Biochim Biophys Acta Rev Cancer*, 1873(2), p. 188356. doi: 10.1016/j.bbcan.2020.188356.

Pineda, S., et al. (2021). 'Tumor-Infiltrating B- and T-Cell Repertoire in Pancreatic Cancer Associated With Host and Tumor Features', *Front Immunol*, 12(p. 730746. doi: 10.3389/fimmu.2021.730746.

Pirinen, R., et al. (2001). 'Prognostic value of hyaluronan expression in non-small-cell lung cancer: Increased stromal expression indicates unfavorable outcome in patients with adenocarcinoma', *Int J Cancer*, 95(1), pp. 12-7. doi: 10.1002/1097-0215(20010120)95:1<12::aid-ijc1002>3.0.co;2-e.

Ponta, H., Sherman, L. and Herrlich, P. A. (2003). 'CD44: from adhesion molecules to signalling regulators', *Nat Rev Mol Cell Biol*, 4(1), pp. 33-45. doi: 10.1038/nrm1004.

Porsch, H., et al. (2013). 'Efficient TGFbeta-induced epithelial-mesenchymal transition depends on hyaluronan synthase HAS2', *Oncogene*, 32(37), pp. 4355-65. doi: 10.1038/onc.2012.475.

Pothula, S. P., et al. (2016). 'Hepatocyte growth factor inhibition: a novel therapeutic approach in pancreatic cancer', *Br J Cancer*, 114(3), pp. 269-80. doi: 10.1038/bjc.2015.478.

Provenzano, P. P., et al. (2012). 'Enzymatic targeting of the stroma ablates physical barriers to treatment of pancreatic ductal adenocarcinoma', *Cancer Cell*, 21(3), pp. 418-29. doi: 10.1016/j.ccr.2012.01.007.

Puissant, E., et al. (2014). 'Subcellular trafficking and activity of Hyal-1 and its processed forms in murine macrophages', *Traffic*, 15(5), pp. 500-15. doi: 10.1111/tra.12162.

Qian, H., et al. (2009). 'Stabilins are expressed in bone marrow sinusoidal endothelial cells and mediate scavenging and cell adhesive functions', *Biochem Biophys Res Commun*, 390(3), pp. 883-6. doi: 10.1016/j.bbrc.2009.10.068.

Rahib, L., et al. (2014). 'Projecting cancer incidence and deaths to 2030: the unexpected burden of thyroid, liver, and pancreas cancers in the United States', *Cancer Res*, 74(11), pp. 2913-21. doi: 10.1158/0008-5472.CAN-14-0155.

Rai, S. K., et al. (2001). 'Candidate tumor suppressor HYAL2 is a glycosylphosphatidylinositol (GPI)-anchored cell-surface receptor for jaagsiekte sheep retrovirus, the envelope protein of which mediates oncogenic transformation', *Proc Natl Acad Sci U S A*, 98(8), pp. 4443-8. doi: 10.1073/pnas.071572898.

Rayahin, J. E., et al. (2015). 'High and low molecular weight hyaluronic acid differentially influence macrophage activation', *ACS Biomater Sci Eng*, 1(7), pp. 481-493. doi: 10.1021/acsbiomaterials.5b00181.

Rice, A. J., et al. (2017). 'Matrix stiffness induces epithelial-mesenchymal transition and promotes chemoresistance in pancreatic cancer cells', *Oncogenesis*, 6(7), p. e352. doi: 10.1038/oncsis.2017.54.

Riecks, J., et al. (2022). 'The hyaluronan-related genes HAS2, HYAL1-4, PH20 and HYALP1 are associated with prognosis, cell viability and spheroid formation capacity in ovarian cancer', *J Cancer Res Clin Oncol*, 148(12), pp. 3399-3419. doi: 10.1007/s00432-022-04127-6.

Rilla, K., et al. (2005). 'Plasma membrane residence of hyaluronan synthase is coupled to its enzymatic activity', *J Biol Chem*, 280(36), pp. 31890-7. doi: 10.1074/jbc.M504736200.

Rilla, K., et al. (2008). 'Pericellular hyaluronan coat visualized in live cells with a fluorescent probe is scaffolded by plasma membrane protrusions', *J Histochem Cytochem*, 56(10), pp. 901-10. doi: 10.1369/jhc.2008.951665.

Roder, P. V., et al. (2016). 'Pancreatic regulation of glucose homeostasis', *Exp Mol Med*, 48(3), p. e219. doi: 10.1038/emm.2016.6.

Ron, D. and Kazanietz, M. G. (1999). 'New insights into the regulation of protein kinase C and novel phorbol ester receptors', *The FASEB Journal*, 13(13), pp. 1658-1676. doi: 10.1096/fasebj.13.13.1658.

Rooman, I. and Real, F. X. (2012). 'Pancreatic ductal adenocarcinoma and acinar cells: a matter of differentiation and development?', *Gut*, 61(3), pp. 449-58. doi: 10.1136/gut.2010.235804.

Saga, R., et al. (2021). '4-Methylumbelliferone administration enhances radiosensitivity of human fibrosarcoma by intercellular communication', *Sci Rep*, 11(1), p. 8258. doi: 10.1038/s41598-021-87850-3.

Sahai, E., et al. (2020). 'A framework for advancing our understanding of cancer-associated fibroblasts', *Nat Rev Cancer*, 20(3), pp. 174-186. doi: 10.1038/s41568-019-0238-1.

Sainio, A., et al. (2010). 'Hyperglycemic conditions modulate connective tissue reorganization by human vascular smooth muscle cells through stimulation of hyaluronan synthesis', *Glycobiology*, 20(9), pp. 1117-26. doi: 10.1093/glycob/cwq076.

Saito, T., et al. (2011). 'Fragmented hyaluronan is an autocrine chemokinetic motility factor supported by the HAS2-HYAL2/CD44 system on the plasma membrane', *Int J Oncol*, 39(5), pp. 1311-20. doi: 10.3892/ijo.2011.1114.

Sanford, D. E., et al. (2013). 'Inflammatory monocyte mobilization decreases patient survival in pancreatic cancer: a role for targeting the CCL2/CCR2 axis', *Clin Cancer Res*, 19(13), pp. 3404-15. doi: 10.1158/1078-0432.CCR-13-0525.

Santi, A., Kugeratski, F. G. and Zanivan, S. (2018). 'Cancer Associated Fibroblasts: The Architects of Stroma Remodeling', *Proteomics*, 18(5-6), p. e1700167. doi: 10.1002/pmic.201700167.

Schneiderhan, W., et al. (2007). 'Pancreatic stellate cells are an important source of MMP-2 in human pancreatic cancer and accelerate tumor progression in a murine xenograft model and CAM assay', *J Cell Sci*, 120(Pt 3), pp. 512-9. doi: 10.1242/jcs.03347.

Schubbert, S., Shannon, K. and Bollag, G. (2007). 'Hyperactive Ras in developmental disorders and cancer', *Nat Rev Cancer*, 7(4), pp. 295-308. doi: 10.1038/nrc2109.

Schutze, A., et al. (2016). 'RHAMM splice variants confer radiosensitivity in human breast cancer cell lines', *Oncotarget*, 7(16), pp. 21428-40. doi: 10.18632/oncotarget.7258.

Shao, S., et al. (2020). 'Positive feedback in Cav-1-ROS signalling in PSCs mediates metabolic coupling between PSCs and tumour cells', *J Cell Mol Med*, 24(16), pp. 9397-9408. doi: 10.1111/jcmm.15596.

Sheng, Y., et al. (2021). 'Hyaluronan synthase 2 (HAS2) regulates cell phenotype and invadopodia formation in luminal-like breast cancer cells', *Mol Cell Biochem*, 476(9), pp. 3383-3391. doi: 10.1007/s11010-021-04165-7.

Shi, Y., et al. (2019). 'Targeting LIF-mediated paracrine interaction for pancreatic cancer therapy and monitoring', *Nature*, 569(7754), pp. 131-135. doi: 10.1038/s41586-019-1130-6.

Shields, M. A., et al. (2011). 'Pancreatic cancer cells respond to type I collagen by inducing snail expression to promote membrane type 1 matrix metalloproteinase-dependent collagen invasion', *J Biol Chem*, 286(12), pp. 10495-504. doi: 10.1074/jbc.M110.195628.

Shiga, K., et al. (2015). 'Cancer-Associated Fibroblasts: Their Characteristics and Their Roles in Tumor Growth', *Cancers (Basel)*, 7(4), pp. 2443-58. doi: 10.3390/cancers7040902.

Siiskonen, H., et al. (2013). 'Inverse expression of hyaluronidase 2 and hyaluronan synthases 1-3 is associated with reduced hyaluronan content in malignant cutaneous melanoma', *BMC Cancer*, 13(1), p. 181. doi: 10.1186/1471-2407-13-181.

Simons, K. and Ehehalt, R. (2002). 'Cholesterol, lipid rafts, and disease', *J Clin Invest*, 110(5), pp. 597-603. doi: 10.1172/JCI16390.

Singleton, P. A. and Bourguignon, L. Y. (2004). 'CD44 interaction with ankyrin and IP3 receptor in lipid rafts promotes hyaluronan-mediated Ca2+ signaling leading to nitric oxide production and endothelial cell adhesion and proliferation', *Exp Cell Res*, 295(1), pp. 102-18. doi: 10.1016/j.yexcr.2003.12.025.

Sivakumar, S., et al. (2021). 'Activated Regulatory T-Cells, Dysfunctional and Senescent T-Cells Hinder the Immunity in Pancreatic Cancer', *Cancers (Basel)*, 13(8). doi: 10.3390/cancers13081776.

Sousa, C. M., et al. (2016). 'Pancreatic stellate cells support tumour metabolism through autophagic alanine secretion', *Nature*, 536(7617), pp. 479-83. doi: 10.1038/nature19084.

Spadea, A., et al. (2019). 'Evaluating the Efficiency of Hyaluronic Acid for Tumor Targeting via CD44', *Mol Pharm*, 16(6), pp. 2481-2493. doi: 10.1021/acs.molpharmaceut.9b00083.

Spicer, A. P., et al. (1997). 'Chromosomal localization of the human and mouse hyaluronan synthase genes', *Genomics*, 41(3), pp. 493-7. doi: 10.1006/geno.1997.4696.

Spitz, D. R., et al. (2000). 'Glucose deprivation-induced oxidative stress in human tumor cells. A fundamental defect in metabolism?', *Ann N Y Acad Sci*, 899(pp. 349-62. doi: 10.1111/j.1749-6632.2000.tb06199.x.

Sritangos, P., et al. (2020). 'Plasma Membrane Ca(2+) ATPase Isoform 4 (PMCA4) Has an Important Role in Numerous Hallmarks of Pancreatic Cancer', *Cancers (Basel)*, 12(1), p. 218. doi: 10.3390/cancers12010218.

Steele, C. W., et al. (2016). 'CXCR2 Inhibition Profoundly Suppresses Metastases and Augments Immunotherapy in Pancreatic Ductal Adenocarcinoma', *Cancer Cell*, 29(6), pp. 832-845. doi: 10.1016/j.ccell.2016.04.014.

Stern, R., Asari, A. A. and Sugahara, K. N. (2006). 'Hyaluronan fragments: an information-rich system', *Eur J Cell Biol*, 85(8), pp. 699-715. doi: 10.1016/j.ejcb.2006.05.009.

Stern, R., et al. (2007). 'The many ways to cleave hyaluronan', *Biotechnol Adv*, 25(6), pp. 537-57. doi: 10.1016/j.biotechadv.2007.07.001.

Strobel, O., et al. (2007). 'In vivo lineage tracing defines the role of acinar-to-ductal transdifferentiation in inflammatory ductal metaplasia', *Gastroenterology*, 133(6), pp. 1999-2009. doi: 10.1053/j.gastro.2007.09.009.

Suarez-Arnedo, A., et al. (2020). 'An image J plugin for the high throughput image analysis of in vitro scratch wound healing assays', *PLoS One*, 15(7), p. e0232565. doi: 10.1371/journal.pone.0232565.

Sullivan, W. J., et al. (2018). 'Extracellular Matrix Remodeling Regulates Glucose Metabolism through TXNIP Destabilization', *Cell*, 175(1), pp. 117-132 e21. doi: 10.1016/j.cell.2018.08.017.

Tahkola, K., et al. (2021). 'Stromal hyaluronan accumulation is associated with low immune response and poor prognosis in pancreatic cancer', *Sci Rep*, 11(1), p. 12216. doi: 10.1038/s41598-021-91796-x.

Talar-Wojnarowska, R., et al. (2009). 'Clinical significance of interleukin-6 (IL-6) gene polymorphism and IL-6 serum level in pancreatic adenocarcinoma and chronic pancreatitis', *Dig Dis Sci*, 54(3), pp. 683-9. doi: 10.1007/s10620-008-0390-z.

Tammi, R., et al. (2001). 'Hyaluronan enters keratinocytes by a novel endocytic route for catabolism', *J Biol Chem*, 276(37), pp. 35111-22. doi: 10.1074/jbc.M103481200.

Tammi, R. H., et al. (2008). 'Hyaluronan in human tumors: pathobiological and prognostic messages from cell-associated and stromal hyaluronan', *Semin Cancer Biol*, 18(4), pp. 288-95. doi: 10.1016/j.semcancer.2008.03.005.

Tang, D., et al. (2015). 'Apoptosis and anergy of T cell induced by pancreatic stellate cells-derived galectin-1 in pancreatic cancer', *Tumour Biol*, 36(7), pp. 5617-26. doi: 10.1007/s13277-015-3233-5.

Taniuchi, K., Yokotani, K. and Saibara, T. (2012). 'BART inhibits pancreatic cancer cell invasion by PKCalpha inactivation through binding to ANX7', *PLoS One*, 7(4), p. e35674. doi: 10.1371/journal.pone.0035674.

Teranishi, F., et al. (2009). 'Phosphoinositide 3-kinase inhibitor (wortmannin) inhibits pancreatic cancer cell motility and migration induced by hyaluronan in vitro and peritoneal metastasis in vivo', *Cancer Sci*, 100(4), pp. 770-7. doi: 10.1111/j.1349-7006.2009.01084.x.

Theocharis, A. D., et al. (2016). 'Extracellular matrix structure', *Adv Drug Deliv Rev*, 97(pp. 4-27. doi: 10.1016/j.addr.2015.11.001.

Theocharis, A. D., et al. (2000). 'Pancreatic carcinoma is characterized by elevated content of hyaluronan and chondroitin sulfate with altered disaccharide composition', *Biochim Biophys Acta*, 1502(2), pp. 201-6. doi: 10.1016/s0925-4439(00)00051-x.

Thompson, C. B., et al. (2010). 'Enzymatic depletion of tumor hyaluronan induces antitumor responses in preclinical animal models', *Mol Cancer Ther*, 9(11), pp. 3052-64. doi: 10.1158/1535-7163.MCT-10-0470.

Tian, C., et al. (2019). 'Proteomic analyses of ECM during pancreatic ductal adenocarcinoma progression reveal different contributions by tumor and stromal cells', *Proc Natl Acad Sci U S A*, 116(39), pp. 19609-19618. doi: 10.1073/pnas.1908626116.

Tian, X., et al. (2013). 'High-molecular-mass hyaluronan mediates the cancer resistance of the naked mole rat', *Nature*, 499(7458), pp. 346-9. doi: 10.1038/nature12234.

Tolg, C., et al. (2010). 'RHAMM promotes interphase microtubule instability and mitotic spindle integrity through MEK1/ERK1/2 activity', *J Biol Chem*, 285(34), pp. 26461-74. doi: 10.1074/jbc.M110.121491.

Tolg, C., et al. (2014). 'Hyaluronan and RHAMM in wound repair and the "cancerization" of stromal tissues', *Biomed Res Int*, 2014(p. 103923. doi: 10.1155/2014/103923.

Tomasz, M. (1995). 'Mitomycin C: small, fast and deadly (but very selective)', *Chem Biol*, 2(9), pp. 575-9. doi: 10.1016/1074-5521(95)90120-5.

Toole, B. P. (2004). 'Hyaluronan: from extracellular glue to pericellular cue', *Nat Rev Cancer*, 4(7), pp. 528-39. doi: 10.1038/nrc1391.

Trovato, R., et al. (2020). 'The Engagement Between MDSCs and Metastases: Partners in Crime', *Front Oncol*, 10(p. 165. doi: 10.3389/fonc.2020.00165.

Trovato, R., et al. (2019). 'Immunosuppression by monocytic myeloid-derived suppressor cells in patients with pancreatic ductal carcinoma is orchestrated by STAT3', *J Immunother Cancer*, 7(1), p. 255. doi: 10.1186/s40425-019-0734-6.

Twarock, S., et al. (2010). 'Hyaluronan stabilizes focal adhesions, filopodia, and the proliferative phenotype in esophageal squamous carcinoma cells', *J Biol Chem*, 285(30), pp. 23276-84. doi: 10.1074/jbc.M109.093146.

Uchino, M., et al. (2010). 'Nuclear beta-catenin and CD44 upregulation characterize invasive cell populations in non-aggressive MCF-7 breast cancer cells', *BMC Cancer*, 10(p. 414. doi: 10.1186/1471-2407-10-414.

Udabage, L., et al. (2005). 'The over-expression of HAS2, Hyal-2 and CD44 is implicated in the invasiveness of breast cancer', *Exp Cell Res*, 310(1), pp. 205-17. doi: 10.1016/j.yexcr.2005.07.026.

Udabage, L., et al. (2004). 'Inhibition of hyaluronan degradation by dextran sulphate facilitates characterisation of hyaluronan synthesis: an in vitro and in vivo study', *Glycoconj J*, 20(7-8), pp. 461-71. doi: 10.1023/B:GLYC.0000038292.71098.35.

Ullman, N. A., et al. (2022). 'Immunologic Strategies in Pancreatic Cancer: Making Cold Tumors Hot', *J Clin Oncol*, 40(24), pp. 2789-2805. doi: 10.1200/JCO.21.02616.

Van Cutsem, E., et al. (2020). 'Randomized Phase III Trial of Pegvorhyaluronidase Alfa With Nab-Paclitaxel Plus Gemcitabine for Patients With Hyaluronan-High Metastatic Pancreatic Adenocarcinoma', *J Clin Oncol*, 38(27), pp. 3185-3194. doi: 10.1200/JCO.20.00590.

Vang Mouritzen, M. and Jenssen, H. (2018). 'Optimized Scratch Assay for In Vitro Testing of Cell Migration with an Automated Optical Camera', *J Vis Exp*, 138). doi: 10.3791/57691.

Vichai, V. and Kirtikara, K. (2006). 'Sulforhodamine B colorimetric assay for cytotoxicity screening', *Nat Protoc*, 1(3), pp. 1112-6. doi: 10.1038/nprot.2006.179.

Vigetti, D., et al. (2011). 'Hyaluronan synthesis is inhibited by adenosine monophosphate-activated protein kinase through the regulation of HAS2 activity in human aortic smooth muscle cells', *J Biol Chem*, 286(10), pp. 7917-7924. doi: 10.1074/jbc.M110.193656.

Vigil, D., et al. (2010). 'Ras superfamily GEFs and GAPs: validated and tractable targets for cancer therapy?', *Nat Rev Cancer*, 10(12), pp. 842-57. doi: 10.1038/nrc2960.

Vincent, A., et al. (2011). 'Pancreatic cancer', *Lancet*, 378(9791), pp. 607-20. doi: 10.1016/S0140-6736(10)62307-0.

Vonlaufen, A., et al. (2008). 'Pancreatic stellate cells: partners in crime with pancreatic cancer cells', *Cancer Res*, 68(7), pp. 2085-93. doi: 10.1158/0008-5472.CAN-07-2477.

Wang, A. and Hascall, V. C. (2004). 'Hyaluronan structures synthesized by rat mesangial cells in response to hyperglycemia induce monocyte adhesion', *J Biol Chem*, 279(11), pp. 10279-85. doi: 10.1074/jbc.M312045200.

Wang, C., et al. (1996). 'Hyaluronan distribution in the normal epithelium of esophagus, stomach, and colon and their cancers', *The American Journal of Pathology*.

Watari, N., Hotta, Y. and Mabuchi, Y. (1982). 'Morphological studies on a vitamin A-storing cell and its complex with macrophage observed in mouse pancreatic tissues following excess vitamin A administration', *Okajimas Folia Anat Jpn*, 58(4-6), pp. 837-58. doi: 10.2535/ofaj1936.58.4-6_837.

Waters, A. M. and Der, C. J. (2018). 'KRAS: The Critical Driver and Therapeutic Target for Pancreatic Cancer', *Cold Spring Harb Perspect Med*, 8(9). doi: 10.1101/cshperspect.a031435.

Weigel, P. H. and DeAngelis, P. L. (2007). 'Hyaluronan synthases: a decade-plus of novel glycosyltransferases', *J Biol Chem*, 282(51), pp. 36777-81. doi: 10.1074/jbc.R700036200.

Weissmueller, S., et al. (2014). 'Mutant p53 drives pancreatic cancer metastasis through cell-autonomous PDGF receptor beta signaling', *Cell*, 157(2), pp. 382-394. doi: 10.1016/j.cell.2014.01.066.

Weng, X., et al. (2022). 'The membrane receptor CD44: novel insights into metabolism', *Trends Endocrinol Metab*, 33(5), pp. 318-332. doi: 10.1016/j.tem.2022.02.002.

Whatcott, C. J., et al. (2015). 'Desmoplasia in Primary Tumors and Metastatic Lesions of Pancreatic Cancer', *Clin Cancer Res*, 21(15), pp. 3561-8. doi: 10.1158/1078-0432.CCR-14-1051.

Wood, L. D., et al. (2022). 'Pancreatic Cancer: Pathogenesis, Screening, Diagnosis, and Treatment', *Gastroenterology*, 163(2), pp. 386-402 e1. doi: 10.1053/j.gastro.2022.03.056.

Wu, M., et al. (2015). 'A novel role of low molecular weight hyaluronan in breast cancer metastasis', *FASEB J*, 29(4), pp. 1290-8. doi: 10.1096/fj.14-259978.

Wu, W., et al. (2020). 'Hyaluronic acid predicts poor prognosis in breast cancer patients: A protocol for systematic review and meta analysis', *Medicine (Baltimore)*, 99(22), p. e20438. doi: 10.1097/MD.0000000000020438.

Xian, X., Gopal, S. and Couchman, J. R. (2010). 'Syndecans as receptors and organizers of the extracellular matrix', *Cell Tissue Res*, 339(1), pp. 31-46. doi: 10.1007/s00441-009-0829-3.

Xie, Z., et al. (2022). 'Exosome-delivered CD44v6/C1QBP complex drives pancreatic cancer liver metastasis by promoting fibrotic liver microenvironment', *Gut*, 71(3), pp. 568-579. doi: 10.1136/gutjnl-2020-323014.

Xing, R. D., et al. (2008). 'Serum hyaluronan levels in oral cancer patients', *Chin Med J (Engl)*, 121(4), pp. 327-30.

Xu, Y., et al. (2018). 'Dextran sulfate inhibition on human gastric cancer cells invasion, migration and epithelial-mesenchymal transformation', *Oncol Lett*, 16(4), pp. 5041-5049. doi: 10.3892/ol.2018.9251.

Xu, Z., et al. (2010). 'Role of pancreatic stellate cells in pancreatic cancer metastasis', *Am J Pathol*, 177(5), pp. 2585-96. doi: 10.2353/ajpath.2010.090899.

Xue, F., Janzen, D. M. and Knecht, D. A. (2010). 'Contribution of Filopodia to Cell Migration: A Mechanical Link between Protrusion and Contraction', *Int J Cell Biol*, 2010(p. 507821. doi: 10.1155/2010/507821.

Yamamoto, H., et al. (2017). 'A mammalian homolog of the zebrafish transmembrane protein 2 (TMEM2) is the long-sought-after cell-surface hyaluronidase', *J Biol Chem*, 292(18), pp. 7304-7313. doi: 10.1074/jbc.M116.770149.

Yan, H. H., et al. (2021). 'ANGPTL4 accelerates KRAS(G12D)-Induced acinar to ductal metaplasia and pancreatic carcinogenesis', *Cancer Lett*, 519(pp. 185-198. doi: 10.1016/j.canlet.2021.07.036.

Yang, B., et al. (1994). 'Identification of a common hyaluronan binding motif in the hyaluronan binding proteins RHAMM, CD44 and link protein', *EMBO J*, 13(2), pp. 286-96. doi: 10.1002/j.1460-2075.1994.tb06261.x.

Yang, C., et al. (2020). 'CD44/HA signaling mediates acquired resistance to a PI3Kalpha inhibitor', *Cell Death Dis*, 11(10), p. 831. doi: 10.1038/s41419-020-03037-0.

Yang, S., Liu, Q. and Liao, Q. (2020). 'Tumor-Associated Macrophages in Pancreatic Ductal Adenocarcinoma: Origin, Polarization, Function, and Reprogramming', *Front Cell Dev Biol*, 8(p. 607209. doi: 10.3389/fcell.2020.607209.

Yen, T. W., et al. (2002). 'Myofibroblasts are responsible for the desmoplastic reaction surrounding human pancreatic carcinomas', *Surgery*, 131(2), pp. 129-34. doi: 10.1067/msy.2002.119192.

Yoshida, H., et al. (2013). 'KIAA1199, a deafness gene of unknown function, is a new hyaluronan binding protein involved in hyaluronan depolymerization', *Proc Natl Acad Sci U S A*, 110(14), pp. 5612-7. doi: 10.1073/pnas.1215432110.

Zadnikova, P., et al. (2022). 'The Degradation of Hyaluronan in the Skin', *Biomolecules*, 12(2), p. 251. doi: 10.3390/biom12020251.

Zhang, A., et al. (2017). 'Cancer-associated fibroblasts promote M2 polarization of macrophages in pancreatic ductal adenocarcinoma', *Cancer Med*, 6(2), pp. 463-470. doi: 10.1002/cam4.993.

Zhang, G., et al. (2016). 'A novel role of breast cancer-derived hyaluronan on inducement of M2-like tumor-associated macrophages formation', *Oncoimmunology*, 5(6), p. e1172154. doi: 10.1080/2162402X.2016.1172154.

Zhao, F., et al. (2009). 'Increase in frequency of myeloid-derived suppressor cells in mice with spontaneous pancreatic carcinoma', *Immunology*, 128(1), pp. 141-9. doi: 10.1111/j.1365-2567.2009.03105.x.

Zhao, P., et al. (2013). 'CD44 promotes Kras-dependent lung adenocarcinoma', *Oncogene*, 32(43), pp. 5186-90. doi: 10.1038/onc.2012.542.

Zhao, S., et al. (2016). 'CD44 Expression Level and Isoform Contributes to Pancreatic Cancer Cell Plasticity, Invasiveness, and Response to Therapy', *Clin Cancer Res*, 22(22), pp. 5592-5604. doi: 10.1158/1078-0432.CCR-15-3115.

Zhou, B., et al. (2000). 'Identification of the hyaluronan receptor for endocytosis (HARE)', *J Biol Chem*, 275(48), pp. 37733-41. doi: 10.1074/jbc.M003030200.

Zhu, Y., et al. (2017). 'Tissue-Resident Macrophages in Pancreatic Ductal Adenocarcinoma Originate from Embryonic Hematopoiesis and Promote Tumor Progression', *Immunity*, 47(2), pp. 323-338 e6. doi: 10.1016/j.immuni.2017.07.014.

Zoller, M. (2011). 'CD44: can a cancer-initiating cell profit from an abundantly expressed molecule?', *Nat Rev Cancer*, 11(4), pp. 254-67. doi: 10.1038/nrc3023.

BLANK